Unraveling the muco-adhesion of Lactococcus lactis : development of biophysical approaches

Thi-Ly Tran

THÈSE

En vue de l'obtention du

DOCTORAT DE L'UNIVERSITÉ DE TOULOUSE

Délivré par :

Institut National des Sciences Appliquées de Toulouse (INSA de Toulouse)

Présentée et soutenue par :
TRAN Thi Ly
Le : jeudi 12 décembre 2013

Titre :

Unraveling the muco-adhesion of *Lactococcus lactis* : development of biophysical approaches

---

École doctorale et discipline ou spécialité :

ED SEVAB : Ingénieries microbienne et enzymatique

Unité de recherche :

Laboratoire Ingénierie des Systèmes Biologiques et des Procédés UMR 5504 CNRS - UMR 792 INRA

Directeur(s) de Thèse :

MERCIER-BONIN Muriel

JURY :

M. SCHMITZ Philippe, Professeur INSA de Toulouse, Président
M. KULAKAUSKAS Saulius, Directeur de Recherche INRA, Rapporteur
M. Di MEGLIO Jean-Marc, Professeur Université Denis Diderot Paris 7, Rapporteur
Mme MERCIER-BONIN Muriel, Chargée de Recherche INRA, Directrice de thèse
M. CASTELAIN Mickaël, Chargé de Recherche INRA, Co-encadrant de thèse

ACKNOWLEDGEMENTS

First of all, I would like to thank Mr. Nic LINDLEY, Director of the "Laboratoirie d'Ingénierie des Systèmes Biologiques et Procédés" of the "Institut National des Sciences Appliquées" (INSA) in Toulouse, where this work was carried out from November 2010 to December 2013, for having welcomed me to his laboratory and provided the materials and equipments that I have needed to produce and complete my thesis.

I would like to thank all members of the jury for agreeing to assess this manuscript and to participate in the thesis defence:

- Mr. Philippe SCHMITZ, Professor of the INSA in Toulouse, the chairman of the jury, for his encouragement, valuable discussions, and good humor.
- Mr. Saulius KULAKAUSKAS, Research Director of the INRA Jouy-en-Josas, for his great enthusiasm and time spent in reading, analyzing, assessing and writing the report.
- Mr. Jean-Marc Di MEGLIO, Professor of "Université Denis Diderot Paris 7", for his particularly rigorous reading, constructive criticism and time spent in writing the report.

I would especially like to express my most sincere gratitude to my supervisor, Mrs. Muriel MERCIER-BONIN, for her excellent guidance, advice and support in all stages of this thesis. I would also like to thank her for helping me to shape my interest and ideas, painstakingly and patiently correct my writing. She cared much about my work and responded to my questions and queries so promptly. Additionally, I will forever be thankful to Mr. Mickaël CASTELAIN, who was willing to provide me a great knowledge of biophysics as well as spend his time and effort during the final year of my PhD. One simply could not wish for a better and friendlier advisor.

I would like to thank Mr. Nicolas DIETRICH, researcher of the "Transfer, Interfaces, Mixing" (TIM) group of the LISBP laboratory in Toulouse, who let me experience the Diffusion Front Tracking method and helped me analyze data using the Monte Carlo Markov Chain program. His motivating collaboration as well as his participation in my doctoral committee meetings was greatly appreciated. I would also like to thank Mrs. Dominique ANNE-ARCHARD, researcher of the "'Institut de Mécanique des Fluides de Toulouse"

(IMFT) in Toulouse, for her particular interest in my work and for taking part in my doctoral committee meetings.

The major part of this thesis is the fruitful result of collaboration with the MICALIS Institute in Jouy-en-Josas, France. I would like to thank Marie-Pierre CHAPOT-CHARTIER and Mickaël MEYRAND for their *Lactococcus lactis* wild-type, mutant and plasmid-cured derivative strains.

I would also like to thank Etienne DAGUE from the “Laboratoire d'Analyse et d'Architecture des Systèmes” (LAAS) in Toulouse for the Atomic Force Microscopy measurement, Yann GUERARDEL from the “Unité de Glycobiologie Structurale et Fonctionnelle” (UGSF) in Lille for pig gastric mucin fractions.

I would particularly and gratefully thank to Mrs. HO Phu Ha and Mr. CHU-KY Son from “Hanoi University of Science and Technology” (HUST), for their confidence in me, recommending me to this project and constant encouragement during my study. Additionally, I would like to thank the “Université des Sciences et Technologies de Hanoï” (USTH), for providing the funding which allowed me to undertake this research. I would also like to thank them for giving me the opportunity to attend the annual USTH workshops which provided a number of the diverse and interesting training courses as well as the career guidance as a teacher-researcher.

I am deeply grateful to Ms. Marie-Pierre DUVIAU who was there for helping me set up the Shear Stress Flow Chamber experiments when I came to the laboratory at the beginning, for her enthusiasm for discussing, caring and giving advices during my thesis.

I would like to thank all the members of my group EAD4 who are extremely friendly, humor and helpful. I would particularly like to thank Mr. Pascal LOUBIÈRE, head of the team, for receiving me to his group. I’m so glad to have worked with the wonderful colleagues. Special thanks go to my young, funny and cheerful office mates (Manon, Marie, Jade, Thomas, Arthur, Pauline, Amandine, Stéphanie, Anne-Laure and Jérôme). I just wish them the best of luck for their thesis and future career.

I would like to thank my countryman, LE Doan Thanh Lam, for his constant help and encouragement while he was doing his thesis and even after he left the laboratory. He was the one whom I wrote up for asking so many questions of science and society. I think of him as a big brother.

Loving thanks to my friends for providing support and friendship that I needed. I will not forget the beautiful moments that we shared in France.

I especially thank my mom, dad and brothers. My hard-working parents have sacrificed their lives for their children and provided unconditional love and care. I know I always have my family to count on when times are rough.

At last, not at least, special thanks to my best friend, soul-mate and boyfriend, Jérémy, who is the only person can appreciate my quirkiness and sense of humor, and his family who all have been supportive and caring.

SUMMARY OF THE THESIS

Context and objectives. The digestive epithelium is covered with a protective mucus layer, regarded as a viscoelastic and permeable hydrogel. This layer serves as an ecological niche for commensal and probiotic bacteria, and plays a role in the defense against pathogens. The mucus layer is described as a secreted mucin-fiber scaffold. Mucins are large glycoproteins with a serine and threonine-rich protein backbone, linked to a wide variety of O-linked oligosaccharide side chains arranged in a bottle-brush configuration. Such O-glycans are nutritive sources for bacteria and/or potential ligands for bacterial adhesins, probably contributing in this way to the selection of the species-specific microbiota.

Many studies on bacterial muco-adhesion have been carried out with commensal *Lactobacillus* species, with the aim to select probiotics based on their ability to persist within the gut. In contrast, little is known about the structural and functional factors involved in the muco-adhesion of *Lactococcus lactis*, the model for Lactic Acid Bacteria.

In this thesis, we focused on unraveling multi-scale interactions between a vegetal *L. lactis* subsp. *lactis* isolate, TIL448 and a model mucin, Pig Gastric Mucin (PGM). In a previous study, *L. lactis* TIL448 was shown to expose at its surface both pili and mucus-binding protein. In contrast to the other tested *L. lactis* strains, specific adhesion to Caco-2 human intestinal epithelial cells was reported. However, no data was available of the TIL448 muco-adhesive phenotype. To address such questions, different biophysical approaches were implemented. Our work was achieved in close collaboration with Micalis Institute in Jouy-en-Josas, France.

Results. In a first part, we performed single-cell scale AFM measurements with dedicated lacto-probes and shear stress flow chamber experiments at the bacterial population level, under laminar flow conditions on the wild type *L. lactis* TIL448. We also tested the plasmid-cured strain and two mutants, obtained by disruption of the genes encoding the major pilin and the mucus-binding protein. Bacterial cells were put in adhesive contact with a biomimetic PGM-coated surface, under static or shear-flow conditions. AFM experiments on TIL448 revealed a high proportion of specific adhesive events (60 %) and a low level of non-adhesive ones (2 %). The strain muco-adhesive properties were confirmed by the weak detachment of

bacteria from the PGM-coated surface under shear flow. In AFM, rupture events were detected at short (100-200 nm) and long distances (up to 600-800 nm). AFM measurements on pili and mucus-binding protein defective mutants demonstrated the comparable role played by these two surface proteinaceous components in adhesion to PGM under static conditions. Under shear flow, a more important contribution of the mucus-binding protein than the pili one was observed. Both methods differ by the way of probing the adhesion force. AFM blocking assays with free PGM or O-glycan fractions purified from PGM demonstrated that neutral oligosaccharides played a major role in adhesion of *L. lactis* TIL448 to PGM. Then, the diffusion ability of *L. lactis* was determined by implementing a novel method, named Diffusion Front Tracking (DFT). It consists of tracking the diffusion front of stained cell suspensions over time within the PGM network. The technique involved tracking a liquid-liquid interface in a Hele-Shaw cell using a digital camera. A suspension of bacterial cells, stained with fuchsine and injected on the top, was allowed to diffuse down to the PGM hydrogel. The feasibility of the method was demonstrated. Then, the diffusion coefficient was determined for all the strains under study, which required solely the diffusing front position over time. A mathematical analysis was developed to solve this problem. Diffusion of bacterial cells follows the Fick's law and was fitted to a model using Monte-Carlo algorithm. The latter allows checking the presence of convection or sedimentation artifacts.

In a second part, in order to have a more thorough understanding of the *L. lactis* muco-adhesive and diffusive ability, the microstructure and mechanical properties of PGM were determined. Gel microstructure for varying PGM concentration was probed by the analysis of diffusivities of 200-nm and 500-nm fluorescent nanoparticles with different surface properties (carboxyl-terminated, negatively charged tracers, with and without PEG coating; amine-terminated, positively charged tracers), using fluorescence Multiple-Particle Tracking. The pore size of the PGM network was evaluated between 240 and 470 nm, depending on the PGM concentration. A high heterogeneity of the mesh pore size was also highlighted. Characterization of the PGM rheological properties was achieved by combining classical bulk rheometry and one-point and two-point microrheometry approaches.

Conclusion. Our study, based on the combination of different biophysical approaches and tools, has allowed dissecting the muco-adhesive and diffusive phenotype of *L. lactis* TIL448, in relation with the nature of the bacterial surface determinants and the structural, mechanical and rheological properties of the PGM network.

RESUME DE LA THESE

Contexte et objectifs. L'épithélium digestif est recouvert d'une couche protectrice de mucus, qui est un hydrogel perméable et viscoélastique. Cette couche sert de niche écologique pour les bactéries commensales et/ou exogènes comme les probiotiques, elle joue également un rôle dans la défense contre les pathogènes. La couche de mucus est formée d'un réseau de fibres de mucines. Ces dernières sont des glycoprotéines de haut poids moléculaire avec un squelette protéique riche en sérine et thréonine, lié à une grande variété de O-glycanes qui représentent une source nutritionnelle pour les bactéries et/ou des ligands potentiels pour les adhésines bactériennes, contribuant ainsi probablement à la sélection et l'implantation d'un microbiote régio-spécifique. De nombreuses études sur la muco-adhésion des bactéries lactiques ont été réalisées avec des lactobacilles, dans le but de sélectionner de nouveaux probiotiques, dotés d'une meilleure faculté de persistance dans l'intestin. En revanche, peu de données sont actuellement disponibles sur les facteurs structurels et fonctionnels impliqués dans la muco-adhésion de *Lactococcus lactis*, le modèle des bactéries lactiques. Dans ce cadre, en collaboration avec l'Institut Micalis de Jouy-en-Josas, nous nous sommes focalisés sur la quantification multi-échelles des interactions entre la souche naturelle d'origine végétale *L. lactis* ssp. *lactis* TIL448 et une mucine modèle, la mucine gastrique de porc (PGM).

Démarche expérimentale et résultats. Nous nous sommes intéressés aux capacités muco-adhésives de *L. lactis* TIL448 par le couplage de (i) la microscopie à force atomique (AFM), à l'échelle de la cellule unique et en mode statique et (ii) la méthode hydrodynamique en chambre à écoulement cisaillé, à l'échelle de l'ensemble de la population bactérienne. Dans l'optique d'identifier la nature et le rôle fonctionnel des déterminants de surface mis en jeu, nous avons testé, outre la souche sauvage, la souche curée de plasmides TIL1230 et deux mutants TIL1289 et TIL1290, altérés dans la synthèse de pili et d'une protéine "mucus-binding", respectivement.

L'adhésion forte de la souche TIL448 à PGM a été démontrée par AFM avec une force de 0,18 ± 0,04 nN, accompagnée d'un pourcentage faible d'événements non adhésifs (2%) et d'un pourcentage élevé d'événements adhésifs spécifiques (60%). La viabilité des bactéries sur la pointe AFM, estimée par un marquage au CFDA, a été établie. Des distances à la rupture ont été détectées à la fois à 100-200 nm et à plus de 600-800 nm, de manière

cohérente avec la présence de pili (structures pouvant atteindre plusieurs µm de longueur). Par ailleurs, nous avons pu montrer la contribution équivalente des pili et de la protéine "mucus-binding ", du fait d'un pourcentage d'événements adhésifs spécifiques proche pour les deux mutants. Enfin, nous avons démontré, à partir d'essais AFM de blocage avec PGM ou des fractions O-glycaniques purifiées (fractions totale, acide et neutre), que les oligosaccharides neutres jouent un rôle majeur dans les interactions TIL448/PGM.

La forte adhésion de TIL448 à PGM a ensuite été confirmée par méthode hydrodynamique, en conditions d'écoulement laminaire. Dans ces conditions, la protéine "mucus-binding" semble jouer un rôle plus important que les pili dans le processus muco-adhésif de TIL448. Il faut toutefois noter que les deux méthodes diffèrent par la façon de "sonder" l'adhésion : par AFM, le contact puis le retrait de la lacto-pointe de la couche de PGM s'effectuent en mode forcé alors que, par méthode hydrodynamique, les conditions de détachement sont plus "douces".

Pour relier les propriétés muco-adhésives et diffusives de *L. lactis*, les capacités de migration de la souche TIL448 et de ses dérivés ont ensuite été évaluées dans des suspensions de PGM à concentration variable (0,5% et 5% (m/v)), en mettant en œuvre une nouvelle méthode "Diffusion Front Tracking" (DFT), précédemment développée au laboratoire pour mesurer le coefficient de diffusion de O_2 dans les liquides. Cette méthode consiste à suivre le front de diffusion de la suspension bactérienne au cours du temps au sein du réseau de PGM, dans une chambre de Hele-Shaw, couplée à une caméra CCD. Les bactéries *L. lactis* sont préalablement marquées avec la fuschine pour mieux visualiser le front de diffusion. A noter que la viabilité et les propriétés de surface (hydrophobie, électronégativité) de l'ensemble des souches testées n'ont pas été modifiées de manière significative après marquage à la fuchsine. La faisabilité de la méthode DFT a tout d'abord été établie. Il a ensuite été démontré que la migration de *L. lactis* dans PGM est régie par un équilibre complexe entre les interactions spécifiques (liaisons du type ligand/récepteur) et non spécifiques (comme l'hydrophobie).

Par ailleurs, nous avons démontré que les bactéries *L. lactis* ont tendance à être plus diffusives dans PGM 0,5% (m/v) que dans PGM 5% (m/v). La microstructure du réseau de mucines a donc été caractérisée par des approches de microrhéométrie 1 point (1P) et 2 points (2P) et de suivi de particules fluorescentes. Cette technique repose sur le suivi de la position des particules en fonction du temps. Ces dernières, de diamètre 200 nm ou 500 nm, sont

chargées négativement par des groupements carboxyl, chargées positivement par des groupements amines ou préalablement fonctionnalisées avec un agent neutre en charge, le polyéthylène glycol (PEG) qui annihile toute interaction d'origine électrostatique avec le milieu suspendant. Il a été montré que le coefficient de diffusion diminue significativement avec la concentration en PGM. De plus, les particules les plus petites sont avantagées ainsi que les particules neutres (i.e. greffées avec PEG). Un modèle d'obstruction, issu de la littérature, a été utilisé et permet d'accéder aux valeurs estimatives caractéristiques de la taille de pore du réseau. Les tailles ainsi obtenues varient de 470 nm à 240 nm pour des concentrations de PGM de 0,5% et 5% (m/v), respectivement. Ces valeurs sont parfaitement corrélées aux données de diffusivité et de microrhéologie. La forte hétérogénéité dans la taille de pore du réseau a toutefois été soulignée.

Conclusions. Notre étude, positionnée à l'interface Biologie/Physique et basée sur la combinaison d'approches biophysiques innovantes, a permis de disséquer le phénotype muco-adhésif de *L. lactis* TIL448, en relation avec la nature des déterminants de surface impliqués et les propriétés structurales, mécaniques et rhéologiques du réseau de PGM.

Publications

- **Le D.T.L*, Tran T.L***, Duviau M.P, Meyrand M., Guérardel Y., Castelain M., Loubière P., Chapot-Chartier M.P, Dague E., Mercier-Bonin M., Unraveling the role of surface mucus-binding protein and pili in muco-adhesion of *Lactococcus lactis*. Published: November 18, 2013. DOI: 10.1371/journal.pone.0079850
  * co-first author

Communications

- **Tran T.L**, Duviau M.P, Castelain M., Loubière P., Chapot-Chartier M.P, Mercier-Bonin M., Unravelling the muco-adhesion of *Lactococcus lactis* using Shear Stress Flow Chamber and Multiparticle Tracking, Journées des Microbiologistes de l'INRA, 13-15 November 2012, L'Isle-sur-la-Sorgue, France (abstract, poster).

- **Tran T.L**, Duviau M.P, Castelain M., Loubière P., Mercier-Bonin M., *In vitro* evaluation of muco-adhesive properties of *Lactococcus lactis* strains, USTH workshop, 10-17 September 2012, Lyon, France (abstract, oral).

- **Tran T.L**, Le D.T.L, Duviau M.P, Meyrand M., Guérardel Y., Castelain M., Loubière P., Chapot-Chartier M.P, Dague E., Mercier-Bonin M., Unraveling the role of surface mucus-binding protein and pili in muco-adhesion of *Lactococcus lactis*. 19ème colloque des Club des Bactéries Lactiques, 16-17-18 October 2013, Bordeaux, France (abstract, oral).

TABLE OF CONTENT

INTRODUCTION

INTRODUCTION

The digestive epithelium is covered with a protective mucus layer that has the consistence of viscoelastic and permeable gel. This layer is the preferential habitat for commensal bacteria and plays a role in the defense against bacterial infections by expelling pathogens from the mucosal surface. Although often overlooked, mucus is also a crucial component of the innate immune system. The mucus layer is organized around secreted mucins that are large glycoproteins, based on protein backbone structures rich in serine and threonine, which are linked to a wide variety of O-linked oligosaccharide side chains, arranged in a bottle-brush configuration and constituting more than 70% of the weight of the molecule. Such O-glycans represent nutrients and energy source for bacteria, and/or potential ligands for microbial adhesins, probably contributing in this way to the selection of the species-specific microbiota.

In the stomach and colon, mucus is divided in two adjacent layers, an easily removable outer loose layer and an inner mucus layer firmly attached to the epithelial cells. MUC5AC and MUC2 are the major secreted mucins, for the stomach and colon, respectively. Under healthy conditions, the inner mucus layer forms a physical barrier that bacteria are unable to penetrate. In contrast to this bi-layered organized structure, the mucus layer in the small intestine is rather discontinuous and less well-defined: the mucus is secreted at the top of the crypts and then moves upward between the villi. The tips of the villi are thus not always covered with mucus.

The molecular mechanisms underlying the composition and functional role of mucus remain to date poorly understood. Elucidating the barrier properties of mucus, i.e. its structure and associated trapping ability, is actually a major concern. At the nanoscale, mucus has been depicted as a heterogeneous mesh network of mucin fibers, with a fiber diameter in the range 5-10 nm, and more particularly 7 nm for intestinal mucins. Numerous works report the use of nano- or micron-sized, and non muco-adhesive nanoparticles as probes to determine the spacing between mucin fibers with Multi-Particle Tracking experiments. The mesh structure obtained (of about several hundreds of nanometers) is generally wider than the pore size expected assuming a random array of individual mucin fibers. In fact, physico-chemical interactions within the mucin network, such as hydrophobic interactions, may cause mucin

fibers to self-condense and/or bundle with others, forming mucin cables thicker than individual mucin fibers, which in turn create larger pores. Trapping ability of mucus is also suspected to be an interplay between size and interaction effects. Under the first assumption, particles with smaller dimensions compared to the mucin network pore are able to migrate freely, while larger particles are obstructed. The latter mechanism is based on specific (ligand/receptor bonding) and non-specific (hydrophobic, electrostatic, Lifshitz-van der Waals) physico-chemical interactions between particles and mucins: muco-adhesive particles are trapped within mucus whereas non-muco-adhesive ones can easily pass through. These barrier properties are thus closely connected to the mucus microstructure but also to its rheological properties, which have been thoroughly investigated in the literature for various mucus sources and forms (scrapped samples vs. commercial products, crude vs. purified extracts).

In contrast to inert particles, the mechanisms underlying the migration of bacteria through mucus have been barely investigated. One striking example is given by the ulcer-causing gastric pathogen *Helicobacter pylori*. It is the only bacterium known to colonize the harsh acidic environment of the human stomach, by producing urease which catalyzes hydrolysis of urea to ammonia, thus elevating the pH of its local environment. Rheology of gastric mucin was found to be pH-dependent, transitioning from a viscous solution at neutral pH to a gel in acidic conditions. Bulk rheology measurements also showed that pH elevation induced by *H. pylori* resulted in a dramatic decrease in mucin viscoelastic moduli. Microscopy studies of the motility of *H. pylori* in gastric mucin at acidic and neutral pH revealed that bacterial cells were able to swim freely at high pH whereas they were strongly constrained at low pH. It was concluded that *H. pylori* moves through mucus by reducing mucin-gel viscoelasticity. Few data are currently available on the migration ability of beneficial bacteria, like Lactic Acid Bacteria (LAB), within mucus gels. However, an increasing attention is paid to their muco-adhesive phenotype, in relation with the cell surface determinants involved. A special interest is dedicated to commensal *Lactobacillus* species, with the aim of identifying novel probiotics based on their capacity to persist within the gut. In this framework, several cell surface proteins have been shown to act as specific mediators of *Lactobacillus* adhesion to mucus, such as mucus-binding proteins and pili.

In contrast to lactobacilli, little is known about the structural and functional factors involved in muco-adhesion of lactococci. *Lactococcus lactis*, considered as the model LAB, is

traditionally used as a starter in manufacturing cheese and other fermented dairy products. Moreover, its beneficial effects on human health have been increasingly depicted, either as a probiotic or delivery vector for therapeutic molecules, notably for treating intestinal diseases. Even though lactococci are not a frequent natural element of the intestinal microbiota, they were sporadically isolated from feces of many different groups of humans. Some particular strains were also shown to transit through the stomach and survive in the gut of rodents. This adaptation ability is probably in line with the genetic, genomic and phenotypic diversity, recently highlighted for *L. lactis*. Such biodiversity was explored in our research group in terms of muco-adhesion by first considering the dairy strain *L. lactis* subsp. *cremoris* IBB477 (PhD thesis of D.T.L. Le, 2011), in collaboration with the Institute of Biochemistry and Biophysics of Warsaw (Poland). The muco-adhesive properties of this strain were clearly assessed by combining *in vitro* approaches from nanoscale with AFM force spectroscopy to multi-cellular level using quartz crystal microbalance with dissipation monitoring. In continuity with these previous studies, the present work aimed at developing a more integrative strategy through unravelling the interplay between biological, physico-chemical and mechanical mechanisms involved in the interaction(s) of *L. lactis* with mucins. To this aim, adhesion and migration through mucin-based gels of the vegetal *L. lactis* subsp. *lactis* isolate TIL448 were characterized, in close relation with, on the one hand, the gel rheology and microstructure and, on the other hand, the *L. lactis* cell surface specific determinants (i.e. pili and mucus-binding protein). To address these questions, the commercial product Pig Gastric Mucin (PGM) of type III was chosen as the model mucin. Different biophysical approaches and tools were combined, including (i) AFM force spectroscopy and shear stress flow chamber for *L. lactis* adhesion to PGM, (ii) Diffusion Front Tracking (DFT) for *L. lactis* migration through PGM-based gels and (iii) fluorescence Multi-Particle Tracking (fMPT) with functionalized nano-sized probes for the microstructure and microrheological properties of PGM-based gels, in comparison with classical bulk rheometry. This work was achieved in close collaboration with the Micalis Institute (Jouy-en-Josas) and with the "Transfert, Interface, Mélange" team of the "Laboratoire d'Ingénierie des Systèmes Biologiques et des Procédés" (Toulouse).

CHAPTER I. LITERATURE REVIEW

Chapter I. Literature review

1. Lactic Acid Bacteria

Lactic Acid Bacteria (LAB) represent a group of Gram-positive bacteria which share common characteristics of morphology, metabolism, and physiology. They are acid-tolerant, generally non-sporing, non-respiring cocci or rods, which produce lactic acid as the major end product during the fermentation of carbohydrates. LAB are generally associated with habitats rich in nutrients, such as various food products (milk, meat, vegetables, beverages), but some are members of the normal microbiota of the mouth, the gastrointestinal tract and the vagina of mammals. Based on their major contribution in food and health, LAB are generally regarded as safe (GRAS status).

1.1 *Lactococcus lactis*

Lactococcus lactis, which is defined as the model LAB, is one of the most important microorganisms in the dairy industry and has been identified as a promising candidate for vaccine delivery (LeBlanc *et al.* 2013). *L. lactis* cells are non motile cocci, which group in pairs and short chains, and, depending on growth conditions, may be ovoid-shaped with typically 0.5 – 1.5 µm in length. To date, eight species of *Lactococcus* have been defined, consisting of *L. lactis, L. garvieae, L. plantarum, L. piscium, L. raffinolactis, L. fujiensis, L. chungangensis* and *L. taiwanensis*. Three new species of lactococci have been recently introduced, based on their morphological, physiological and phylogenetic features: *L. chungangensis* sp. nov., isolated from activated sludge foam (Cho *et al.* 2008), *L. fujiensis* sp. nov., isolated from the outer leaves of Chinese cabbages (Cai *et al.* 2010), and *L. taiwanensis* sp. nov., isolated from fresh cummingcordia (Chen *et al.* 2012). Among these species, only *L. lactis* is found in the dairy industry. Four subspecies of *L. lactis* can be distinguished: *L. lactis* subsp. *lactis* (including the *L. lactis* subsp. *lactis* biovar diacetylactis), *L. lactis* subsp. *cremoris*, *L. lactis* subsp. *hordniae* and the recently proposed subspecies *L. lactis* subsp. *tructae* subsp. nov, isolated from the intestinal mucus of trout (Pérez *et al.* 2011).

The completely-sequenced genomes of some *L. lactis* strains (**Table I.1**) have been published during the last decade, which may provide some important traits in the dairy industry, as well

as for other applications. *L. lactis* strains are of a high biodiversity, exhibiting great adaptation ability for their environment. Indeed, a number of studies have shown that the gene pool plays a pivotal role both in evolution and in the environmental adaptation of *L. lactis* (Siezen *et al.* 2005, Górecki *et al.* 2011, Siezen *et al.* 2011). A comparative evaluation of the genetic and genomic diversity within a collection of 36 strains isolated from different ecological sources and geographical areas revealed a high variability at both gene and genome levels and gave clues about population structure and evolution. Therefore, the authors proposed a new classification based on ecological separation corresponding to "domesticated" and "environmental" strains (Passerini *et al.* 2010). Similarly, an extensive whole-genome diversity analysis on 39 *L. lactis* strains, isolated from dairy and plant sources, showed that *L. lactis* has a very flexible genome: strain variability in terms of functions included proteolysis, lactose fermentation, citrate uptake, metal ion resistance and exopolysaccharides biosynthesis (Siezen *et al.* 2011).

Table I.1. List of *L. lactis* strains which have been completely sequenced

Strain	Resource	Reference
***L. lactis* subsp. *lactis* IL1403**	A plasmid-free derivative of the strain IL594, isolated from cheese starter culture	(Bolotin *et al.* 2001)
***L. lactis* subsp. *cremoris* SK11**	Dairy origin	(Siezen *et al.* 2005)
***L. lactis* subsp. *cremoris* MG1363**	A plasmid-free derivative of the strain *L. lactis* subsp. *lactis* NCDO712*	(Wegmann *et al.* 2007)
***L. lactis* subsp. *lactis* KF147**	Mung bean sprouts	(Siezen *et al.* 2010)
***L. lactis* subsp. *lactis* A76**	Dairy origin	(Bolotin *et al.* 2012)
***L. lactis* subsp. *lactis* CV56**	Vagina of healthy women	(Gao *et al.* 2011)
***L. lactis* subsp. *lactis* IO-1**	Water in the drain pit of a kitchen sink	(Kato *et al.* 2012)

*NCDO strains were from the National Collection of Dairy Organisms, National Institute for Research in Dairying, England.

1.2 Application of *L. lactis* for food and health issues

1.2.1 Application of *L. lactis* for food products

L. lactis is extensively used in the production of cheese, sour cream and fermented milk (Madigan 2005), which has a significant economic value. As shown in **Table I.2**, which reports the global sale value of dairy products in 1998, 2003 and 2007, cheese represented about 30% of total dairy products with a 9.8% growth from 2003 to 2007 (Farkye 2004).

Table I.2. Global value sales of dairy products (US$ million, retail selling price) (Farkye 2004)

	1998	2003	2007	% Growth 2003-2007
Total of dairy products	218 881.5	222 971.3	247 994.2	11.2
Milk	76 080.0	73 067.7	78 242.8	1.4
Cheese	66 584.5	67 810.0	74 439.1	9.8
Yoghurt	24 363.0	23 334.4	34 002.1	20.0
Cream	8 863.7	8 934.4	9 769.9	13.7
Flavored milk	7 424.2	8 367.1	9 963.1	19.1
Milk powder	6 539.3	6 003.1	7 309.1	21.8

Starter cultures consisting of *L. lactis* are added at the beginning of the cheese making process, which are essential for texture profile and taste of products. *L. lactis* subsp. *lactis* is used for making soft cheese while the subspecies *cremoris* is preferred for hard cheese. Analysis of the *L. lactis* strains present either in raw milk or from non-dairy source has gained interest in the dairy industry. For instance, for some wild-type lactococci from raw milk, traditional cheese ripening is faster and the flavor is more intense than the one achieved with pasteurized or micro-filtered milk (Corroler *et al.* 1998). Ayad *et al.* (Ayad *et al.* 1999, Ayad *et al.* 2001) reported the specific-flavor forming abilities of *L. lactis* isolates from artisanal and non-dairy origin. Wild-type strains produced relatively high levels of primary alcohols and branched aldehydes by degrading amino acids, which could explain their ability to produce distinct flavors. Other examples of *L. lactis*-based dairy fermented products are kefir and viili. Kefir is a cultured milk beverage from Russia, made with the milk of cow, ewes, goats and buffalos. Kefir is produced by kefir grains consisting of a symbiotic community of 90-95% bacteria (mainly *L. lactis* subsp. *lactis* and *L. lactis* subsp. *cremoris*) and 5-10% of various lactose-fermenting yeasts (Farnworth 2006). Viili is a type of traditional yogurt from Scandinavian countries and produced by the dual microbial action of

LAB and yeasts. The LAB identified in viili include *L. lactis* subsp. *cremoris, L. lactis* subsp. *lactis* biovar diacetylactis (Leporanta 2003).

Moreover, the non-dairy *L. lactis* strains, isolated for instance from plants, animals and soil, may also offer advantages such as bacteriocin-producing capacities, probably to withstand competition with other bacteria (Ayad *et al.* 2002). Among 123 strains of LAB isolated from mixed salad and fermented carrots, Uhlman *et al.* (Uhlman *et al.* 1992) identified and characterized two *Lactococcus* strains which produced a heat-stable bacteriocin. This bacteriocin was found to inhibit species of *Listeria, Lactobacillus, Lactococcus, Pediococcus, Leuconostoc, Carnobacterium, Bacillus and Staphylococcus.* Likewise, the nisin-like bacteriocin produced by *L. lactis* A164, which was isolated from Korean traditional fermented vegetables, was active against closely related LAB and some food borne pathogens (Choi *et al.* 2000).

1.2.2 *L. lactis* as a new potential probiotic

Probiotics are defined as living microorganisms that, when administered in adequate amounts, confer a health benefit on the host (according to WHO - the World Health Organization - and FAO - the Food and Agriculture Organization of the United States). Some criteria have been defined to select a probiotic strain, including its tolerance to the hostile conditions of the stomach and the small intestine, i.e. low pH and bile salts, and its ability to adhere to intestinal surfaces (Morelli 2000). Most of the probiotics belong to LAB and exert their beneficial effects within the gastrointestinal tract (Holzapfel *et al.* 1998). Possible mechanisms involved are the following: (i) balancing the gut ecology (e.g., reducing harmful microorganisms); (ii) protecting the underlying epithelial cells; (iii) stimulating the body immune response (Vanderpool *et al.* 2008). Reported beneficial effects of probiotics on host health include the treatment/prevention of some diseases like lactose intolerance (Vasiljevic and Shah 2008), diarrhea, *H. pylori* infection (Khulusi *et al.* 1995, Felley *et al.* 2001, Linsalata *et al.* 2004), Inflammatory Bowel Disease (IBD) (Gionchetti *et al.* 2000, Guandalini 2002), mutagenicity and carcinogenicity (Hirayama and Rafter 2000, Lo *et al.* 2004).

The patented probiotic strain *L. lactis* L1A, which is present in Scandinavian fermented milk, has been shown to have a positive effect on the immune and digestive system. Intake of this probiotic could decrease chronic bowel discomfort following radiotherapy (Henriksson *et al.*

1995). Another probiotic strain is *L. lactis* CV56, isolated from vaginal secretions of healthy women and which has been completely sequenced (Gao *et al.* 2011). CV56 was found to exhibit strong antimicrobial activity by producing nisin A, as well as a greater adhesion ability to vaginal epithelial cells than that of other *Lactococcus* strains such as *L. lactis* MG1363. It also contains the genes encoding the riboflavin (vitamin B2) biosynthesis (Capozzi *et al.* 2012).

Moreover, other studies investigated the potential use of *L. lactis* as a probiotic. The tolerance to harsh conditions within the gastrointestinal tract was tested for different strains (Kimoto *et al.* 1999). The strains *L. lactis* NIAI 527 and *L. lactis* biovar diacetylactis N7, which are originally from the Japanese National Institute of Animal Industry, exhibited a good ability to tolerate contact with a low-pH juice (pH 2.5), followed by exposure to bile salts at concentrations as high as 0.5 - 0.9% for 30 minutes. A high *in vitro* adhesion to Caco-2 cells was also observed for the NIAI 527 strain. Furthermore, the strain *L. lactis* HV219, isolated from human vaginal secretions, was shown to display adaptation properties, i.e. resistance to hostile conditions within the intestinal tract, adhesion capacity to Caco-2 cells and secretion of the bacteriocin HV219 (Todorov *et al.* 2007). In addition, using a macrophage-like cell line, Kimoto *et al.* (2004) (Kimoto *et al.* 2004) demonstrated that the strain *L. lactis* subsp. *lactis* G50 was able to induce a high level of cytokines IL-12, IL-6 and TNF-α. Accordingly, using the same kind of cell line, Suzuki *et al.* (2008) investigated the probiotic immunomodulatory activity of 46 different *L. lactis* strains through their capacity to induce production of the same panel of cytokines (IL-6, IL-12 and TNF-α). The extent of induction of IL-6, IL-12 and TNF-α was strain-specific and was not related to subspecies, biovariety or the source of the isolates. All these findings converge on the probiotic potential of *L. lactis*, even though it is undoubtedly strain-specific.

1.2.3 *L. lactis* as a delivery vector for therapeutic molecules

The use of *L. lactis* in biomedical applications, as a delivery vector for therapeutic proteins, DNA and vaccine antigens, is a fast-evolving area of interest. During the two past decades, approximately 20 new articles have been published each year (LeBlanc *et al.* 2013), and have depicted novel strategies, notably for the treatment of human gut diseases (Nouaille *et al.* 2003). For instance, interleukin IL10-producing *L. lactis* (Steidler *et al.* 2003, Braat *et al.*

2006) and, more recently, Elafin-producing *L. lactis* (Motta *et al.* 2012) have provided significant effects against intestinal inflammation. In addition, the use of *L. lactis* as a delivery vehicle at the mucosal level was reported for DNA (Guimaraes *et al.* 2006, de Azevedo *et al.* 2010) or virucide against HIV-1 (Pusch *et al.* 2005). The example of live lactococci for the treatment of human papilloma virus type 16 (HPV-16) infection was also depicted (Bermudez-Humaran *et al.* 2005).

As mentioned above, adhesion to intestinal surfaces may be viewed as an important property for the selection of probiotics. The intestinal epithelium is separated from the lumen by the mucus layer. Understanding the structural and functional properties of mucus has gained interest during the past decade. In the next section, we will present the most important findings on this “key” interface within the gastrointestinal tract.

2. Gastrointestinal mucus

2.1 Components, organization and functions

Mucus, which lines the gastrointestinal (GI) tract, is directly exposed to a potentially noxious environment and constitutes a protective barrier for the underlying epithelial cells. The mucus layer serves as a selective barrier that prevents from the translocation of toxins, viruses (e.g. herpes simplex virus) (Olmsted *et al.* 2001, Lai *et al.* 2010) and pathogens (Johansson *et al.* 2008), while allowing gases, ions and nutrients to diffuse (Powell 1987, McLaughlin 2002).

Generally, mucus contains water (90 – 98% w/v), mucins and other components such as salts, lipids, DNA, IgA, defensins. The concentration of mucins, as obtained from the scrapping of pig mucosal surfaces, reaches ~5% (w/v) in stomach/duodenum, ~ 2% (w/v) in small intestine and ~3% (w/v) in colon (Allen 1989). Mucus is also a dynamic layer, which is continuously secreted and transported. Nearly 10 L of mucus are secreted into the GI tract each day with a flow rate of 1-100 µL/s (Cone 2009). Most of the secreted mucus is then digested and shed in feces. Mucus turnover is balanced by continuous secretion outwards and mechanical erosion that flushes away the external layer containing potentially harmful material (pathogens, drugs, etc.).

Mucins are one of the most important components of mucus. They are extracellular and large glycoproteins. At least 19 human mucin (MUC) genes have been distinguished, cloned and partially sequenced – MUC1, MUC2, MUC3A, MUC3B, MUC4, MUC5A, MUC5B, MUC6, MUC7, MUC8, MUC12, MUC13, MUC15, MUC16, MUC17 and MUC20, and homologues to many of them have been identified in rodent models (Perez-Vilar and Hill 1999). Mucins can be classified as either secreted or membrane-bound. The secreted mucins confer to mucus its gel-forming properties due to the highly glycosylated regions (see below).

The mucin monomers consist of ~ 80% carbohydrates and the remaining 20% is the protein core, which is arranged into distinct regions. Mucin glycoproteins experience high-frequency domains composed of Pro, Thr and Ser amino acids residues (PTS domains). These domains are often made up by repetitive sequences ordered in tandem and thus referred to as tandem repeats. Flanking the PTS domains are regions that are cysteine-rich (nearly 10%), giving rise to hydrophobic patches (Turner *et al.* 1999). The PTS domains become highly *O*-

glycosylated within the Golgi apparatus. Once decorated with glycans, the PTS domains form "mucin domains" that have a long and extended rod configuration, like a "bottle brush". Glycans are composed of 5-15 monomers, including N-acetylgalactosamine (GalNAc), N-acetylglucosamine (GlcNAc), fucose (Fuc), galactose (Gal), and sialic acid or N-acetylneuraminic acid (Neu5Ac) and sulfate residues (Meyer and Silberberg 1979). The mucin *O*-glycan chain is initiated by a GalNAc attachment to Ser or Thr residues and consists of three regions, named the core, the backbone and the peripheral region.

Pig gastric mucin (PGM) has been widely used for investigating the properties of mucus, such as its rheological behavior (Allen 1989, Celli *et al.* 2005, Celli *et al.* 2007). This will be detailed in the section 2.2. In terms of composition, Nordman *et al.* (Nordman *et al.* 1997) showed that PGM contains a number of different mucin populations varying in buoyant density, size, "acidity", glycosylation, sulphation and tissue origin. Furthermore, the analysis of glycan composition showed the prevalence of LacNAc-based O-glycans partially fucosylated in α1,2 on Gal residues and sulfated in 1,6 position of GlcNAc residues (Karlsson *et al.* 1997, Tsubokawa *et al.* 2007). A schematic representation of PGM is shown in **Figure I.1.**

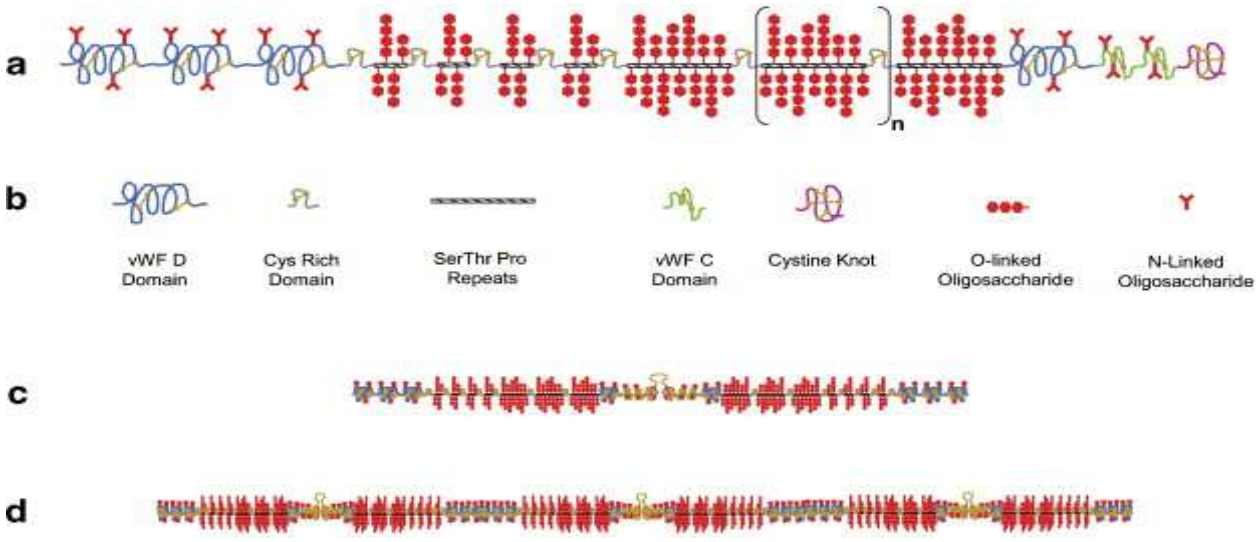

Figure I.1. A schematic drawing of the PGM monomer (a); its elementary components (b); PGM dimer (c) and PGM polymer (d) (Bansil and Turner 2006).

The structure and spatial organization of the mucus layer are different according to the intestinal region under study. In the colon, mucus is divided in two distinct physical layers (**Figure I.2**): (i) an inner layer which is firmly adhering to the epithelial cells and approximately 50-µm thick and (ii) an outer, loose layer which is approximately 100-µm

thickness, as measured in rodent models (Johansson *et al.* 2011). These mucus layers are organized around the highly glycosylated MUC2 mucin, that is secreted by the goblet cells. The inner mucus layer is dense and does not allow bacteria to penetrate, thus keeping the epithelial cell surface devoid of bacteria (Johansson *et al.* 2008). The inner mucus layer is converted into the outer layer, which is the preferential habitat of the gut commensal bacteria. It can be speculated that bacteria contribute to dissolving the outer loose mucus since germ-free mice exhibit a thicker layer than that of conventional rodents (Johansson *et al.* 2011). Furthermore, the outer mucus layer has an expanded volume, due to proteolytic activities provided by the host but also probably by commensal bacteria. The numerous *O*-glycans on the MUC2 mucin not only serve as nutritive substrates for bacteria but also as adhesion sites, thus contributing in this way to the selection of the species-specific microbiota (Juge 2012).

As in the colon, the stomach has relatively well-defined mucus layers made up by the major mucins MUC5AC and MUC6 (McGuckin *et al.* 2011) (**Figure I.2**). In the small intestine, in contrast with the stomach and the colon, the mucus layer is rather discontinuous (**Figure I.2**). Mucus is secreted at the top of the crypts and then moves upward between the villi. Therefore, the tips of the villi are not systematically covered with mucus (Johansson *et al.* 2011). The main secreted mucin is MUC2, as in the colon.

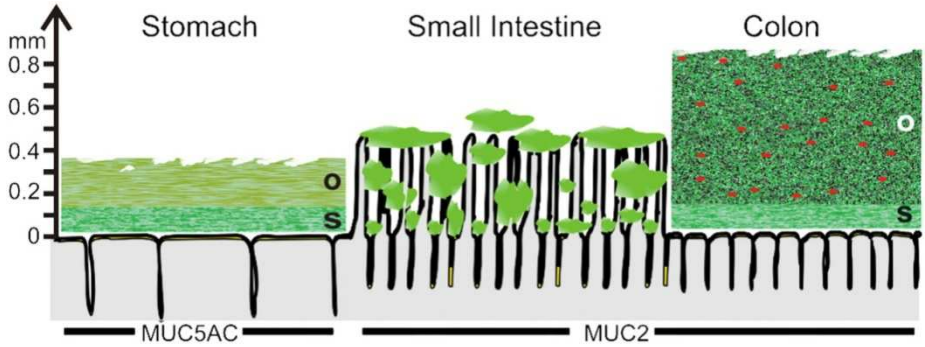

Figure I.2. Schematic representation of the mucus layer(s) along the gut (Johansson *et al.* 2011). Note that the thicknesses given are derived from data on rat and adapted from the work of Atuma *et al.* (Atuma *et al.* 2001). The symbols in red are representative of the bacteria trapped inside the outer mucus layer. The name of the gel-forming mucins in each intestinal region is indicated. **O** stands for "outer loose mucus layer" and **S** for "inner and firmly attached mucus layer".

Analysis of the *O*-glycan structures associated with Muc2 in small and large intestines of rats showed that the large intestine was enriched for sulphated residues whereas the small

intestine was enriched in sialylated residues (Karlsson *et al.* 1997). This region-specific glycosylation was also found in humans with a decreasing gradient of fucose from ileum to rectum and an increased gradient of sialic acid (Robbe *et al.* 2003). This acidic gradient was shown to be acquired after birth, perhaps due to bacterial colonization or initiation of digestive and absorptive functions within the gut (Robbe-Masselot *et al.* 2009).

Concerning the relationship between mucus and intestinal diseases, numerous studies described the role of alterations in the structure and/or quantity of mucins in initiating and maintaining mucosal inflammation in IBD and in driving cancer development in the intestine, as recently reviewed (Kim and Ho 2010, Sheng *et al.* 2012). Reduction in MUC2 synthesis and/or goblet cell number, resulting in a barrier defect, was shown to be involved in the onset or development of IBD. For instance, patients with ulcerative colitis (UC) were first characterized by depletion of goblet cells in the colonic epithelium (Theodossi *et al.* 1994). More recent studies in mouse models of colitis highlighted the importance of mucins in maintaining integrity of the protective mucus barrier, the breakdown of which could result in colitis. Indeed, Muc2-deficient mice, with no morphologically identifiable goblet cells and absence of Muc2 expression in the intestine, were reported to display markedly deficient mucus layers with increased permeability and enhanced bacterial adhesion to the mucosal cell surface. Moreover, these mice developed spontaneous colitis and were more susceptible to dextran sulfate sodium-induced colitis (Van der Sluis *et al.* 2006). Later, Johansson *et al.* (Johansson *et al.* 2013) reported that mucus secreted from human sigmoid colon was normally dense and thick whereas that in patients with active UC was thinner and more penetrable to 2-µm sized fluorescent beads and bacteria.

2.2 Rheological properties of GI mucus

In order to understand how LAB evolve within the mucus, rheology needs to be scrutinized, i.e. mucus flow behavior law has to be characterized. From a general point of view, mucus is a viscoelastic pH-dependent gel with functional consequences (Cao *et al.* 1999, Celli *et al.* 2007, Celli *et al.* 2009). For instance, Celli *et al.* (2009) reported that the pathogen *H. pylori* utilizes such properties to reach the stomach epithelium. To manage so, bacteria secrete urease that elevates the pH of their microenvironment, resulting in a transition gel-sol. This is a striking evidence of the interplay between biochemical and mechanical interactions that

must not be ignored. In line with these results, Celli *et al.* (2007) demonstrated a sol-gel transition of PGM with a solid-like viscoelastic behavior below pH 4 and liquid-like above. This is probably due to the neutralization of some amino acid residues with pKa values of ~4, Glu and Asp, which facilitates the cross-linking among macromolecules through hydrophobic interactions (Lee *et al.* 2005). Furthermore, the presence of monovalent cations, such as K^+ and Na^+, impacts mucin rheology (Martin *et al.* 1978, Celli *et al.* 2007). For instance, Celli *et al.* (2007) reported that PGM exhibits a gel structure at a NaCl concentration of 100 mM but evolves toward a liquid-like behavior for a higher concentration of 200 mM. This can be explained by the decrease in electrostatic interactions within the mucin network. Likewise, other substances are capable of interacting with mucins, including (phospho)lipids, albumin (Martin *et al.* 1978). In addition, the mechanical properties of mucus can be significantly altered by proteolytic enzymes, e.g. pepsin (Allen *et al.* 1984), or by reduction of disulfide bridges with mercaptoethanol, dithiothreitol or N-acetylcysteine (Allen 1989).

Mucus is a non-Newtonian shear-thinning fluid (Allen 1989, Zhou *et al.* 2004, Celli *et al.* 2007), i.e. its viscosity decreases with increasing shear rate (**Figure I.3**). **Figure I.3** also shows that mucus from different sources, such as pig stomach, small intestine, colon; human lung, sputum and cervix; bovine cervix; and rat epididymis (Cone 2005), share a common behavior modeled by a power law.

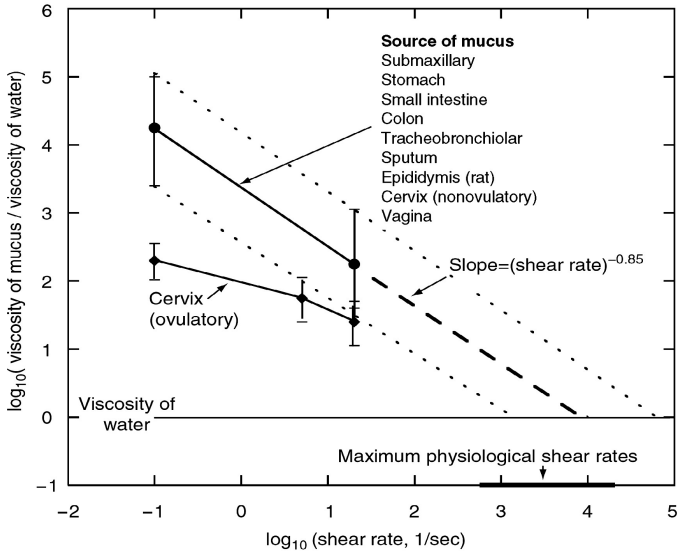

Figure I.3. Flow curve (apparent viscosity (Pa.s) vs. shear rate (s^{-1})). The data summarized are derived from many different mucosal sites (Cone 2005). The apparent viscosity of these

various sources of mucus is rather comparable and follows a power law, reaching the viscosity of water at high physiological shear rates.

Studies of PGM secretions obtained by gentle scrapping of pig stomach showed a greater elastic modulus G' (or storage modulus) than its viscous modulus G" (or loss modulus) throughout the frequency range studied (10^{-2} to 10^{2} rad/s) (Allen *et al.* 1984). Delgado-Reyes *et al.* (Delgado-Reyes *et al.* 2013) studied the viscoelasticity of two types of commercial PGM (Sigma-Aldrich), type II and type III referred to as non-purified and purified, respectively. Flow curves were described by the shear-thinning Ostwald de Waele model that solely takes into account the flow behavior index (*n*), and the consistency coefficient (*K)* as free fitting parameters in the form $\eta_{app} = K\dot{\gamma}^{n-1}$, as it is the case in **Figure I.3**. Rheological properties of PGM were function of its concentration and varied with the types of PGM. At a shear rate of 100 s^{-1}, non-purified mucin preparations showed a lower apparent viscosity (0.22–8.37 Pa.s) than that of purified ones (0.43–29.29 Pa.s). At a PGM concentration of 10% (w/v), the gel was a viscoelastic liquid (G">G') whereas at a higher concentration (40% (w/v)), it rather exhibited viscoelastic solid properties (G'>G"). The latter showed remarkable recovery during the creep compliance tests. Using atomic force microscopy, the topography of non-purified PGM was rough and regular whereas purified PGM presented a smoother, granular and inhomogeneous surface (Delgado-Reyes *et al.* 2013).

Furthermore, these two types of PGM commercial products have been widely used as a model mucus system, for (i) muco-adhesion assays (Rojas *et al.* 2002, Tian *et al.* 2005, Dague *et al.* 2010), (ii) investigation of mucin composition and properties (Zenteno *et al.* 1995, Corfield 2000, Dawson *et al.* 2004, Le *et al.* 2011) or (ii) isolation of gut-associated LAB (Kraatz 2011). Apart from the simplicity of use (easy preparation, reproducibility, long-term stability) and reduced costs, reasons for employing such lyophilized mucins are primarily linked to the difficulties in collecting native human or animal mucins and guaranteeing stability (i.e. effect of age, healthy status and diet, etc.). However, Kocevar-Nared *et al.* (1997) reported a difference between the natural PGM, i.e. scraped from pig stomach and purified, and the commercial type II and type III PGM products. Asides with others (Madsen *et al.* 1996, Kocevar-Nared *et al.* 1997), Celli *et al.* (Celli *et al.* 2005, Celli *et al.* 2007) concluded that commercial PGM could not resemble the natural PGM. Nevertheless, we will show in ***Chapter III*** that those conclusions are rather swift and

commercial PGM, in addition to be easily prepared, follows the rheological behavior required.

In order to decipher the selective and filtering properties of the mucin network, many tools are currently used to connect the rheological properties with the microstructure, that both affect the migration of particles or bacteria such as pathogens, as presented for *H. pylori* (Celli *et al.* 2009). Worth mentioning is the **Multi-Particle Tracking (MPT)**, used in this study and explained in details below.

2.3 Mucus microrheology and microstructure

2.3.1 Introduction of MPT technique

This technique consists of tracking the position of tracers over time. Tracers are beads, typically 200-500 nm in diameter (*a*) and termed here as nanoparticles (NPs). At the microscale level, matter is subjected to thermal agitation described by the Brownian motion. Particles are bombarded by atoms and induce stochastic displacement of them. Technically, particles suspended in a fluid are simply visualized under microscope using a high-resolution charge-coupled device (CCD) camera (**Figure I.4**). In crowded environment, the tendency is to use fluorescent particles to discriminate the probe with the fluid and this is commonly observed *via* epifluorescence. The exciting light could affect the motion by exerting an optical force but it remains small (<5%) compared to the thermally driven force of the beads (Gardel *et al.* 2005).

MPT has unique advantages: (i) MPT can directly measure the mechanical properties of specialized medium, such as cytoplasm (Wirtz 2009), because of the intimate contact between probing beads and material microstructure; (ii) MPT requires short times of data collection, typically 10-20s, to track mobility of tens to hundreds of embedded NPs at the same time and to obtain statistically significant data; (iii) the spatial resolution of detecting nanoparticle centers typically ranges from 3 nm to 10 nm (Wirtz 2009), allowing the investigation of the microstructure as well as the heterogeneous degree of soft matter.

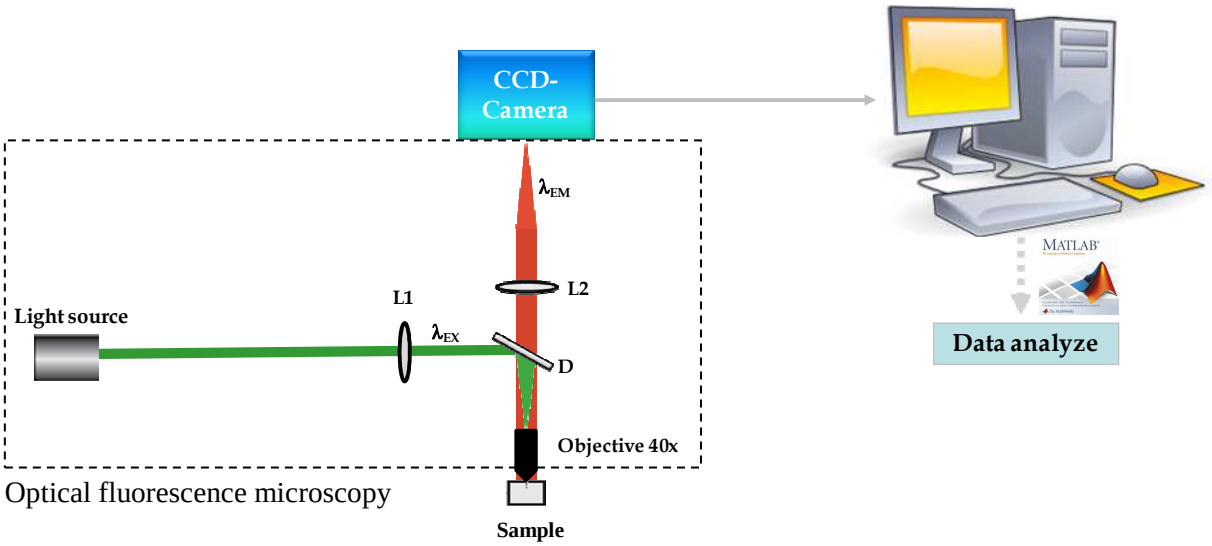

Figure I.4. An example of MPT set-up is composed of an optical fluorescence microscopy with a light source; an excitation filter **L1**, allowing the transfer of the short-wavelength light; an emission filter **L2**, allowing the transfer of the long-wavelength light; a dichroic beam splitter **D**; and a charge-coupled device (CDD) camera.

The important definitions in MPT method are time scale, mean-square displacement and mode of transport.

(i) ***Time scale.*** The shortest time scale achievable for a given experimental set-up is determined by the maximum speed of the camera and the necessary acquisition hardware. Assuming a camera is able to capture images at video rate 30 frames per second (fps), the shortest time scale is 33 ms. The longest time scale depends on the length of the movie. In gels or porous networks with small mesh sizes, NPs may undergo subdiffusive transport at short time scale, however at longer time scale nanoparticle mobility may be more diffusive due to the relaxation time of polymer gel structures (Suh *et al.* 2005).

(ii) ***Mean-square displacement (MSD).*** MSD $\left\langle \Delta r^2(\tau) \right\rangle$ describes the NP mobility in a material over time, and is given by:

$$\begin{aligned} \left[r(\Delta t+\tau) - r(\Delta t) \right]^2 &= \left[x(\Delta t+\tau) - x(\Delta t) \right]^2 + \left[y(\Delta t+\tau) - y(\Delta t) \right]^2 \\ \left\langle \Delta r^2(\tau) \right\rangle &= \frac{1}{N} \sum_{i=0}^{N} \left[r(i\Delta t+\tau) - r(i\Delta t) \right]^2 = 2nDt \end{aligned} \qquad \text{(I.1)}$$

t is time elapsed (s), τ the time lag, *D* is diffusion coefficient and n the dimensionality. In 2D, n=2.

The embedded NPs are smaller than 1 µm so that they undergo Brownian motion, while gravity or convections are negligible. If active transport is also negligible, only two types of forces act on the NPs inside viscous liquids: (i) the thermal energy k_BT and the movements of the local structure of the material; (ii) the counteracting frictional force $\xi = 6\pi\eta a$ which results from the movement of NPs driven by the thermal energy. In this case of Brownian motion, the diffusion coefficient (independent of time scale) *D* is also measured by the Stokes-Einstein relation:

$$D = \frac{k_B T}{3\pi\eta a} \tag{I.2}$$

where k_B is Boltzmann constant 1.38×10^{-23} $m^2.kg.s^{-2}.K^{-1}$, T is temperature (^oK), η is water viscosity ($9.03\ 10^{-4}$ Pa.s), *a* is size of the spherical NPs in diameter (m).

(iii) ***Mode of transport.*** Active and subdiffusive transport of NPs can be described by:

$$\left\langle \Delta r^2(\tau) \right\rangle = 2nDt^{\alpha} \tag{I.3}$$

α is the anomalous exponent. For the motion of actively transported (also called "super-diffusive") NPs, which is due to the relaxation of polymer gels, convection or gravity in systems, α equals to more than 1. In contrast, the subdiffusive transport α equals to less than 1, which describes motion impeded by obstacles or by NP binding to physical structures in the environment. NPs are classified as immobile transports when their movements are smaller than spatial resolution, i.e. their diffusion coefficients are lower than that of the same NPs attached to glass slides. Moreover, MPT allows determining the degree of heterogeneity of particle diffusion inside mucus gels by the relative width of the diffusion coefficient distribution (Lieleg *et al.* 2010):

$$\sigma_{rel} = \frac{\sigma}{\overline{D}} \tag{I.4}$$

σ is the standard deviation and $\overline{D}$ is the mean value of diffusion coefficients. This assumes that the distribution is normal. It will be seen later (***Chapter III***) that it tends to lognormal.

2.3.2 Microrheological characterization

In addition to determine the diffusion coefficient and the anomaly of diffusion, MSD obtained by using MPT can help quantifying the dynamic rheological moduli of the microenvironment of a tracer embedded in fluid, and to some extent in complex media.

In this review, two passive microrheology methods are distinguished (Levine and Lubensky 2000): one-point and two-point rheology. The first uses MSD of an individual particle, i.e. the autocorrelation of the motion of beads, and the second assumes that the motion of one tracer affects its neighbor. Therefore, two-point microrheology makes use of the cross-correlation of two beads introducing a new variable, the bead separation *r*.

a. One-point microrheology – conventional way

From Eq. (I.2) the viscosity of the material can be estimated by:

$$\eta = \frac{4k_B T}{3\pi a} \frac{t}{\left\langle \Delta r^2(\tau) \right\rangle}, \tag{I.5}$$

In the case of purely viscous material, MSD follows the thermal limit giving rise constant viscosity that solely depends to temperature.

In the case of complex media, the time-dependent MSD of the NPs can be transformed into the frequency-dependent viscoelastic moduli $G^*(\omega)$ (Mason and Weitz 1995, Gittes *et al.* 1997) *via* the Laplace transform inversion method:

$$\tilde{r}^2(s) = \frac{2k_B T}{\pi s a \tilde{G}(s)}, \tag{I.6}$$

where $\tilde{r}^2(s)$ is the Laplace transform of the tracer's MSD, as function of Laplace frequency *s*, *a* their diameter and $\tilde{G}(s)$ the Laplace transform of the complex modulus G*=G"+iG'. Equation (I.6) is the Stokes-Einstein equation generalized (GSER) form of a frequency-dependent viscosity (Mason and Weitz 1995). Another inversion method consists of approximating the Fourier transform *via* an analytic continuation that handles noise arising for the Fourier transform (Mason 2000). MSD plot is fitted to a local power law and the logarithmic differential is then calculated:

$$\alpha(\tau) = \frac{d \ln \left\langle \Delta r^2(\tau) \right\rangle}{d \ln \tau}, \tag{I.7}$$

This parameter, which is the anomalous exponent described above, is used in an algebraic form of the GSER:

$$G(\omega) \approx \left. \frac{4k_B T}{3\pi a \left\langle \Delta r^2(\tau) \right\rangle \Gamma\left(1+\alpha(\tau)\right)} \right|_{\tau=1/\omega}, \tag{I.8}$$

where $\Gamma(x) = (x-1)!$ is the gamma function. Defining $\delta(\omega)$ the phase angle as:

$$\delta(\omega) = \frac{\pi}{2} \frac{d \ln \left| G^*(\omega) \right|}{d \ln \omega}, \tag{I.9}$$

The storage G' and loss G'' moduli with respect to frequency ω can be obtained:

$$\begin{aligned} G'(\omega) &= \left| G^*(\omega) \right| \cos\left(\delta(\omega)\right), \\ G''(\omega) &= \left| G^*(\omega) \right| \sin\left(\delta(\omega)\right). \end{aligned} \tag{I.10}$$

b. Two-point microrheology

This method correlates the motion of two tracers separated by the distance *r*. It was developed to connect the microscale with the macroscopic methods that usually exhibit several orders of magnitude discrepancies (Crocker *et al.* 2000). Limitations of Eqs. (I.6) and (I.8) from GSER arise in majority from the inhomogeneity of the medium. Since one particle strain field will affect a second, it is therefore possible to measure the strain field by cross correlating two-particle motions. In the homogenous case, the strain field is proportional to the tracer motion and decays ~ *a/r*.

Recent experiments have probed such correlated motion in viscous (Crocker 1997) and elastic (Bausch *et al.* 1999) materials. MPT enables to measure the vector displacements of the beads $\Delta r_\alpha(t,\tau) = r_\alpha(t+\tau) - r_\alpha(t)$ where t is the absolute time and τ the lag time as aforementioned. The ensemble averaged tensor product of the tracer displacements yields:

$$D_{\alpha\beta}(t,\tau) = \left\langle \Delta r_\alpha^i(t,\tau) \Delta r_\beta^j(t,\tau) \delta\left[r - R^{ij}(t) \right] \right\rangle_{i \neq j, t}, \tag{I.11}$$

where *i* and *j* label different particles, α and β label different coordinates, and R^{ij} is the distance between particles *i* and *j*. The average takes over the distinct terms ($i \neq j$) and the self-terms are $\left\langle \Delta r^2(\tau) \right\rangle \times \delta(r)$. As described by (Crocker *et al.* 2000), for an incompressible medium, the expected two-point correlation resulted in the product of the displacement given by Eq. (I.6) and the strain field of a point stress (Landau and Lifshitz 1986), in the limit $r \gg a$ gives rise to:

$$\begin{aligned} \tilde{D}_{rr}(r,s) &= \frac{k_B T}{2\pi r s \tilde{G}(s)}, \\ D_{\theta\theta} = D_{\phi\phi} &= \frac{1}{2} D_{rr}, \end{aligned} \tag{I.12}$$

where $\tilde{D}_{rr}(r,s)$ is the Laplace transform of $D_{rr}(r,\tau)$ and off-diagonal tensor neglected. Note that Eq. (I.12) does no longer depend on *a*, suggesting that $D_{\alpha\beta}(r,\tau)$ is independent of the tracer size or shape, still in the limit of $r \gg a$. Still reported by (Crocker *et al.* 2000), a distinct MSD can be introduced and defined as:

$$\left\langle \Delta r^2(\tau) \right\rangle_D = \frac{2r}{a} D_{rr}(r,\tau). \tag{I.13}$$

This quantity describes the thermal motion obtained by extrapolating the long-wavelength thermal undulations of the medium down the bead size. Under Stokes assumptions and in homogeneous medium $\left\langle \Delta r^2(\tau) \right\rangle_D = \left\langle \Delta r^2(\tau) \right\rangle$. Practically, $D_{rr} \sim 1/r$ indicates that the medium can be treated as (coarse-grained) homogeneous continuum over scales of typically 3-50 µm (Pelletier *et al.* 2009). The average value of $rDrr$ over that range is used to determine $\left\langle \Delta r^2(\tau) \right\rangle_D$ from Eq. (I.13). Finally, two-point complex modulus can be deduced by substituting $\left\langle \Delta r^2(\tau) \right\rangle_D$ into Eq.(I.6) or Eq.(I.8) in place of $\left\langle \Delta r^2(\tau) \right\rangle$.

Therefore, Crocker *et al.* (2000) have demonstrated that two-point microrheology agrees with bulk rheology and since it is not dependent of shape or size, this technique opens up new doors for studying living cell rheology for example (Lau *et al.* 2003).

2.3.3 Microstructure of mucus

Wang *et al.*, (2011a) presented an obstruction-scaling model in order to estimate the size of pores between mucin fibers of cervicovaginal mucus. The model describes the ratio of diffusion in a gel and in water:

$$\frac{D_g}{D_w} = \exp\left(\left(-\frac{\pi}{4}\right)\left(\frac{a+r_f}{r_g+r_f}\right)^2\right), \qquad \text{(I.14)}$$

D_g is the diffusion coefficient of the probe NPs in the mucus gel, D_w is its diffusion coefficient in water, a is the NP radius, r_f is the gel fiber radius, and r_g is the effective radius of the gel pore. An r_f of 3.5 nm was used as the best estimate for the radius of individual mucin fiber (Wang *et al.* 2011). Mucin net pore can be estimated when NPs migrate freely through the mucin suspension. Free motion can be attainable when almost no interaction with the mucins occurs. Mucin network has been shown to act as a selective filtering wherein electrostatics prevails (Lieleg *et al.* 2009, Lieleg *et al.* 2010). Indeed, Lieleg *et al.* (2010) proposed two possible filtering strategies of mucin network: size filtering and interaction filtering. The first allows NPs (also valid for viruses or bacteria), with smaller dimensions compared to the mucin network pore, to migrate while larger particles are entangled. The latter is based on interactions between NPs and mucins, i.e. mucoadhesive NPs are trapped within mucus whereas non-mucoadhesive ones can pass through. To address the issue of reducing such interactions, carboxylate-modified NPs may be coated with amine-terminated polyethylene glycol (PEG) *via* carbodiimide reaction (Panorchan *et al.* 2004, Valentine *et al.* 2004, Lai *et al.* 2007). PEG is an aqueous-soluble, uncharged and hydrophilic polymer, which is routinely used in pharmaceutics. Coating NPs with PEG polymer minimizes electrostatic adhesive interactions between NPs and the mucin network (Lieleg *et al.* 2010).

So far, some studies have used the MPT technique, for instance, for investigating the human cervicovaginal mucus (CVM). Lai *et al.* (2010) found that herpes simplex virus (HSV) (180-nm diameter) was strongly trapped in CVM through adhesive interactions, with a motion at least 8,000-fold slower than that of the same-sized non-mucoadhesive PEG-coated NPs (200-nm diameter) (**Figure I.5**).

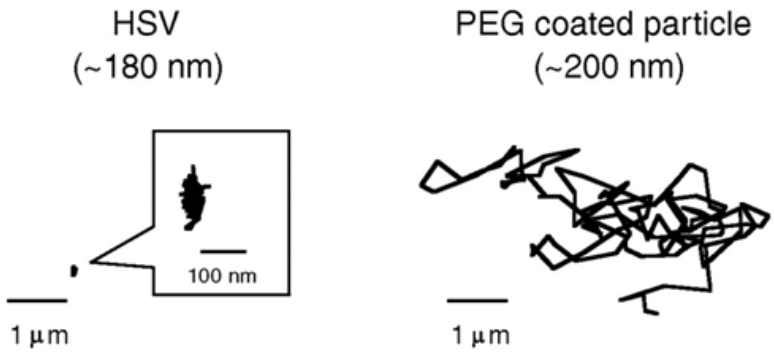

Figure I.5. Representative trajectories of 180-nm HSV and 200-nm PEG-coated particles in CVM (from Lai *et al.* 2010).

Furthermore, PEG-coated 100-, 200-, and 500-nm sized NPs exhibited a 6,000-, 600-, and 400-fold higher diffusion rate in CVM, respectively, than that of their uncoated (mucoadhesive) counterparts (Lai *et al.* 2010). On this basis, the CVM pore size was estimated at 340 ± 70 nm (Lai *et al.* 2010). Collectively, these results, together with those depicted by Lieleg *et al.* (2010) for the translocation of PEG-coated NPs within PGM gels, strongly suggest that muco-adhesion, rather than steric obstruction, is critically important for the migration of biological particles (e.g. viruses, bacteria) through mucus.

Complementary to MPT, other techniques have been implemented for investigating the microrheology and microstructure of mucus. For instance, using dynamic light scattering (DLS), Celli *et al.* (2005) found that PGM was a highly heterogeneous network with a pore size ranging from 400 to 650 nm (Celli *et al.* 2005). In another study, using fluorescent recovery after photobleaching (FRAP) and multiple image photography (MIP), Olmsted *et al.* (2001) indicated that capsid viruses, such as Norwalk virus (38-nm diameter) and human papilloma virus (HPV) (55-nm diameter), diffused as rapidly in CVM as they did in phosphate buffered saline (PBS). In contrast, the diffusion of HSV (180-nm diameter) in mucus was ~ 1000-fold reduced compared to the value obtained in PBS. The distribution of CVM mesh size was here estimated in the range 20 – 200 nm (Olmsted *et al.* 2001). Recently, Kirch *et al.* (2012) used Cryo-SEM imaging for investigating the pore size distribution in native respiratory mucus. The authors pointed out the strongly heterogeneous nature of the mucus polymer mesh: large pores were heterogeneously combined with very small pores. Pore sizes of mucus ranged between ∼100 nm and voids of several micrometers in diameter (**Figure I.6**).

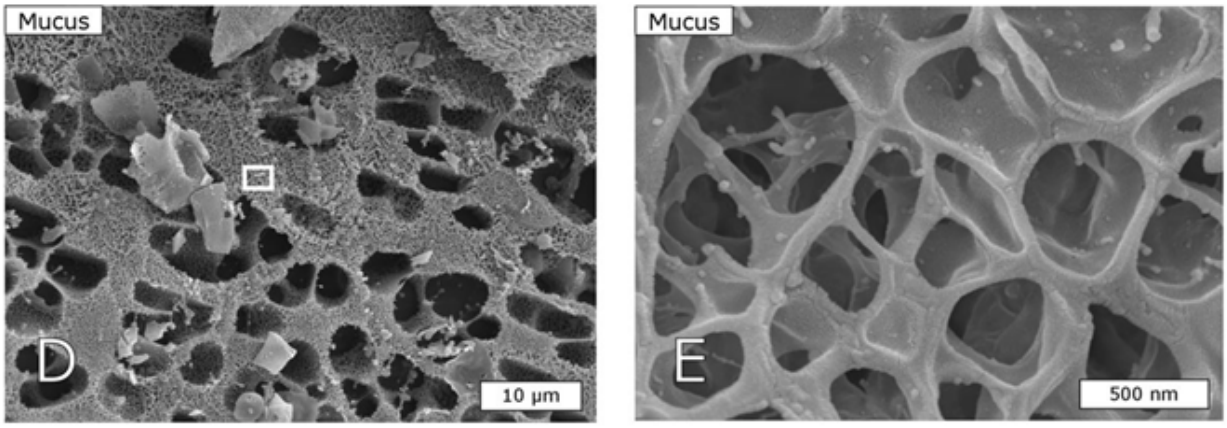

Figure I.6. Representative cryo-SEM images of mucus (*D* and *E*), showing the strongly heterogeneous nature of the mucus polymer mesh. Large as well as very small pores can be observed (Kirch *et al.* 2012).

In the following sections, adhesion of LAB, and especially *L. lactis*, to intestinal mucosa and mucus, will be discussed. A special attention will be paid to the cell surface determinants generally involved in adhesion and muco-adhesion.

3. Interactions between LAB and mucus

3.1 Determinants of the bacterial cell surface involved in adhesion and muco-adhesion

The role of numerous physico-chemical and biochemical factors, in particular the cell surface (composition, structure, conformation), has been depicted in terms of bacterial adhesion and adhesion to mucus. According to the classical approaches, i.e. DLVO theory (Derjaguin 1941, Verwey *et al.* 1999) and extended DLVO theory (Van Oss *et al.* 1986), the force of interaction between two entities (e.g. bacterial cell and solid surface) depends on physico-chemical parameters, such as surface-free energy and charge density. The corresponding interaction events (electrostatic, Lifshitz-van der Waals, Lewis acid/base) contribute to non-specific adhesion. However, the trend in current research is to consider specific interactions, like ligand/receptor bonding, between the bacterial cell wall and the surface, and to measure associated forces, as done with atomic force microscopy for probing the interactions between *L. lactis* and PGM (Dague *et al.* 2010, Le *et al.* 2011).

For *L. lactis* adhesion, and more generally for LAB, the cell wall determinants involved are notably **teichoic acids (TA), polysaccharides (PS) and surface proteins**.

3.1.1 Teichoic acids

The teichoic acid (TA) molecules, which were initially characterized in *L. plantarum* (Baddiley 1989), are divided into two categories: WTAs, which are covalently bound to *N*-acetylmuramic acid of peptidoglycan, and LTAs, which are anchored to the cell membrane *via* a diacylglycerol (Kleerebezem *et al.* 2010). Both types are decorated by D-alanine esters, in which the *dlt* gene encodes the proteins required for the incorporation of D-alanine esters into TA. Such molecules are important for acid tolerance, adhesion, biofilm formation, as well as the general defense against antimicrobial molecules because of their positively charged amino groups (Kleerebezem *et al.* 2010). LTAs are responsible for the cell surface hydrophobicity (Miorner *et al.* 1983) and charge (Mozes *et al.* 1988). In lactobacilli, LTAs may promote adhesive capacity to Caco-2 human intestinal cells, as observed with *L.*

johnsonii La1 (Granato *et al.* 1999). Walter *et al.* (2007) showed that D-Alanine ester depletion of TAs in *L. reuteri* 100-23 resulted in an impaired biofilm formation on the forestomach epithelium and a subsequent impaired colonization of the mouse gastrointestinal tract. The authors concluded that D-alanylation is an important cell function of *L. reuteri* that seems to protect this commensal organism against the hostile conditions prevailing in the murine forestomach. Further, Giaouris *et al.* (Giaouris *et al.* 2008) studied the relation between D-alanylation degree of TAs in lactococci, and more specifically *L. lactis* MG1363, and resistance to cationic antimicrobials (nisin, lysozyme), as well as adhesion to abiotic surfaces. An increase in the degree of D-alanylation of TAs resulted in a significant increase in *L. lactis* resistance toward nisin and lysozyme whereas the absence of D-alanylation led to a decreased resistance toward the same compounds. However, charge and hydrophobicity of *L. lactis* cell surface were not modified; consequently adhesion of *L. lactis* to polystyrene and glass remained the same.

3.1.2 Polysaccharides

Polysaccharides of Gram-positive bacteria (PS) are composed of various sugars, including rhamnose, glucose and glucosamine (Schleifer and Kilpper-Balz 1987). Polysaccharides can be divided into the following three major groups: capsular PS (CPS), which are in most cases covalently bound to peptidoglycan and form a thick outer layer; wall polysaccharides (WPS), which may be attached to the cell wall covalently or not; and extracellular polysaccharides (EPS), which may be released into the surrounding medium. In lactococci, the presence of EPS, which play an important role in fermented milk or for health benefits (Ruas-Madiedo *et al.* 2002), has been found in many *L. lactis* strains, such as *L. lactis* subsp. *cremoris* KH (Valyasevi *et al.* 1990), *L. lactis* subsp. *cremoris* SK110 and SK112 (Sijtsma *et al.* 1991), *L. lactis* subsp. *cremoris* SBT0495 (Nakajima *et al.* 1992), *L. lactis* subsp. *cremoris* LC330 (Marshall *et al.* 1995), five slime-forming *L. lactis* subsp. *cremoris* strains (ARH53, ARH74, ARH84, ARH87 and B30) isolated from Finnist fermented milk (Yang *et al.* 1999), *L. lactis* NIZO B40 and B891 (Kleerebezem *et al.* 1999, Looijesteijn *et al.* 2000), *L. lactis* HO2 (Forde and Fitzgerald 1999), *L. lactis* IL1403 (Bolotin *et al.* 2001), *L. lactis* NZ4010 (Looijesteijn *et al.* 2001), and *L. lactis* MG1363 (Chapot-Chartier *et al.* 2010). The nature

and role of PS on adhesive properties of LAB have been more particularly investigated for lactobacilli. For instance, Francius *et al.,* (2008) showed by single-molecule force spectroscopy (SMFS) with specific lectin tips that the cell surface of *L. rhamnosus* GG (LGG) wild-type cells contained two major types of cell wall-associated polysaccharides: the longest and most abundant polysaccharides are galactose-rich whereas shorter ones are glucose-rich. Later, Lebeer *et al.* (2009) identified a gene cluster that encodes the enzymes and regulatory and transporter proteins for the different steps in the biosynthesis of the extracellular polysaccharides of LGG. Subsequent mutation of the *welE* gene, encoding the priming glycosyltransferase within this cluster, and comparative phenotypic analyses of wild-type versus mutant strains confirmed the specific function of this gene cluster in the biosynthesis of high-molecular-weight, galactose-rich heteropolymeric PS molecules. Further characterization of the *welE* mutant showed that deprivation of these long, galactose-rich EPS molecules results in an increased adherence of LGG to commercial PGM and Caco-2 epithelial cells, as well as an increased biofilm formation. This was probably due to less shielding of adhesins such as fimbria-like structures, as revealed by TEM (Lebeer *et al.* 2012). For *L. lactis*, a chromosomally-encoded pellicle, designed as a novel thin compact PS, has been discovered in the MG1363 strain (Chapot-Chartier *et al.* 2010).

3.1.3 Surface proteins

In Gram-positive bacteria such as LAB, surface proteins constitute a diverse group of molecules with key functions, particularly the adherence and interaction with the host or the environment (Dramsi *et al.* 2005). Surface proteins can be associated to the cell wall by two basic mechanisms, cell wall sorting and targeting (Navarre and Schneewind 1999). In the first case, the surface proteins contain the C-terminal motif LPxTG recognized by the sortase enzyme (SrtA), which cleaves between the T and G residues, and covalently links the threonine carboxyl group to the amino groups of peptidoglycan (Marraffini *et al.* 2006). The product of the sortase action is a covalently anchored protein, which is incorporated into the envelope and displayed on the microbial surface. In the second case, cell-wall targeted proteins involve their non-covalent attachment to the cell surface *via* hydroxyl bonds or hydrophobic interactions. The group of targeted proteins includes muralytic enzymes such as autolysins, lysostaphin and phage lytic enzymes. In lactococci, three surface proteins have

been to date depicted as cell-wall located ones (Navarre and Schneewind 1999): the chromosomally-encoded sex factor aggregation protein CluA (Godon *et al.* 1994), the plasmid-encoded proteinase NisP (van der Meer *et al.* 1993) and the plasmid-encoded serine proteinase PrtP (Reid and Coolbear 1999). This protein, which catalyzes the hydrolysis of milk caseins, is involved in cell surface hydrophobicity and plays a positive role in adhesion of *L. lactis* to glass and tetrafluoroethylene (Habimana *et al.* 2007). In terms of LAB adhesion to mucus, cell surface proteins described to date are S-layer proteins, MUB (MUcus Binding) proteins and other proteins displaying specific functions.

(i) S-layers, which are regular paracrystalline surface protein arrays, are composed of single proteins or glycoprotein species that form the S-layer lattice by an intrinsic self-assembly process. Diverse functions have been proposed for S-layers, such as cell-protective coats, molecular sieves, molecule and ion traps, and cell adhesion mediators (Sleytr and Beveridge 1999). S-layers are exclusively found in some species of *Lactobacillus* (Von Kleist *et al.* 1975, Masuda and Kawata 1983, Yanisch-Perron *et al.* 1985). S-layer proteins were found to be able to bind to porcine small intestinal mucus and gastric mucin in *L. fermentum* 104R (Rojas *et al.* 2002), and to intestinal epithelial cells in *L. acidophilus* NCFM (Buck *et al.* 2005). However, we should note that these studies were based on the use of different chemical detergents (lithium chloride, guanidinium chloride) for the extraction or the removal of the S-layer proteins, thus probably affecting other proteins.

(ii) Mucus-binding proteins. As mentioned above, some cell surface proteins contain the C-terminal LPxTG anchor motif, recognized by the enzyme sortase (SrtA) which has the capacity to covalently attach the protein to the peptidoglycan. Majority of these proteins do not have to date an identified precise function, however certain proteins contain domains which are directly involved in binding to mucus: the MUB domains. These MUB domains vary in size, ranging from approximately 100 to more than 200 residues per domain. Indeed, by searching protein databases, Boekhorst *et al.* (2006) identified 48 proteins with at least one MUB domain in nine different lactic acid bacterial species. MUB-domain-containing proteins were most abundant in lactobacilli (**Figure I.7**) that are mainly found in the gastrointestinal tract, supporting the hypothesis that the domain is involved in adherence to intestinal mucus. For *L. lactis*, both for *L. lactis* subsp. *lactis* IL1403 and *L. lactis* subsp. *cremoris* SK11, only a single MUB-domain-containing protein was found, probably due to the fact, according to

the authors, that "domesticated" *L. lactis* strains live in a more restricted habitat than lactobacilli. However, we should note that only laboratory plasmid-free *L. lactis* strains were considered in this study. More recently, an *in silico* analysis of extracellular proteomes of lactobacilli revealed 47 proteins from six *Lactobacillus* genomes contained mucus-binding domains(s) (Kleerebezem *et al.* 2010), confirming that the MUB domain is a functional unit specific to LAB, that may fulfill an important function in host–microbe interactions.

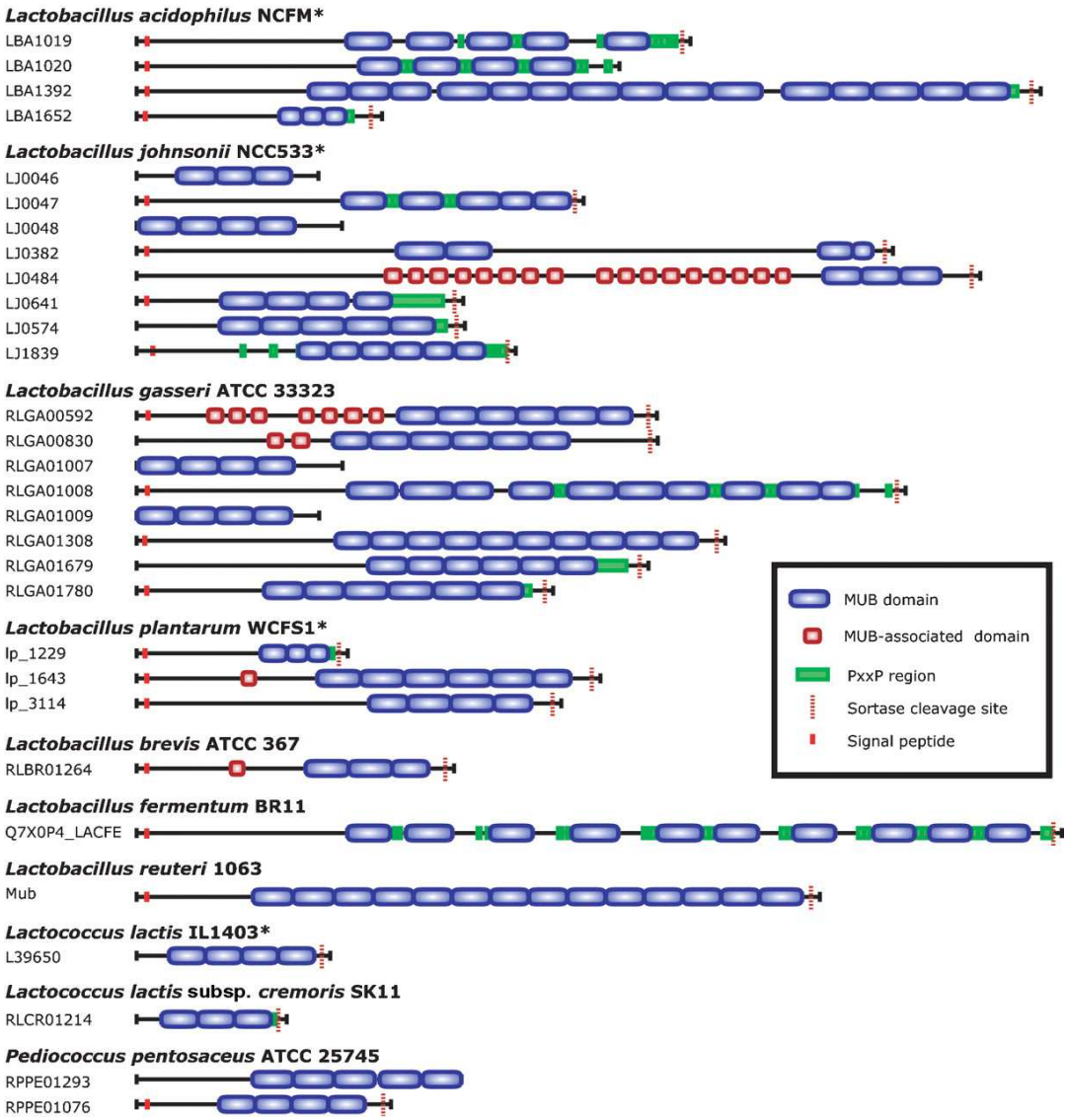

Figure I.7. A schematic overview of the 30 proteins with three or more MUB domains (Boekhorst *et al.* 2006). An asterisk indicates a species for which the complete genome sequence is available. MUB-associated domains were similar to domains with a known function or structure. The PxxP region separates the N-terminal part of the MUB domain from the rest of the domain. The C-terminal sortase recognition sites target the protein for

covalent attachment to the peptidoglycan layer. The N-terminal signal peptides target the protein for secretion.

(iii) Pili. Pili of Gram-positive bacteria, which are proteinaceous appendages of 1-10 nm in diameter and 2-3 µm in length, have been first characterized and well-documented in pathogens and were shown to be involved in cell adhesion and virulence (Telford *et al.* 2006). In the LAB *L. rhamnosus* GG (LGG), cell surface pili were more recently discovered and characterized (Kankainen *et al.* 2009, Lebeer *et al.* 2012). LGG bacterial cells contain multiple pili averaging 10-50 per cell and with lengths up to 1 µm (Kankainen *et al.* 2009). As shown in **Figure I.8**, LGG pili, found to be encoded by the spaCBA gene cluster, are composed of three pilin subunits: SpaA is the major pilin subunit forming the pilus shaft, SpaB an ancillary minor pilin subunit and SpaC a large-sized minor pilin subunit likely functioning as an adhesin (Kankainen *et al.* 2009). Note that, despite the presence of the *spaFED* genes in the genome, the SpaCBA pili appeared to be the only pili produced by LGG (Reunanen *et al.* 2012). According to the authors, the absence of SpaFED pili was likely resulting from the lack of appropriate environmental stimuli to activate the expression of the *spaFED* genes. However, it could not be excluded that the SpaFED pili are produced in the intestinal tract. Further, SpaC was shown to have a central role in adhesion as it is involved in binding to human mucus (Kankainen *et al.* 2009) and intestinal epithelial cells (Kankainen *et al.* 2009, Lebeer *et al.* 2012). This subunit was found to be not only localized at the pilus tip but also along the length of the pilus shaft, enabling bacteria to establish both long distance and intimate contact with host tissues (Reunanen *et al.* 2012). More recently, using single-molecule atomic force microscopy, Tripathi *et al.* (2013) investigated the biophysical properties of pili from LGG. The authors showed that SpaC formed homophilic trans-interactions engaged in bacterial aggregation and specifically bound mucin and collagen. LGG pili also exhibited two unique mechanical responses, that is, zipper-like adhesion involving multiple SpaC molecules distributed along the pilus length and nanospring properties enabling pili to resist high force (Tripathi *et al.* 2013).

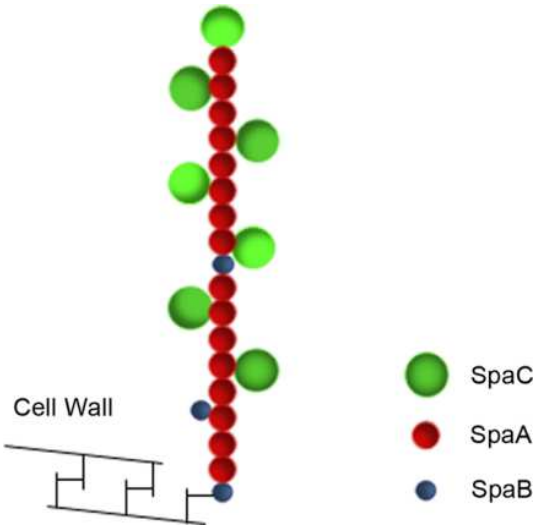

Figure I.8. Schematic model of *L. rhamnosus* GG SpaCBA pili (from Reunanen *et al.*, 2012). In the model proposed by the authors, the SpaCBA pili in LGG are composed of shaft-forming SpaA major pilins together with SpaB and SpaC as minor pilins. The SpaC adhesin can be found not only at the pilus tip but also throughout the pilus at a ratio with SpaA of approximately 1:2. The SpaB minor pilin is located at the pilus base, and few SpaB subunits can be found on the pilus fiber.

Concerning the pili biogenesis and function in lactococci, Dieye *et al.* (Dieye *et al.* 2010) first provided genetic and biochemical evidence that *L. lactis* owns a housekeeping sortase A able to anchor at least 5 LPxTG proteins to its cell wall. The presence of another putative sortase of class C, suggesting the presence of a pilus cluster in *L. lactis* genome, was revealed (Dieye *et al.* 2010). In a further work of the same group, Oxaran *et al.* (2012) confirmed that the genome of *L. lactis* strain IL1403 harbors a putative pilus biogenesis cluster consisting of a sortase C gene flanked by 3 LPxTG protein encoding genes (yhgD, yhgE, and yhhB), called pil. Pili were not detected under standard growth conditions. However, over-expression of the pil operon resulted in production and display of pili over the surface. Indeed, imaging with atomic force microscopy revealed the presence of filamentous structures on the bacterial cell surface that were frequently tangled, with several fibers wrapping around each other (**Figure I.9**). The fibers reached up to 3 µm in length and around 5 nm in width. Interestingly, these pili were only present at distinct foci on the bacterial surface and only part of the bacterial population seemed piliated (Oxaran *et al.* 2012).

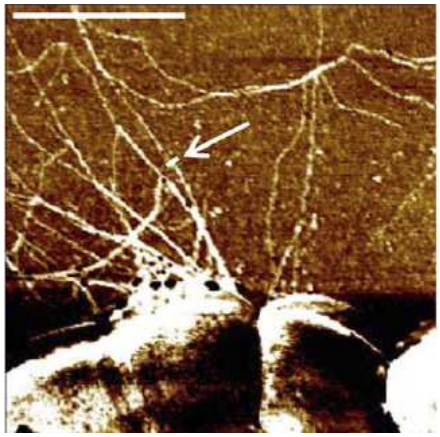

Figure I.9. Observation by AFM of lactococcal pili in *L. lactis* IL1403 over-expressing the *pil* operon (Oxaran *et al.* 2012). Pili were proteinaceous appendages of 1-10 nm in diameter. A white bar shown by an arrow indicated where the pilus diameter was measured. Scale bar: 1 µm.

Moreover, functional analysis of the pilus biogenesis machinery indicated that: (i) the pilus shaft was formed by oligomers of the YhgE pilin, (ii) the pilus cap was formed by the YhgD pilin and (iii) YhhB was the basal pilin allowing the tethering of the pilus fibers to the cell wall. Oligomerization of pilin subunits was catalyzed by sortase C while anchoring of pili to the cell wall was mediated by sortase A. In terms of specific phenotype, piliated *L. lactis* cells exhibited auto-aggregation in liquid cultures, which was attributed to the polymerization of the major pilin YhgE. In addition, the piliated lactococci formed thicker, more aerial biofilms compared to those produced by non-piliated bacteria (Oxaran *et al.* 2012). This phenotype was attributed to YhgE oligomers. Interestingly, in contrast to the model strain *L. lactis* IL1403, pili production was assessed under standard laboratory growth conditions for natural *L. lactis* isolates from clinical or vegetal environments (Oxaran *et al.* 2012). This pili-related specificity of *L. lactis* was exploited in our study and will be detailed in the next sections.

(iv) Other proteins. Some of cell surface proteins are multifunctional molecules with independent intracellular and extracellular functions. For instance, in *L. johnsonii* NCC533 (La1), apart its central role in protein synthesis in the cytoplasm (Granato *et al.* 2004), the elongation factor Tu (EF-Tu) was shown to be also localized at the cell surface and involved in binding to Caco-2 and HT29 intestinal epithelial cells, and mucins purified from HT29-MTX cells. Also, in this La1 strain, a heat shock protein from Hsp60 class (GroEL) was found to be present at the cell surface and display binding properties towards HT29 cells and

mucins obtained from HT29-MTX cells (Bergonzelli *et al.* 2006). Moreover, glyceraldehyde-3-phosphate dehydrogenase (GAPDH), isolated from the cell surface of *L. plantarum* LA318, was functionally characterized as binding to human colonic mucin (Kinoshita *et al.* 2008).

3.2 Adhesion of *L. lactis* to the intestinal mucosa and mucus: *in vitro* and *in vivo* approaches

Even though lactococci are not a frequent natural element of the intestinal microbiota, they were sporadically isolated from feces of many different groups of humans (Finegold *et al.* 1983). Certain strains were also shown to transit through the stomach and survive in the gut of rodents (Boguslawska *et al.* 2009). In particular, the fluorescent *L. lactis* WH-C1-GFP strain was able to adhere to the intestinal mucosa in mice (Wang *et al.* 2011) (**Figure I.10**).

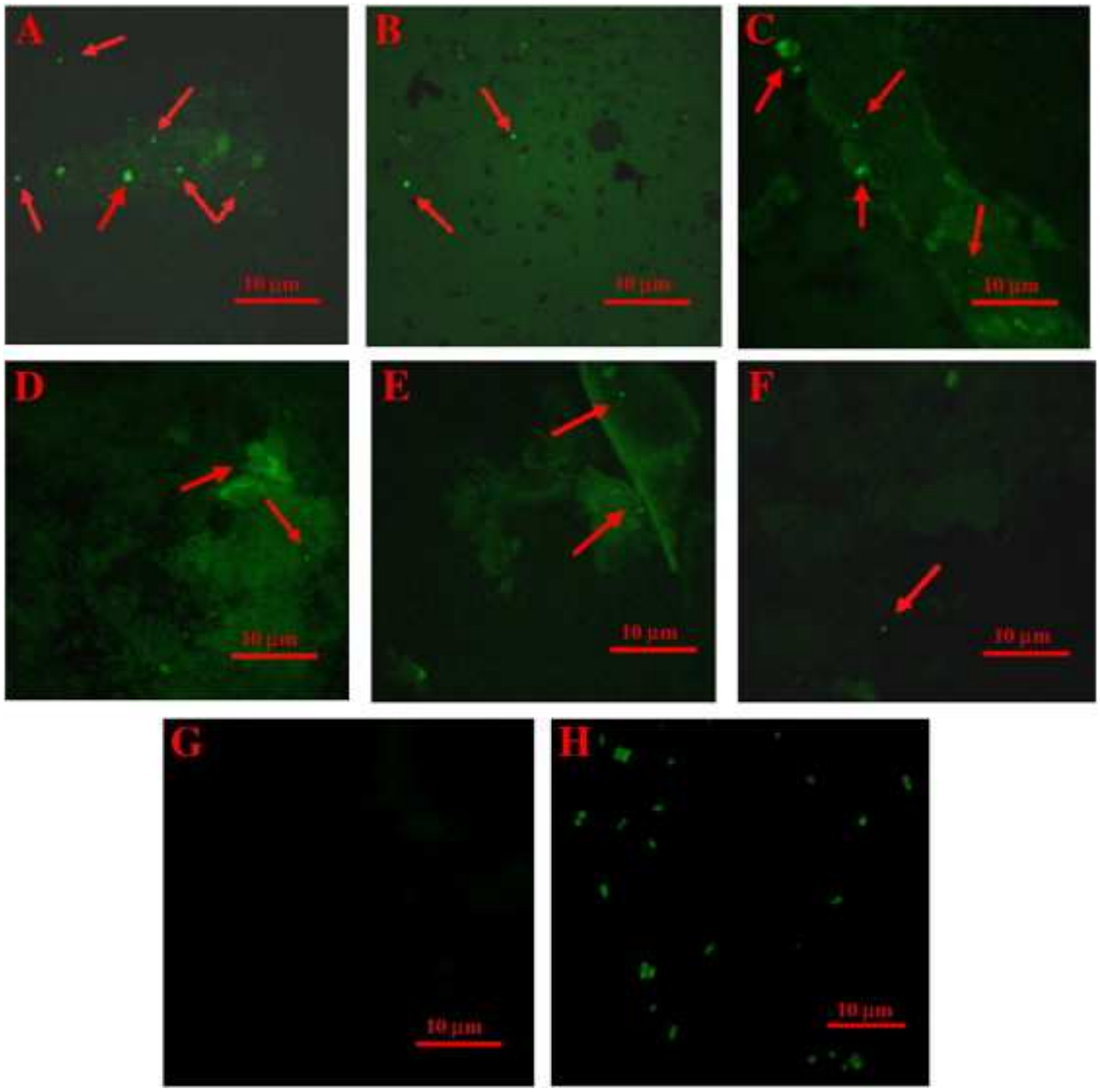

Figure I.10. Fluorescent detection of GFP-tagged *L. lactis* WH-C1 present in the contents of intestinal tissues and adhered to the intestinal mucosa. A to F: the inoculated group; G the non-inoculated group; H: cultured fluorescent *L. lactis* cells (Wang *et al.* 2011).

Recently, Lukic *et al.* (2012) assessed the adhesive properties of *L. lactis* subsp. *lactis* BGKP1, based on its strong auto-aggregation phenotype mediated by the AggL protein and the presence of the mucin binding protein (MbpL). *In vivo* and *in vitro* experiments revealed potentially different physiological roles of these two proteins in the process of adherence to the intestine during the passage of the strain through the gastrointestinal tract. The authors correlated the *in vitro* and *in vivo* AggL-mediated aggregation to binding to the colonic mucus through non-specific hydrophobic interactions. The expression of AggL on the bacterial cell surface significantly increased the hydrophobicity of the strain. On the other

hand, the presence of AggL in the strain reduced its ability to adhere to the ileum. Moreover, MbpL protein showed an affinity to bind gastric-type mucin proteins such as MUC5AC. However, this protein did not contribute to the binding of *L. lactis* to the ileal or colonic part of the intestine (Lukic *et al.* 2012).

In previous works of our group, the use of AFM force spectroscopy provided new insights into the interaction mechanisms *in vitro* between *L. lactis* and the commercial PGM of type III. The natural strain *L. lactis* subsp. *cremoris* IBB477 strain (and its control strain MG1820), isolated from a dairy environment and which was shown to exhibit *in vivo* persistence in the rat gastrointestinal tract (Boguslawska *et al.* 2009), was studied. Interaction forces were directly quantified at nanoscale between an AFM tip functionalized with living *L. lactis* cells ("lacto-probe") and PGM-coated polystyrene (Dague *et al.* 2010). Both non-specific (showing no extension before rupture) and specific forces (ligand/receptor bonding) were shown to be involved in *L. lactis* adhesion to PGM. Some typical force-distance curves obtained displayed one, two or three specific events, with each force peak due to a disruption of intra- and intermolecular interactions which represent a barrier against unfolding. When the externally applied force overcomes the strength of these molecular interactions in a given domain, all entities in that domain unfold spontaneously, together with an abrupt drop of the measured force to zero. High percentages of specific adhesive events were observed for IBB477 (20%), compared to their low-adhesive counterparts (about 5%) (Le *et al.* 2011). Blocking assays with free PGM and O-glycans demonstrated that oligosaccharides played a major role in interactions between *L. lactis* and PGM. Specific interactions were then analysed in terms of kinetic constants. On the one hand, an increase in the loading rate of AFM tip led to a higher adhesion force between interacting biological entities, which is directly linked to the kinetic dissociation constant (K_{off}). On the other hand, enhancing the contact time between the tip and the sample allowed an increase in the interaction probability, which can be related to the kinetic association constant (K_{on}). Variations of loading rate and contact time enabled to determine K_{off} (0.46 s^{-1}) and K_{on} (3.3 x 10^2 $M^{-1}.s^{-1}$), for the first time with living cell probes and mucins. The K_{off} parameter was consistent with values given in the literature for sugar/protein interactions (Le *et al.* 2011). Later, the higher adhesion of IBB477 to PGM than that of MG1820 was confirmed at the population level under controlled hydrodynamics, using real-time quartz crystal microbalance with dissipation monitoring (QCM-D). Indeed, a sharp increase in QCM-D outputs (change in frequency and energy

dissipation, Δf and ΔD, and ΔD/Δf ratio) was observed, which was related to a higher number of attached cells to the PGM-coated crystal surface, as shown by DAPI staining (Le *et al.* 2012). However, in these studies, it was not possible to relate *L. lactis* muco-adhesive profile, as probed by AFM and QCM-D, to cell surface determinants potentially involved. Studies for identifying such components in the IBB477 strain are under progress (Kowalczyk M., personal communication).

In the following section, we will present literature data on the vegetal isolate *L. lactis* subsp. *lactis* TIL448, used throughout our study. Details on its surface properties, its cell surface determinants and their role in adhesion will be given.

4. Identification of the natural *L. lactis* subsp. *lactis* isolate TIL448: cell surface determinants and adhesive properties to abiotic and biotic surfaces

4.1. Diversity of *L. lactis* strains in terms of physico-chemical properties

First studies concerning the surface properties of *L. lactis* were conducted either on a unique strain (Boonaert *et al.* 2000, Boonaert *et al.* 2001, Habimana *et al.* 2007) or on a limited number of natural strains, only isolated from milk products (Crow *et al.* 1995, Ly *et al.* 2006, Ly *et al.* 2006). However, in the work of Giaouris *et al.* (2009), the diversity of *L. lactis* strains in terms of surface physico-chemical properties (cell surface hydrophobicity and Lewis acid–base properties, electrical charge) was highlighted. Indeed, 50 strains, belonging to *lactis* or *cremoris* subspecies (or unknown subspecies), and isolated from different sources (dairy, vegetal or animal origin), were classified in three main groups. While 52% of the strains presented a hydrophilic and electronegative cell wall surface, as generally found, a group of hydrophobic strains (12% of the strains) and a group of strains with low charged surface (18%) were identified. In addition, surface physico-chemical properties were correlated with adhesion to abiotic polystyrene: the most adhesive strains in a low ionic strength suspending medium were hydrophobic or low charged. Collectively, these results on the differences observed between *L. lactis* strains in terms of cell surface characteristics suggested that different components are exposed at the outermost layer of the cell wall, which

in turn may influence bacterial adhesion not only to abiotic but also probably to biotic surfaces.

4.2. Specific adhesion of TIL448 to Caco-2 human intestinal epithelial cells

To test this last hypothesis, in a further study of the same team (Meyrand *et al.* 2013), the authors chose different *L. lactis* strains representative of the three above groups (Giaouris *et al.* 2009) and compared their ability to adhere to Caco-2 human intestinal epithelial cells. Among them, only *L. lactis* subsp. *lactis* TIL448, a vegetal isolate previously characterized as a very hydrophobic strain, strongly adhered to Caco-2 cells, as shown by epifluorescence microscopy and plate counting, and this behavior was not dependent on the cell surface hydrophobicity (**Figure I.11**).

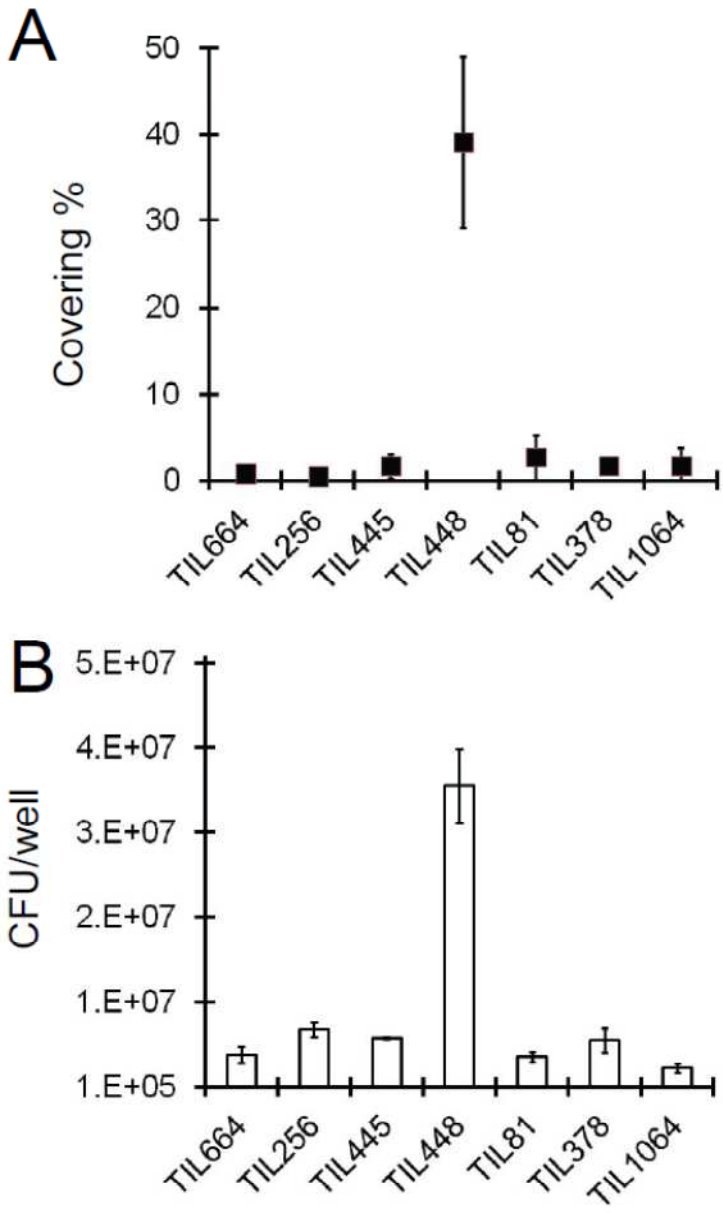

Figure I.11. Adhesion of *L. lactis* strains to Caco-2 intestinal epithelial cells. (A) Adhesion was quantified as the percentage of surface covered by GFP-labeled bacteria, estimated by epifluorescence microscopy; (B) Adhesion of non-labeled bacteria was quantified by plate counting and expressed as CFU/well (Meyrand *et al.* 2013).

Data on the origin and the cell surface properties of *L. lactis* strains are derived from Giaouris *et al.* (2009):

- **TIL81:** MG1363, *L. lactis* subsp. *cremoris*, plasmid-free and prophage-cured derivative of NCDO712, hydrophilic and electronegative surface,

- **TIL256:** C2, *L. lactis* subsp. *cremoris*, dairy strain, hydrophobic and electronegative surface;
- **TIL378:** NCDO2118, *L. lactis* subsp. *lactis* isolated from beans, hydrophilic and low surface charge;
- **TIL445:** NCDO2108, *L. lactis* subsp. *lactis* isolated from peas, hydrophobic and electronegative surface;
- **TIL448:** NCDO2110, *L. lactis* subsp. *lactis* isolated from peas, hydrophobic and electronegative surface;
- **TIL664:** CNRZ739, *L. lactis* subsp. *lactis*, dairy strain, hydrophobic and electronegative surface;
- **TIL1064:** KH, *L. lactis* subsp. *cremoris*, dairy strain, hydrophobic surface and low surface charge.

4.3. Identification and functional role of TIL448 surface proteins in adhesion to Caco-2 cells

The adhesion determinants of *L. lactis* TIL448 to Caco-2 cells were shown to be plasmid-encoded (Meyrand *et al.* 2013). To identify surface proteins in *L. lactis* TIL448 involved in adhesion, a proteomic approach was used, consisting in digesting surface-exposed proteins on whole bacteria with a proteolytic enzyme, followed by the identification of the released peptides by LC-MS/MS. Among the 32 surface-predicted proteins that were detected in TIL448, two of them, encoded by plasmids, were identified and defined as adhesin candidates (Meyrand *et al.* 2013):

(i) the first protein, named YhgE2, displayed pilin characteristics.

The plasmidic gene cluster involved has the typical organization of genes specifying sortase-dependant heterotrimeric pili biosynthesis. It encodes four putative proteins including a major pilin, a class-C sortase involved in major pilin polymerization, a minor pilin and a tip pilin. This putative tip pilin, probably located at the extremity of the pili appendages, is a large LPxTG-protein and, interestingly, contains a lectin-type domain (PF00139 or *Lectin_leg* domain) with predicted carbohydrate binding specificity. It was shown that the IL1403 chromosomal locus, depicted by Oxaran *et al.* (2012), and the TIL448 plasmidic one exhibited similarities but also marked differences, as revealed by sequence analysis. In

particular, the tip pilin has no homolog in IL1403 chromosome or in other known *L. lactis* genome sequences. Further, it was found that this plasmidic pilin gene cluster, expressed in classical laboratory conditions, was responsible for the synthesis of pili, as revealed by electron microscopy and negative staining (**Figure I.12**). However, the pili density at the cell surface was rather low, for instance in comparison with *L. rhamnosus* GG (Tripathi *et al.* 2013).

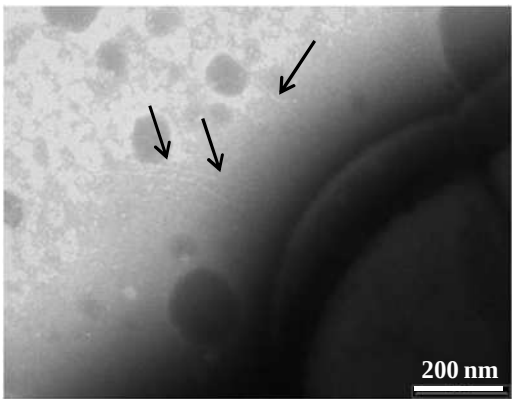

Figure I.12. Electron micrograph of *L. lactis* TIL448 after negative staining. Scale bar: 200 nm. Pili are indicated by arrows.

(ii) The second protein exhibited high sequence similarity with putative mucus-binding (MUB) proteins (Boekhorst *et al.* 2006) of *Leuconostoc citreum* KM20 and *Lactobacillus fermentum*. It contains two MucBP domains (PF06458), followed by a LPxTG motif for peptidoglycan anchoring at the C-terminal end and a N-terminal signal peptide (**Figure I.13**).

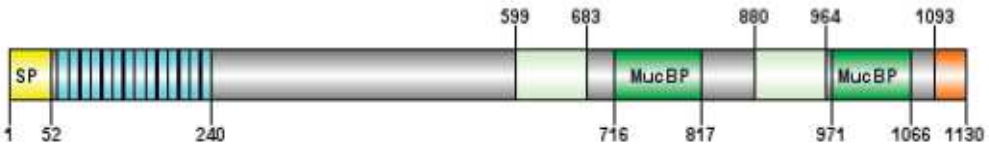

Figure I.13. Schematic representation of the MUB-protein identified in *L. lactis* TIL448.
SP, signal peptide. MucBP, mucus-binding domain (PF06458). In blue are represented 14 repeated sequences with consensus sequence SSA(V,T)NA(D,E)(S,T)T(S,G)A. In light green are indicated two completely identical sequences. In orange are shown the C-terminal peptidoglycan-anchoring motif constituted of LPxTG, followed by a hydrophobic domain and a positively charged tail (Meyrand *et al.* 2013).

It was shown that inactivation of the pilin gene abolished adhesion to Caco-2 cells whereas inactivation of the mucus-binding protein gene had no effect on adhesion (Meyrand *et al.* 2013), showing that pili appendages are responsible for the original adhesion properties of *L. lactis* TIL448 to human intestinal epithelial cells, like Caco-2. However, the muco-adhesive phenotype of TIL448, in relation with the cell surface determinants involved, remained so far unknown.

CHAPTER II. OBJECTIVES OF THE STUDY

Chapter II. Objectives of the study

As mentioned in the ***Chapter I***, *L. lactis* has an important contribution in the food industry, particularly for dairy products. Moreover, increasing attention is paid to beneficial effects of *L. lactis* on human health as a probiotic or delivery vector for therapeutic molecules, notably for treating intestinal diseases. Recently, a vegetal isolate of *L. lactis*, TIL448, was shown to display original properties in terms of surface determinants (presence of both mucus-binding protein and pili) and adhesion to biotic surfaces, such as Caco-2 intestinal epithelial cells. **However, the mucus-related phenotype of TIL448 remained unknown. In this framework, our work, conducted in "Laboratoire d'Ingénierie des Systèmes Biologiques et des Procédés" (LISBP, Toulouse), in close collaboration with Micalis Institute, Jouy-en-Josas (team of M-P. Chapot-Chartier), was devoted to evaluating adhesion of *L. lactis* TIL448 to mucins, considering PGM of type III. It also aimed at elucidating the respective contribution of both pili and mucus-binding protein by using targeted defective-mutants. The migration ability of *L. lactis* within PGM-based hydrogels was also determined, in relation with their rheological properties and microstructure. To address these questions, different biophysical approaches and tools were combined.**

The description of the results obtained in our study is organized as follows:

1. Adhesion and migration of *L. lactis* TIL448 inside PGM-based hydrogels: role of pili and mucus-binding protein

1.1. Unraveling the role of surface mucus-binding protein and pili in muco-adhesion of *Lactococcus lactis*

Complementary to the use of atomic force microscopy (AFM) with static and single-cell force spectroscopy measurements, as previously described for *L. lactis* IBB477 (Dague *et al.*, 2010; Le *et al.*, 2011), shear stress flow chamber (SSFC) was implemented for estimating adhesion of *L. lactis* to PGM-coated polystyrene, at the bacterial population level and under well-controlled hydrodynamics. To this end, shear-flow induced detachment experiments

were performed, according the experimental procedure developed for yeast and bacterial cells (Mercier-Bonin *et al.* 2011, Mercier-Bonin *et al.* 2012, Saulou *et al.* 2012). The strains studied throughout this part were the following*:* the wild-type *L. lactis* TIL448, the plasmid-cured derivative TI1230, the pilin mutant TIL1289 and the mucus-binding protein mutant TIL1290. Results obtained are described in our publication, recently accepted in PLOS ONE (see the ***Chapter III 1.1***).

1.2. Further investigations on the migration ability of *L. lactis* inside PGM-based hydrogels

In contrast to pathogens, only few data are to date available on the migration ability of beneficial bacteria, like *L. lactis*, particularly within intestinal mucus gels. In this framework, diffusivities of the wild-type *L. lactis* and its derivatives within PGM-based hydrogels were investigated at the population level. To this end, a novel method named Diffusion Front Tracking (DFT) was implemented (Jimenez *et al.*, 2013), based on evaluating the displacement of a bacteria front diffusing through the flat bacteria/PGM hydrogel interface in a dedicated chamber. The respective contribution of *L. lactis* adhesive and muco-adhesive properties was elucidated. Results are presented in the ***Chapter III.1.2.***

2. Scrutinizing the microstructure of porcine gastric mucins by fluorescence multiple particle tracking and microrheometry

In order to get a deeper understanding of the *L. lactis* muco-adhesive and diffusive ability, the microstructure and mechanical properties of PGM were determined. Gel microstructure was probed by the analysis of diffusivities of 200-nm and 500-nm fluorescent nanoparticles with different surface properties (carboxyl-terminated, negatively charged tracers, with and without PEG coating; amine-terminated, positively charged tracers), using fluorescence Multiple-Particle Tracking (Lai *et al.*, 2007; Lai *et al.*, 2010; Lieleg *et al.*, 2010). The pore size of the PGM network was evaluated. Characterization of the PGM rheological properties was achieved by combining classical bulk rheometry in collaboration with “Institut de

Mécanique des Fluides de Toulouse" (IMFT) and microrheometry approaches. Results are detailed in the ***Chapter III.2***. This chapter is a work about to be submitted.

CHAPTER III. RESULTS

Chapter III. Results

1. Adhesion and migration of *L. lactis* TIL448 inside PGM-based hydrogels: role of pili and mucus-binding protein

Context and objectives. Adhesion of bacteria to mucus may favor their persistence within the gut and their beneficial effects to the host. Few studies have to date investigated muco-adhesion of lactococci. In this framework, the present study was devoted to unraveling at multi-scale interactions between the model mucin Pig Gastric Mucin (PGM) and a vegetal *L. lactis* subsp. *lactis* isolate, TIL448, in close relation with the nature of the bacterial surface determinants involved. To this end, other strains were tested: the plasmid-cured strain (TIL1230) and two mutants (TIL1289 and TIL1290), obtained by disruption of the genes encoding the major pilin and the mucus-binding protein, respectively. Single-cell scale and static AFM measurements with dedicated lacto-probes were performed and compared to shear stress flow chamber experiments at the bacterial population level, under laminar flow conditions (see Chapter III.1.1). Then, the impact of *L. lactis* adhesive/muco-adhesive properties on its migration inside PGM-based hydrogels at varying PGM concentration was evaluated on the same panel of strains, using Diffusion Front Tracking (DFT) method (see Chapter III.1.2).

Methods. AFM force spectroscopy measurements were performed for the four strains under study (TIL448, TIL1230, TIL1289 and TIL1290) at room temperature and in MilliQ-grade water. The viability of bacterial cells attached to the AFM tip was evaluated with CFDA labeling. In addition, AFM blocking assays were performed with free PGM and O-glycan fractions (total, acidic or neutral fraction), which were analyzed by mass spectrometry. In parallel, detachment of *L. lactis* bacterial cells from PGM coating was characterized in the shear stress flow chamber. Surface analysis of the PGM-coated coupons was carried out (surface wettability, elemental composition using X-ray photoelectron spectroscopy XPS). Detachment experiments were performed in phosphate buffered saline (PBS) and at room temperature. Then, DFT measurements were performed on PGM-based hydrogels for all the strains in order to determine the diffusivity of fuchsine-labelled bacteria in each condition.

The effect of such fuchsine labelling on cell viability and physico-chemical properties was evaluated. Two PGM concentrations (0.5% and 5% (w/v)) were tested.

Results. AFM experiments revealed a strong adhesion of the wild type TIL448 strain to PGM, with a high proportion of specific adhesive events (60 %) and a low level of non-adhesive ones (2 %). In contrast, the plasmid-cured derivative TIL1230 showed low muco-adhesive properties. Viability of attached cells was established for both strains. The muco-adhesive properties were confirmed for TIL448 by the weak detachment of bacterial cells from the PGM-coated surface under shear flow. For TIL1230, no adhesion to PGM occurred. In AFM, rupture events were detected for TIL448 at short (100-200 nm) and long distances (up to 600-800 nm), consistent with the characteristics of the cell surface determinants involved. AFM measurements on pili and mucus-binding protein defective mutants demonstrated the comparable role played by these two surface proteinaceous components in adhesion to PGM under static conditions. However, under shear flow, a more important contribution of the mucus-binding protein than the pili one was observed. Both methods differ by the way of probing the adhesion force, i.e. negative force contact vs. sedimentation and normal-to-substratum retraction vs. tangential detachment conditions, using AFM and flow chamber, respectively. AFM blocking assays with free PGM or O-glycan fractions purified from PGM demonstrated that oligosaccharides, and more particularly neutral ones, played a major role in adhesion of *L. lactis* TIL448 to PGM. In addition, the feasibility of the DFT method for determining the *L. lactis* diffusion coefficient inside PGM-based hydrogels was demonstrated. Fuchsine labelling had only a limited impact on viability and cell surface properties of the wild type *L. lactis* and its derivatives. Whatever the PGM concentration, the lowest diffusion coefficient was obtained for the wild type TIL448 strain whereas the highest one was achieved for the plasmid-cured derivative TIL1230. The pilin mutant TIL1289 had a diffusion coefficient lower than that observed for the mucus-binding protein mutant TIL1290. Moreover, independently of the strain, bacterial cells tended to be more diffusive in a 0.5% (w/v) than in a 5% (w/v) PGM gel.

Conclusion. This work was focused on the muco-adhesion/migration phenotype of the vegetal isolate *L. lactis* subsp. *lactis* TIL448 at multi-scale, by coupling AFM force spectroscopy, shear stress flow chamber and Diffusion Front Tracking method. The Pig

Gastric Mucin (PGM) was chosen as the model mucin. Using the wild-type strain, in conjunction with pilin and mucus-binding protein defective mutants, the combined role played by both surface proteins in adhesion to PGM was established, with a contribution closely depending on how interactions are probed. The importance of the sugar receptors of PGM, mainly of neutral type, was demonstrated. The need for well-controlled hydrodynamics was also highlighted, especially when shear-flow sensitive appendages like pili are involved. In addition, migration of *L. lactis* inside PGM-based hydrogels was shown to be a complex interplay between specific (bacterial adhesin(s)/sugar receptors) and non-specific (e.g. electrostatic and/or hydrophobic interactions) interactions. All these findings allowed a better understanding of interactions of *L. lactis* with the mucosal environment in the gastrointestinal tract, further offering novel strategies for medical and food-related applications.

Unraveling the Role of Surface Mucus-Binding Protein and Pili in Muco-Adhesion of *Lactococcus lactis*

Doan Thanh Lam Le[1,2,3,4,5,6#], Thi-Ly Tran[1,2,3#], Marie-Pierre Duviau[1,2,3], Mickael Meyrand[7,8], Yann Guérardel[9,10], Mickaël Castelain[1,2,3], Pascal Loubière[1,2,3], Marie-Pierre Chapot-Chartier[7,8], Etienne Dague[4,5,6*], and Muriel Mercier-Bonin[1,2,3*]

[1] Université de Toulouse; INSA,UPS, INP; LISBP, 135 Avenue de Rangueil, F-31077 Toulouse, France

[2] INRA, UMR792 Ingénierie des Systèmes Biologiques et des Procédés, F-31400 Toulouse, France

[3] CNRS, UMR5504, F-31400 Toulouse, France

[4] CNRS ; LAAS ; 7 avenue du colonel Roche, F-31400 Toulouse, France

[5] CNRS ; ITAV-UMS3039 ; F31106 Toulouse, France

[6] Université de Toulouse, LAAS, F-31400 Toulouse, France

[7] INRA, UMR1319 Micalis, F-78350 Jouy-en-Josas, France

[8] AgroParisTech, UMR Micalis, F-78350 Jouy-en-Josas, France

[9]Université de Lille1, Unité de Glycobiologie Structurale et Fonctionnelle, UGSF, F-59650 Villeneuve d'Ascq, France

[10]CNRS, UMR 8576, F-59650 Villeneuve d'Ascq, France

[#] D.T.L. Le and T.L. Tran contributed equally to this work.

This work has been accepted for publication in PLOS ONE.

* To whom correspondence should be addressed: Muriel Mercier-Bonin, Commensal and Probiotics-Host Interactions Team, MICALIS, UMR 1319 INRA/AgroParisTech, Domaine de Vilvert, 78350 Jouy en Josas, France, Tel: +33 (0) 1 34 65 22 87, Fax: +33 (0) 1 34 65 23 11, E-mail: Muriel.Mercier-Bonin@jouy.inra.fr; Etienne Dague, LAAS-CNRS, Université de Toulouse, 7 avenue du colonel Roche, F-31400 Toulouse, France, Tel:+33 (0) 5 61 33 78 41, Fax: +33 (0) 5 61 33 62 08, E-mail: edague@laas.fr

Abstract

Adhesion of bacteria to mucus may favor their persistence within the gut and their beneficial effects to the host. Interactions between pig gastric mucin (PGM) and a natural isolate of *Lactococcus lactis* (TIL448) were measured at the single-cell scale and under static conditions, using atomic force microscopy (AFM). In parallel, these interactions were monitored at the bacterial population level and under shear flow. AFM experiments with a *L. lactis* cell-probe and a PGM-coated surface revealed a high proportion of specific adhesive events (60 %) and a low level of non-adhesive ones (2 %). The strain muco-adhesive properties were confirmed by the weak detachment of bacteria from the PGM-coated surface under shear flow. In AFM, rupture events were detected at short (100-200 nm) and long distances (up to 600-800 nm). AFM measurements on pili and mucus-binding protein defective mutants demonstrated the comparable role played by these two surface proteinaceous components in adhesion to PGM under static conditions. Under shear flow, a more important contribution of the mucus-binding protein than the pili one was observed. Both methods differ by the way of probing the adhesion force, i.e. negative force contact vs. sedimentation and normal-to-substratum retraction vs. tangential detachment conditions, using AFM and flow chamber, respectively. AFM blocking assays with free PGM or O-glycan fractions purified from PGM demonstrated that neutral oligosaccharides played a major role in adhesion of *L. lactis* TIL448 to PGM. This study dissects *L. lactis* muco-adhesive phenotype, in relation with the nature of the bacterial surface determinants.

Introduction

The digestive epithelium is covered with a protective mucus layer, regarded as a visco-elastic and permeable hydrogel. This layer serves as an ecological niche for commensal and probiotic bacteria, and plays a role in the defense against enteric bacterial infections by expelling pathogens from the mucosal surface [1]. The mucus layer is described as a secreted mucin-fiber scaffold [2]. Mucins are large glycoproteins with a serine and threonine-rich protein backbone, linked to a wide variety of O-linked oligosaccharide side chains arranged in a bottle-brush configuration [2]. Such O-glycans are nutritive sources for bacteria and/or

potential ligands for bacterial adhesins [3], probably contributing in this way to the selection of the species-specific microbiota [4].

Many studies on bacterial muco-adhesion have been carried out with commensal *Lactobacillus* species, with the aim to select probiotics based on their ability to persist within the gut [5-8]. Several cell surface proteins have been shown to act as mediators of specific *Lactobacillus* adhesion to mucus [9-12]. By searching protein databases within different lactic acid bacteria (LAB) species, including lactococci and lactobacilli, Boekhorst *et al.* [13] and Kleerebezem *et al.* [14] concluded that the mucus-binding (MUB) repeat plays a pivotal role in host-bacteria interactions. Furthermore, the presence of pili structures and related muco-adhesion properties were reported in *Lactobacillus rhamnosus* GG [15].

Lactococcus lactis, considered as the model LAB, is traditionally used as a starter in manufacturing cheese and other fermented dairy products. Even though lactococci are not a frequent natural element of the intestinal microbiota, they were sporadically isolated from feces of many different groups of humans [16]. Certain strains were also shown to transit through the stomach and survive in the gut of rodents [17,18]. To date, in contrast with lactobacilli, little is known about the structural and functional factors involved in lactococci muco-adhesion. The presence of only one single MUB-domain-containing protein was reported in the study depicted by Boekhorst *et al.* [13], in the genome of laboratory plasmid-free *L. lactis* strains. Nevertheless, Giaouris *et al.* [19] and Passerini *et al.* [20] highlighted the genetic, genomic and phenotypic diversity, such as surface physico-chemical properties, within large collections of *L. lactis* strains isolated from different ecological niches. Such biodiversity was further explored in terms of muco-adhesive ability. Indeed, we focused on elucidating interactions between *L. lactis* strains and a model mucin (pig gastric mucin (PGM)), using the natural strain *L. lactis* subsp. *cremoris* IBB477, isolated from a dairy environment and which was shown to persist *in vivo* in rat gut [17]. The higher adhesion force measured between IBB477 cells and PGM, compared to the control strain MG1820, was assessed at nanoscale with AFM force spectroscopy [21] and further confirmed at the bacterial population level, using quartz crystal microbalance with dissipation monitoring [22].

In the present contribution, we focused on unraveling multi-scale interactions between PGM and a vegetal *L. lactis* subsp. *lactis* isolate, TIL448, in close relation with the nature of the bacterial surface determinants involved. In a previous study, *L. lactis* TIL448 was shown to

expose pili at its surface, conferring specific adhesion to Caco-2 human intestinal epithelial cells in contrast to the other tested *L. lactis* strains [23]. The gene cluster involved in pili synthesis is located on a plasmid and has the typical organization of genes specifying sortase-dependant heterotrimeric pili biosynthesis. Similarly to the gene cluster identified in the chromosome sequence of *L. lactis* IL1403 [23], the TIL448 plasmidic gene cluster encodes four putative proteins including a major pilin, a class-C sortase involved in major pilin polymerization, a minor pilin and a tip pilin. In addition, the presence of a mucus-binding protein, displaying two MucBP domains (PF06458) and which differs from the one identified by *in silico* analysis in the chromosome of sequenced *L. lactis* strains, was demonstrated at the surface of *L. lactis* TIL448. Noteworthy, this protein is also encoded by a plasmid-located gene.

In this framework, we performed single-cell scale AFM measurements with dedicated lacto-probes [24] and shear stress flow chamber experiments at the bacterial population level, under laminar flow conditions on the wild type *L. lactis* TIL448. We also tested the plasmid-cured strain (TIL1230) and two mutants (TIL1289 and TIL1290), obtained by disruption of the genes encoding the major pilin-encoding gene (*yhgE2*) and the mucus-binding protein (*muc*), respectively. Bacterial cells were put in adhesive contact with a biomimetic PGM-coated surface, under static or shear-flow conditions. Special attention was paid to the importance of specific interactions, as probed with AFM and the effect of variable flow conditions on shear-flow induced *L. lactis* detachment. Data of both sets of experiments were then combined to establish the role of surface mucus-binding protein and pili in *L. lactis* muco-adhesion, with a contribution closely depending on the static or dynamic nature of the environment and how interactions are probed.

Materials and Methods

Bacterial strains, plasmids, growth conditions and preparation of suspensions

The bacterial strains used in this study are listed in Table 1. Bacterial stock cultures were kept at -80°C in M17 broth (Oxoid), containing 0.5 % (w/v) glucose and 20 % (v/v) glycerol. Bacteria were first sub-cultured overnight at 37°C in M17-glucose (0.5 % (w/v)) medium

(M17Glc). This preculture was then used to inoculate M17Glc at 37°C. Erythromycin (5 µg/mL) was added when required. Bacteria were harvested during the exponential growth phase (optical density at a wavelength of 600 nm (OD_{600}) of 1.2) by centrifugation (4000 rpm, 10 min, room temperature) and washed twice with MilliQ-grade water or phosphate buffered saline (PBS), according to further experiments to be performed (AFM and shear stress flow chamber, respectively).

Preparation of the PGM-coated polystyrene surfaces

The pig gastric mucin (PGM) was commercially available as a lyophilized powder (Sigma M1778, partially purified type-III mucin from porcine stomach). PGM was directly dissolved in PBS at pH 7.5 at a final concentration of 10 mg/mL. The solutions were prepared just before use.

Polystyrene was used as the substratum in the form of square (10.0 mm x 10.0 mm x 1.0 mm) or rectangular coupons (25.2 mm x 6.3 mm x 2.0 mm), for AFM and flow chamber experiments, respectively. Coupons were immersed in 2 % (v/v) liquid detergent RBS 25 (Traitements Chimiques de Surfaces, Frelinghien, France) at 50°C for 15 min, rinsed in five successive baths of tap water at 50°C and five successive baths of tap water at room temperature, rinsed with copious amounts of MilliQ-grade water (50°C and room temperature) and finally air-dried for 15 min under a vertical flow hood (Cytosafe 2000, Faster, Italy). Surfaces were either used immediately for the following steps or stored in a desiccator at room temperature until use.

PGM adsorption onto polystyrene was performed as previously described [24] with slight modifications. Briefly, polystyrene coupons, prepared according to the above procedure, were exposed overnight to a 10 mg/mL PGM solution in PBS pH 7.5 at 4°C, under gentle agitation. After incubation, surfaces were copiously rinsed to remove loosely bound material using, in sequence, PBS and MilliQ-grade water and finally air-dried under a vertical flow hood (Cytosafe 2000, Faster, Italy).

The characteristics of the PGM layer after adsorption onto square polystyrene coupons have been described in details in a previous study [25]. Thus, before AFM force measurements, the

shape of the water droplet partially wetting the PGM-coated surface was just compared to that obtained for the bare substratum in order to verify the enhanced wettability due to PGM adsorption. Reproducible results were obtained (data not shown). For rectangular polystyrene coupons, a more thorough surface analysis was carried out. First, surface wettability was evaluated before and after PGM coating, using the sessile drop technique with a Digidrop goniometer (Contact Angle Meter– GBX Scientific Instruments, Romans sur Isère, France), coupled with the WinDrop^{++} software to capture and analyse images. Reported values are the average of at least three advancing deionised water contact angle measurements per sample. Then, the physico-chemical properties of bare and PGM-coated surfaces were assessed with X-ray photoelectron spectroscopy (XPS), as previously detailed [25]. As for square coupons, before each experiment in the shear stress flow chamber, the shape of the water droplet formed on rectangular coupons was verified and a higher surface wettability due to PGM coating was systematically observed in a reproducible manner (data not shown).

Isolation and separation of oligosaccharide-alditols from PGM

Commercial PGM was submitted to reductive β-elimination for 72 h at 37°C in 100 mM NaOH containing 1 M $NaBH_4$. The reaction was stopped by the addition of cation exchange resin Dowex 50 x 8 (25–50 mesh, H^+form) at 4°C until pH 6.5. After filtration on glass wool and evaporation to dryness, boric acid was eliminated by repetitive distillation as its methyl ester in the presence of methanol. The material was submitted to a cation exchange chromatography on Dowex 50 x 2 (200–400 mesh, H^+ form) to remove residual peptides. The released O-glycans were desalted on Bio-Gel P2 column (Bio-Rad), eluted in water. Neutral and acidic O-glycans were separated by anion exchange chromatography fractionation on Dowex 1 x 2 (200–400 mesh, $HCOO^-$ form). Neutral glycans were eluted from the resin by water and acidic glycans by stepwise concentrations of pyridine acetate (5 to 100 mM). Carbohydrate containing neutral and acidic fractions were pooled and desalted on Bio-Gel P2 column (Bio-Rad), eluted in water.

Mass spectrometry analyses

MALDI-TOF mass spectra were acquired on a voyager Elite DE-STR mass spectrometer (Perspective Biosystems, Framingham, MA) in the reflection positive mode by delayed

extraction using an acceleration mode of 20 kV, a pulse delay of 200 ns and grid voltage of 66%. Samples were prepared by mixing directly on the target 1 µL of oligosaccharide solution (1-5 pmol) with 1 µL of 2,5dihydroxybenzoic acid matrix solution (10 mg/mL in CH_3OH/H_2O, 50/50 v/v). Between 50 and 100 scans were averaged for each spectrum.

AFM lacto-probe preparation

OTR4 (Si_3N_4) probes, purchased from Bruker Corporation (Palaiseau, France), were used for the lacto-probe preparation, as described elsewhere [24]. Briefly, cantilevers and tips, first cleaned for 15 min with UV/O_3 treatment, were immersed for 5 hours in a polyethylenimine (PEI) solution (0.1 % (w/v)), rinsed with a copious amount of MilliQ-grade water and stored under light vacuum. The negatively-charged *L. lactis* cells [19], suspended in MilliQ-grade water, were attached to the positively charged PEI-coated probes through a 20-min contact time. The presence of immobilized bacteria on the AFM tip was detected by scanning electron microscopy (SEM; Hitachi S-3700N). In addition, viability of attached cells was evaluated, as previously described [21]. In brief, the lacto-probe was first observed under bright field microscopy to visualize the total amount of immobilized cells. Then, the lacto-probe was labeled with carboxyfluorescein diacetate 100 µM (5(6)-CFDA: 5-(and-6)-carboxyfluorescein diacetate - mixed isomers, C195, Molecular Probes, 492-517 nm) for 1 h at 30 °C, thoroughly rinsed with MilliQ-grade water, and reexamined under epifluorescence microscopy. Cells exhibiting an esterase activity are seen in green. Note that viability was checked on planktonic cells harvested at the exponential growth phase (complete CFDA labeling, data not shown). Control experiments were also performed with planktonic and attached dead cells after heat treatment (2 h, 95°C) and, as expected, no green fluorescence was detected (data not shown).

AFM force spectroscopy

In order to ensure a firm immobilization of the *L. lactis* cells on the probe during the experiment, AFM measurements were performed in MilliQ-grade water and at room temperature, using the Catalyst system from Bruker Corporation (Santa Barbara, USA). Interactions between the lacto-probe and the PGM-coated polystyrene surface were assessed, for each strain tested, by recording at a loading rate of 161250 pN/s single force-distance

curves and matrix of 32 x 32 force-distance curves on 5 x 5 µm² squares, giving 1024 force curves to be analyzed. Experiments were performed with five independent PGM-coated surfaces and lacto-probes. For each lacto-probe, two zones (5 x 5 μm^2) with homogeneous PGM coating [25] were probed. Blocking assays were performed with free PGM (10 mg/mL in PBS) and O-glycan fractions (total, acidic or neutral fraction, 10 mg/mL in PBS), prepared as described above. The spring constants of the tips, measured for each probe, were in the range 0.02 - 0.03 N/m. Adhesion forces were deduced from the force-distance curves and quantified using Research Nanoscope 8.31 software from Bruker Corporation. In brief, deflection data were recorded during the retraction of the tip from the PGM-coated surface and converted to force after multiplication with the spring constant of each individual cantilever, whereas the real tip-substrate distance was obtained by subtracting the deflection from the piezo movement. The point of zero distance was assigned at the intersection of the experimental curve with the straight line fitting the tail of the curve. Bond-rupture distances were deduced from the force vs. distance curves as the point of zero distance, subtracted from the point at which a negative deflection returns to zero.

Detachment of *L. lactis* bacterial cells from PGM coating in the shear stress flow chamber

PGM-coated polystyrene coupons were subjected to shear flow-induced detachment experiments for each *L. lactis* strain under study. The experimental procedure, previously described for *Escherichia coli* in adhesive contact with plasma-modified stainless steel [25], was slightly modified, notably for the cell-counting mode. In brief, shear-flow induced *L. lactis* detachment was analyzed in a rectangular flow channel (12-mm width, 25.2-mm length and 200-µm thickness). The wall shear stress τ_W is given by:

$$\tau_w = \frac{3\mu Q}{4h^2 l}$$

where μ is the fluid dynamic viscosity (Pa.s), Q (m^3/s) is the flow rate, l and h are respectively the channel half-width and half-thickness (m).

In order to have more "physiological" conditions for *L. lactis*, experiments were performed in PBS and at room temperature. The flow chamber and all tubes were filled with PBS, while care was taken to remove air bubbles from the system. The bacterial suspension (OD_{600} of

0.3, volume of 700 µL) was slowly injected into the flow chamber and bacterial cells were allowed to attach to PGM coating for 3 hours under “static” conditions. Images, collected using the reflection mode of an upright optical microscope (Nikon Eclipse LV100) equipped with a 40x ultra-long working distance objective, were recorded by a camera (digital STGHT DS-2MBW, Nikon) and the NIS-Elements F3.0 video acquisition software. The field of view was 144 µm by 108 µm with a resolution of 0.09 µm per pixel. Owing to previous results on velocity field in the flow chamber [26], special care was taken to properly choose the observation area, in order to satisfy requirements with respect to uniform flow conditions. Images were analyzed for estimating the percentage of the surface occupied by attached cells with the free software MacbiophotonicsImageJ (www.macbiophotonics.ca) and the Matlab software (Mathworks Inc., USA).

After the 3-h adhesion step, rinsing with PBS was achieved at a low flow rate of 0.001 mL/s (corresponding to a wall shear stress of about 0.012 Pa) in order to stabilize the system and remove loosely-adhering bacteria. The percentage of remaining attached cells was thereafter referred as to A_0. We should note that the A_0 value was in the range 1 % - 3 % of the total surface area, so that any interactions between neighboring bacteria were considered as minimal. Laminar flow of PBS was then imposed, with a stepwise increase in the flow rate (maximal value of 6.7 mL/s), with 3-min step duration. Flow rates ranging from 0.001 to 0.3 mL/s were generated by gravity, controlling through a toothed rack the height of a constant head vessel located upstream of the chamber. Higher flow rates were obtained using a gear pump (Ismatec, Fisher Bioblock Scientific). The maximal Reynolds number was equal to 560 (laminar flow conditions). The wall shear stress τ_W was in the range 0–80 Pa.

At the end of each step, the surface coverage by attached bacteria (A) was estimated. The detachment profile, representing the ratio A/A_0 as a function of the wall shear stress τ_W, was plotted. For each strain, experiments were performed at least in triplicate with different PGM-coated coupons and independently grown cultures.

Results

Using AFM for probing the adhesive properties of *L. lactis* TIL448 to PGM

A lacto-probe consisting of bacterial cells immobilized on the AFM tip was prepared with *L. lactis* TIL448 and examined by SEM (Figure 1A). We should note that small clusters of cells were typically attached to the AFM tip. To check cell viability, the lacto-probe was first observed under bright field microscopy (supplemental Figure S1A), then labeled with carboxyfluorescein diacetate (CFDA), for which cells exhibiting an esterase activity are seen in green, thoroughly rinsed with MilliQ-grade water and reexamined under epifluorescence microscopy. *L. lactis* bacterial cells on the probe were shown to be viable, or at least esterase active (supplemental Figure S1B). Furthermore, after 2-h AFM force measurements, cells were still viable (data not shown).

Histograms of adhesion forces together with typical force-distance curves obtained when probing interactions between TIL448 bacterial cells and PGM-coated polystyrene are displayed in Figures 1B and 1C, respectively. The adhesion force and the repartition of the percentages corresponding to non-adhesive, non-specific adhesive and specific adhesive events are also summarized in Table 2, for one representative experiment. The muco-adhesive properties of TIL448 were clearly assessed with a low level of non-adhesive events (only 2 %) and a high proportion of specific ones (60 %). An adhesion force of 0.18 ± 0.04 nN was obtained. Rupture events were observed at short (100-200 nm) and long distances (up to 600-800 nm) (Figure 2A).

Noteworthy most *L. lactis* strains contain mobile genetic elements such as plasmids, responsible for the natural diversity among strains [27,28]. Thus, genetic determinants for the observed muco-adhesive phenotype of *L. lactis* TIL448 (e.g. genes encoding surface proteins) could be located on plasmids that are present in the strain. To verify this hypothesis, a plasmid-cured derivative TIL1230 [23] was tested for its muco-adhesive properties by force spectroscopy. SEM image of TIL1230 lacto-probe, histograms of adhesion forces and typical force-distance curves are displayed in Figures 1D, 1E and 1F, respectively. Note that, as for TIL448, bacterial cells attached to the AFM probe were viable before and after 2-h force measurements (supplemental Figure S2 and Figure S3, respectively). The adhesion force and the repartition of the percentages corresponding to non-adhesive, non-specific adhesive and

specific adhesive events are indicated in Table 2. The plasmid-cured TIL1230 strain exhibited an adhesion force of 0.09 ± 0.02 nN, 37 % of non-adhesive events and only 8 % of specific adhesive events, close to levels depicted for the low-adhesive control MG1820 [24]. Taken together, these results clearly demonstrated that the genetic determinants involved in the muco-adhesive phenotype of *L. lactis* TIL448 are plasmid-located.

Assessing with AFM the role of surface proteins in adhesion of *L. lactis* TIL448 to PGM under static conditions

Two genes encoding surface proteins and located on plasmids were previously identified in TIL448 [23]. These genes, named *yhgE2* and *muc*, encode a pilin and a mucus-binding protein, respectively. These two genes were previously inactivated in TIL448, leading to mutant strains TIL1289 (pilin mutant, devoid of pili) and TIL1290 (mucus-binding protein mutant), respectively (Table 1).

First, as for the wild-type strain (TIL448) and the plasmid-cured derivative (TIL1230), AFM force spectroscopy measurements were carried out on TIL1289 and TIL1290 mutants. Since both of them are erythromycin-resistant (see Table 1), we checked that the presence of erythromycin in the culture medium had no effect on adhesion of TIL448 to PGM. To this end, AFM force spectroscopy measurements on PGM coating were performed with a control erythromycin-resistant derivative of TIL448 (TIL1295) (Table 1). The histogram of adhesion forces was similar to that of TIL448 grown in the absence of antibiotic (data not shown).

Adhesion force levels for TIL1289 (pilin-mutant) and TIL1290 (mucus-binding protein mutant) were lower than that of the parental strain TIL448 (Table 2). Furthermore, the percentage of specific adhesive events was substantially reduced (26 % and 29 % for TIL1289 and TIL1290, respectively vs. 60 % for TIL448), which was correlated to a significant increase in the occurrence of non-adhesive events (31 % and 20 % for TIL1289 and TIL1290, respectively vs. 2 % for TIL448) (Table 2). The equivalent percentage of specific adhesive events, recorded for both variants, was a clear indication that pili and mucus-binding protein equally contribute to the muco-adhesive properties of TIL448, as probed with “static” AFM.

To deeper investigate mechanisms involved, rupture distances extracted from specific adhesive events were scrutinized. Corresponding histograms are presented in Figure 2. Interestingly, for wild-type TIL448, rupture events were observed at short (100-200 nm) and long distances (up to 600-800 nm) (Figure 2A) whereas for the pilin mutant (TIL1289), long-distance adhesive events were suppressed (Figure 2B). In contrast, for the mucus-binding protein mutant (TIL1290), short-distance adhesive events disappeared (Figure 2C). According to these results, we hypothesize that short-distance events reflect interactions of the mucus-binding protein with PGM whereas long-distance ones are rather representative of pili involvement.

Assessing with the shear-stress flow chamber the role of surface proteins in adhesion of *L. lactis* TIL448 to PGM under dynamic conditions

In parallel, to unravel the role of mucus-binding protein and pili under dynamic conditions, detachment of *L. lactis* from PGM coating was evaluated in a shear stress flow chamber, for the same strains as those tested above with "static" AFM force spectroscopy. Accordingly, bacterial cells attached to PGM coating were subjected to a stepwise increase in wall shear stress (0-80 Pa), under well-controlled hydrodynamics (laminar flow conditions). Cells are thus exposed to hydrodynamic drag and torque that both increase with applied wall shear stress [29]. The rate of bacteria removal directly correlates to their muco-adhesive behaviour.

The surface characteristics of the PGM-coated coupons were determined, in comparison with those of bare polystyrene. Surface wettability was first evaluated using the sessile drop technique. For the bare substratum, a water contact angle of 88.9° ± 2.9° was reached. After PGM adsorption, it dropped down to 73.7° ± 4.1°. An increase in hydrophilic properties was thus obtained, albeit at a lesser extent than that previously reported [25], probably due to differences in the elemental surface composition of polystyrene, as analyzed by X-ray photoelectron spectroscopy (data not shown). Then, XPS experiments were carried out to confirm the presence of adsorbed PGM. C1s and N1s core level spectra after PGM coating are displayed in supplemental Figure S4. Two C1s contributions, other than those specific to polystyrene, were observed [25]: one peak at 286.4 eV associated to C-O and/or C-N bonds and another one at 288.4 eV assigned to COOH or CONH compounds. Both peaks were characteristic of chemical groups present in the protein core and the glycan side chains of

PGM. The N1s signal, not detected for the bare substratum as expected. was composed of one peak at 400.4 eV, which was indicative of the PGM protein core [25]. Altogether, these results clearly demonstrated an efficient PGM adsorption onto polystyrene.

Detachment profiles (i.e. normalized surface coverage vs. applied wall shear stress) of wild-type TIL448, plasmid-cured TIL1290 and mutant TIL1289 and TIL1290 strains from the PGM-coated surfaces are presented in Figure 3. We should note that the surface wettability was evaluated before and after a thorough PBS washing in the flow chamber in a stepwise manner, with a 3-min duration for each wall shear stress step, tested in the range 0-80 Pa. Water contact angle remained the same (data not shown), indicating that no PGM desorption occurred, despite the high wall shear stresses applied. Detachment data were interpreted by evaluating three representative parameters [25]: $\tau_{W50\%}$ (wall shear stress needed to remove 50% of the bacterial cells initially attached to PGM coating), $\tau_{W5\%}$ (threshold value for bacterial cell detachment) and $\tau_{W90\%}$ (for evaluating the ability of quasi-complete detachment). Values obtained for all strains under study are reported in Table 3.

Shear-flow induced detachment of *L. lactis* from PGM coating was shown to be strongly strain-dependent (Figure 3). Wild-type TIL448 strain exhibited high PGM-adhesive properties, in contrast with its plasmid-cured derivative TIL1230, which was not able to adhere to PGM-coated polystyrene, even after 3-h contact time (data not shown). Indeed, for TIL448, the fraction of detached bacteria was low, even for increasing wall shear stress and, at the end of the experiment with a maximal wall shear stress of about 80 Pa, nearly 80% of the initial bacterial population remained attached to PGM coating (Figure 3). Such results are in good agreement with those previously described at the single-cell level and static conditions with AFM (see above). We also confirmed that the control TIL1295 exhibited the same muco-adhesive properties as TIL448 (data not shown).

Moreover, the respective role of *L. lactis* surface determinants involved in muco-adhesion was elucidated with the shear stress flow chamber, considering TIL1289 and TIL1290 mutants. Both mutants exhibited weaker adhesion than that of the wild type (Figure 3). Nevertheless, detachment profiles were quite different. Indeed, the fraction of detached cells was high for TIL1290 (mucus-binding protein mutant) throughout the experimental range whereas, for TIL1289 (pilin-mutant), cell removal was significantly lower. This was

confirmed by the analysis of $\tau_{W5\%}$, $\tau_{W50\%}$ and $\tau_{W90\%}$ values (Table 3). Indeed, $\tau_{W5\%}$ was the lowest for TIL1290 (i.e. no threshold) with close values for TIL448 and TIL1289 (0.2 ± 0.1 Pa against 10.1 ± 0.4 Pa and 12.9 ± 12.0 Pa for TIL1290, TIL448 and TIL1289, respectively) whereas, as expected, $\tau_{W50\%}$ was intermediate for TIL1289 (56.8 ± 8.6 Pa vs. 4.0 ± 2.2 Pa for TIL1290, not reached for TIL448). $\tau_{W90\%}$ reached 62.2 ± 2.4 Pa for TIL1290 (not reached for TIL1289 and TIL448). Taken together, these results indicate a more important contribution of the mucus-binding protein than pili in the muco-adhesive phenotype of *L. lactis*, as probed under shear flow.

Deciphering with AFM the role of mucin O-glycans in adhesion of *L. lactis* TIL448 to PGM

In order to get a deeper insight into the specificity of the adhesive events depicted for *L. lactis* TIL448, AFM blocking assays were carried out, first with free PGM (Figure 4). Subsequently, the TIL448 lacto-probe was incubated in PGM solution, before putting it in contact with the PGM-based coating. The number of curves showing adhesive events as well as the measured binding forces were dramatically reduced, indicating that the adhesion forces measured using the lacto-probe were specific to the *L. lactis*/PGM interaction. Indeed, on one representative experiment, the percentage of non-adhesive events substantially increased, from 2 % to 84 % (Figures 4A and 4B). The shape of force-distance curves after the lacto-probe incubation with free PGM (Figure 4D) confirmed the presence of non-adhesive events.

On this basis, further blocking assays were performed with total, acidic and neutral fractions of O-glycans, after their isolation and purification from PGM. Percentages of non-adhesive events after blocking with each tested fraction are displayed in Table 4. A substantial increase, compared to before-blocking conditions (2 %, see above), was systematically observed. Indeed, inhibition of adhesion with total O-glycans (76 ± 5 %) was of the same order of magnitude as the value reported for free PGM (80 ± 4 %). Moreover, the neutral oligosaccharidic fraction exerted a higher blocking effect than the acidic one (42 ± 10 % vs. 11 ± 5 %) (Table 4).

Discussion

The lacto-probe concept and the associated AFM measurements were applied to *L. lactis* subsp. *lactis* TIL448 and its derivatives for probing interaction mechanisms with the model mucin PGM. The shear stress flow chamber was then implemented for monitoring the shear-flow induced detachment of the same panel of *L. lactis* strains under laminar flow conditions. Data derived from a single-cell scale "static" method (AFM) vs. a multi-cellular scale "dynamic" one (flow chamber) were then combined to establish the role of mucus-binding protein and pili in *L. lactis* muco-adhesion.

For TIL448, an adhesion force of 0.18 ± 0.04 nN was reached, which is consistent with the value previously reported for *L. lactis* subsp. *cremoris* IBB477 (0.22 ± 0.05 nN) [21]. Further, such values may be related to the adhesive force recently reported for the specific interactions between a lectin-coated surface and the cell surface glycopolymers of the probiotic *Lactobacillus plantarum* (0.251 ± 0.146 nN) using single-cell force spectroscopy [30]. Moreover, as previously reported for *L. lactis* subsp. *cremoris* IBB477 [21,24], adhesion of *L. lactis* TIL448 to PGM was driven by an interplay between specific and non-specific forces. During AFM force spectroscopy, three representative curve shapes were obtained, as shown in supplemental Figure S5: (1) no adhesive event detected upon retraction of the tip from the PGM-coated surface; (2) non-specific adhesive events (showing no extension before rupture) corresponding to hydrophobic, electrostatic, or Lifshitz-van der Waals interactions; and (3) one, two, or three specific adhesive events, occurring at several nanometers after the contact point. Such multiple adhesive events, attributed to specific interactions involving ligand-receptor bonding, like here cell surface protein/sugar complexes [21], were recently more deeply investigated using AFM tips functionalized with different types of lectin, in contact with purified PGM [31]. For TIL448, 60% of the force curves were assigned to specific adhesive events, which was significantly higher than the value previously reported for IBB477 (20% [21]). We should also note that the inhibition percentage achieved during blocking tests with total O-glycans was higher than that obtained for IBB477 (mean value of 76 % against 48 %, for TIL448 and IBB477 [21], respectively), probably due to differences between these two strains in terms of type and characteristics of cell surface proteins involved in muco-adhesion. However, no data are to date available for *L. lactis* IBB477.

With the use of two targeted defective-mutants, the role of both mucus-binding protein and pili in adhesion of TIL448 to PGM was clearly established. Their contribution was shown to be equivalent, as "sensed" under AFM static conditions, since nearly identical percentages of specific adhesive events were reached (26 % and 29 % for the pilin and mucus-binding protein mutants, respectively). This conclusion is reinforced by the adhesion force values which were quite similar between both mutants (0.10 ± 0.03 nN and 0.12 ± 0.04 nN for the pilin and mucus-binding protein mutants, respectively), in comparison with the wild-type strain (0.18 ± 0.04 nN). Such force levels are consistent with the mean rupture force of 95 pN, reported for type-IV piliated *Pseudomonas aeruginosa* cell probe in contact with mica [32]. Elsewhere, the retraction forces for type-IV pili of *Neisseria gonorrhoeae*, as determined by optical tweezers, reached 0.11 ± 0.03 nN [33].

All these results were supported by the further analysis of the bond-rupture distance, which is defined as the distance from the start of retraction to the point of final rupture. This essentially corresponds to the distance between the AFM tip and the substrate when the ligand-receptor complex is fully extended. For wild-type TIL448, we observed rupture events at short (100-200 nm) and long distances (up to 600-800 nm). The short rupture distances, observed with the wild-type strain and further confirmed with the pilin mutant (TIL1289), undoubtedly reflect interactions between the mucus-binding protein present on the *L. lactis* cell wall with sugars of PGM (see below). The existence of long rupture distances, also detected with the mucus-binding protein mutant (TIL1290), is indeed consistent with the elongated architecture of pili [34,35]. In the AFM study probing interactions between type-IV piliated *P. aeruginosa* and mica surface [32], the authors observed long rupture distances (up to 1 µm). When they tested the non-piliated mutant, rupture lengths were drastically reduced (10 to 100 nm), which is fully consistent with our own results. The presence of pili and related muco-adhesion properties were previously reported in *L. rhamnosus* GG [15,36]. Such properties are expected to confer to *L. rhamnosus* GG a distinct advantage over non-piliated probiotics for maintaining stable, or at least, extended residence within the gastrointestinal tract [36].

Parallel to AFM measurements, muco-adhesion of *L. lactis* was evaluated under well-defined flow field conditions, which are more relevant from a physiological point of view. Dynamic conditions are indeed encountered in many compartments within the gastrointestinal tract (e.g. shear fluctuations caused by salivary washing or intestinal peristalsis [37]). The effect of

shear stress on the adhesion of bacteria, yeast cells and colloidal particles has been addressed in numerous works, using specially-dedicated laminar flow chambers. A decrease in the total number of adhesion events as a function of shear has often been depicted [25,29,38-40]. However, to our knowledge, data on the use of flow-induced shear forces to probe bacterial muco-adhesion are scarce. Likewise, no study has previously evaluated how muco-adhesion may be modulated by cell surface proteins (as here, mucus-binding protein and pili), separately in mutants and in combination within the wild-type strain. Indeed, we observed that an increase in the wall shear stress facilitated *L. lactis* bacterial cell detachment, albeit at a variable extent depending on the strain under study. In contrast with AFM results, a more important contribution of the mucus-binding protein than pili in the muco-adhesive phenotype of *L. lactis* was assessed under shear flow. Nevertheless, worth mentioning is the different mode used for both methods for probing the force, as pointed out by Xu *et al*. [41]: with AFM, the tip of the cantilever pushes the bacteria cells against the surface and then bring them away, normal to the surface. In contrast, the flow-chamber method operates under "mild conditions" using the drag force to detach cells, parallel to the surface, mainly *via* rolling [26]. During AFM measurements, all the individual surface determinants acting against detachment are stressed together while, with the second method, only a part of them located at the trailing edge of the bacterial cell dissociate, described as a peeling process [42]. The weaker adhesion under shear flow of the piliated mutant (TIL1290), compared to its non-piliated counterpart (TIL1289), could be related to the presence of long pili (rupture events up to 600-800 nm, as found with AFM), which prevented, through steric repulsions, maximum contact of *L. lactis* bacterial cells with PGM coating. In their study on adhesion of the Gram-negative *Xylella fastidiosa* bacteria (possessing both type-I and type-IV pili) to glass, based on the use of a microfluidic flow chamber in conjunction with the wild-type strain and two pilus-defective mutants, De la Fuente *et al.* [43] reported the tendency of the mutant with the longer type-IV pili to require lower drag forces for detachment from the substratum compared to results obtained with the other mutant only exhibiting short type-I pili. However, in the case of Gram-positive bacteria, pili have been shown to be extremely flexible [44] albeit inextensible structures [45]. Therefore, they would not be a large obstacle to get close to the substratum but could not withstand the drag force due to their inextensibility. Another possible explanation of weak adhesion of the piliated mutant under shear flow would be the low density of pili present at the cell surface for TIL448 [23]. The wild-type TIL448 adhered much better to PGM than the two mutants, showing that the co-expression of both short and long structures is required, as was alluded to previous work [43].

In addition, blocking assays with free PGM or with total, acidic and neutral fractions of O-glycans purified from PGM demonstrated that neutral oligosaccharides play a major role in interactions between PGM and *L. lactis* TIL448, with a percentage of non-adhesive events of 42 ± 10 % after blocking against 11 ± 5 % for the acidic fraction. We established the profiles of neutral and acidic O-glycans isolated from PGM. As revealed by MALDI-MS analysis of the released glycans, PGM is substituted by a complex mixture of neutral and sulfated glycans, with size ranging from two to twelve monosaccharides (Table 5). Nordman *et al.* [46] showed that pig gastric mucus contains a number of distinctly different mucin populations varying in buoyant density, size, "acidity", glycosylation, sulphation and tissue origin. Furthermore, the glycan composition that we observed is fully in agreement with previous studies reporting the prevalence of LacNAc-based O-glycans partially fucosylated in α1,2 on Gal residues and sulfated in 1,6 position of GlcNAc residues [47,48].

In agreement with the above findings, the TIL448 plasmid-encoded tip pilin, probably located at the extremity of the pili appendages, contains a lectin-type domain (PF00139 or *Lectin_leg* domain) characteristic of leguminous lectins, which bind typically hexoses and/or hexosamines [49], as found here for the neutral O-glycan fraction of PGM (Table 5). In addition, since fucose was identified in many of the neutral oligosaccharides (Table 5), it could be involved in the interactions between PGM and the mucus-binding protein of *L. lactis* TIL448. To support this hypothesis, in a previous work on *Lactobacillus reuteri* [9], the mucus-binding protein was shown to recognize carbohydrate structures in mucus and fucose could be part of the recognized structure. Further, the Fuc-binding lectin (*Ulex europaeus* agglutinin I (UEA)) was found to exhibit the strongest affinity for purified PGM compared to Gal-binding lectins (namely, *Ricinus communis* agglutinin I (RCA) and peanut (*Arachis hypogaea*) agglutinin (PNA)) [31].

In conclusion, this work was focused on the muco-adhesive phenotype of the vegetal isolate *L. lactis* subsp. *lactis* TIL448 at multi-scale, by coupling AFM force spectroscopy and shear stress flow chamber. Using the wild-type strain, in conjunction with pilin and mucus-binding protein defective mutants, the combined role played by both surface proteins was established, with a contribution closely depending on how interactions are probed. The importance of the sugar receptors of PGM, mainly of neutral type, was also demonstrated. The need for well-

controlled hydrodynamics was highlighted, especially when shear-flow sensitive appendages like pili are involved. We hope that these findings on *L. lactis* muco-adhesion will lead to a better understanding of interactions of this LAB with the mucosal environment in the gastrointestinal tract, further offering novel strategies for medical and food-related applications.

Acknowledgements

This work was supported by INRA (CEPIA and MICA Departments) through the doctoral grant of Doan Thanh Lam Le (2008-2011). Thi-Ly Tran was recipient of a Ph.D. grant from the University of Science and Technology of Hanoi (USTH), Vietnam. The authors wish to thank Sandrine Zanna (Laboratoire de Physico-Chimie des Surfaces, Paris, France) for XPS measurements. Thanks are also due to Mélodie Goin (MICALIS, Jouy-en-Josas, France) for her technical support.

References

1. Bergstrom KS, Kissoon-Singh V, Gibson DL, Ma C, Montero M, et al. (2010) Muc2 protects against lethal infectious colitis by disassociating pathogenic and commensal bacteria from the colonic mucosa. PLoS Pathog 6: e1000902.
2. Bansil R, Turner BS (2006) Mucin structure, aggregation, physiological functions and biomedical applications. Curr Opin Colloid Interf Sci 11: 164-170.
3. Juge N (2012) Microbial adhesins to gastrointestinal mucus. Trends Microbiol 20: 30-39.
4. Johansson MEV, Holmén Larsson JM, Hansson GC (2010) The two mucus layers of colon are organized by the MUC2 mucin, whereas the outer layer is a legislator of host–microbial interactions. PNAS.
5. Tuomola EM, Ouwehand AC, Salminen SJ (2000) Chemical, physical and enzymatic pre-treatments of probiotic lactobacilli alter their adhesion to human intestinal mucus glycoproteins. Int J Food Microbiol 60: 75-81.
6. Ouwehand AC, Tuomola EM, Tolkko S, Salminen S (2001) Assessment of adhesion properties of novel probiotic strains to human intestinal mucus. Int J Food Microbiol 64: 119-126.
7. Uchida H, Fujitani K, Kawai Y, Kitazawa H, Horii A, et al. (2004) A new assay using surface plasmon resonance (SPR) to determine binding of the *Lactobacillus acidophilus* group to human colonic mucin. Biosci Biotechnol Biochem 68: 1004-1010.
8. Kinoshita H, Uchida H, Kawai Y, Kitazawa H, Miura K, et al. (2007) Quantitative evaluation of adhesion of lactobacilli isolated from human intestinal tissues to human colonic mucin using surface plasmon resonance (BIACORE assay). J Appl Microbiol 102: 116-123.
9. Roos S, Jonsson H (2002) A high-molecular-mass cell-surface protein from *Lactobacillus reuteri* 1063 adheres to mucus components. Microbiology 148: 433-442.
10. Buck BL, Altermann E, Svingerud T, Klaenhammer TR (2005) Functional analysis of putative adhesion factors in *Lactobacillus acidophilus* NCFM. Appl Environ Microbiol 71: 8344-8351.
11. Pretzer G, Snel J, Molenaar D, Wiersma A, Bron PA, et al. (2005) Biodiversity-based identification and functional characterization of the mannose-specific adhesin of *Lactobacillus plantarum*. J Bacteriol 187: 6128-6136.
12. Mackenzie DA, Jeffers F, Parker ML, Vibert-Vallet A, Bongaerts RJ, et al. (2010) Strain-specific diversity of mucus-binding proteins in the adhesion and aggregation properties of *Lactobacillus reuteri*. Microbiology 156: 3368-3378.
13. Boekhorst J, Helmer Q, Kleerebezem M, Siezen RJ (2006) Comparative analysis of proteins with a mucus-binding domain found exclusively in lactic acid bacteria. Microbiology 152: 273-280.
14. Kleerebezem M, Hols P, Bernard E, Rolain T, Zhou M, et al. (2010) The extracellular biology of the lactobacilli. FEMS Microbiol Rev 34: 199-230.
15. Kankainen M, Paulin L, Tynkkynen S, von Ossowski I, Reunanen J, et al. (2009) Comparative genomic analysis of *Lactobacillus rhamnosus* GG reveals pili containing a human-mucus binding protein. PNAS 106: 17193-17198.
16. Finegold S, Sutter V, Mathisen G (1983) Human intestinal microflora in health and disease; DJ H, editor. New York: Academic Press.
17. Boguslawska J, Zycka-Krzesinska J, Wilcks A, Bardowski J (2009) Intra- and interspecies conjugal transfer of Tn916-like elements from *Lactococcus lactis* in vitro and in vivo. Appl Environ Microbiol 75: 6352-6360.
18. Wang Y, Wang J, Dai W (2011) Use of GFP to trace the colonization of *Lactococcus lactis* WH-C1 in the gastrointestinal tract of mice. Journal of microbiological methods 86: 390-392.
19. Giaouris E, Chapot-Chartier MP, Briandet R (2009) Surface physicochemical analysis of natural *Lactococcus lactis* strains reveals the existence of hydrophobic and low charged strains with altered adhesive properties. Int J Food Microbiol 131: 2-9.
20. Passerini D, Beltramo C, Coddeville M, Quentin Y, Ritzenthaler P, et al. (2010) Genes but not genomes reveal bacterial domestication of *Lactococcus lactis*. PLoS One 5: e15306.

21. Le D-T-L (2011) Identification et caractérisation des déterminants physico-chimiques et biologiques mis en jeu dans l'adhésion de Lactococcus lactis à la mucine modèle PGM. Toulouse: INSA
22. Le DT, Zanna S, Frateur I, Marcus P, Loubiere P, et al. (2012) Real-time investigation of the muco-adhesive properties of *Lactococcus lactis* using a quartz crystal microbalance with dissipation monitoring. Biofouling 28: 479-490.
23. Oxaran V, Ledue-Clier F, Dieye Y, Herry JM, Pechoux C, et al. (2012) Pilus biogenesis in *Lactococcus lactis*: molecular characterization and role in aggregation and biofilm formation. PLoS One 7: e50989.
24. Dague E, Le DT, Zanna S, Marcus P, Loubiere P, et al. (2010) Probing in vitro interactions between *Lactococcus lactis* and mucins using AFM. Langmuir 26: 11010-11017.
25. Mercier-Bonin M, Duviau MP, Ellero C, Lebleu N, Raynaud P, et al. (2012) Dynamics of detachment of *Escherichia coli* from plasma-mediated coatings under shear flow. Biofouling 28: 881-894.
26. Mercier-Bonin M, Dehouche A, Morchain J, Schmitz P (2011) Orientation and detachment dynamics of Bacillus spores from stainless steel under controlled shear flow: modelling of the adhesion force. Int J Food Microbiol 146: 182-191.
27. Siezen RJ, Bayjanov JR, Felis GE, van der Sijde MR, Starrenburg M, et al. (2011) Genome-scale diversity and niche adaptation analysis of *Lactococcus lactis* by comparative genome hybridization using multi-strain arrays. Microb Biotechnol 4: 383-402.
28. van Hylckama Vlieg JE, Rademaker JL, Bachmann H, Molenaar D, Kelly WJ, et al. (2006) Natural diversity and adaptive responses of *Lactococcus lactis*. Curr Opin Biotechnol 17: 183-190.
29. Lorthois S, Schmitz P, Angles-Cano E (2001) Experimental study of fibrin/fibrin-specific molecular interactions using a sphere/plane adhesion model. J Colloid Interface Sci 241: 52-62.
30. Beaussart A, El-Kirat-Chatel S, Herman P, Alsteens D, Mahillon J, et al. (2013) Single-Cell Force Spectroscopy of Probiotic Bacteria. Biophys J 104: 1886-1892.
31. Gunning AP, Kirby AR, Fuell C, Pin C, Tailford LE, et al. (2013) Mining the "glycocode"--exploring the spatial distribution of glycans in gastrointestinal mucin using force spectroscopy. FASEB journal : official publication of the Federation of American Societies for Experimental Biology 27: 2342-2354.
32. Touhami A, Jericho MH, Boyd JM, Beveridge TJ (2006) Nanoscale characterization and determination of adhesion forces of *Pseudomonas aeruginosa* pili by using atomic force microscopy. J Bacteriol 188: 370-377.
33. Maier B, Potter L, So M, Long CD, Seifert HS, et al. (2002) Single pilus motor forces exceed 100 pN. PNAS 99: 16012-16017.
34. Mandlik A, Swierczynski A, Das A, Ton-That H (2008) Pili in Gram-positive bacteria: assembly, involvement in colonization and biofilm development. Trends Microbiol 16: 33-40.
35. Proft T, Baker E (2009) Pili in Gram-negative and Gram-positive bacteria — structure, assembly and their role in disease. Cell Mol Life Sci 66: 613-635.
36. von Ossowski I, Reunanen J, Satokari R, Vesterlund S, Kankainen M, et al. (2010) Mucosal adhesion properties of the probiotic *Lactobacillus rhamnosus* GG SpaCBA and SpaFED pilin subunits. Appl Environ Microbiol 76: 2049-2057.
37. Jeffrey B, Udaykumar HS, Schulze KS (2003) Flow fields generated by peristaltic reflex in isolated guinea pig ileum: impact of contraction depth and shoulders. Am J Physiol Gastrointest Liver Physiol 285: G907-G918.
38. Pierres A, Touchard D, Benoliel AM, Bongrand P (2002) Dissecting streptavidin-biotin interaction with a laminar flow chamber. Biophys J 82: 3214-3223.
39. Mercier-Bonin M, Adoue M, Zanna S, Marcus P, Combes D, et al. (2009) Evaluation of adhesion force between functionalized microbeads and protein-coated stainless steel using shear-flow-induced detachment. J Colloid Interface Sci 338: 73-81.
40. Nejadnik MR, van der Mei HC, Busscher HJ, Norde W (2008) Determination of the shear force at the balance between bacterial attachment and detachment in weak-adherence systems, using a flow displacement chamber. Appl Environ Microbiol 74: 916-919.

41. Xu CP, Boks NP, de Vries J, Kaper HJ, Norde W, et al. (2008) *Staphylococcus aureus*-fibronectin interactions with and without fibronectin-binding proteins and their role in adhesion and desorption. Appl Environ Microbiol 74: 7522-7528.
42. Décavé E, Garrivier D, Brechet Y, Bruckert F, Fourcade B (2002) Peeling process in living cell movement under shear flow. Phys Rev Lett 89: 108101.
43. De La Fuente L, Montanes E, Meng Y, Li Y, Burr TJ, et al. (2007) Assessing adhesion forces of type I and type IV pili of *Xylella fastidiosa* bacteria by use of a microfluidic flow chamber. Appl Environ Microbiol 73: 2690-2696.
44. Castelain M, Koutris E, Andersson M, Wiklund K, Bjornham O, et al. (2009) Characterization of the biomechanical properties of T4 pili expressed by Streptococcus pneumoniae--a comparison between helix-like and open coil-like pili. Chemphyschem 10: 1533-1540.
45. Alegre-Cebollada J, Badilla CL, Fernandez JM (2010) Isopeptide bonds block the mechanical extension of pili in pathogenic Streptococcus pyogenes. J Biol Chem 285: 11235-11242.
46. Nordman H, Davies JR, Herrmann A, Karlsson NG, Hansson GC, et al. (1997) Mucus glycoproteins from pig gastric mucosa: identification of different mucin populations from the surface epithelium. Biochem J 326 (Pt 3): 903-910.
47. Karlsson NG, Nordman H, Karlsson H, Carlstedt I, Hansson GC (1997) Glycosylation differences between pig gastric mucin populations: a comparative study of the neutral oligosaccharides using mass spectrometry. Biochem J 326 (Pt 3): 911-917.
48. Tsubokawa D, Goso Y, Sawaguchi A, Kurihara M, Ichikawa T, et al. (2007) A monoclonal antibody, PGM34, against 6-sulfated blood-group H type 2 antigen, on the carbohydrate moiety of mucin. The FEBS journal 274: 1833-1848.
49. Sharon N, Lis H (1990) Legume lectins--a large family of homologous proteins. The FASEB Journal 4: 3198-3208.

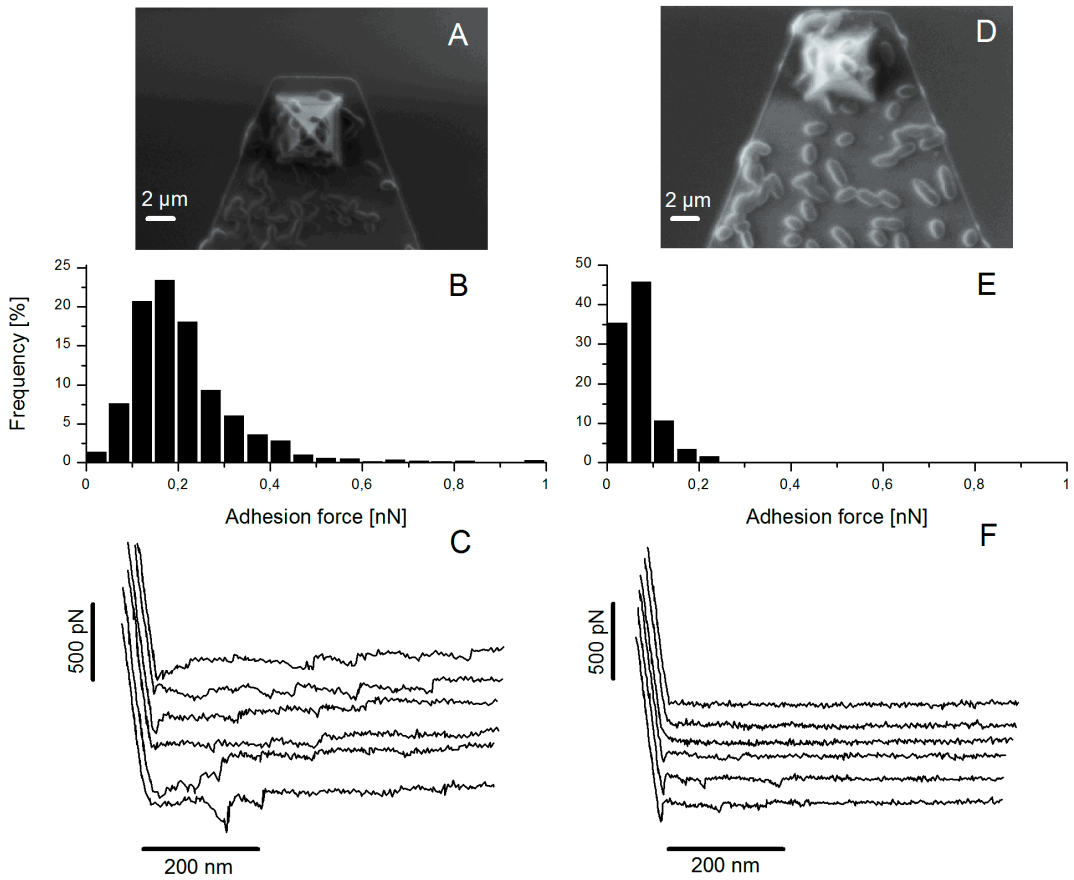

Figure 1. **AFM force spectroscopy for the wild-type TIL448 and the plasmid-cured derivative TIL1230.**

(A, D) Representative SEM images of *L. lactis* bacterial cells immobilized onto AFM tip and cantilever; (B, E) histograms of adhesion forces and (C, F) typical force-distance curves obtained when probing interactions between the wild-type TIL448 (A, B, C) and the plasmid-cured derivative TIL1230 (D, E, F) and PGM-coated polystyrene using AFM force spectroscopy in milliQ-grade water. One representative experiment (1024 force curves) is shown.

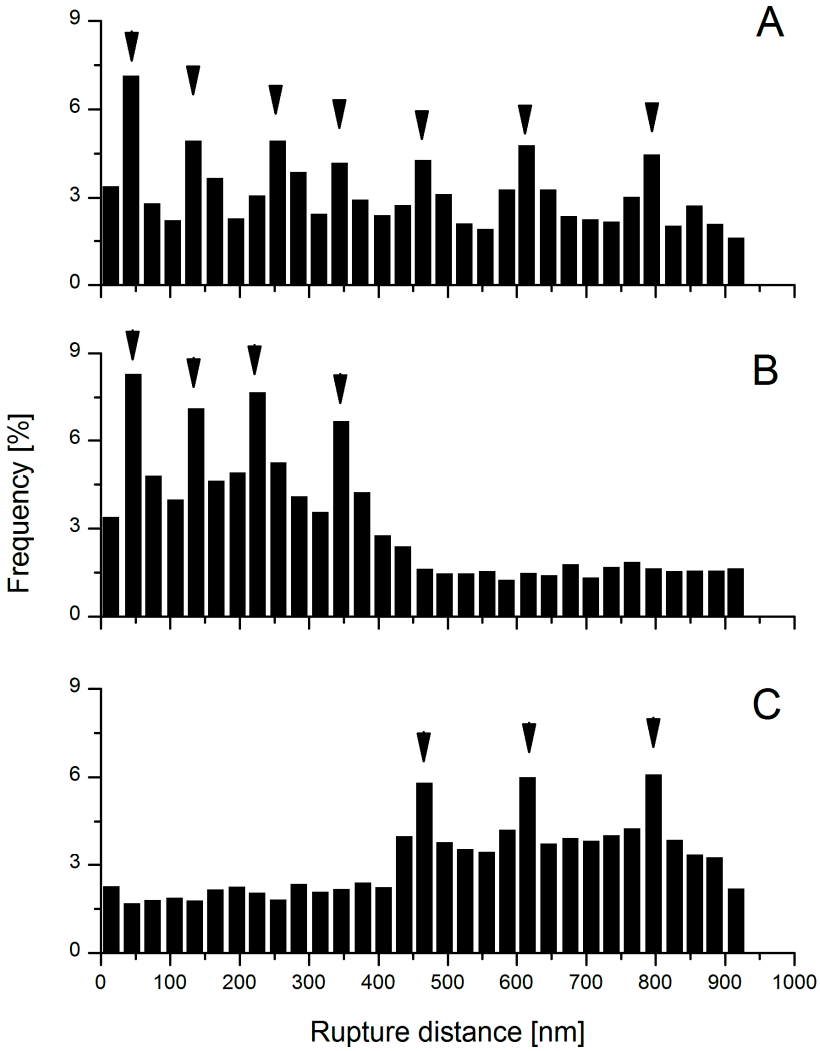

Figure 2. **Rupture distances for the wild-type TIL448, the pilin mutant TIL1289 and the mucus-binding protein mutant TIL1290.**

Histograms of rupture distances corresponding to specific adhesive events for (A) wild-type TIL448; (B) pilin mutant TIL1289 and (C) mucus-binding protein mutant TIL1290 for one representative experiment (1024 force curves). Some typical rupture distances are indicated by arrows

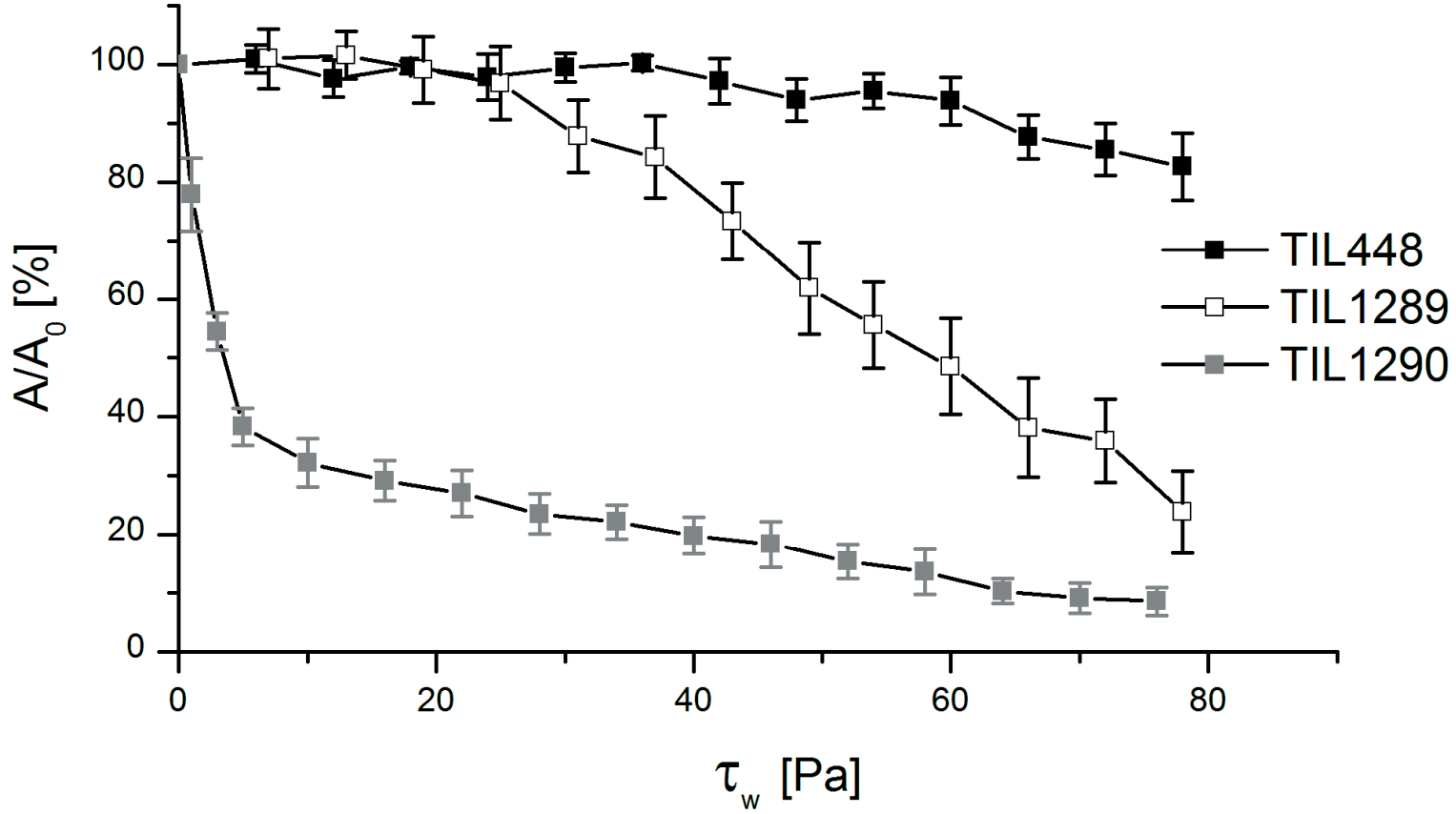

Figure 3. Detachment under shear flow of the wild-type TIL448, the pilin mutant TIL1289 and the mucus-binding protein mutant TIL1290.

Shear-flow induced detachment profiles of *L. lactis* bacterial cells attached to PGM-coated polystyrene in PBS; wild-type TIL448 (black square); pilin mutant TIL1289 (white square) and mucus-binding protein mutant TIL1290 (light grey square). The given results are the average values and standard deviations over at least three different coupons and independently grown cultures.

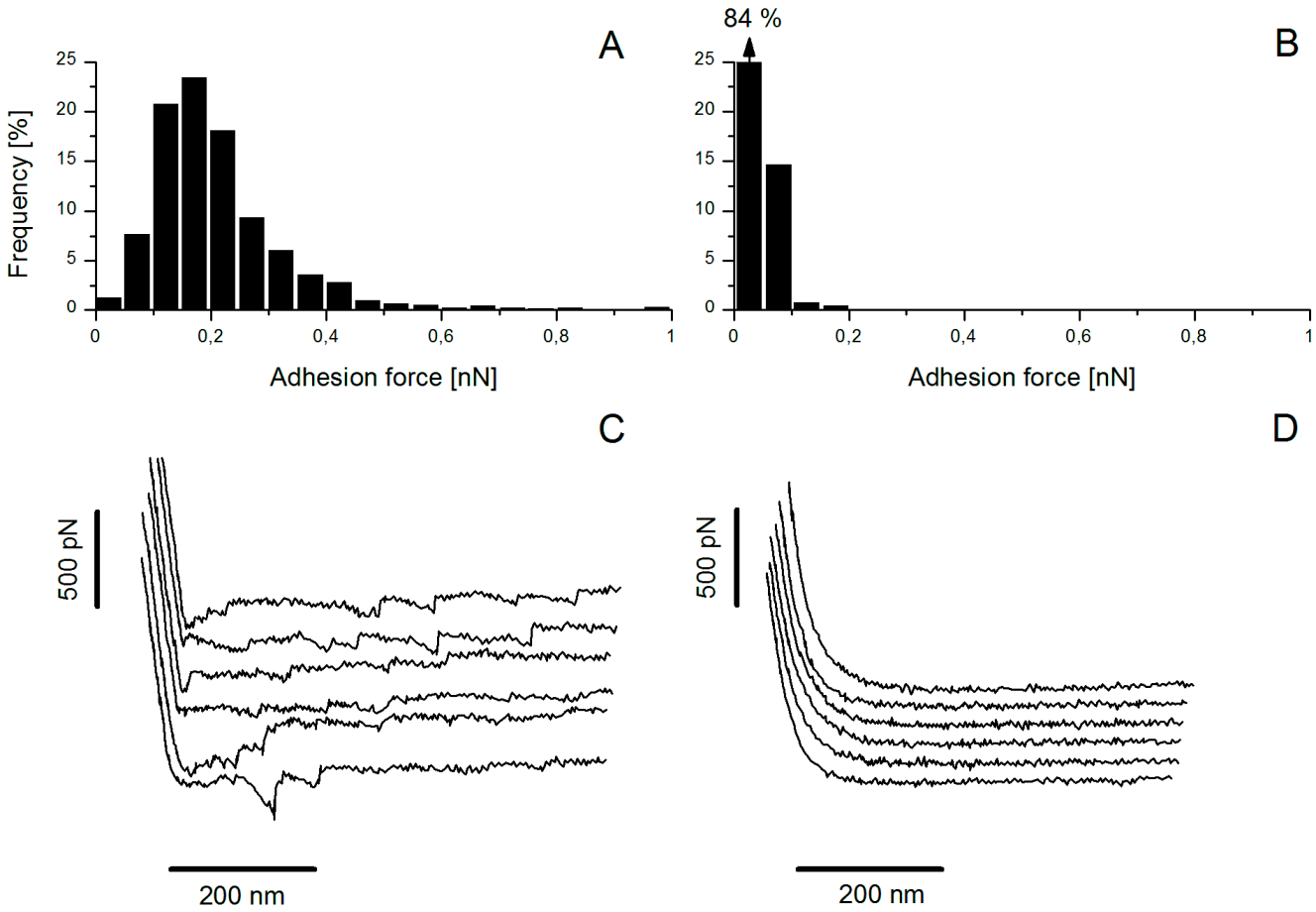

Figure 4. AFM blocking assays with free PGM for the wild-type TIL448.

(A, B) Histograms of adhesion forces and (C, D) typical force-distance curves for wild-type TIL448 lacto-probe in interaction with PGM-coated polystyrene, using AFM force spectroscopy in milliQ-grade water, before (A, C) and after (B, D) incubation with free PGM. One representative experiment (1024 force curves) is shown.

SUPPLEMENTATRY DATA

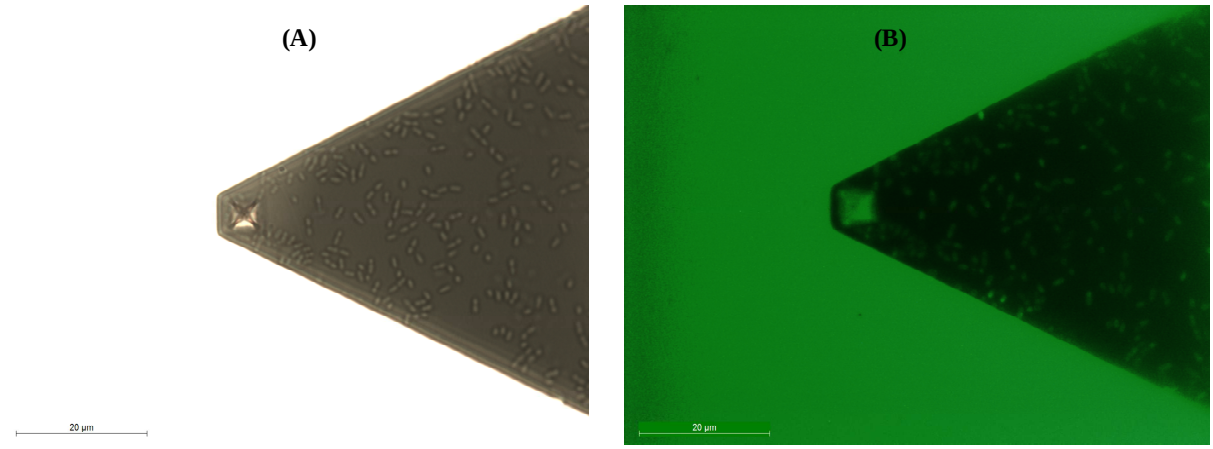

Figure S1. Fluorescence images of the biologically functionalized AFM probe, for *L. lactis* TIL448 cells immobilized onto AFM tip and cantilever. (A) Bright-field microscopy image of the TIL448 lacto-probe (total bacterial cells attached). (B) Fluorescence image of the TIL448 lacto-probe after CFDA labeling. Viable cells are seen in green. Scale bar: 20 µm.

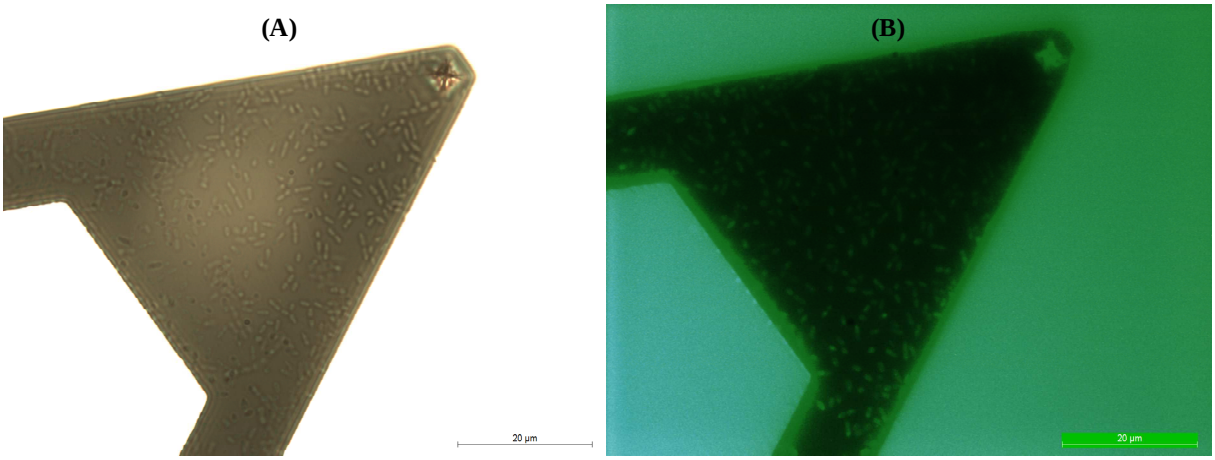

Figure S2. Fluorescence images of the biologically functionalized AFM probe, for *L. lactis* TIL1230 cells immobilized onto AFM tip and cantilever. (A) Bright-field microscopy image of the TIL1230 lacto-probe (total bacterial cells attached). (B) Fluorescence image of the TIL1230 lacto-probe after CFDA labeling. Viable cells are seen in green. Scale bar: 20 µm.

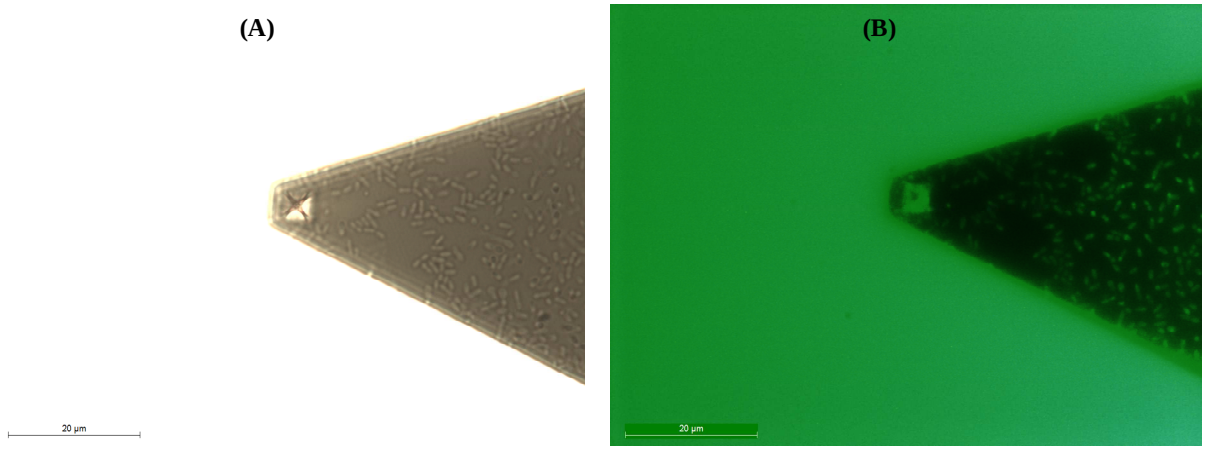

Figure S3. Fluorescence images of the biologically functionalized AFM probe, for *L. lactis* TIL1230 cells immobilized onto AFM tip and cantilever, and imaged after 2 hours of force measurements. (A) Bright-field microscopy image of the TIL1230 lacto-probe (total bacterial cells attached). (B) Fluorescence image of the TIL1230 lacto-probe after 2-h force measurements and CFDA labeling. Scale bar: 20 µm.

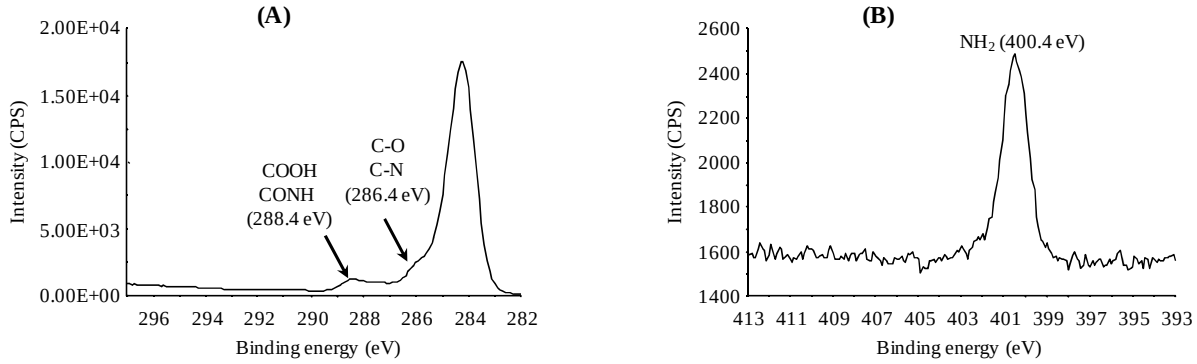

Figure S4. (A) C1s core-level spectrum and (B) N1s core-level spectrum recorded by XPS for PGM-coated polystyrene surface. Chemical groups representative of PGM (protein core and glycan side chains) are indicated, together with their binding energy.

Table 1. Bacterial strains used in this study.

Strain	Characteristics	Source
TIL448	*L. lactis* subsp. *lactis* NCDO2110, isolated from peas	INRA collection
TIL1230	Derivative of TIL448 obtained after curing plasmids by acridine orange treatment	M.-P. Chapot-Chartier[a]
TIL1289	Ery^R; pilin mutant of TIL448 obtained by disruption of *yhgE2* gene encoding the major pilin, with the use of thermosensitive plasmid pGhost 9	M.-P. Chapot-Chartier[a]
TIL1290	Ery^R; mucus-binding protein mutant of TIL448 obtained by disruption of *muc* gene encoding a mucus-binding protein, with the use of thermosensitive plasmid pGhost 9	M.-P. Chapot-Chartier[a]
TIL1295	Ery^R; control strain TIL448 containing empty plasmid pGKV259	M.-P. Chapot-Chartier[a]

[a]Micalis, INRA, Jouy-en-Josas, France

Table 2. Adhesion forces and percentage of non-adhesive, non-specific adhesive and specific adhesive events obtained using AFM force spectroscopy in milliQ-grade water on TIL448, TIL1230, TIL1289 and TIL1290 lacto-probes in contact with PGM-coated polystyrene.

		TIL448 (wild-type)	**TIL1230** (plasmid-cured)	**TIL1289** (pilin minus)	**TIL1290** (mucus-binding protein minus)
Force (nN)		0.18 ± 0.04	0.09 ± 0.02	0.10 ± 0.03	0.12 ± 0.04
Percentage of events	NA[a]	2 %	37 %	31 %	20 %
	NSA[b]	38 %	55 %	43 %	51 %
	SA[c]	60 %	8 %	26 %	29 %

[a] NA: non-adhesive event
[b] NSA: non-specific adhesive event
[c] SA: specific adhesive event

Table 3. $\tau_{W5\%}$, $\tau_{W50\%}$ and $\tau_{W90\%}$ values (Pa) obtained in the shear stress flow chamber for *L. lactis* bacterial cells attached to PGM coating in PBS. The given results are the average values and standard deviations over at least three different PGM-coated coupons and independently grown cultures.

	TIL448 (wild-type)	**TIL1289** (pilin minus)	**TIL1290** (mucus-binding protein minus)	**TIL1230** (plasmid-cured)
$\tau_{W5\%}$ (Pa)	10.1 ± 0.4	12.9 ± 12.0	0.2 ± 0.1	No adhesion
$\tau_{W50\%}$ (Pa)	Not reached	56.8 ± 8.6	4.0 ± 2.2	
$\tau_{W90\%}$ (Pa)	Not reached	Not reached	62.2 ± 2.4	

Table 4. AFM blocking assays with PGM or O-glycan fractions (total, acidic, neutral) purified from PGM for *L. lactis* TIL448 lacto-probe in contact with PGM-coated polystyrene in milliQ-grade water. The given results are the average values and standard deviations over five independent PGM-coated coupons and lacto-probes. Before blocking, the percentage of non-adhesive events for *L. lactis* TIL448 was 2 % (see in the Results section).

Solution	PGM	Total O-glycans	Acidic fraction	Neutral fraction
Percentage of NA[a] events after blocking	80 ± 4 %	76 ± 5 %	11 ± 5 %	42 ± 10 %

[a] NA: non-adhesive

Table 5. Compositions of (A) neutral and (B) acidic fractions of O-glycans released from PGM. Monosaccharide composition of individual glycans was established by MALDI-TOF-MS based on the m/z values of monosaccharides. Nature of monosaccharides (Gal, GlcNAc and Fuc) was based on GC composition analysis and on previous reports [47]. *m/z* values of neutral and sialylated glycans correspond to $[M+Na]^+$ adducts whereas sulphated glycans exhibited $[M+2Na-H]^+$ adducts.

(A)

m/z	GalNAc-ol	Gal	GlcNAc	Fuc
408	1	1	0	0
449	1	0	1	0
554	1	1	0	1
611	1	1	1	0
757	1	1	1	1
773	1	2	1	0
814	1	1	2	0
919	1	2	1	1
976	1	2	2	0
1017	1	1	3	0
1065	1	2	1	2
1122	1	2	2	1
1138	1	3	2	0
1179	1	2	3	0
1284	1	3	2	1
1325	1	2	3	1
1430	1	3	2	2
1471	1	2	3	2
1487	1	3	3	1
1544	1	3	4	0
1585	1	3	5	0
1633	1	3	3	2
1649	1	4	3	1
1690	1	3	4	1
1706	1	4	4	0
1747	1	3	5	0
1795	1	4	3	2
1836	1	3	4	2
1852	1	4	4	1
1894	1	3	5	1
1910	1	4	5	0
1942	1	4	3	3
1999	1	4	4	2
2040	1	3	5	2
2056	1	4	5	1
2114	1	2	4	5
2161	1	5	4	2
2202	1	4	5	2
2217	1	5	5	1
2260	1	4	6	1

(B)

m/z	GalNAc-ol	Gal	GlcNAc	Fuc	Neu5Ac	SO_3
902	1	1	1	0	1	0
1078	1	2	2	0	0	1
1021	1	2	1	1	0	1
1224	1	2	2	1	0	1
1281	1	2	3	0	0	1
1370	1	2	2	2	0	1
1386	1	3	2	1	0	1
1427	1	2	3	1	0	1
1532	1	3	2	2	0	1
1573	1	2	3	2	0	1
1589	1	3	3	1	0	1
1735	1	3	3	2	0	1
1751	1	4	3	1	0	1
1898	1	4	3	2	0	1
1955	1	4	4	1	0	1

1.2. Further investigations on the migration ability of *L. lactis* inside PGM-based hydrogels

1.2.1. Connecting adhesion of *L. lactis* to PGM to its migration inside PGM-based hydrogels: introduction of the DFT method

In the previous section, the adhesion of the vegetal *L. lactis* subsp. *lactis* isolate TIL448 to the model mucin PGM was clearly established by combining single-cell scale and static (AFM) vs. multi-cellular and dynamic (SSFC) conditions. The respective role exerted by the surface mucus-binding protein and pili in TIL448 adhesion to PGM was elucidated, with a contribution closely depending on the static or dynamic nature of the environment and how interactions are probed. The next step was to connect muco-adhesion of *L. lactis* to its migration inside mucin gels by addressing the following questions: what is the diffusivity of *L. lactis* in mucin gels? How do muco-adhesion properties influence bacterial migration through mucin gels? To address these questions, which have never been investigated in the literature, the migration ability of *L. lactis* inside PGM-based hydrogels was characterized, using the same panel of strains as that previously tested, i.e. the wild type strain, its plasmid-free derivative and the two defective-mutants. A novel method, named Diffusion Front Tracking (DFT) was implemented in the present study. This technique was recently developed in the team "Transfert, Interface, Mélange" of "Laboratoire d'Ingénierie des Systèmes Biologiques et des Procédés" for O_2 diffusion coefficient measurements in liquids (Jimenez *et al.* 2013). The diffusivity of bacterial cells was thus determined, based on evaluating the displacement of a bacteria front diffusing from the flat bacteria/PGM hydrogel interface in a Hele-Shaw chamber (Hele-Shaw 1898).

L. lactis bacterial cells had to be enough concentrated (see part 1.2.3.3) and also stained with the magenta dye fuchsine in order to properly visualize and track the diffusion front of bacteria inside PGM hydrogels. Fuchsine stains the cytoplasm of the bacteria cells, causing a pink suspension and allowing to record the bacteria migration through the colourless PGM. Fuchsine dye has been extensively used for revealing bacterial cell structures (Maneval 1941), in particular flagella and capsules (Leifson 1930, Mayfield and Inniss 1977). The effect of such fuchsine labelling on cell viability and physico-chemical properties was first

evaluated (see part 1.2.2). We should note that, at the beginning of this study, another method, named Diffusion Fluorescent Front Tracking (DFFT) and based on the use of planar laser for tracking the migration of green fluorescent protein (GFP)-tagged strains, was employed. To this end, in collaboration with the Micalis Institute, the GFP-tagged counterparts of TIL448 and TIL1230 (named TIL1248 and TIL1250, respectively) were constructed and tested. Equivalent cell surface physico-chemical properties and muco-adhesive behaviours between GFP-tagged strains and the original ones were obtained, i.e high hydrophobicity, high surface charge and high adhesion to PGM (as probed in the SSFC) for TIL448/TIL1248 and low hydrophobicity, high surface charge and low adhesion to PGM (as probed in the SSFC) for TIL1230/TIL1250 (data not shown). Unfortunately, DFFT experiments could not be successfully performed, due to the weak fluorescence intensities emitted by GFP-tagged lactococci at the laser wavelength of 532 nm. Nevertheless, the TIL1248 and TIL1250 strains were still considered for further DFT experiments, in combination with the pilin and mucus-binding protein defective-mutants (TIL1289 and TIL1290, respectively).

1.2.2. Effect of fuchsine labelling on *L. lactis* viability and cell surface physico-chemical properties

First, viability of *L. lactis* bacterial cells was estimated by plate counting for the four strains tested, before and immediately after staining, and after 2 h and 4 h corresponding to the maximal duration for DFT measurements. Experimental protocols are detailed in the Appendix. After fuchsine staining, whatever the strain under study, a one-log decrease in viable counts was observed (**Figure III.1**). Nevertheless, for all the strains, the number of viable cells remained unchanged afterwards.

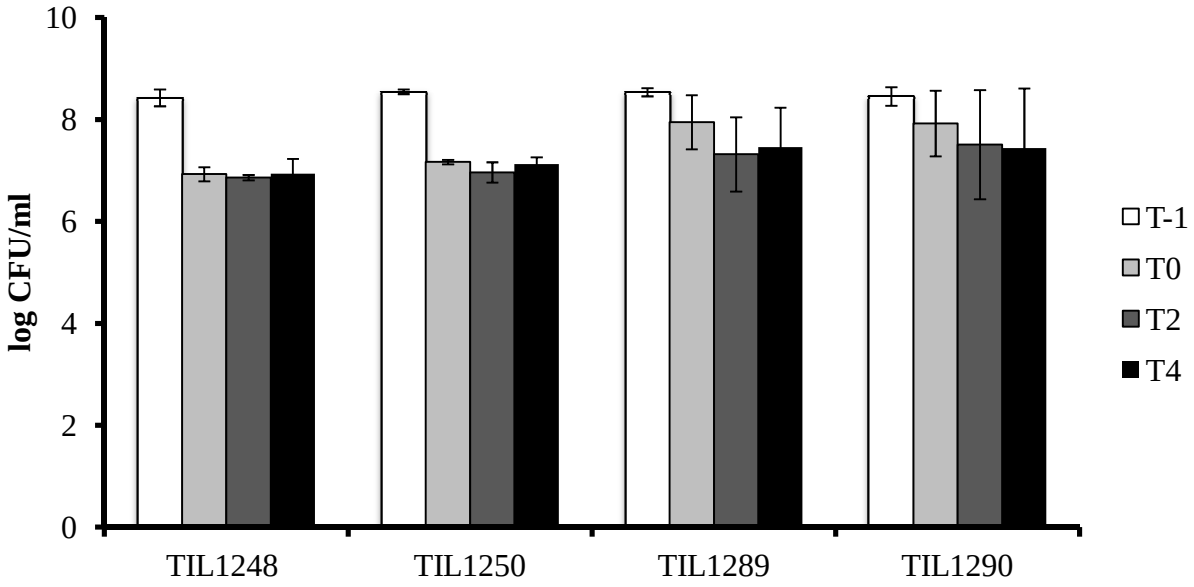

Figure III.1. *L. lactis* viable counts before and after fuchsine staining for the four strains under study (wild type TIL1248*, plasmid-cured derivative TIL1250*, pilin mutant TIL1289 and mucus-binding protein mutant TIL1290). T-1: before staining; T0: just after staining, T2: after 2 h and T4: after 4 h.* GFP-tagged strains.

Then, hydrophobic/hydrophilic properties and electrophoretic mobilities were evaluated for the four strains under study, according to the protocols detailed in the Appendix. Results are displayed in **Figures III.2** and **III.3**, respectively. Before fuchsine staining, the TIL1248 strain was highly hydrophobic, as expected. The TIL1250 strain was mildly hydrophilic, which was consistent with previous results (M-P. Chapot-Chartier, unpublished data). The same profile was obtained for the mucus-binding protein mutant (TIL1290). As for TIL1248, the pilin mutant (TIL1289) was highly hydrophobic, albeit at a lesser extent (**Figures III.2**). After fuchsine staining, no significant change in the cell surface hydrophobicity was found for the four strains under study (**Figures III.2**). The surface charge before and after fuchsine staining is presented in **Figures III.3**. All the strains were negatively charged, with the lowest value achieved for TIL1248 (average values of -2.1×10^{-8} $m^2.V^{-1}.s^{-1}$, -3.1×10^{-8} $m^2.V^{-1}.s^{-1}$, -2.6×10^{-8} $m^2.V^{-1}.s^{-1}$ and -3.1×10^{-8} $m^2.V^{-1}.s^{-1}$ for TIL1248, TIL1250, TIL1289 and TIL1290, respectively) After staining, the surface charge was only slightly increased, probably due to the positive charge of fuchsine (**Figures III.3**). In conclusion, viability and cell surface

properties of the wild type *L. lactis* and its derivatives were not significantly modified after fuchsine labelling.

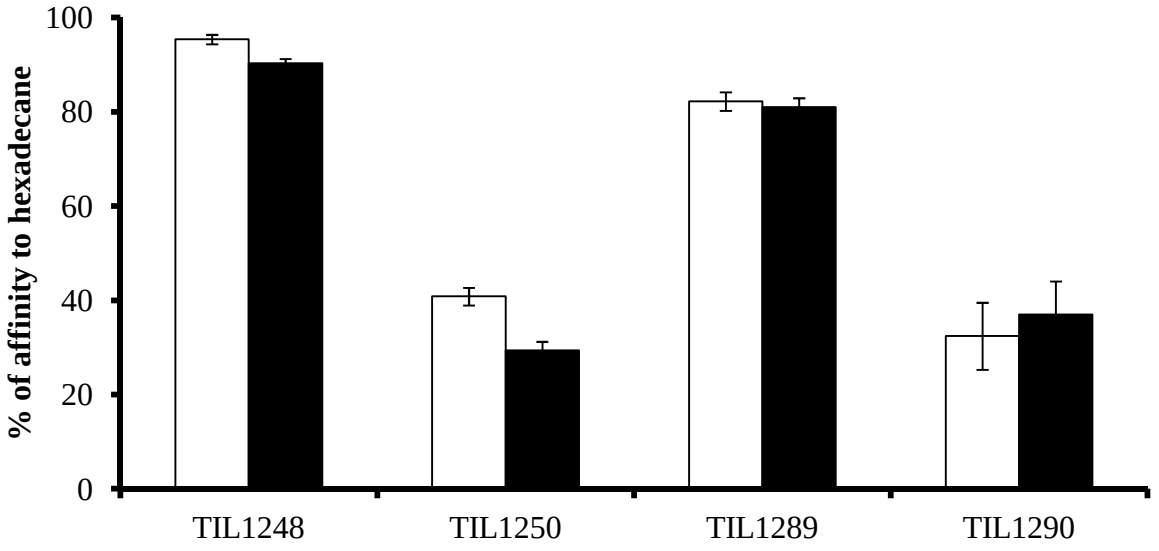

Figure III.2 Affinity to hexadecane for the four strains under study (wild type TIL1248*, plasmid-cured derivative TIL1250*, pilin mutant TIL1289 and mucus-binding protein mutant TIL1290); no fuchsine staining (□) and after fuchsine staining (■); * GFP-tagged strains.

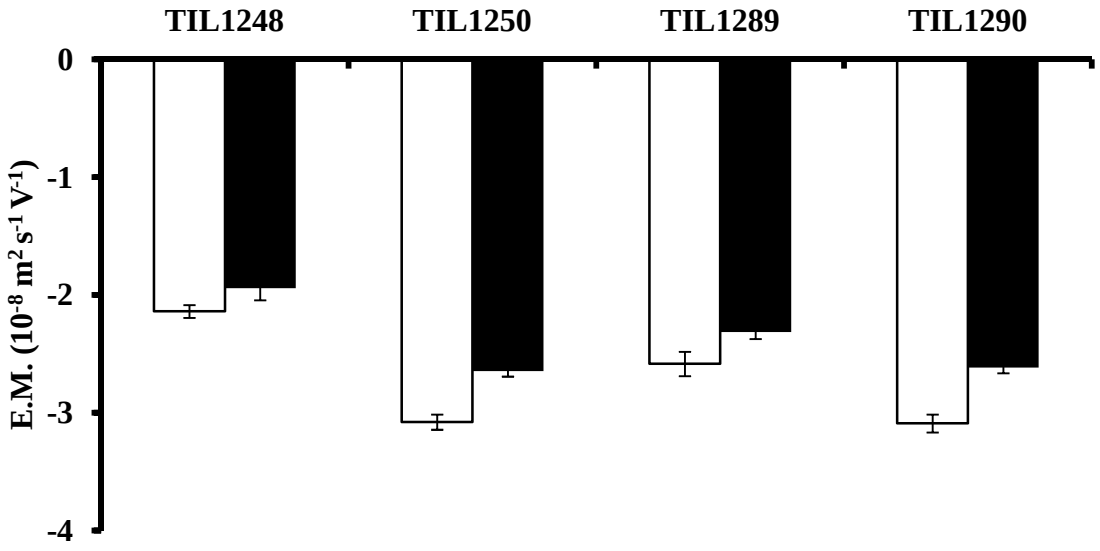

Figure III.3. Electrophoretic mobility at pH 7 in KNO_3 1 mM for the four strains under study (wild -type TIL1248*, plasmid-cured derivative TIL1250*, pilin mutant TIL1289 and mucus-binding protein mutant TIL1290); no fuchsine staining (□) and after fuchsine staining (■); * GFP-tagged strains.

1.2.3 DFT methodological developments

1.2.3.1 Principle of the DFT method

The DFT technique is based on a flat liquid-liquid interface of the cell suspension over a PGM hydrogel, which is carried out in a small Hele-Shaw chamber. According to the second law of thermodynamics, systems which are not in equilibrium tend toward equilibrium due to a difference in the chemical potential of a component between one region and another. There are many factors that can give rise to a difference in chemical potential, such as concentration, temperature, density and external forces (e.g. gravity, magnetic forces). In this study, the only driving force considered is a difference in cell concentration. A classical diffusion equation based on a material balance for cells can be used to calculate diffusion coefficients (Fick 1855):

$$\frac{\partial C}{\partial t} = D\left(\frac{\partial^2 C}{\partial x^2} + \frac{\partial^2 C}{\partial y^2} + \frac{\partial^2 C}{\partial z^2}\right), \qquad \text{(III.1)}$$

where C is the cell concentration (mg/L); t is the exposure time (s) and D is the diffusion coefficient of cells (m^2/s); and x, y, z are the positions in rectangular coordinates.

Experiments were carried out in a small Hele-Shaw chamber (5 x 10 x 0.2 cm^3) (see **Figure III.4**). Such a configuration affords important conclusions: (i) the diffusion is two-dimensional due to the absence of the z-axis contribution, which has been previously demonstrated by a Particle Image Velocimetry (PIV) analysis (Jimenez *et al.* 2013); (ii) the concentration gradient only appears along the x-axis, thus the diffusion along the y-axis can be suppressed. In addition, at the vicinity of interfaces, there is no convection along the x-axis (Jimenez *et al.* 2013). Therefore, cell diffusion occurs along the x-axis only and can be obtained from (III.1) as the following:

$$\frac{\partial C}{\partial t} = D\,\frac{\partial^2 C}{\partial x^2} \qquad \text{(III.2)}$$

1.2.3.2. Theoretical frameworks and a Markov-Chain Monte-Carlo method for determining the diffusion front

(A) Theoretical frameworks

In order to solve Eq.(III.2), several assumptions have to be formulated. The boundary and initial conditions of the diffusion equation must be considered as follows:

Boundary condition (1): $C = C_{max}$ at $x = 0$ and $t \geq 0$

Boundary condition (2): $C = 0$ at $x = L$ and $t \geq 0$

Initial condition (3): $C = 0$ at $t = 0$ and $0 \leq x \leq L$

where C_{max} is the highest cell concentration, x is the position where the cell concentration is measured, L is the height of the hydrogel in the chamber.

The analytical solution for Eq.(III.2) with these conditions is assumed (Crank 1975):

$$\frac{C - C_0}{C_{\max} - C_0} = 1 - erf\left[\frac{x}{2\sqrt{Dt}}\right] \quad \text{(III.3)}$$

with the error function *erf* (-) defined as:

$$erf(u) = \frac{2}{\sqrt{\pi}} \int_0^u \exp(-u^2) \cdot du \quad \text{(III.4)}$$

(B) A MCMC method

A Markov Chain Monte Carlo (MCMC) method was used as a strong solver for the Equation (III.3) (Jimenez, 2013). The solver compares experimental and theoretical concentration profiles at different time and optimizes several parameters in order to fit experimental and theoretical data. In this study, the input parameters of MCMC solver are:

- A matrix *C*, with size (n_L *x* n_t), of the average cell concentration on each line and for n_L lines of image and n_t time.
- A vector *x*, with size (n_L *x 1*), of the characteristic distance between the *x*-position line and cell-PGM hydrogel interface.
- A vector *t*, with size (n_t *x 1*), of the interval times of recorded images.

The output parameters of MCMC solver are:

- C_0 and C_{max}, the minimum and maximum cell concentration in the bulk, respectively.
- δ_x, error of x from the experimental input.
- δ_t, error of t from the experimental input.
- D, the cell diffusion coefficient.

1.2.3.3 Experimental set-up and procedure

Experimental set-up. The set-up for DFT experiments is displayed in **Figure III.4**. The Hele-Shaw chamber sides were transparent and made of polymethyl methacrylate (PMMA). A led lighting panel (Photonline, France) was placed behind the chamber. The diffusive process was recorded by a CCD camera (Guppy PRO - Allied Vision Technologies, 14 bits, 1292×964 pixels, 31 fps). A 105-mm objective (Micro-Nikkor 105 mm f/8, Nikon, Champigny, France) was added to the CCD camera to obtain a measurement area of 4 × 6 mm². Data were then collected using specific acquisition software (AVTCamera, Allied Vision Technologies, Germany).

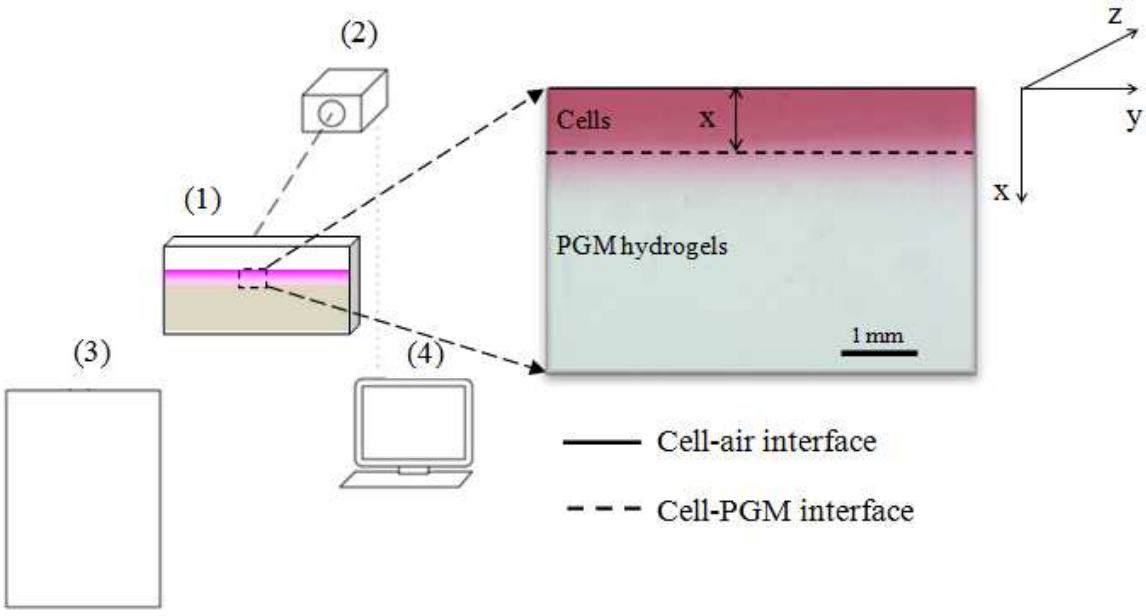

Figure III.4. DFT set-up: (1) Hele-Shaw chamber filled with PGM and fuchsine-stained cells of *L. lactis* injected at the top surface; (2) CCD camera; (3) lighting panel; (4) acquisition set-up. Note that x is the vertical axis in this case.

Experimental procedure. A volume of 9 mL of the PGM hydrogel of 0.5% or 5% (w/v) was added into the Hele-Shaw chamber to reach a height of 3 cm. The fuchsine-stained cells (OD_{600nm} of 3.5, volume 1 mL) were cautiously injected on the top of PGM, ensuring the cell-PGM hydrogel interface was completely flat. The cell layer height was thus set to about 5 mm. Measurements were performed at room temperature. Images were then recorded every 75 s for a period of 2 h (see **Figure III.5**). Note that a period of 30 min was allowed to elapse before recording in order to prevent any artefact. At the end of the experiment, a ruler was inserted in the Hele-Shaw chamber in order to determine the geometric calibration factor (conversion between pixel and mm). Each experiment was performed twice with independent cell cultures.

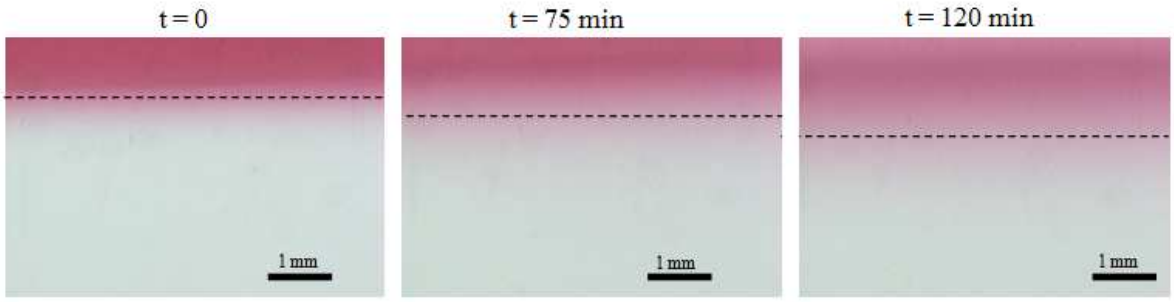

Figure III.5. Example of images recorded for the diffusion process of the mucus-binding protein mutant TIL1290 in PGM 0.5% (w/v).

1.2.3.4 Data analysis

Firstly, the pixel colour of the images is converted into grey values (GV), which indicate the brightness of pixels, by using a MATLAB-based program. The average GV of each line along the x-axis is determined with the following equation:

$$GV(x,t) = \frac{1}{n_C} \sum_{y=1}^{y=n_C} GV\left(x,y,t\right), \qquad \text{(III.5)}$$

with GV(x, y, t) is the grey value at a pixel at time t and n_C is the number of pixels along the y-axis in the observed zone. **Figure III.6** shows an example of profile of GV function of x over time. Note that the minimum grey value, i.e. GV_0 at x = L, is not zero due to the greyish colour of the PGM hydrogel but corresponds to a null cell concentration.

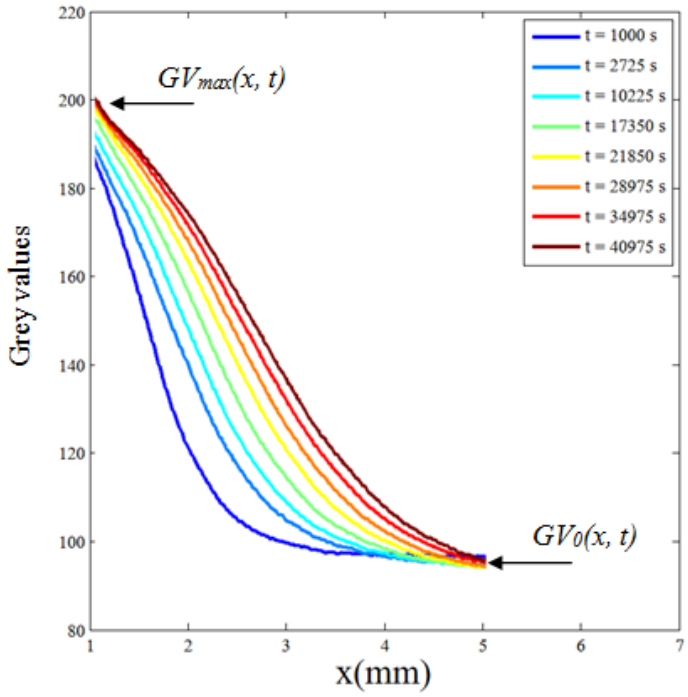

Figure III.6. Example of an experimental profile of GV function of *x* for the mucus-binding protein mutant TIL1290 in PGM 0.5% (w/v).

In order to determine the relationship between grey values and cell concentration, measurements were carried out for various cell concentrations. Results showed that grey values are directly proportional to the cell concentration, i.e. by a linear equation (**Figure III.7** and Eq.(III.6)).

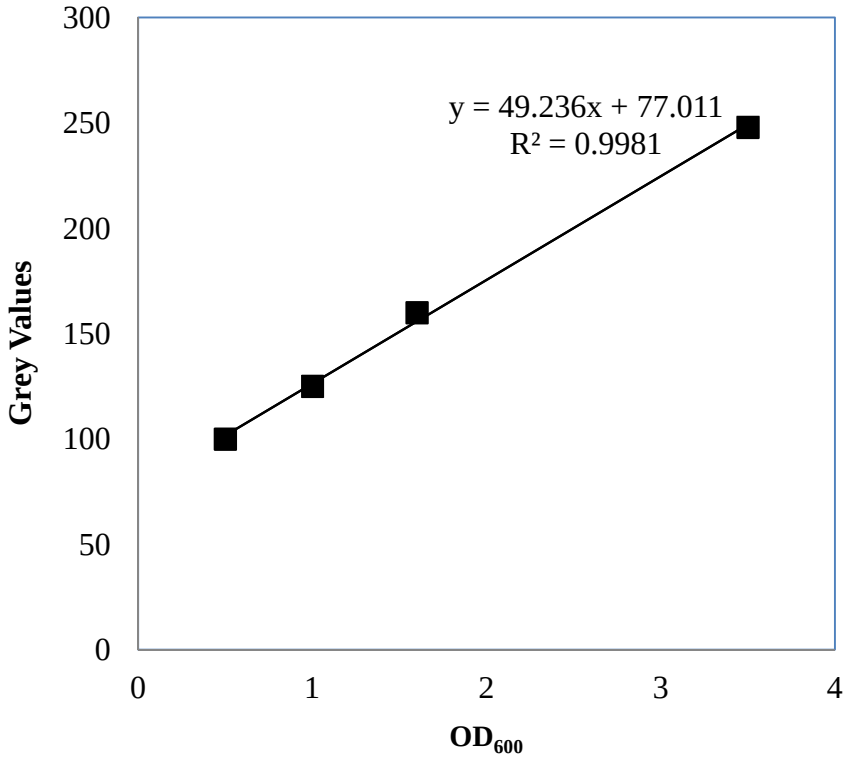

Figure III.7. Variation of the grey values extracted from experimental images with the OD $_{600\ nm}$ of the cell suspension (example of the wild type TIL1248 strain).

Note that the cell concentration (mg/L) is also a linear function of the OD $_{600\ nm}$. The linear equations between grey values and cell concentrations were thus characterized as follows:

$$GV(\mathrm{x},\mathrm{t}) = \alpha C \tag{III.6}$$

$$GV_{\max}(x,t) = \alpha C_{\max} \tag{III.7}$$

$$GV_0(x,t) = \alpha C_0 \tag{III.8}$$

From this point, only *GV(x,t)* will be considered in order to simplify the resolution of diffusion equation. One can note that:

(i) The profile of grey values obtained from experimental images demonstrated that the boundary and initial conditions were in agreement with our assumptions.

(ii) Based on Eq.(III.3), the diffusion determination is given by:

$$\frac{\frac{1}{\alpha}GV(x,t)-\frac{1}{\alpha}GV_0(x,t)}{\frac{1}{\alpha}GV_{\max}(x,t)-\frac{1}{\alpha}GV_0(x,t)}=1-erf\left[\frac{x}{2\sqrt{Dt}}\right]. \quad \text{(III.9)}$$

Eliminating $1/\alpha$ in Eq.(III.9) leads to Eq.(III.10):

$$\frac{GV(x,t)-GV_0(x,t)}{GV_{\max}(x,t)-GV_0(x,t)}=1-erf\left[\frac{x}{2\sqrt{Dt}}\right]. \quad \text{(III.10)}$$

Therefore, the MCMC method could be used directly with GV from images instead of concentration value for solving Eq.(III.10). The input parameters of the MCMC solver are:

- A matrix $GV(x, t)$, with size (n_L x n_t), of the average GV on each line and for n_L lines of image and n_t time.
- A vector x, with size (n_L x 1), of the characteristic distance between the x-position line and the cell-PGM hydrogel interface.
- A vector t, with size (n_t x 1), of the interval times of recorded images.

The output parameters of the MCMC solver are:

- $GV_0(x, t)$ and $GV_{max}(x, t)$, the minimum and maximum grey values, respectively.
- δ_x, error of x from the experimental input.
- δ_t, error of t from the experimental input.
- D, the cell diffusion coefficient.

The MCMC method provided a highly accurate estimation of the parameters of interest, e.g. an error of 4.3% on diffusion coefficient was obtained. An example of a minimum error between $GV(x,t)_{\text{experiment}}$ and $GV(x,t)_{\text{estimation}}$ is displayed in **Figure III.8**. The distribution of the parameters of interest (diffusion coefficient, error of x, error of t) can be evaluated (**Figure III.9**).

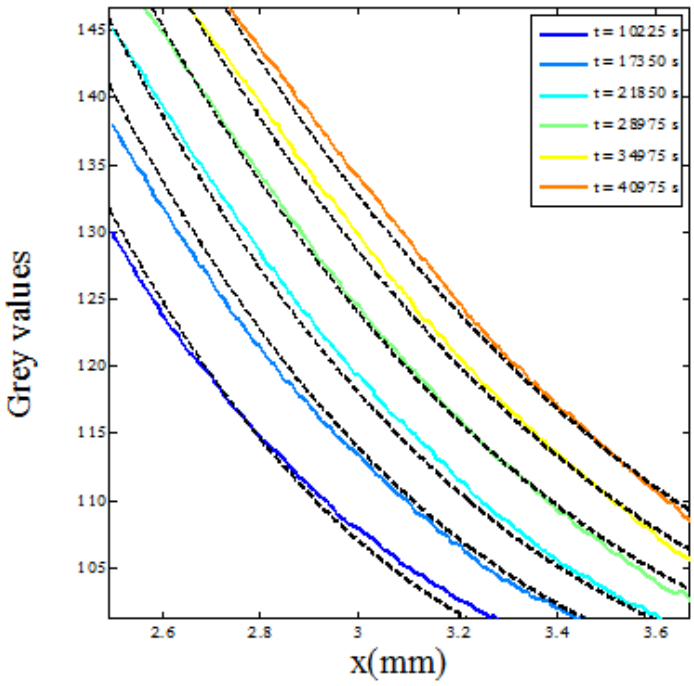

Figure III.8. Example of a regression profile of grey values function of *x*; comparison between experiment (plain lines) and estimation (dashed lines) for the mucus-binding protein mutant TIL1290 in PGM 0.5% (w/v).

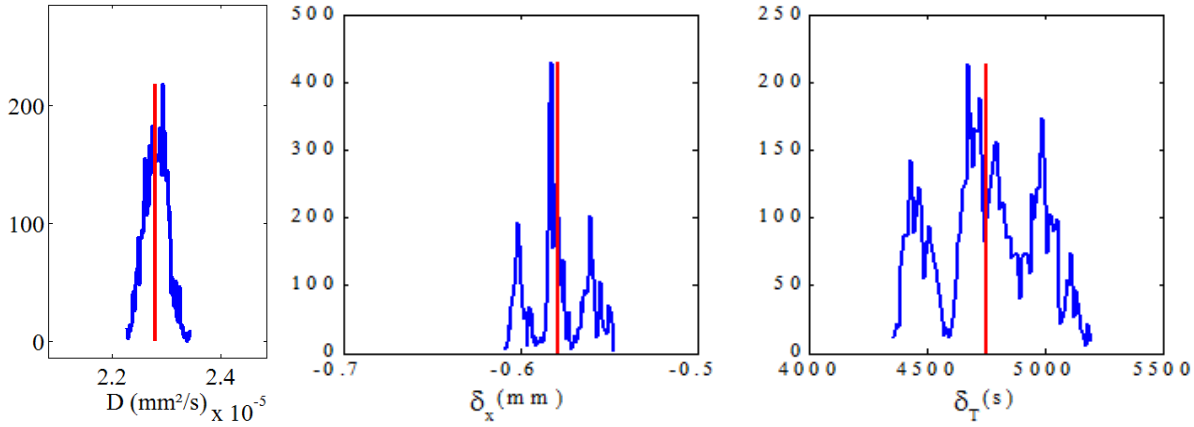

Figure III.9. Example of distribution for the diffusion coefficient D (left), error of *x* (δ_x) (middle) and error of t (δ_t) (right) by the MCMC solver, for the mucus-binding protein mutant TIL1290 in PGM 0.5% (w/v).

The advantage of the DFT method is to determine the diffusion coefficient of bacteria without calculating the cell concentration, thanks to the linear relationship with brightness of pixel, i.e. grey values. Classical techniques used in the literature to study the diffusivity of bacteria require to quantify the cell concentration or to count the cell number (Kim 1996). The DFT method may thus be considered as a novel and promising technique to measure: (i) the GV profile along the x-axis near the cell-medium interface; (ii) the diffusion coefficient of bacterial cells at the population level in a given medium with good accuracy. Results for *L. lactis* and PGM are presented in the next section.

1.2.4 Results

The diffusion coefficient of the wild type *L. lactis* strain and its derivatives inside PGM hydrogels was deduced from DFT experiments for a PGM concentration of 0.5% and 5% (w/v). Results are presented in **Table III.1**. Since *L. lactis* is non-motile, its movement through PGM gels was mainly governed by Brownian diffusion (Nelson 2004).

Table III.1. Diffusion coefficient (10^{-12} m^2/s) of *L. lactis* inside PGM hydrogels for the four strains under study and for a PGM concentration of 0.5% and 5% (w/v).

	TIL1248 Wild type	**TIL1289** Pilin mutant	**TIL1290** Mucus-binding protein mutant	**TIL1250** Plasmid-cured derivative
PGM 0.5% (w/v)	8.16 ± 0.41	12.9 ± 0.65	22.8 ± 1.14	89.8 ± 4.49
PGM 5% (w/v)	7.45 ± 0.37	9.00 ± 0.45	10.4 ± 0.52	68.8 ± 3.44

Whatever the PGM concentration, the lowest diffusion coefficient was obtained for the wild type strain whereas the highest one was achieved for the plasmid-cured derivative. These trends were a first indication that migration of *L. lactis* inside PGM hydrogels may be significantly influenced by its muco-adhesive profile, i.e. the strain exhibiting the strongest interactions with PGM tends to be more entangled than a less muco-adhesive one. This was confirmed by the analysis of the *L. lactis* mutants. The pilin mutant TIL1289 had a diffusion coefficient lower than that observed for the mucus-binding protein mutant TIL1290, which was fully consistent with previous findings on a more important contribution of the mucus-binding protein than pili in adhesion to PGM, as probed under dynamic conditions with the shear stress flow chamber (see part III.1.1). Nevertheless, the role of non-specific interactions, e.g. electrostatic and/or hydrophobic interactions, could not be ignored. All strains tested were electronegative with close electrophoretic mobility values, thus indicating

that differences could not be ascribed to electrostatic effects. Furthermore, due to the high ionic strength medium used (PBS), charge shielding occurred. Strikingly, the lowest diffusion coefficients were obtained for the most hydrophobic strains, i.e. TIL1248 and TIL1289, which were probably able to interact with hydrophobic patches of PGM, such as the naked protein core (e.g. cystein-rich regions). This underlines that migration of *L. lactis* inside PGM hydrogels is a complex interplay between specific and non-specific interactions. The size and morphology of bacterial cells were also probably involved. Furthermore, for piliated strains, auto-aggregation could occur (Oxaran *et al.* 2012). Another point to deal with was the effect of PGM concentration on the diffusion coefficients: independently of the strain and its adhesive/muco-adhesive properties, bacterial cells tended to be more diffusive in a 0.5% (w/v) PGM gel than in a 5% (w/v) one, surely indicating different gel structure and mesh size. In the following chapter, we will thus present our results on the microstructure and rheological properties of PGM hydrogels for various concentrations, including the extreme values tested here (0.5 and 5% (w/v)).

Chapter III. Results

2. Scrutinizing the microstructure of porcine gastric mucins by fluorescence multiple particle tracking and microrheometry

Context and objectives. The mucus layer covers a large surface of the human body and protects the host from threats such as viruses, pathogens and toxins. Such defenses have been optimized in order to intake in the meantime essential materials, e.g. nutrients. It works as a bandpass where desired molecules are allowed to diffuse. The knowledge of the microstructure has been covered over the past decades and mucin models were required. The main model used was the porcine gastric mucin (PGM), close to human stomach mucin and composed in majority by MUC5AC mucin. Commercial PGM is available but its use remains controversial. Therefore, this section aims at scrutinizing the microstructure in terms of mechanical properties and diffusivities of commercial Type III PGM in order to address the question of bacteria versus mucins interactions.

Methods. Fluorescence Multi-Particle Tracking (fMPT) consists of monitoring the position of probe nanosized-particles over time to extract information about their surrounding medium. 200-nm and 500-nm sized polymeric beads were either positively or negatively-charged and were modified by PEG-coating (polyethylene-glycol) to neutralize the surface charge. Their characterization in terms of size and electrophoretic mobility was performed. Reconstituted type III PGM was studied in a concentration range of 0.5-20% (w/v). The mean-square displacement (MSD) provides a way to get apparent diffusion coefficient (over the first 10 steps of individual trajectories), the anomaly of diffusion when fitting the Generalized Stoke-Einstein Relation (GSER) over the full-length individual MSD. The complex modulus can be determined using MSDs with one-point and two-point microrheology. The first is related to the self-correlation of tracer motion while the second considers the long-wavelength fluctuations of the medium and gives the cross-correlation of two tracers motion. Finally, bulk rotational rheometry is presented by shear stress–controlled and sweep frequency assays.

Results. It was demonstrated that PGM is shear-thinning complex fluid with solid-like settings at low concentration. The findings bring to counter-intuitive conclusions since it is observed that the increase in concentration was displayed by solid-like to liquid-like fluid. It is thereby postulated that hydration controls such properties since highly concentrated and partially hydrated mucins cannot move properly in the mesh. The analysis of diffusivities of polymeric particles with varying size and surface properties showed that the mesh was highly heterogeneous and the average pore size was situated from 470 nm to 240 nm for PGM 0.5% to 5% (w/v), respectively. For the first time, this paper reports lognormal distribution of apparent diffusion coefficient that reflects the heterogeneity and the preferential size exclusion and electrostatic bandpass. Finally, 500-nm and 200-nm charged particles underwent anomalous diffusion while 200-nm neutral-modified ones remained almost free-diffusive within the PGM network.

Conclusions. Using fluorescence Multi-Particle Tracking (fMPT), this work provided a scrutiny on the microstructure of partially purified PGM solutions by the analysis of the diffusivities of uncoated and PEG-coated nanoparticles and the microrheology. This analysis gave a valuable input by displaying the distribution of apparent coefficient of diffusion. The obstruction-scaling model, used largely to estimate the network pore size, worked suitably but had to be used solely as a size bandpass indicator. The PGM network appeared to be highly heterogeneous and this information was accessible by the lognormal distribution. For this work purpose, PGM of type III remained an adequate model to study the properties of nanoparticle transport and further works will be devoted to investigate the migration of bacteria using the fMPT technique.

Scrutinizing the microstructure of porcine gastric mucins by fluorescence multiple particle tracking and microrheometry

Mickaël Castelain[1,2,3,*], Thi-Ly Tran[1,2,3], and Muriel Mercier-Bonin[1,2,3]

[1] Université de Toulouse; INSA,UPS, INP; LISBP, 135 Avenue de Rangueil, F-31077 Toulouse, France
[2] INRA, UMR792 Ingénierie des Systèmes Biologiques et des Procédés, F-31400 Toulouse, France
[3] CNRS, UMR5504, F-31400 Toulouse, France

* Corresponding author: Mickaël Castelain

Abstract

The mucus layer covers a large surface of the human body and protects the host from threats such as viruses, pathogens and toxins. Such defenses have been optimized in order to intake in the meantime essential materials, e.g. nutrients. It works as a bandpass where desired molecules are allowed to diffuse. The knowledge of the microstructure has been covered over the past decades and mucin models were required. The main model used was the porcine gastric mucin (PGM), close to human stomach mucin and composed in majority by MUC5AC mucin. Commercial PGM is available but its use remains controversial. A deep characterization is therefore proposed in the present paper in terms of mechanical properties and diffusivities of probe particles. It is demonstrated that PGM is shear-thinning complex fluid with solid-like settings at low concentration. The findings bring to counter-intuitive conclusions since it is observed that the increase in concentration was displayed by solid-like to liquid-like fluid. It is thereby postulated that hydration controls such properties since highly concentrated, and partially hydrated mucins cannot move properly in the mesh. The analysis of diffusivities of polymeric particles with varying size and surface properties shows that the mesh is highly heterogeneous and the average pore size was situated from 470 nm to 240 nm for PGM 0.5% to 5% (w/v), respectively. For the first time, this paper reports lognormal distribution of apparent diffusion coefficient, which reflects the heterogeneity and the preferential size exclusion and electrostatic bandpass. It has been shown that 500-nm and 200-nm charged particles underwent anomalous diffusion while 200-nm neutral-modified ones remained almost free-diffusive.

Key-words: Diffusion, microrheology, viscoelastic, rheology, mucins

Introduction

The mucus is a biological viscoelastic fluid that lines the host epithelium and protects from threats by selectively filtering the required solutes, nutrients, gases and preventing from infections. Such properties have been widely investigated in terms of biochemical composition or mechanical properties, even though a comprehensive understanding is still lacking.

Mucus is not a homogenous fluid, but rather comprises a nanoscopically heterogeneous mesh network of flexible, highly glycosylated protein fibers called mucins (see for example this review from Bansil and Turner [1]). With the exception of specific disease states, the mucin content found in the human body usually ranges between 1 and 5% (w/v). Likewise, water content is highly similar across various mucosal surfaces and usually within the 90-98% range. Mucus also comprises DNA, lipids, salts, proteins and cellular debris. Mucus is a non-Newtonian shear-thinning fluid [2-4], i.e. its viscosity decreases with increasing shear rate. A variety of mucus sources, including pig stomach, small intestine, colon; human lung, sputum and cervix; bovine cervix; and rat epididymis [5], share a common rheological behavior modeled by a power law.

The primary function of mucus is to act as a filter, permitting the selective passage of molecules that are beneficial to the body, while serving as a barrier against potential harmful ones, such as viruses and pathogens. Understanding the filter properties of the mucosal barrier has gained significant interest for the development of novel drug delivery strategies, such as nanoparticle application systems [6]. Potentially, such systems could be used for therapeutic purposes: as due to their nanometric size, the drugs would be able to penetrate the mucosal barrier and thus access the underlying epithelium, in turn providing a controlled and sustained release of drugs locally.

Nanoparticle diffusion has previously been determined in various human mucus secretions, including cervicovaginal mucus [7], cystic fibrosis sputum [8], chronic rhinosinusitis mucus [9] and, more recently, respiratory mucus [10]. Reconstituted hydrogels of porcine gastric mucins, obtained from scraping of fresh pig stomachs, have also been considered (Lieleg et al., 2010). Due to their typical surface physico-chemical properties (high hydrophobicity,

negative charge), conventional, uncoated polymeric nanoparticles strongly interact with the mucin fiber network. To minimize such muco-adhesive effects, Lai et al. [7] first used protocol from Valentine et al. [11] consisting of coating the polymeric nanoparticles with a dense layer of low molecular weight polyethylene glycol (PEG). Using PEG-coated nanoparticles, it was thus possible to probe the microstructure of cervicovaginal mucus [12], cystic fibrosis sputum [8] and respiratory mucus [10]. Tracking the motion of individual PEG-coated particles and their uncoated counterparts offers significant advantages compared to traditional approaches for unravelling mucus gel structure and trapping ability. In particular, bulk diffusion measurements do not allow transport rates to be estimated at the single-particle scale, thus potentially neglecting sub-populations of interest, like sub-diffusive or actively-transported particles.

Based on this background, this paper aims at scrutinizing the microstructure of commercial Type III porcine gastric mucins (PGM) in order to address the question of bacteria versus mucins interactions. To do so, mobility of 200-nm and 500-nm PEG-coated and uncoated polymeric nanoparticles was measured in reconstituted porcine gastric mucins (PGM) gels with fluorescence Multi-Particle Tracking (fMPT). The PGM gel structure and its barrier function towards nanoparticle diffusion were further investigated by comparing bulk rheology, as measured using a cone-plate rheometer, with microrheology, as probed by PEG-coated particles.

Material and Methods

Mucins preparation

The lyophilized powder PGM (Sigma-Aldrich batch #M1778, partially purified type III) was rehydrated in PBS or deionized water. In the case of particle tracking experiments, PGM was first rehydrated at various concentrations 1; 2; 4 and 10% (w/v) and kept 24 h under gentle shaking at 4°C. Nanoparticle dispersions were then added to the PGM-based hydrogels with a ratio 1:1 to obtain an expecting final concentration of bead (0.0008% (w/v)) and PGM hydrogels (0.5; 1; 2; 5% (w/v)). In the case of bulk rheology measurements, PGM was rehydrated at concentrations 0.5, 1, 2, 5, 10 and 20% (w/v). Aliquots of 20 mL were put under gentle agitation on roller at 4°C about 24 h to 48 h to reach equilibration and complete

dissolution of bubbles if any (case of 20% (w/v)). pH was measured prior experiments and was 7.3 ± 0.1 at 23°C. All measurements were performed at 23°C.

Preparation and characterization of nanoparticles

PEG-coating protocol was modified from Parnorchan *et al.* [13]. All reagent and solvents were purchased from Sigma-Aldrich (St. Louis, MO). Red (ex. 580 nm/ em. 605 nm) fluorescent polystyrene particles sized 200 nm (carboxylate-modified and amine-modified) and 500 nm (carboxylate-modified) were obtained from Invitrogen (Carlsbad, CA) and Sigma-Aldrich (St. Louis, MO), respectively. 200-nm beads were dialyzed extensively against PBS 1X (pH 7.5) and 500-nm beads were washed three times with PBS by centrifugation (3300 *g*, 4^{o}C, 15 min) with 3-min bath sonic to break aggregates. 2-kDa polyethylene glycol (PEG) was covalently attached to particles via carboxyl-amine reaction. To do so, 30 mg/mL PEG bis-amine in 50 mM (pH 6) of 2-(N-morpholino)ethanesulfonic acid (MES) was mixed at a 1:1 ratio with a 2% (w/v) aqueous suspension of different sized beads and incubated for 15 min at room temperature. 1-ethyl-3-(3-dimethylaminopropyl)carbodiimide (EDC, Thermo Scientific, US) was then added to a final concentration of 4 mg/mL and the pH of the solution was adjusted to 6.5 using 100 mM NaOH, and incubated on an orbital shaker for 2 h. To quench the reaction, glycine was added to a final concentration of 100 mM. The solution was incubated for 30 min at room temperature. PEG-coated beads were collected by dialyze (200-nm beads) or centrifugation (500-nm beads; 3300 *g*, 4^{o}C, 15 min). 500-nm PEG-coated beads were washed three times with PBS or water according to further experiments.

Size and electrophoretic mobility of particles were measured by dynamic light scattering using a Zetasizer Nano ZS (Malvern Instruments, US) under a 50-V electric field. The beads were suspended in KNO_3 1 mM pH 7.0 at an optical density of 0.2–0.3 at 600 nm and sonicated 3 min before each measurement.

Fluorescence multi-particle tracking (fMPT)

Mucin samples were mixed 1:1 (v/v) with nanoparticles (in PBS to reach the final concentration used in this paper, i.e. 0.5, 1, 2, 5% (w/v) and 0.0008% of nanoparticles). The mixture was gently stirred and sonicated 3 min before experiments. It was then placed between slide and coverslide. The final volume was confined in air-tight chamber

(GeneFrame 25µL, ABGene, Thermo Scientific, US). The sample was incubated 2 h at 30°C prior to any particle tracking experiment and loaded onto an upright Olympus BX51 microscope equipped with a 40x semi-apochromat fluorescence objective (LUCPlanFL N, Olympus, France). The setup was placed on an active optical table to reduce the effects of low-frequency noise. Sequences of 20 s were taken with 30-ms exposure time using a pco.1200hs fast charged-coupled camera (PCO imaging, Germany) and an arc-lamp source using epifluorescence path and filter set (ex. 575 nm / em. 610 nm). Motion of about one hundred of particles was captured and 4 zones on the sample were explored. The measurements were performed at about 20 µm away from the bottom slide to prevent from any boundary effect. The position of the nanoparticles (NP) was extracted using a customized version of the MATLAB-based Poly particle tracker software [14]. It is based on a polynomial fit of the intensity around each feature point, weighted by a Gaussian function of the distance from the center. This method offers a sub-pixel determination of the center with a 6.5-nm spatial resolution on our system. To reach such value, the center of mass of the whole sample was determined and the drift obtained over time was removed on the individual trajectories [15]. The individual tracks were then converted into mean-square displacement (MSD) for the available time lags τ (i.e. multiples of the time Δt between the images):

$$\left\langle \Delta r^2(\tau) \right\rangle = \frac{1}{N}\sum_{i=0}^{N}\left[r\left(i\Delta t+\tau\right) - r\left(i\Delta t\right)\right]^2 = 2n_d Dt, \quad (1)$$

With D the diffusion coefficient and n_d the dimensionality (n_d=2 for isotropic case).

Free diffusion of particles is governed by the Stokes-Einstein relation:

$$D = \frac{kT}{6\pi\eta R} \quad (2)$$

Where k_B is Boltzmann constant $1.38\text{x}10^{-23}$ $m^2.kg.s^{-2}.K^{-1}$, T is temperature (^oK), η is water viscosity ($9.03\text{x}10^{-4}$ Pa.s), R is size of the spherical NPs in radius (m). This equation helped validating our tracking method by measuring the diffusion coefficient of PEG NPs of 500 nm and 200 nm in water at 23 °C. Equation (2) yields 0.97 and 2.42 µm²/s, respectively. From the experimental size distribution (Figure 3A) where 500-nm and 200-nm NPs are 508 ± 47 nm and 284 ± 33 nm, the theoretical values were corrected to give 0.97 ± 0.09 µm²/s and 1.70 ± 0.20 µm²/s, respectively. Experimental diffusion coefficients were then obtained and were found to be 0.98 ± 0.01 µm²/s and 1.77 ± 0.03 µm²/s, respectively.

The MSD versus τ plots were analyzed by a weighted fit of the anomalous diffusion model [16]. Active and sub-diffusive transport of NPs can be described by:

$$\left\langle \Delta r^2(\tau) \right\rangle = 2n_b D t^{\alpha} \tag{3}$$

α is the anomalous exponent. For the motion of actively-transported (also called "super-diffusive") NPs, which is due to the relaxation of polymer gels, convection or gravity in the system, α equals to more than 1. In contrast, the sub-diffusive transport α equals to less than 1, which describes motion impeded by obstacles or by NPs binding to physical structures in the environment. NPs are classified as immobile when their movements are smaller than spatial resolution, i.e. their diffusion coefficients are lower than that of the same NPs attached to the glass slide. By analyzing the trajectories according to this anomalous diffusion model, distributions of the corresponding α-values can be obtained. The distribution of the apparent diffusion coefficient was calculated by the first time lag Δt using Eq.(1), as $D_a = MSD/4\Delta$t. The MSDs can be ensemble-averaged to obtain the mean diffusion coefficient.

One-point (1P) and two-point (2P) microrheology methods were used in this paper to quantify the complex shear modulus G^*, separable into elastic and viscous moduli, $G^*(\omega) = G'(\omega) + iG''(\omega)$ [17]. Only the 500-nm PEG-coated particles were used for this purpose since no substantial cage hopping events were observed in the tracks of such probe spheres, which have been shown to lead to artifacts with actin solutions [18].

One-point microrheology utilizes the analytical solution [19]:

$$G(\omega) \approx \left. \frac{4k_B T}{3\pi a \left\langle \Delta r^2(\tau) \right\rangle \Gamma\left(1+\alpha(\tau)\right)} \right|_{\tau=1/\omega}, \tag{4}$$

Where Γ is the gamma function, and α the anomaly. 2P microrheology uses pairwise correlated motions with a probed length (separation between two correlated tracers) on the order of 3-100 μm. We calculated the tensor of pairwise cross-correlated bead displacements as a function of separation distance r and lag time τ, and the component in the direction of r, $D_{rr}(r,\tau)$ is used to determine the MSD^{2P} as:

$$\left\langle \Delta r^2(\tau) \right\rangle_{2P} = \frac{2r}{a} D_{rr}(r,\tau). \tag{5}$$

Practically, $D_{rr} \sim 1/r$ indicates that the medium can be treated as (coarse-grained) homogeneous continuum over scales of typically 3-50 µm [20]. The average value of rD_{rr}

over that range is used to determine MSD^{2P} from Eq.(I.13). Finally, two-point complex modulus can be deduced by substituting $\left\langle \Delta r^2(\tau) \right\rangle_D$ into Eq.(I.8) in place of $\left\langle \Delta r^2(\tau) \right\rangle$.

Therefore, Crocker *et al.* [17] have demonstrated that two-point microrheology agrees with bulk rheology and since it is not dependent of shape or size, this technique opens up new doors for studying living cell rheology for example [21].

Rheometry

Rheological measurements were performed with a rotational rheometer (Haake Mars III, Thermo Fischer Scientific, USA), with microstress control, using a cone-plate geometry (CP2/60), 60-mm diameter, 2° cone angle on PGM with concentration ranging 0.5-20% (w/v). Temperature was controlled at 23°C with a Peltier device. Shear rate interval was from 10^{-3} to 300 s^{-1}. Before starting experiments, samples were sheared at 300 s^{-1} over 240 s. The viscosity was obtained under steady flow at a given shear rate and a stability criterion on the viscosity over time was given at 10^{-4} Pa.s/s over 240 s. If the criterion is satisfied, the value is reported.

Additionally, oscillatory amplitude sweeps were applied at 6.28 rad/s (1Hz) to determine the linear viscoelasticity regime, i.e. when the storage modulus (G') and the loss modulus (G'') are independent of the oscillatory shear stress, typically at 1-2 % deformation. Later, the samples were subjected to a shear stress in the sweep frequency interval of 6.3 10^{-2} – 125.6 rad/s (10^{-2} - 20 Hz). This protocol allowed to determine *G'*, *G''* and the phase angle δ as function of frequency (rad/s) given by: $\tan\delta = G''/G'$. All frequency sweeps were performed in Hz and converted in rad/s for better comparison with the literature data.

PGM mesh pore size

The size of pores was estimated using the scaling-obstruction model [22,23] developed by Amsden *et al.* for covalently cross-linked hydrogels, but applicable to gels with physical entanglements such as mucus [24]. This model describes the ratio of diffusion in a gel and diffusion in water as:

$$\frac{D_a}{D_w} = \exp\left[-\frac{\pi}{4}\left(\frac{r_s + r_f}{r_g + r_f} \right)^2 \right] \tag{6}$$

Where D_a and D_w are the apparent diffusion coefficients of the beads in mucus and in water, respectively, r_s is the particle radius, r_f is the gel fiber radius, and r_g is the effective radius of

the pore. The model is valid when there is no chemical interaction between the probe particles and the gel mesh. An r_f of 3.5 nm was used as the current best estimate for the radius of individual mucin fibers, as deduced from biochemical data, and electron microscopy and atomic force microscopy (AFM) observations [25,26].

Results

Macrorheological properties of mucins

To allow the comparison with the microscale characterization of PGM by fMPT (1P and 2P microrheology), the bulk viscoelasticity has been determined using a sensitive strain-controlled cone-plate rheometer. The apparent viscosity was characterized as function of the shear rate, ranging from 10^{-3} to 300 s^{-1} (Figure 1A). The curves exhibit a strong shear-thinning behavior with viscosity declining by 2000 fold over 5 decades in the case of PGM 0.5% (w/v). In addition, the viscosity shows a Newtonian plateau at low rates (10^{-3} s^{-1}) that is only accessible to date with the new technology. When the concentration increased, the plateau became larger (from 4.1 to 71.3 Pa.s) and expanded to higher rates until 10^{-2} s^{-1} in the case of PGM 20% (w/v). Flow curves have been fitted to a power law model (Figure 1B) as $\tau \sim \dot{\gamma}^n$ with *n* the behavior index. As can be seen in Table 1, this index describing the slope decreases with the concentration that gives rise to a steeper curve at high concentration since $\eta \sim \dot{\gamma}^{n-1}$. Also, the presence of salts (PBS) with respect to deionized water (DI) does not drastically influence the flow behavior. The generalized power-law model as Ostwald–de Waele relationship describes power-law fluid as $\tau = K\dot{\gamma}^n$. In the case of PGM, this was not the best model that could fit our experimental characterization. It appears that the Herschel-Bulkley model, in the form $\tau = \tau_0 + K\dot{\gamma}^n$, fits to the data to more than 99.5% (R^2) versus 89.1 % (data not shown) in the case of simple power-law fluid. This model introduces a parameter τ_0 that gives more flexibility in the fitting process. Physically, this parameter, referred to as *yield stress*, is described as the stress needed for the fluid to flow. Below this stress value, the fluid can be described as plastic. In our case, this notion has to be taken with extreme caution since the yield stress was determined around 10^{-2}-10^{-1} Pa (see Table 1) which is at the lowest limit of accuracy. The flow consistency coefficient *K* increases with the PGM concentration and is generally similar in both DI and PBS.

The dynamic response of PGM to shear was tested by applying an oscillatory deformation of small amplitude (1-2%) in the linear regime. Frequency sweeps show that storage (*G'*) modulus dominates at frequency below 6.28 rad/s (Figure 2B) at low PGM concentrations (0.5% (w/v)). In Figure 2A, the phase angle variation reveals that elasticity dominates for all the preparations in the range 0.5-2% (w/v). Those profiles resemble as a viscoelastic solid according to their low phase angle. However, Figure 2B depicting the moduli versus sweep frequency shows that there is a strong dependence of frequency with a polymer entanglement signature of a macromolecular solution, according to the classification of Clark and Ross-Murphy [27] and the graph proposed by Steffe [28] (fig 5.24 in this reference). The low phase angle can be explained by the low viscosity (Figure 1) in this frequency range. When concentration increases from 2% to 20% (w/v), the viscosity dominates over the elasticity, which gives rise to a phase angle larger than 45°. The moduli balanced, i.e. $\delta = 45°$, at frequencies increasing with C_m. This means that the phase angle is strongly affected by the viscosity variation, more than elasticity. When the frequency is lower than the cross point (e.g. 5.1 rad/s for the 10% (w/v) case), the cross-links could be formed by chain association until a critical sweep frequency is reached resulting in a sol-gel transition, that breaks down the structure in which the elasticity dominates over the viscosity. Note that the sol-gel transition is shifted to higher frequencies as the Newtonian plateau expands for increasing PGM concentration (Figure 1A).

In Figure 2B, the elastic modulus *G'* follows a power-law in the form $G'(\omega) \sim \omega^b$, at low and intermediate frequencies. The exponent *b* is plotted against the PGM concentration (Figure 2C) and shows an increase from 0.17 to 0.72. This tendency seems counter-intuitive since the exponent should decrease from 1 for diluted solutions to ~0.8 for concentrated solutions and ~0.03 for gels [28]. Nevertheless, elasticity has shown to be preponderant at low concentrations whereas viscosity shields the viscoelasticity at higher concentration. We thus hypothesized that PGM behaves as *self-assembled semi-dilute solutions* at low concentrations and *diluted solutions* at high concentrations, made of flexible (n~0.5 at 5% and 10% (w/v)) to semi-rigid polymers (n~0.75 at 20 % (w/v)) [29]. This will be discussed further. The latter, which can be considered as semi-rigid polymers, would also result in less water available in the sample, reducing drastically the rehydration process.

Transport of individual particles in PGM

The characterization of migration properties of entities travelling within the PGM network has been available by following the trajectories of such over time. PGM concentrations have been chosen in the physiological range i.e. 0.5-5% (w/v). 200-nm and 500-nm fluorescent particles have been used with different surface properties to study the effect of charge on their migration ability. To do so, carboxyl-terminated (negatively charged) and amine-terminated (positively charged) beads were used, as well as modified ones with PEG coating. Figure 3A and B shows the size and charge distribution for each type of beads, respectively. It appears that the 200-nm beads are larger than the value given by the provider, i.e. ~284 nm instead of 200 nm. In contrast, the 500-nm bead size is very close to the theoretical value. The ζ-potential, as expected, is positive for amine-terminated beads, reaching 30.5 mV and negative for carboxylated beads with -45.3 mV and -32.6 mV for 200-nm and 500-nm beads, respectively, in KNO_3 at 1 mM and pH 7. The efficiency of the PEG coating procedure was checked by the same method since PEG is assumed to partially shield the particle surface charge. After PEG grafting, ζ-potential was measured at -8.4 mV and -7.2 mV for 500-nm and 200-nm beads, respectively. The PEG-coating was thus reliable and data acquired are in line with the literature; Lieleg *et al.* [30] obtained a mean ζ-potential of -6.7 mV for 1-µm beads, using the same PEG reaction, at pH 7 and in a 20 mM Tris, 20 mM NaCl buffer.

The coordinates of the centroids of hundreds of fluorescent microspheres embedded in PGM were captured and transformed into time-averaged MSDs $\left\langle \Delta r^2(\tau) \right\rangle$. At short time scales, MSDs are linearly related to diffusion coefficients as $\left\langle \Delta r^2(\tau) \right\rangle = 2n_d Dt$ with n_d the dimensionality (here n_d=2). For each condition, the 10 first steps of 2000 trajectories are averaged and linearly fitted to give rise to the apparent diffusion coefficient, as shown in Figure 3C. The averaged apparent diffusion shows relative small standard deviation with a maximum for the 200-nm PEG-coated beads in the case of PGM concentrations of 0.5-2% (w/v). This value is rather constant, indicating that no obstruction is detected by such NPs until a 5% (w/v) PGM concentration is reached where diffusion drastically drops down to a common level shared by the other beads. Note that the standard deviation is large that cannot confirm any variation of the types of beads. In contrast, 500-nm PEG-coated NPs seemed to be much more obstructed as PGM concentration increased, with a standard deviation becoming larger and larger. This suggests that heterogeneity increases with concentration,

allowing some neutral beads to move or not, depending on their location. Diffusion coefficient of charged beads is similar for a given PGM concentration, i.e. no dependence on the type of charge, with a decrease in this value when concentration increases. PGM solutions seem to exhibit both positive and negative patches at pH 7 and in the presence of salts. Lieleg *et al.* [30] stated that high concentration of salts facilitates the transport of amine-modified beads. In that case, the diffusion properties of negatively and positively charged beads are equivalent, reflecting a similar density of negative/positive charges over the mucin network.
The diffusion coefficients have been determined by fitting individual MSD over the 10 first steps of trajectory and plotted as distributions (Figure 4 A-D). For the first time in the literature, instead of only considering averaged values, the distribution has been unveiled and found to be lognormal with multimodality in some cases. On inset A, the values of 200-nm and 500-nm NPs diffusion in water at T = 23°C were determined as reference for the log-log plots. It shows that the maximum values equal 0.94 $\mu m^2/s$ (with mean 0.98 ± 0.01 $\mu m^2/s$) and 1.75$\mu m^2/s$ (with mean 1.77 ± 0.03 $\mu m^2/s$) for 500-nm and 200-nm NPs, respectively. The theoretical values given by Eq.(2) yield 0.97 and 2.42 $\mu m^2/s$ for 500-nm and 200-nm NPs, respectively. The first agrees very well but not the latter. However, one should remind that the experimental size distribution of 200-nm NPs was determined (Figure 3A), and if the corrected value for particle size (considering 2R as 284 nm) was taken into account, a theoretical value of 1.70 ± 0.20 $\mu m^2/s$ was reached, which is fully in line with the experimental data (Table 2).

Generally, the distributions were shifted toward low diffusion values as PGM concentration increased (panel A to D). The 500-nm beads are the first affected by this increase since negatively-charged NPs (solid black line) are almost hindered at 2% (w/v). Neutral 500-nm PEG-coated NPs (dashed black line) exhibit multimodality with 2 peaks. The larger is centered at 0.29 $\mu m^2/s$ and the second around 0.047 $\mu m^2/s$. This multimodality, present in almost all cases, is reflected by large standard deviation in Table 2 for higher PGM concentrations. Noteworthy, the peaks did not shift with increasing concentration but rather change in value, that is, at PGM 1% (w/v) for the 500-nm PEG-coated NPs, the secondary peak became the maximum peak and in turn the maximum the secondary. At PGM 2% (w/v), a tertiary peak appeared at lower diffusion values. It looked like the distribution crept down to lower values as concentration increased (Figure 4). The distribution of 500-nm PEG-coated NPs almost followed the charged 200- and 500-nm NPs ones, except that it was

expanded showing that a proportion of neutral beads remains mobile. The 200-nm PEG-coated NPs are the only case that delayed the shift to lower values, even at 5% (w/v). This suggests that neutral 200-nm NPs were not as obstructed as the 500-nm ones were. A mesh size between 280 and 500 nm would thus reasonable to envision and confirm that the network had size exclusion but also interaction filtering properties. Furthermore, the heterogeneity of the mucin network was pointed out, as the distribution of neutral particles with critical sizes exhibited so spread profiles. The mesh size was then estimated using Eq.(6) and reported in Table 2. The pore size seems to be reduced when PGM concentration increases, which is reasonable. Also, the order of magnitude corresponds to the size exclusion previously commented with Figure 4.

The mode of transport was estimated by determining the exponent of anomalous diffusion given by $MSD = 2n_dDt^{\alpha}$ (Eq.(3)). The full length MSD was fitted with this equation and the anomaly α reported as distributions (Figure 4 E-H). When anomaly equals to unity, the diffusion can be treated as free (vertical dashed line). Distributions are rather centered on this value, with positive skewness (oriented to the left). Indeed, when α is lower than 1, the transport is considered as sub-diffusive, meaning that the particle motion is obstructed and not as free as it would be. When it is larger than 1, the transport is called super-diffusive, meaning that external forces are acting (molecular motors, polymer relaxation, propellers). In our case, most of the population tended to be sub-diffusive with $\alpha<1$. When PGM concentration increased, the low α values increased until profiles tended to be almost monotonic (PGM 5% (w/v)). In the case of neutral NPs, both of 200-nm and 500-nm types, this behavior was not seen, the unimodal shape remained, showing that the obstruction does not tend to impede the beads. In contrast, the largest proportion of charged beads was found to be hindered. Figure 5 illustrates this observation by plotting the trajectory of both 200-nm positively-charged NPs and 500-nm PEG-coated NPs over 12 s for increasing PGM concentration. It is noteworthy that neutral particles even larger that the charged ones in that plot underwent larger displacement. Again, the increase in PGM concentration would lead to shrink the PGM network, giving rise to obstructed movement but no hindrance. Positively-charged NPs, albeit smaller, seem to be stuck on the mesh. It can be hypothesized then that the motion recorded for such particles reflects the motion of the mesh itself.

Local viscosity in voids

As seen in Figure 3 and Figure 4, the neutral 200-nm PEG-coated NPs did not appear to be obstructed within the PGM network, at least until 2% (w/v). Also, it has been described by the macrorheology (Figure 1) that PGM behaves as shear-thinning viscoelastic fluid. Elastic properties dominate over viscosity at low PGM concentration, displaying therefore signature of concentrated solution of macromolecules, while higher concentration displays dilute solution behavior due to its high loss modulus. If 200-nm PEG-coated particles are able to evolve almost freely within such fluids, especially within voids of the network where they are actually confined, the local viscosity is attainable using Eq.(2). In Table 2 are reported the ensemble-averaged values of apparent diffusion coefficient normalized by the corresponding value in water. The local viscosity displayed values close to water for C_m = 0.5-2% (w/v). This would reflect the value within the void since 200-nm PEG-coated beads were still able to move in the mesh. For higher concentration, the viscosity dropped by 1200 fold. This reveals that beads were obstructed within the mesh and could no longer report microviscosity of the voids. Note that bulk viscosities are about 4000 times higher.

Microrheology

To probe the mechanical properties of PGM gels at length scales representative of the NPs size, one-point (1P) and two-point (2P) microrheology measurements have been performed by adapting the work of Maria Kilfoil's group [15] and previously introduced by Crocker *et al.* [17].The two methods are based upon the trajectories of the neutral 500-nm PEG-coated NPs that have been found to be caged by the network (Figures 3 and 4) and therefore are able to probe its intrinsic mechanical properties.

From the MSD defined by Eq.(1), the complex modulus G^* can be determined using Eq.(4) plotted in Figure 6 as function of the sweep frequency. As it was described above, the 2P method uses the correlation of the motion of two tracers separated by a distance r represented by D_{rr}. Once the condition of rD_{rr} is valid for a given range of r, this product is averaged and used to calculate the 2P MSD and the complex modulus given by Eq.(5) in place of the conventional MSD into Eq.(4).

In Figure 6A, representative results at 5% (w/v) PGM concentration reveal a relative good agreement of the 2P microrheometry that correctly captured the cross-over while 1P

microrheometry completely failed to retrieve it. Upper inset shows the cross correlation of motion along *r* direction as *~1/r* over 30 µm. At such distances, PGM can be treated as coarse-grained homogeneous medium where tracer motions influence each other and/or the fluctuations inherent to the network undergo Brownian motion. Tracers would carry along these random undulations of the medium that statistically correlate the motion of the two tracers. 2P elastic modulus behaves as $\sim\omega^{1/2}$ at low frequencies (below 1 rad/s) while exponent tends to ¾ above 50 rad/s. At this frequency, rheometry experienced instability due to inertia, inherent to the geometry and the low-viscosity sample, indicated by orange filled circles. 1P moduli converged to 2P ones to follow also ¾ exponent. This is confirmed by determining the phase angle δ (lower inset in Figure 6A). 2P agreed well with rheometry, but 1P showed a solid-like fluid with rather constant angle below 20°. At higher frequencies (above 50 rad/s), angles seemed to converge. Heterogeneity of 5% (w/v) PGM biased the 1P approach even if D_{rr} evolved as *~1/r* over 30-µm separation distance.

At a lower PGM concentration of 0.5% (w/v) (Figure 6B), rheometry appeared to be much more instable around 1 rad/s that limited the characterization. Microrheometry was confirmed as a powerful tool since the analysis gained one decade more. Motion correlation rD_{rr} was fitted to constant up to 80 µm (upper inset). The three methods agreed well with a cross-over that would be extrapolated at about 0.005 rad/s. The slope of each curve was lower than ½ until they converged to $\sim\omega^{1/2}$. No ¾ exponent has been observed throughout the experiments. The phase angle was also determined in this case and showed the same tendency with a plateau under 45° at intermediate frequencies. At low frequency, 2P method determined a liquid-like behavior characteristic of concentrated solutions. Not depicted in this paper, at PGM concentrations of 1% and 2% (w/v), 2P dynamic moduli behaved similarly to 0.5% (w/v), as they showed observable cross-overs, while 1P resembled 5% (w/v) case as 1P failed to retrieve cross-overs. The 0.75 exponent was not observable and representative of 5% (w/v) case.

As shown in Figure 6, the 1P method suffered from homogenous-sample limitations that did not reflect the low frequencies behavior but, nevertheless, appeared to converge to 2P approach. Both methods proved their exceptional performance by gaining one decade on frequency as compared with conventional rheometry (see Figure 6B). Indeed, Figure 2C provided the power-law exponent of ¾ only for PGM 20% (w/v). Using microrheometry, we

have measured such high-frequency power-law exponent at PGM 5% (w/v), which describes the PGM as semi-rigid polymer.

Discussion

This study scrutinized the microstructure and mechanical properties of commercial type III PGM. Porcine Gastric Mucins have been widely used in the literature as a model for understanding the migration of nutrients [31], diffusion of solutes or viruses [32]. To study intrinsic characteristics of such biological material, different works have investigated the mechanical as well as the diffusion properties. Mucus is made of a network of mucin fibers with a more-or-less degree of cross-linking that confers viscoelasticity behavior. In this work, the microstructure was probed by the analysis of diffusivities of tracers with varying size and surface properties and rheology characterization has been performed alongside with microrheometry approaches.

Rheology demonstrated that PGM fluid, with concentration ranging from 0.5% to 20% (w/v) and at neutral pH in PBS, is non-Newtonian and viscoelastic with shear-thinning properties as was already shown elsewhere [33-35]. Studies of PGM secretions obtained by gentle scrapping of pig stomach showed a greater elastic modulus G' (or storage modulus) than its viscous modulus G" (or loss modulus) throughout the frequency range studied (10^{-2} to 10^{2} rad/s). Delgado-Reyes *et al.* [36] studied the viscoelasticity of two types of commercial PGM (Sigma-Aldrich), type II and type III referred to as *non-purified* and *purified*, respectively. Flow curves were described by the shear-thinning Ostwald-de Waele model that solely takes into account the flow behavior index (n) and the consistency coefficient (K) as free fitting parameters in the form $\eta_{app} = K\dot{\gamma}^{n-1}$. Despite we used Herschel-Bulkley model to reach better fitting, the flow behavior index decreased as PGM concentration increased. However, the authors reported much higher indices of type III PGM than that we measured since they obtained the same value of n at 10% (w/v) as ours at 1% (w/v). At 20% (w/v), values were similar. This would be ascribed to the presence of buffering salts in our case versus distilled water and warming step to 40°C in their case.Their work would also have suffered from the geometry that introduced R^3 error (cone-plate 60 mm (this work) versus plate-plate 20 mm [36]), with R the radius of the mobile part.

Sriamornsak *et al*. [37] studied the rheological enhancement of pectin solutions by adding 5% PGM type III. Their results are in good agreement with the present work, showing the cross-over at similar frequency. However, exponent was deduced from their data and found to be around 1.4, which is rather high and reflects diluted viscoelastic solutions [28].

Moreover, the dynamics diverged notably. We have described elastic modulus as $\sim\omega^n$ in Figure 2C with *n* increasing with PGM concentration, in the range 0.3-0.75. This means that the mucus network would be treated as *flexible* to *semi-rigid* polymer scaffold [29] with increase in PGM concentration. This was not the case for the previous study [36] that described the exponent as decreasing from 2 to 0.6 as mucin concentration increased from 10% to 40%. It is intuitive to think that elasticity of dilute Newtonian fluids that equals to 2 would decrease to such values, below 1 as concentration increases from dilute to entangled semi-dilute solutions. The overlap concentration was estimated to 12 mg/mL [38]. Therefore, the range 10-40% is above this limit and probably above the entanglement concentration as well wherefore the results obtained were probably biased by artifacts. The preparation of PGM 20% (w/v) sample needed particular care to avoid any bubbles trapped by such high viscosities. In addition, the time required for a suitable rehydration was 24 to 48 h at 4°C in order to avoid bacterial contamination and enzymatic degradation. Working at such high viscosity introduced natural errors that could reach substantial value. Indeed, unless stated otherwise, the shear stress varies as the cubic radius, which means that any disturbances on the edges lead to dramatic changes on the shear determination. Bubbles that are usually going outwards may reach about 0.5-1 mm in size and produce valuable capillary forces. We have experienced errors by 50% on the shear stress above the PGM 20% (w/v) limit.

Rheological characterization of PGM is still controversial in the literature and, even as a convenient model, its preparation leads to tremendous variability. To unveil such mysteries, the microscale was probed in terms of diffusivities and microrheometry.

More than one decade ago, Crocker *et al.* [17] introduced the 2P microrheometry as a more reliable method than the 1P one, and suggested that data in the literature should be reconsidered, especially those concerning heterogeneous systems (e.g. cytoplasm of cells). However, Liu *et al.* [39] compared both methods on F-actin solutions. The authors concluded that 1P microrheology was more suitable for measurements of cross-linked networks of semi-

flexible filaments. We have demonstrated that even high PGM concentration would lead to behave as dilute solutions since the viscosity is much higher than elasticity but it showed a frequency-dependence that is compatible with $\omega^{3/4}$. At PGM 5% (w/v), this behavior was not retrieved by bulk rheometry since it was located above the technical limit, but the 2P method characterized this behavior, only seen for PGM 20% (w/v). Despite the homogeneous conditions for 1P, the discrepancies between 1P and 2P methods would be explained by the contributions from long-wavelength longitudinal fluctuations that are reduced if the mucins are treated as semi-rigid or semi-flexible polymers [39]. It seems therefore that fibers either aggregate to form bundles, which are stiffer, or are stiffer by themselves because of the low amount of water available for a proper rehydration. At this 5% (w/v) concentration, it was also found that heterogeneity drastically increased. Indeed, the 500-nm PEG-coated particles exhibited diffusivities widely spread with multimodality (Figure 4D) wherefore 1P method could not be applied suitably [17]. Nevertheless, such method was more adequate when treating lower concentration as semi-dilute solution of flexible polymers where elastic modulus evolves as $\sim\omega^{1/2}$; typical of flexible polymers. Very recent work has characterized the concentration–dependence of PGM and showed that it behaved like dilute solutions below 1.2%, the overlap concentration to semi-dilute solutions where the mucins start to overlap and therefore interact [38]. Due to the neutral pH,it is possible that cross-linking did not occur and did not form a gel [33,34,36]. However, electrostatic interactions would enhance non-covalent cross-linking, giving rise to "weak" gels. The addition of salts (PBS) shielded such interactions [30] but we observed (i) the presence of salts (PBS) or not (DI) did not affect viscoelasticity (Table 1) and (ii) the diffusion of charged particles was affected, showing that active charged patches remained within the PGM network.

From this remark, it is worth describing PGM as (i) a weak viscoelastic gel, exhibiting low moduli but phase angle around 20° at low PGM concentration (0.5-2% (w/v)), (ii) an unentangled semi-dilute solution with flexible polymers at intermediate PGM concentration (5-10% (w/v)), and (iii) an entangled semi-dilute solution with semi-rigid polymers due to partially-hydration conditions for extreme PGM concentration (20% (w/v)). The latter exhibited a high viscosity with phase angle close to 45°.

Such rheological properties appeared to be modulated essentially by the hydration during the reconstitution. Considering the other parameters potentially involved (pH, charge,

purification degree, measurement type), it becomes obvious that all the interpretations through the literature are somewhat controversial.

The characterization of mucin network in terms of mechanical properties helps correlating with diffusivities of particles. High elasticity can arrest them while viscosity can delay their transport. Nevertheless, this is the case at the mesoscopic scale, i.e. when the particle size is similar to the entanglement size. In this paper, we scrutinized the diffusion of particles within the PGM fluids previously described, by modulating their size and surface properties. Lieleg *et al.* used 1-µm microspheres to estimate their diffusion over natural PGM [30] or extracellular matrices [40]. The authors reported that the mucin network presented an electrostatic bandpass suppressing the diffusion of both positively and negatively-charged particles. They also found that high salt concentration inhibited such trapping capacity by shielding electrostatic interactions. In our case, the buffer used (PBS) altered the electrostatic bandpass only at a moderate extent since diffusion of negatively and positively-charged particles was strongly affected compared to neutral PEG-coated NPs (Figure 4). This was also reflected by anomalous diffusion displaying exponent below 0.2 (Figure 4G-H). Many works have used fMPT to investigate the migration of NPs within mucus network, such as the works from Lai *et al.* [7,12,41,42] who showed that viruses were trapped by the cervical mucus, even though the mesh pore size was larger than them [12]. Again, the pore size was in the range 50-1800 nm, displaying a high heterogeneity. Using Eq.(6), the pore size was estimated using the obstruction-scaling model proposed by Amsden *et al.* [23]. Mesh pore size seemed to vary from 470 nm to 240 nm as the PGM concentration increased, which was in good agreement with what was observed in Figure 4; 500-nm PEG-coated NPs underwent a large proportion under free diffusion while others tended to be caged at a PGM concentration of 0.5% (w/v), consistent with the 470-nm estimated pore size. At PGM 5% (w/v), 500-nm PEG-coated particles seemed hindered while 200-nm PEG-coated ones remained almost free diffusive, reflected by an estimation of 240 nm in pore size. Wang *et al.* [24] utilized such model to assess the influence of muco-adhesive particles on the microstructure of cervical mucus. The authors reported that it increased from 380 nm to 470 nm but the bulk rheology was unaffected. They postulated that such particles affected the microstructure by adhering to mucins that triggered bundling and resulted in the increase in pore size.

Those conclusions, even drawn easily, are not fully representative of the heterogeneity but give a limit of size bandpass. With respect to stochastic fluctuations of the mesh, this size exclusion does not obey static rules and ignore any diffusion of the mucins themselves or even reptation. For the first time in the literature, apparent diffusion coefficient of NPs within PGM was resolved as a distribution, showing more than values of mean and error as displayed in Figure 3C. This opens the possibility to give a complete picture of the bandpass spectrum of the mucus mesh. It was then possible to observe the distribution as lognormal with multimodality, reflecting the high heterogeneity of the network. Very recently, Yang *et al.* [43] described the interaction of pseudo-rabies virus with tracheal respiratory mucus and depicted the diffusion as lognormal distribution as well. In addition, the authors experimentally quantified the mesh pore size using AFM, which was found to be between 80 nm and 1500 nm as extremes.

Conclusion

Using fluorescence particle tracking, this work provided a scrutiny on the microstructure of partially purified PGM solutions by the analysis of the diffusivities of nanoparticles and the microrheology. This analysis gave a valuable input by displaying the distribution of apparent coefficient of diffusion that revealed the high heterogeneity of the mesh size. The obstruction-scaling model, used largely to estimate the network pore size, worked suitably but had to be used solely as a size bandpass indicator. The PGM network appeared to be highly heterogeneous and this information was accessible by the lognormal distribution. The modality revealed that the diffusivities had preferential values and the profiles seemed to creep down to low values as PGM concentration increased. The increase in concentration tended to crowd the medium with mucins that forced the solution to be entangled semi-dilute while retaining the large neutral beads. The charged beads were rapidly captured, whatever their size, even smaller than the pore size, as was demonstrated in the literature.

The bulk rheology was connected to the local microrheology by the cross-correlation microrheology, convenient for inhomogenous media. Those methods had to be used jointly for mapping adequately the mechanical properties of the mucin network. They revealed that PGM at low concentration (0.5–2% (w/v)) displayed weak gel properties as semi-dilute solution of flexible polymer exhibiting low moduli but phase angle around 20°, as unentangled semi-dilute solution with flexible polymers at intermediate concentration (5-10%

(w/v)), and as entangled semi-dilute solution with semi-rigid polymers due to partially-hydration conditions at extreme concentrations of 10-20% (w/v). The later still showed viscoelasticity with a remarkable high phase angle value (above 45°). In this work, we postulated that hydration modulated viscoelasticity that does not stick to conventional classification.

The use of partially purified PGM from commercial stocks was controversial. As few other authors, we believe that commercial PGM was pooled, which reduced the biological variability. In this work, this was the case, robust and reliable results were then obtained. On the other side, it was thought that such PGM did not reflect the natural native mucin, due to partial enzymatic degradation. Care was thus taken to reconstitute PGM at 4°C. For this work purpose, PGM of type III remained an adequate model to study the properties of nanoparticle transport and further works will be devoted to investigate the migration of bacteria using the fMPT technique.

REFERENCES

1. Bansil R, Turner B (2006) Mucin structure, aggregation, physiological functions and biomedical applications. Current Opinion in Colloid and Interface Science 11: 164-170.
2. Zhou D, Li J, Li N, Yan G (2004) Study on viscosity property of gastrointestinal mucus. Journal of biomedical engineering 21: 72.
3. Celli JP, Turner BS, Afdhal NH, Ewoldt RH, McKinley GH, et al. (2007) Rheology of gastric mucin exhibits a pH-dependent sol-gel transition. Biomacromolecules 8: 1580-1586.
4. Allen A (1989) Gastrointestinal mucus. Comprehensive Physiology.
5. Cone R (2005) Mucus. In: Mestecky J, Lamm ME, Strober W, Bienenstock J, McGhee JR et al., editors. Handbook of mucosal immunology. London: Academic Press. pp. 49-72.
6. Kirch J, Schneider A, Abou B, Hopf A, Schaefer UF, et al. (2012) Optical tweezers reveal relationship between microstructure and nanoparticle penetration of pulmonary mucus. Proceedings of the National Academy of Sciences of the United States of America 109: 18355-18360.
7. Lai SK, O'Hanlon DE, Harrold S, Man ST, Wang YY, et al. (2007) Rapid transport of large polymeric nanoparticles in fresh undiluted human mucus. Proceedings of the National Academy of Sciences of the United States of America 104: 1482-1487.
8. Suk JS, Lai SK, Wang YY, Ensign LM, Zeitlin PL, et al. (2009) The penetration of fresh undiluted sputum expectorated by cystic fibrosis patients by non-adhesive polymer nanoparticles. Biomaterials 30: 2591-2597.
9. Lai SK, Suk JS, Pace A, Wang YY, Yang M, et al. (2011) Drug carrier nanoparticles that penetrate human chronic rhinosinusitis mucus. Biomaterials 32: 6285-6290.
10. Schuster BS, Suk JS, Woodworth GF, Hanes J (2013) Nanoparticle diffusion in respiratory mucus from humans without lung disease. Biomaterials 34: 3439-3446.
11. Valentine MT, Perlman ZE, Gardel ML, Shin JH, Matsudaira P, et al. (2004) Colloid surface chemistry critically affects multiple particle tracking measurements of biomaterials. Biophys J 86: 4004-4014.
12. Lai SK, Wang YY, Hida K, Cone R, Hanes J (2010) Nanoparticles reveal that human cervicovaginal mucus is riddled with pores larger than viruses. Proceedings of the National Academy of Sciences of the United States of America 107: 598-603.
13. Panorchan P, Wirtz D, Tseng Y (2004) Structure-function relationship of biological gels revealed by multiple-particle tracking and differential interference contrast microscopy: The case of human lamin networks. Physical review E 70: 041906.
14. Rogers SS, Waigh TA, Zhao XB, Lu JR (2007) Precise particle tracking against a complicated background: polynomial fitting with Gaussian weight. Phys Biol 4: 220-227.
15. Pelletier V, Gal N, Fournier P, Kilfoil ML (2009) Microrheology of microtubule solutions and actin-microtubule composite networks. Physical review letters 102: 188303.
16. Qian H, Sheetz MP, Elson EL (1991) Single-particle tracking - analysis of diffusion and flow in 2-dimensional systems. Biophysical Journal 60: 910-921.
17. Crocker JC, Valentine MT, Weeks ER, Gisler T, Kaplan PD, et al. (2000) Two-point microrheology of inhomogeneous soft materials. Physical review letters 85: 888-891.
18. He J, Tang JX (2011) Surface adsorption and hopping cause probe-size-dependent microrheology of actin networks. Physical review E, Statistical, nonlinear, and soft matter physics 83: 041902.

19. Mason TG (2000) Estimating the viscoelastic moduli of complex fluids using the generalized Stokes-Einstein equation. Rheol Acta 39: 371-378.
20. Pelletier V, Gal N, Fournier P, Kilfoil ML (2009) Microrheology of microtubule solutions and actin-microtubule composite networks. Physical review letters 102: 188303.
21. Lau AW, Hoffman BD, Davies A, Crocker JC, Lubensky TC (2003) Microrheology, stress fluctuations, and active behavior of living cells. Physical review letters 91: 198101.
22. Amsden B (1998) Solute diffusion within hydrogels. Mechanisms and models. Macromolecules 31: 8382-8395.
23. Amsden B (1999) An obstruction-scaling model for diffusion in homogeneous hydrogels. Macromolecules 32: 874-879.
24. Wang YY, Lai SK, So C, Schneider C, Cone R, et al. (2011) Mucoadhesive nanoparticles may disrupt the protective human mucus barrier by altering its microstructure. PLoS One 6: e21547.
25. Olmsted SS, Padgett JL, Yudin AI, Whaley KJ, Moench TR, et al. (2001) Diffusion of macromolecules and virus-like particles in human cervical mucus. Biophysical Journal 81: 1930-1937.
26. Shen H, Hu Y, Saltzman WM (2006) DNA diffusion in mucus: effect of size, topology of DNAs, and transfection reagents. Biophys J 91: 639-644.
27. Clark A, Ross-Murphy S (1987) Structural and mechanical properties of biopolymer gels. Biopolymers: Springer Berlin Heidelberg. pp. 57-192.
28. Steffe JF (1992) Rheological Methods in Food Process Engineering: Freeman Press.
29. Dawson M, Wirtz D, Hanes J (2003) Enhanced viscoelasticity of human cystic fibrotic sputum correlates with increasing microheterogeneity in particle transport. The journal of biological chemistry 278: 50393-50401.
30. Lieleg O, Vladescu L, Ribbeck K (2010) Characterization of particle translocation through mucin hydrogels. Biophysical journal 98: 1782–1789.
31. Lafitte G, Thuresson K, Söderman O (2007) Diffusion of nutrients molecules and model drug carriers through mucin layer investigated by magnetic resonance imaging with chemical shift resolution. Journal of Pharmaceutical Sciences 96: 258-263.
32. Lieleg O, Lieleg C, Bloom J, Buck CB, Ribbeck K (2012) Mucin Biopolymers As Broad-Spectrum Antiviral Agents. Biomacromolecules 13: 1724-1732.
33. Celli JP, Gregor B, Turner B, Afdhal N, Bansil R, et al. (2005) Viscoelastic properties and dynamics of porcine gastric mucin. Biomacromolecules 6: 1329-1333.
34. Celli JP, Turner BS, Afdhal NH, Ewoldt RH, MaKindley GH, et al. (2007) Rheology of gastric mucin exhibits a pH-dependent Sol-gel transition. Biomacromolecules 8: 1580-1586.
35. Zhou D, Li J, Li N, Yan G (2004) Study on viscosity property of gastrointestinal mucus. Sheng Wu Yi Xue Gong Cheng Xue Za Zhi 21: 72-73.
36. Delgado-Reyes DA, Ramos-Ramirez EG, Cruz-Orea A, Salazar-Montoya JA (2013) Flow and dynamic viscoelastic characterization of non-purified and purified mucin dispersions. International Journal of Polymer analysis and characterization 18: Published online.
37. Sriamornsak P, Wattanakorn N (2008) Rheological synergy in aqueous mixtures of pectin and mucin. Carbohydr Polym 74: 474-481.
38. Georgiades P, Pudney PDA, Thornton DJ, Waigh T (2013) Particle tracking microrheology of purified gastrointestinal mucins. Biopolymers: n/a-n/a.
39. Liu J, Gardel ML, Kroy K, Frey E, Hoffman BD, et al. (2006) Microrheology Probes Length Scale Dependent Rheology. Physical review letters 96: 118104.

40. Lieleg O, Baumgartel RM, Bausch AR (2009) Selective Filtering of Particles by the Extracellular Matrix: An Electrostatic Bandpass. Biophysical Journal 97: 1569-1577.
41. Lai SK, Wang YY, Cone R, Wirtz D, Hanes J (2009) Altering mucus rheology to "solidify" human mucus at the nanoscale. PLoS One 4: e4294.
42. Wang YY, Lai SK, Suk JS, Pace A, Cone R, et al. (2008) Addressing the PEG mucoadhesivity paradox to engineer nanoparticles that "slip" through the human mucus barrier. Angewandte Chemie 47: 9726-9729.
43. Yang XY, Forier K, Steukers L, Van Vlierberghe S, Dubruel P, et al. (2012) Immobilization of Pseudorabies Virus in Porcine Tracheal Respiratory Mucus Revealed by Single Particle Tracking. PLoS One 7.

Figures

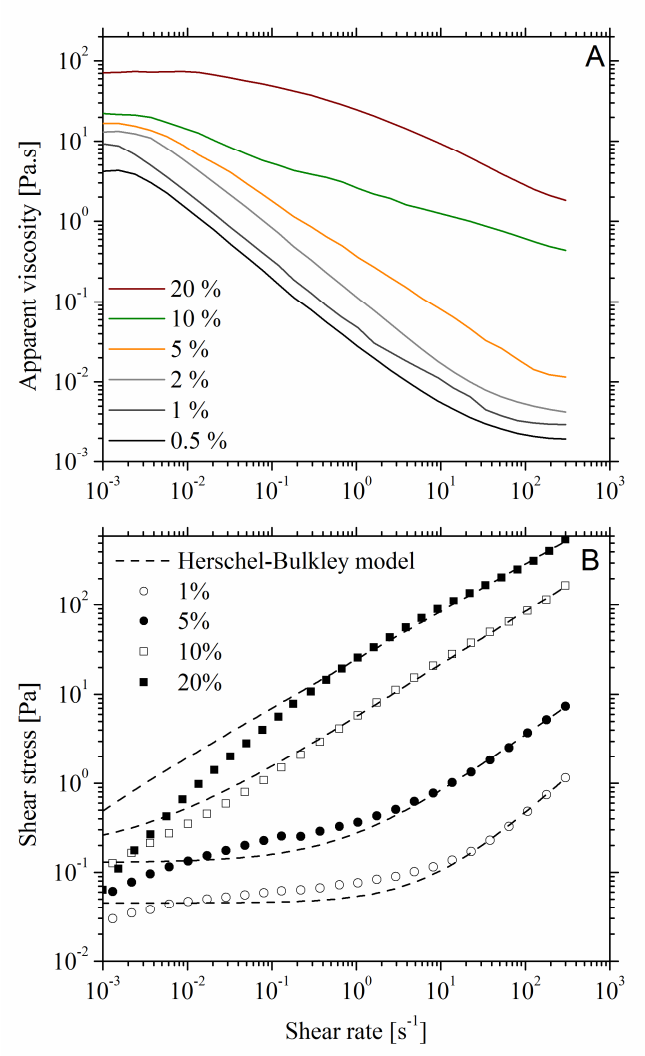

Figure 1: (A) Apparent viscosity versus shear rate and (B) flow curves fitted to the Herschel-Bulkley model (dashed lines) for different mucin concentrations (0.5–20% (w/v)) at T=23°C.

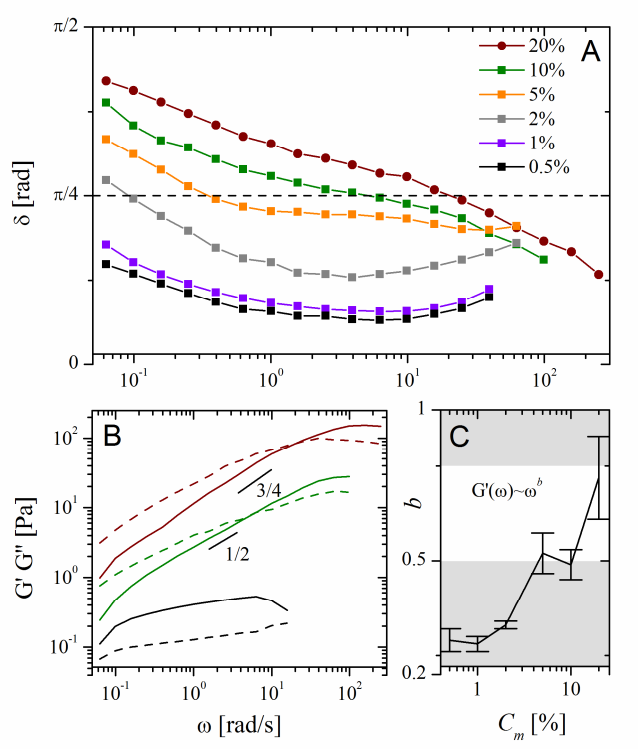

Figure 2: (A) Phase angle as $\tan^{-1}\left(G''/G'\right)$ in radians as function of frequency (rad/s) for concentration C_m (%) in PGM (0.5-20% (w/v)). (B) Loss (G'', dashed lines) and storage (G', solid lines) moduli versus frequency. Only data of 20, 10 and 0.5% (w/v) are depicted for representative purpose. Slopes of 3/4 and 1/2 on G' show the power-law behavior as $G'(\omega)\sim\omega^b$, where the exponent b is indicated in (C) as function of concentration C_m.

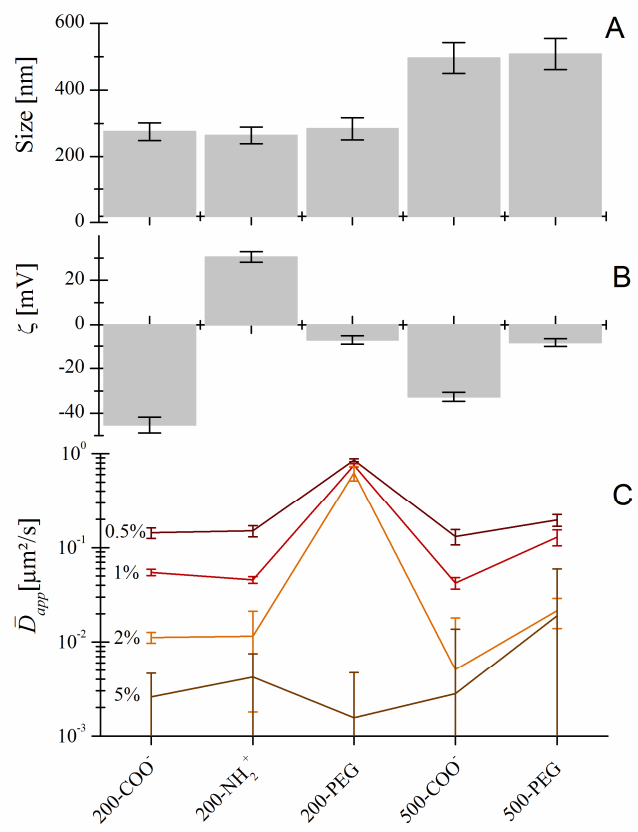

Figure 3 : (A) Size distribution of the NPs measured by light dynamic scattering. Error bars indicate the standard deviation (SD). (B) ζ-potential of the NPs obtained for the electrophoretic mobility using the Smoluchowski theorem in KNO_3 1 mM at pH 7. Error bars indicate SD. (C) Apparent diffusion coefficient of the NPs. Coefficients ensemble-averaged $\bar{D}_{app}$ were determined by particle tracking of ensembles of 2000 particles for each condition. Error bars indicate SD.

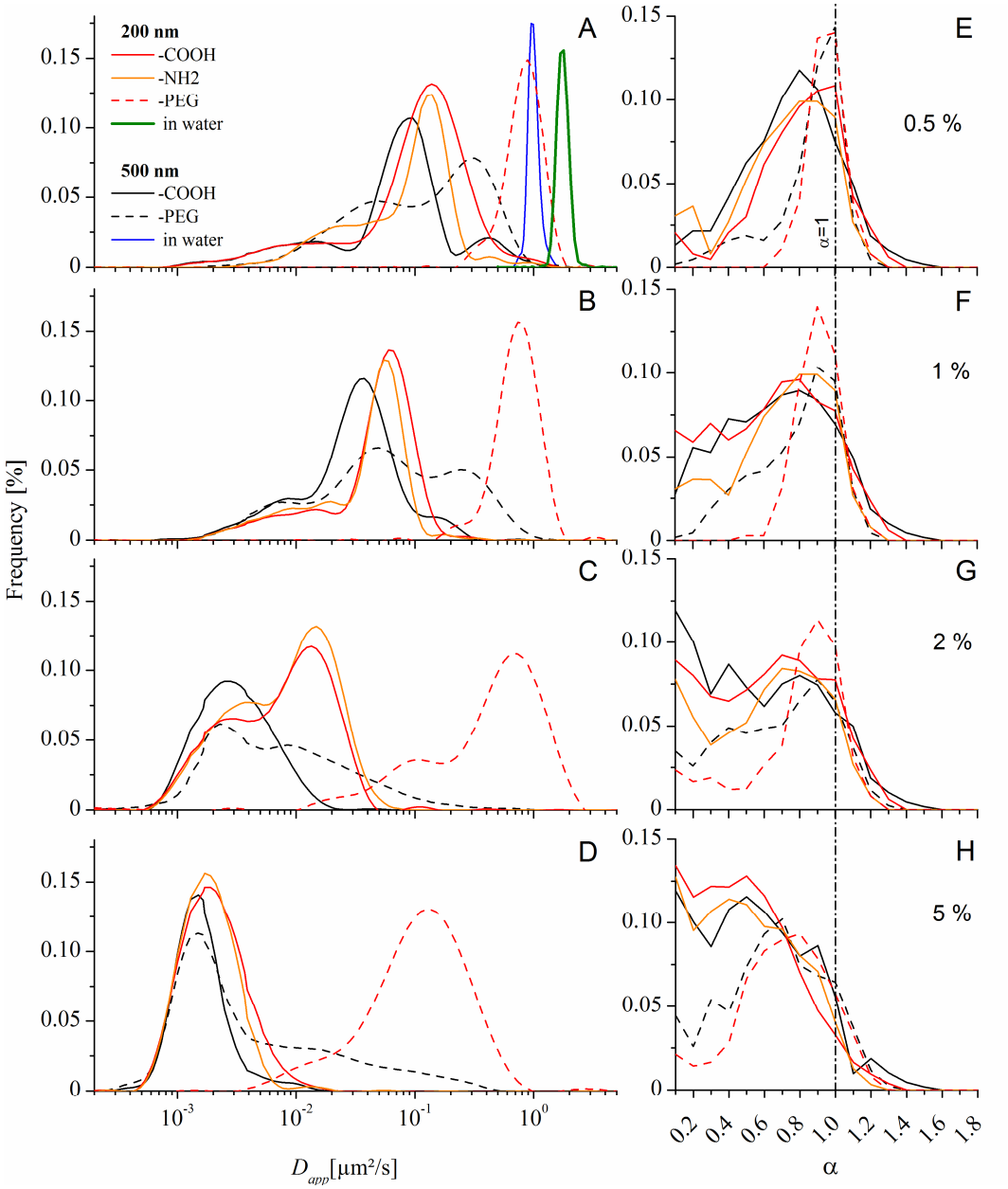

Figure 4: (A-D) Distributions of the apparent diffusion coefficient of carboxyl-, amine- or PEG-modified fluorescent 200-nm and 500-nm nanoparticles (NPs). Trajectories of 10 steps were analyzed for each of the 2000 diffusion coefficients. References peaks are obtained in water. All experiments were conducted at 23°C. (E-H) Transport modes of NPs indicated by α value. Dashed-point vertical line indicates α as unity (free diffusion). More than 2000 trajectories from at least 3 independent experiments were tested to obtain α. Each experiment was performed in PGM at different concentration (w/v) of 0.5% (A,E), 1% (B,F), 2% (C,G) and 5% (D,H).

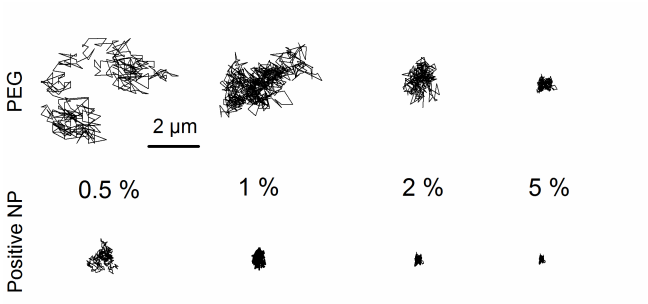

Figure 5: Representative trajectories of PEG-coated 500-nm and positively-charged 200-nm nanoparticles (NPs) over 12 s in PGM solutions (0.5–5% (w/v)). The diffusion of large PEG-coated NPs decreases with PGM concentration, reflecting the mucin mesh shrinkage but diffusion of smaller positively charged NPs is significantly suppressed, even at low concentration.

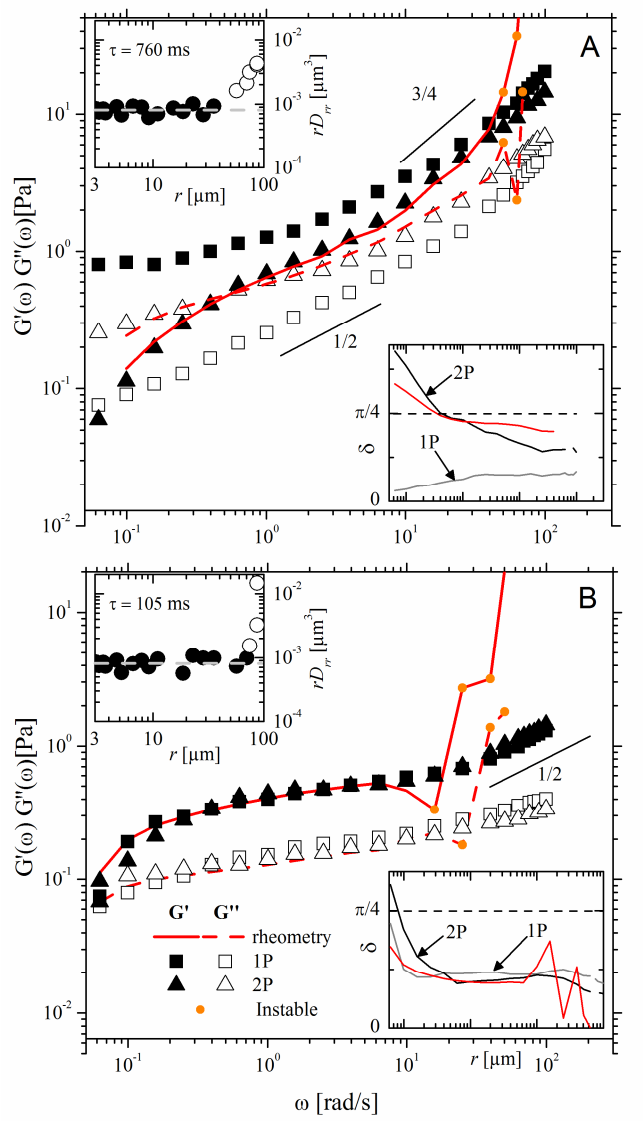

Figure 6: Apparent moduli for (A) 5% (w/v) and (B) 0.5% (w/v) PGM solution using conventional cone-plate rheometry, 1P and 2P microrheometry. Orange filled circles represent instable data originated from geometry inertia from 50 rad/s. Upper insets: fits of rD_{rr} (μm^3) to constant at lag time 0.76 s and 0.105 s, respectively, used to obtain the data for $G^*(\omega)$. Fit was performed over solid symbols; open symbols are outside the range D_{rr}~$1/r$. Lower insets: Phase angle δ over frequency (rad/s) using the same scale of the main plot. Red solid line is the value of rheometry (Figure 2A); black and grey solid lines are obtained from 2P and 1P methods, respectively.

Tables

Table 1. Rheological parameters of PGM suspended in PBS and deionized water (DI) at different concentrations (C_m). η_0 is the apparent viscosity at the lowest shear rate measured (10^{-3} s^{-1}), which is in that case the magnitude of the Newtonian plateau. *K* is the flow consistency coefficient, τ_0 the yield stress, *n* the flow behavior index, $<R^2>$ the regression coefficient and *N* the number of experiments. All variables are accompanied by their standard deviation.

C_m [% w/v]	η_0 [Pa.s]	K [Pa.s^n]	τ_0 [Pa]	n	$<R^2>$	N
PBS (pH 6.6-7.4)						
0.5	4.12 ± 0.25	0.0031 ± 0.0012	0.021 ± 0.002	0.91 ± 0.01	0.998	10
1	9.32 ± 0.79	0.0083 ± 0.0013	0.035 ± 0.005	0.90 ± 0.02	0.999	12
2	12.65 ± 1.56	0.0230 ± 0.0023	0.083 ± 0.004	0.82 ± 0.02	0.998	9
5	16.66 ± 2.01	0.147 ± 0.009	0.128 ± 0.017	0.68 ± 0.01	0.998	11
10	22.32 ± 2.10	5.49 ± 0.24	0.171 ± 0.048	0.59 ± 0.01	0.998	10
20	70.54 ± 4.65	24.60 ± 1.38	-0.113 ± 1.791	0.53 ± 0.01	0.997	12
DI (pH 6.4-7.8)						
0.5	2.47 ± 1.02	0.0082 ±0.0018	0.010 ± 0.002	0.81 ± 0.01	0.998	9
1	7.36 ± 1.33	0.0152 ± 0.0047	0.020 ± 0.004	0.79 ± 0.04	0.997	8
2	10.32 ± 2.52	0.0102 ± 0.0098	0.051 ± 0.005	0.67 ± 0.05	0.998	10
5	14.25 ± 4.65	0.456 ± 0.013	0.074 ± 0.021	0.51 ± 0.07	0.997	10
10	18.64 ± 8.31	4.02 ± 1.69	0.102 ± 0.154	0.61 ± 0.03	0.995	10
20	56.01 ± 12.36	21.32 ± 2.06	-0.231 ± 2.012	0.49 ± 0.02	0.998	10

Table 2. Diffusion with maxima. Standard deviation (SD) over N=2000. *Mesh size obtained from Eq. (6) on individual PEG-coated beads.

C_m (% (w/v))	NP	Maximum (μm²/s)	$\overline{D}_a$ (SD) (μm²/s)	$\overline{D}_a / \overline{D}_w$	Mesh size* (nm)
water	200-PEG	1.7657	1.7737 ± 0.0328	1	-
water	500-PEG	0.9635	0.9892 ± 0.0119	1	-
0.5	200-COOH	0.1385	0.1436 ± 0.0185	0.0810	
	200-NH_2	0.1239	0.1509 ± 0.0203	0.0851	
	200-PEG	0.8902	0.8532 ± 0.0281	0.4810	474
	500-COOH	0.0870	0.1315 ± 0.0241	0.1329	
	500-PEG	0.2915	0.1967 ± 0.0286	0.1988	
1	200-COOH	0.0658	0.0548 ± 0.0043	0.0309	
	200-NH_2	0.0546	0.0457 ± 0.0038	0.0258	
	200-PEG	0.7391	0.7536 ± 0.0295	0.4249	389
	500-COOH	0.0343	0.0423 ± 0.0060	0.0428	
	500-PEG	0.0453	0.1294 ± 0.0249	0.1308	
2	200-COOH	0.0135	0.0112 ± 0.0015	0.0063	
	200-NH_2	0.0148	0.0115 ± 0.0097	0.0065	
	200-PEG	0.6734	0.6242 ± 0.1079	0.3519	250
	500-COOH	0.0028	0.0051 ± 0.0129	0.0052	
	500-PEG	0.0023	0.0215 ± 0.0076	0.0217	
5	200-COOH	$1.803\ 10^{-3}$	$(2.601 \pm 4.790)\ 10^{-3}$	$1.466\ 10^{-3}$	
	200-NH_2	$1.761\ 10^{-3}$	$(4.215 \pm 1.896)\ 10^{-3}$	$2.376\ 10^{-3}$	
	200-PEG	$1.301\ 10^{-3}$	$(1.561 \pm 0.315)\ 10^{-3}$	$0.8801\ 10^{-3}$	245
	500-COOH	$1.451\ 10^{-3}$	$(2.814 \pm 10.86)\ 10^{-3}$	$2.845\ 10^{-3}$	
	500-PEG	$1.512\ 10^{-3}$	$(19.02 \pm 11.72)\ 10^{-3}$	$19.23\ 10^{-3}$	

CHAPTER IV. DISCUSSION-

GENERAL CONCLUSION

Chapter IV. Discussion - General conclusion

Context

The digestive epithelium is covered with a protective mucus layer that has the consistence of viscoelastic and permeable gel. This layer is the preferential habitat for commensal bacteria and plays a role in the defense against bacterial infections by expelling pathogens from the mucosal surface. Mucus is organized around secreted mucins that are large glycoproteins, based on protein backbone structures rich in serine and threonine, which are linked to a wide variety of O-linked oligosaccharide side chains, arranged in a bottle-brush configuration and constituting more than 70% of the weight of the molecule. Such O-glycans represent nutrients and energy source for bacteria, and/or potential ligands for microbial adhesins, probably contributing in this way to the selection of the species-specific microbiota.

Elucidating the barrier properties of mucus, i.e. its structure and associated trapping ability, is actually a major concern. At the nanoscale, mucus has been depicted as a heterogeneous mesh network of mucin fibers, with a fiber diameter in the range 5-10 nm, and more particularly 7 nm for intestinal mucins. Numerous works report the use of nano- or micron-sized, and non muco-adhesive nanoparticles as probes to determine the spacing between mucin fibers for various mucus sources with Multi-Particle Tracking experiments (Lai *et al.*, 2007; Lai *et al.*, 2010; Lai *et al.*, 2011; Schuster *et al.*, 2013; Suk *et al.*, 2009). The mesh structure obtained (of about several hundreds of nanometers) is generally wider than the pore size expected assuming a random array of individual mucin fibers. In fact, physico-chemical interactions within the mucin network, such as hydrophobic interactions, may cause mucin fibers to self-condense and/or bundle with others, forming mucin cables thicker than individual mucin fibers, which in turn create larger pores. Trapping ability of mucus is also suspected to be an interplay between size and interaction effects, in close relation with its microstructure and rheological properties.

To date, only few data are available on the migration ability of beneficial bacteria, like Lactic Acid Bacteria (LAB), within intestinal mucus gels. However, an increasing attention is paid to their muco-adhesive phenotype, in relation with the cell surface determinants involved. Indeed, adhesion ability of LAB to mucus may be correlated to their residence time and subsequent beneficial activities to host health. A special interest is dedicated to commensal *Lactobacillus* species, with the aim of identifying novel probiotics based on their capacity to persist within the gut. In this framework, several cell surface proteins have been shown to act as specific mediators of *Lactobacillus* adhesion to mucus, like mucus-binding proteins and pili.

In this framework, our research group at the "Laboratoire d'Ingénierie des Systèmes Biologiques et des Procédés" of Toulouse has focused on the model LAB *L. lactis*. Since 2008, we have developed numerous studies on the structural and functional factors involved in muco-adhesion of lactococci by coupling *in vitro* approaches from nanoscale with AFM force spectroscopy to multi-cellular level using quartz crystal microbalance with dissipation monitoring (Dague *et al.* 2010; Le *et al.* 2011; Le *et al.* 2012). The present work was based on a more integrative strategy combining Microbiology, Physico-chemistry and Biophysics, in collaboration with the Institute Micalis of Jouy-en-Josas and with the "Transfert, Interface, Mélange" team of the "Laboratoire d'Ingénierie des Systèmes Biologiques et des Procédés". We chose the *L. lactis* subsp. *lactis* isolate TIL448, due to its outstanding properties, including high hydrophobicity, electronegativity and strong adhesion to polystyrene (Giaouris *et al.* 2009), and specific attachment to Caco-2 intestinal cell line. This atypical behavior was assigned to the presence of pili (Meyrand *et al.* 2013). A mucus-binding protein, which exhibited high sequence similarity with putative MUB proteins (Boekhorst *et al.* 2006) of *L. citreum* KM20 and *L. fermentum* and contained two MucBP domains (PF06458), was also depicted. Both surface proteins were defined as adhesin candidates (Meyrand *et al.* 2013). However, their interactions with mucus and, more particularly, mucins remained so far unknown. In this framework, adhesion and migration through mucin (Pig Gastric Mucin (PGM))-based gels of *L. lactis* TIL448 were characterized, in close relation with, on the one hand, the *L. lactis* cell surface specific determinants (pili and mucus-binding protein) and, on the other hand, the rheology and microstructure of the PGM network.

Pili and surface mucus-binding protein contribute to the adhesion of *L. lactis* TIL448 to PGM, depending on the static or dynamic nature of the environment and how interactions are probed.

AFM measurements were performed on *L. lactis* subsp. *lactis* TIL448 and its derivatives (plasmid-cured derivative TIL1230, pilin mutant TIL1289 and mucus-binding protein mutant TIL1290) for probing interaction mechanisms with PGM, in collaboration with the "Laboratoire d'Analyse et d'Architecture des Systèmes" and "Institut des Technologies Avancées" en Sciences du Vivant of Toulouse. The AFM lacto-probe was first characterized using SEM. As previously depicted for other *L. lactis* strains (Dague *et al.*, 2010; Le *et al.*, 2011), with the PEI-based immobilization method, clusters of cells were typically attached and the sensitivity of a "true" single cell on the AFM tip could not be achieved. A recent study has developed the concept of single-cell AFM tip, using colloidal probe cantilevers combined with bioinspired polydopamine polymers (Beaussart *et al.*, 2013). However, worth is mentioning the heterogeneity of the physiological state/surface physico-chemical properties within a given bacterial population. In particular, Oxaran *et al.* (2012) recently depicted that, for a *L. lactis* piliated strain, only part of the bacterial population seemed piliated. According to the cell which is trapped on the tip, adhesive and muco-adhesive profiles may thus differ. That is the reason why AFM measurements were performed with different independent probes and scanning zones (5 x 5 μm^2, homogeneous PGM layer, see Dague *et al.*, 2010) and results were shown to be highly reproducible. Then, the lacto-probe viability was evaluated, using CFDA labelling. For TIL448 and TIL1230 strains, attached bacterial cells remained viable, or at least esterase active, even after 2-h contact time.

In parallel, shear-flow induced detachment was characterized for the same panel of *L. lactis* strains under laminar well-defined flow field conditions, which are more relevant from a physiological point of view. In fact, dynamic conditions are encountered in many compartments within the gastrointestinal tract (e.g. shear fluctuations caused by salivary washing or intestinal peristalsis (Jeffrey *et al.*, 2003)). Thus, the advantages of the flow chamber method are not only the *in situ* observation of the detachment process without any air/liquid interface and the well-controlled shear stress but also the dynamic conditions mimicking, at least to some extent, the gastro-intestinal tract environment. *L. lactis* bacterial cells attached to the PGM coating were exposed to hydrodynamic drag and torque that both increase with applied wall shear stress.

For the first time in the literature, data derived from a single-cell scale “static” method (AFM) vs. a multi-cellular scale “dynamic” one (flow chamber) were combined to demonstrate the strong and specific adhesion of *L. lactis* TIL448 to PGM and to establish the role of mucus-binding protein and pili in its muco-adhesive phenotype, by using targeted defective-mutants. Contribution of these cell surface determinants, previously shown to be key parameters in lactobacilli muco-adhesion (Boekhorst *et al.*, 2006; von Ossowski *et al.*, 2010) was equivalent, as “sensed” under AFM conditions. Indeed, nearly identical characteristic values were reached for both mutants: (i) percentage of specific adhesive events of 26 % and 29 % (wild type strain: 60%) and (ii) adhesion force of 0.10 ± 0.03 nN and 0.12 ± 0.04 nN (wild type strain: 0.18 ± 0.04 nN), for the pilin and mucus-binding protein mutants, respectively. In contrast with AFM, a more important contribution of the mucus-binding protein than pili in the muco-adhesive phenotype of *L. lactis* was assessed under shear flow. However, one should mention the difference of the nature of external force applied for each method. With AFM, the tip of the cantilever pushes the bacterial cells against the surface and then bring them away, normal to the surface, while the flow chamber method uses the hydrodynamic force to detach cells, mainly *via* rolling. Furthermore, (Boonaert *et al.* 2001) indicated that the loading force in AFM may influence *L. lactis* adhesion to the substratum. The easier detachment under shear flow of the piliated mutant (TIL1290), compared to its non-piliated counterpart (TIL1289), was related to the presence of long pili (detection with AFM of rupture events up to 600-800 nm), and their characteristics, including low density and nanomechanical properties (flexibility and inextensibility). Nevertheless, one could not ignore the influence of non-specific physico-chemical properties, as probed by AFM and flow chamber, since the four strains under study exhibited different cell surface hydrophobicity: TIL448 and TIL1289 were highly hydrophobic whereas TIL1230 and TIL1290 were mildly hydrophilic. In contrast, surface charge values were close.

In addition, MALDI-MS analysis of O-glycans, performed in collaboration with the "Unité de Glycobiologie Structurale et Fonctionnelle" of Villeneuve d'Ascq, revealed that PGM is substituted by a complex mixture of neutral and sulfated glycans, the size of which ranges from two to twelve monosaccharides. Then, AFM blocking assays demonstrated that neutral oligosaccharides, like fucose, were rather mainly involved in interactions between PGM and *L. lactis* TIL448. In agreement with these findings, the TIL448 plasmid-encoded tip pilin, probably located at the extremity of the pili appendages, contains a lectin-type domain

(PF00139 or *Lectin_leg* domain) characteristic of leguminous lectins, which bind typically hexoses and/or hexosamines (Sharon and Lis, 1990). In addition, fucose was assumed to be involved in the interactions between PGM and the mucus-binding protein of *L. lactis* TIL448, based on previous works on *L. reuteri* (Roos and Jonsson, 2002) and, more recently, on lectins (Gunning *et al.*, 2013). A schematic representation of the *L. lactis* TIL448/PGM specific interactions is given in **Figure IV.1.**

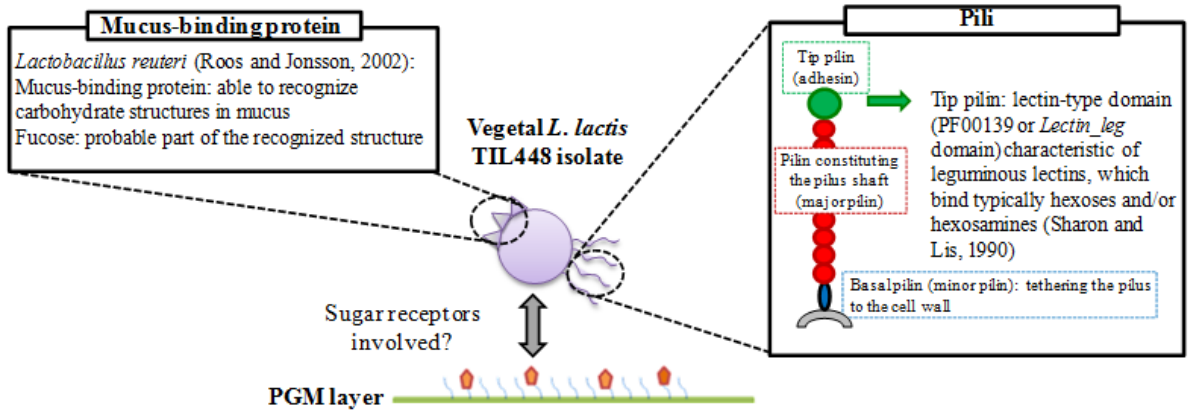

Figure IV.1. Schematic representation of the *L. lactis* TIL448/PGM specific interactions, showing the sugar receptors of PGM potentially involved. The pilus model has been adapted from the data Reunanen *et al.* (2012) presenting the SpaCBA pili of *L. rhamnosus* GG.

In conclusion, the nature and functional role of cell surface specific mediators of binding to mucins was the first time unraveled for lactococci. The contribution of both mucus-binding protein and pili was clearly assessed. This was previously demonstrated in lactobacilli, for instance for *L. reuteri* (Mackenzie *et al.*, 2010) and *L. rhamnosus* GG (Kankainen *et al.*, 2009; Tripathi *et al.*, 2013), for MUB and pili, respectively. We showed that such contribution was closely related to the static or dynamic nature of the environment and how interactions are probed. Furthermore, the interactions of cell surface determinants with mucins was found to be a direct recognition through ligand/receptor bonding, as presented in **Figure IV.1** and/or an indirect mechanism through non-specific interactions, due to different *L. lactis* surface physico-chemical properties, like hydrophobicity.

The migration of *L. lactis* TIL448 inside PGM-based hydrogels is governed by a complex interplay between adhesive and muco-adhesive properties.

As mentioned above, the mucus layer forms a protective barrier of intestinal epithelial cells, notably against pathogens. However, certain pathogens have developed strategies for avoiding to be trapped by mucus in order to reach the underlying mucosa. For instance, they can secrete toxins that disrupt epithelial cells and consequently alter the production of mucins and the barrier function of mucus (McGuckin *et al.* 2011). They can also produce enzymes, such as glycosidases and proteases (McGuckin *et al.* 2011), the activity of which results in the breakdown of mucin structure, the substantial decrease in mucus viscoelasticity, and its facilitated dispersal. *Vibrio cholera* was shown to be able to translocate through a mucin-containing gel by producing the mucinolytic haemagglutinin/protease (Hap) (Silva *et al.* 2003). In addition, *H. pylori* may overcome the mucus barrier by changing the local pH (Moore *et al.* 2011). Besides, one common feature of enteric pathogens is the presence of flagella, which allow them to propel within the mucus gel (Ottemann and Lowenthal 2002, Ramos *et al.* 2004). Flagellated bacteria possess a remarkable motility system, based on a rotary motor driving the cell toward chemical gradients (chemotaxis). For instance, the motility of a flagellated *Escherichia coli* strain was found as high as 30 μm/s (Turner *et al.* 2000) and, in general, motile cells can diffuse about 1000 times faster than non-motile ones (Kim 1996). Contrary to pathogens, few data are currently available on the diffusivity of beneficial bacteria, like Lactic Acid Bacteria (LAB), and their migration ability within mucus gels. Based on this background, we aimed at estimating the diffusion coefficient of fuchsine-stained *L. lactis* TIL448 and its derivatives (plasmid-cured derivative, pilin mutant and mucus-binding protein mutant) inside PGM-based hydrogels. Note that fuchsine labelling had no significant impact on cell viability and surface physico-chemical properties. To achieve the above aim, a novel method, named Diffusion Front Tracking (DFT) and recently developed in the team "Transfert, Interface, Mélange" of "Laboratoire d'Ingénierie des Systèmes Biologiques et des Procédés" for O_2 diffusion coefficient measurements in liquids (Jimenez *et al.*, 2013) was implemented. The method feasibility was first demonstrated. Then, diffusion coefficients were evaluated for the four strains under study. For instance, for a PGM concentration of 0.5% (w/v), values of 8.2×10^{-12} m^2/s, 89.8×10^{-12} m^2/s, 12.9×10^{-12} m^2/s, 22.8×10^{-12} m^2/s and were reported for the wild type, the plasmid-cured derivative, the pilin mutant and the mucus-binding protein mutant, respectively. The lowest diffusion

coefficient was obtained for the wild type strain whereas the highest one was achieved for the plasmid-cured derivative. The pilin mutant had a diffusion coefficient lower than that observed for the mucus-binding protein mutant. Altogether, these results underline that migration of *L. lactis* inside PGM-based hydrogels is significantly influenced by its muco-adhesive profile, i.e. the strain exhibiting the strongest interactions with PGM tends to be more entangled than a less muco-adhesive one. Nevertheless, as previously pointed out, the contribution of non-specific interactions, like hydrophobic ones, could not be ignored.

Since *L. lactis* is non-motile, its movement through PGM gels was mainly governed by Brownian diffusion. However, we should note that the diffusivity values are 1 or 2 orders of magnitude higher than that previously reported for non-motile cells (of about $5x10^{-13}$ m^2/s, Kim, 1996). This discrepancy could be due to cell aggregation, as previously depicted for *Klebsiella pneumoniae* (Kim, 1996). This is all the more probable since piliated *L. lactis* bacteria tend to form aggregates (Oxaran *et al.*, 2012). Another possible explanation was sedimentation of PGM within the Hele-Shaw chamber. Further experiments will thus be devoted to elucidate such biological and physical effects (see below).

The trapping potential of PGM is governed by its microstructure, mechanical and rheological properties.

In the previous part, independently of the strains and their adhesive/muco-adhesive properties, bacterial cells were shown to be more diffusive in a 0.5% (w/v) PGM gel than in a 5% (w/v) one. On this basis, a thorough analysis of the microstructure and mechanical properties of commercial PGM of type III was performed. Gel microstructure was probed by the analysis of diffusivities of 200-nm and 500-nm fluorescent nanoparticles with different surface properties (carboxyl-terminated, negatively charged tracers, with and without PEG coating; amine-terminated, positively charged tracers), using fluorescence Multiple-Particle Tracking as previously depicted (Lai *et al.*, 2007; Lai *et al.*, 2010; Lieleg *et al.*, 2010). Rheology characterization was carried out alongside with microrheometry approaches.

The mean mesh pore size, as derived from the obstruction-scaling model, was shown to vary between 470 nm and 240 nm, as the PGM concentration increased from 0.5% to 5% (w/v), which was fully consistent with the nanoparticle migration behavior inside the gel. However this model had to be solely used as a size bandpass indicator, since the distribution of

apparent diffusion coefficient was found lognormal with multimodality, reflecting the high heterogeneity of the network. Except the recent work depicted by Yang *et al.* (2012) for probing interaction of pseudo-rabies virus with tracheal respiratory mucus, this kind of approach has never been investigated in the literature, thus now offering the possibility to give a complete picture of the bandpass spectrum of the mucus mesh. We could imagine to experimentally confirm the mesh pore size distribution using, for instance, AFM (Yang *et al.*, 2012). In agreement with our findings, in a recent study (Teubl *et al.* 2013), the 3-dimensional network properties of commercial PGM at a concentration of 10% (w/v) were evaluated by SEM. Parallel and crossing mucin fibers were observed (**Figure IV.2**), with pore sizes up to 0.9 µm in diameter.

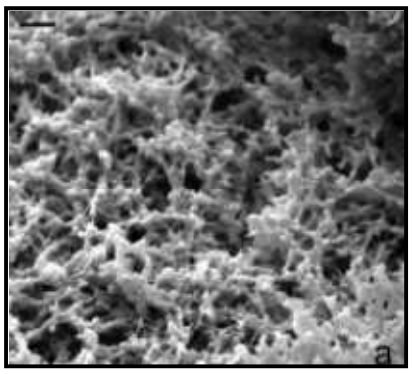

Figure IV.2. SEM image of the network formed by the porcine stomach mucin; scale bar = 1 µm (from Teubl *et al.*, 2013).

Furthermore, the bulk rheology was connected to the local microrheology by the cross-correlation microrheology, convenient for inhomogenous media. Those methods had to be used jointly for mapping adequately the mechanical properties of the mucin network. Delgado-Reyes *et al.* (2013) described PGM of type III accordingly with the theory of viscoelasticity, i.e. the frequency-dependence as $G' \sim \omega^n$ with n decreasing roughly from 2 to 0.5 with concentration. Our results do not confirm such findings; at low concentration (0.5-2% (w/v)), PGM behaves as a semi-dilute solution of flexible polymer described by gel properties (phase angle below 45°). Extreme PGM concentrations (>20% (w/v)) lead to counter-intuitive observations: PGM behaves as a dilute solution of semi-flexible polymers, with liquid-like properties at low frequency. This was not retrieved by other works. In fact, high concentrations experienced difficulties to rehydrate (more than 24 h at 4°C) and it was not possible to circumvent the presence of bubbles. Unfortunately, such mm-sized bubbles are the main source of disturbances during rotational rheometry (note that the stress evolves as $1/R^3$ with R the radius of the mobile geometry, bubbles are expelled to the periphery and

capillary forces biased by 50-100% the apparent shear stress). Demonstrating that rheology on commercial PGM was not similar to that achieved with native mucin was not significantly convincing to state that PGM of type III is not a relevant model. At physiological concentrations (0.5-5% (w/v), results were robust and reflected the low biological variability obtained by the commercial PGM. Indeed, many samples were initially pooled before purification.

In addition, diffusivities of 200-nm and 500-nm agreed with previous works in terms of mesh size and charge filtering. Pore size was determined to be between 240 and 470 nm for PGM 5% and 0.5% (w/v), respectively. In section III.1.2 using the DFT method, *L. lactis* strains were prone to diffuse at about 10 µm²/s in order of magnitude. This means that 1 or 2-µm sized bacteria were able to migrate about 1000-fold faster than beads, with respect to size 2 to 5 times smaller than the bacterial cell dimensions. These results were thus not consistent and to account for such unexpected differences, several assumptions may be formulated. Firstly, in fMPT, the samples were allowed to equilibrate 2 h prior experiment and sequences lasted 20 s. On the other hand, in DFT, even reflecting diffusion process described by fitting the diffusion leading front by the Fick's law, the conditions were situated at the first contact time between the PGM solution and the cell suspension at the top and the experiments were much longer in time. Conditions were therefore not comparable and different regimes may be revealed; the sedimentation was not detected on the front curve, but sedimentation of both bacterial cells and PGM could ascribe such high diffusion. Additionally, the mucus layer stands on few hundreds of micrometers *in vivo*, which was reproduced in the fMPT method (250-µm thick) but far not in DFT (few centimeters). Even in rheometry, the gap between cone and plate was 5 mm at the periphery. The network was probably not fully formed and very large voids may be present. A threshold in gap thickness (2 mm in DFT versus 0.25 mm in fMPT) could explain those discrepancies and insure the integrity of the mucus network. Finally, it has been observed in section III.2 that the mucus network exhibits high heterogeneity in pore size. Since DFT measures the diffusion front, only the fastest population seemed to be monitored, therefore giving a part of the population. With these hypotheses in mind, a straightforward perspective could be reducing the gap by a factor of 4 in order to stabilize the PGM suspension.

As a general conclusion, the muco-adhesion and migration phenotype of the vegetal isolate *L. lactis* subsp. *lactis* TIL448 was unraveled at multi-scale, by coupling different biophysical

tools such as AFM force spectroscopy, shear stress flow chamber, Diffusion Front Tracking method and fluorescence Multi-Particle Tracking. Commercial Pig Gastric Mucin (PGM) of type III, once properly reconstituted, was demonstrated to be a robust and reliable model for investigating adhesive, rheological and trapping properties of mucus. Using the wild type *L. lactis* strain, in conjunction with pilin and mucus-binding protein defective mutants, the combined role played by both surface proteins in adhesion to PGM was established, with a contribution closely depending on how interactions are probed. The importance of the sugar receptors of PGM, mainly of neutral type, was demonstrated. In addition, adhesion and migration of *L. lactis* inside PGM-based hydrogels were governed by a complex interplay between specific (bacterial adhesin(s)/sugar receptors) and non-specific (e.g. electrostatic and/or hydrophobic interactions) interactions. Trapping properties were also influenced by the microstructure and the mechanical properties of the PGM network. A high heterogeneity of the mesh pore size was highlighted. This study, positioned at the interface between Biology and Physics, will undoubtedly provide new insights into the interactions of *L. lactis* with the mucosal environment in the gastrointestinal tract, contributing to further applications in human health as a probiotic or a delivery vector for therapeutic molecules.

APPENDIX

APPENDIX. Experimental protocols for DFT measurements

I. Preparation of PGM hydrogels

The lyophilized powder PGM (Sigma-Aldrich M1778, partially purified type III) was rehydrated in PBS at two concentrations 0.5 and 5% (w/v) and kept overnight under gentle shaking at 4°C. Prior to each experiment, the PGM hydrogel was subjected to a process of degassing to remove any unwanted air bubbles.

II. Preparation of bacterial cells

The strains TIL1248 (GFP-tagged wild type strain), TIL1250 (GFP-tagged plasmid-cured derivative), TIL1289 (pilin mutant) and TIL1290 (mucus-binding protein mutant) were considered throughout this study. Bacterial stock cultures were kept at -80°C in M17 broth (Oxoid), containing 0.5 % (w/v) glucose and 20 % (v/v) glycerol. Bacteria were first sub-cultured overnight at 37°C in M17-glucose (0.5 % (w/v)) medium (M17Glc). This preculture was then used to inoculate M17Glc at 37°C. Erythromycin or chloramphenicol (5 µg/mL) was added when required. Bacteria were harvested during the exponential growth phase (optical density at a wavelength of 600 nm (OD_{600nm}) of 1.2) by centrifugation (4000 rpm, 10 min, room temperature), washed twice with phosphate buffered saline (PBS), and concentrated to an OD_{600nm} of 3.5. The cell suspension was mixed with the magenta dye fuchsin (Merck KGaA, Germany) with a ratio 4:6 and left for 10 min. The mixture was then centrifuged at 4000 rpm for 15 min at room temperature and subsequently washed twice with PBS.

III. Viability test by counting colony-forming units (CFU/ml)

Viability of *L. lactis* bacterial cells was evaluated before staining as a control, immediately after fuchsine staining, and after 2 h and 4 h, corresponding to the maximal duration for DFT measurements. Serial dilutions of the cell suspension in PBS were plated on M17Glc agar with the appropriate antibiotic. Plates were then incubated at 37°C for 24 h. Results are expressed in CFU/mL. For each strain under study, three independent cultures were considered.

IV. Cell surface hydrophobicity

To determine the *L. lactis* cell surface hydrophobicity, hexadecane was chosen as the apolar solvent. Bacterial cells before and after fuchsin staining were diluted in PBS at a final OD_{600nm} of 0.5-0.6. The cell suspension (2.4 mL) was mixed with 0.4 mL of hexadecane (Sigma) for 10 s by manual shaking and 50 s at maximum intensity on a vortex-type agitator. The mixture was allowed to stand for 15 min to ensure that the two phases were completely separated before a sample of 1 mL was carefully removed from the aqueous phase. Its optical density was measured at 600 nm. The microbial affinity to hexadecane was calculated as follows:

$$\% \text{ affinity} = \left(1 - \frac{OD}{OD_0}\right) \times 100 \qquad \text{(A.1)}$$

where OD_0 is the optical density at 600 nm of the bacterial suspension before mixing with hexadecane and OD is the optical density at 600 nm of the bacterial suspension after mixing and phase separation. Each measurement was performed in triplicate and, for each strain, three independent cultures were considered.

V. Cell surface charge

The global electrical properties of the *L. lactis* cell surface were assessed by measuring the electrophoretic mobility of bacterial cells. Experimentally, *L. lactis* cells with and without fuchsin staining were washed by three centrifugations (4000 rpm, room temperature, 10 min) and re-suspended in KNO_3 1 mM pH 7.0 at an OD_{600nm} of 0.2-0.3. The electrophoretic mobility was measured with an automated laser zetasizer Nano (Malvern Instruments, USA) under a 50-V electric field. Each measurement was performed in triplicate and, for each strain, three independent cultures were considered.

REFERENCES

Alegre-Cebollada, J., C. L. Badilla and J. M. Fernandez (2010). *Isopeptide bonds block the mechanical extension of pili in pathogenic Streptococcus pyogenes*. J Biol Chem **285**(15): 11235-11242.

Allen, A. (1989). *Gastrointestinal mucus*. Comprehensive Physiology.

Allen, A., W. Cunliffe, J. Pearson, L. Sellers and R. Ward (1984). *Studies on gastrointestinal mucus*. Scandinavian journal of gastroenterology. Supplement **93**: 101.

Amsden, B. (1998). *Solute diffusion within hydrogels. Mechanisms and models*. Macromolecules **31**(23): 8382-8395.

Amsden, B. (1999). *An obstruction-scaling model for diffusion in homogeneous hydrogels*. Macromolecules **32**(3): 874-879.

Atuma, C., V. Strugala, A. Allen and L. Holm (2001). *The adherent gastrointestinal mucus gel layer: thickness and physical state in vivo*. American Journal of Physiology-Gastrointestinal and Liver Physiology **280**(5): G922-G929.

Ayad, E. H., A. Verheul, C. de Jong, J. Wouters and G. Smit (1999). *Flavour forming abilities and amino acid requirements of Lactococcus lactis strains isolated from artisanal and non-dairy origin*. International Dairy Journal **9**(10): 725-735.

Ayad, E. H., A. Verheul, J. Wouters and G. Smit (2001). *Population dynamics of lactococci from industrial, artisanal and non-dairy origins in defined strain starters for Gouda-type cheese*. International Dairy Journal **11**(1): 51-61.

Ayad, E. H., A. Verheul, J. Wouters and G. Smit (2002). *Antimicrobial-producing wild lactococci isolated from artisanal and non-dairy origins*. International Dairy Journal **12**(2): 145-150.

Baddiley, J. (1989). *Bacterial cell walls and memebranes. Discovery of the teichoic acids*. Bioessays **10**: 207-210.

Bansil, R. and B. S. Turner (2006). *Mucin structure, aggregation, physiological functions and biomedical applications*. Current Opinion in Colloid & Interface Science **11**(2): 164-170.

Bausch, A. R., W. Moller and E. Sackmann (1999). *Measurement of local viscoelasticity and forces in living cells by magnetic tweezers*. Biophysical Journal **76**(1): 573-579.

Beaussart, A., S. El-Kirat-Chatel, P. Herman, D. Alsteens, J. Mahillon, P. Hols and Yves F. Dufrêne (2013). *Single-Cell Force Spectroscopy of Probiotic Bacteria*. Biophysical journal **104**(9): 1886-1892.

Bergonzelli, G. E., D. Granato, R. D. Pridmore, L. F. Marvin-Guy, D. Donnicola and I. E. Corthesy-Theulaz (2006). *GroEL of Lactobacillus johnsonii La1 (NCC 533) is cell*

surface associated: potential role in interactions with the host and the gastric pathogen Helicobacter pylori. Infection and immunity **74**(1): 425-434.

Bergstrom, K. S., V. Kissoon-Singh, D. L. Gibson, C. Ma, M. Montero, H. P. Sham, N. Ryz, T. Huang, A. Velcich, B. B. Finlay, K. Chadee and B. A. Vallance (2010). *Muc2 protects against lethal infectious colitis by disassociating pathogenic and commensal bacteria from the colonic mucosa*. PLoS Pathogens **6**(5): e1000902.

Bermudez-Humaran, L. G., N. G. Cortes-Perez, F. Lefevre, V. Guimaraes, S. Rabot, J. M. Alcocer-Gonzalez, J.-J. Gratadoux, C. Rodriguez-Padilla, R. S. Tamez-Guerra and G. r. Corthier (2005). *A novel mucosal vaccine based on live Lactococci expressing E7 antigen and IL-12 induces systemic and mucosal immune responses and protects mice against human papillomavirus type 16-induced tumors*. The Journal of Immunology **175**(11): 7297-7302.

Boekhorst, J., Q. Helmer, M. Kleerebezem and R. J. Siezen (2006). *Comparative analysis of proteins with a mucus-binding domain found exclusively in lactic acid bacteria*. Microbiology **152**(1): 273-280.

Boguslawska, J., J. Zycka-Krzesinska, A. Wilcks and J. Bardowski (2009). *Intra- and interspecies conjugal transfer of Tn916-like elements from Lactococcus lactis in vitro and in vivo*. Appl Environ Microbiol **75**(19): 6352-6360.

Bolotin, A., B. Quinquis, S. D. Ehrlich and A. Sorokin (2012). *Complete genome sequence of Lactococcus lactis subsp. cremoris A76*. Journal of bacteriology **194**(5): 1241-1242.

Bolotin, A., P. Wincker, S. p. Mauger, O. Jaillon, K. Malarme, J. Weissenbach, S. D. Ehrlich and A. Sorokin (2001). *The complete genome sequence of the lactic acid bacterium Lactococcus lactis ssp. lactis IL1403*. Genome Research **11**(5): 731-753.

Boonaert, C., P. Rouxhet and Y. Dufrene (2000). *Surface properties of microbial cells probed at the nanometre scale with atomic force microscopy*. Surface and interface analysis **30**(1): 32-35.

Boonaert, C. J. P., Y. F. Dufrêne, S. R. Derclaye and P. G. Rouxhet (2001). *Adhesion of Lactococcus lactis to model substrata: direct study of the interface*. Colloids and surfaces B: Biointerfaces **22**: 171-182.

Braat, H., P. Rottiers, D. W. Hommes, N. Huyghebaert, E. Remaut, J. P. Remon, S. J. van Deventer, S. Neirynck, M. P. Peppelenbosch and L. Steidler (2006). *A phase I trial with transgenic bacteria expressing interleukin-10 in Crohn's disease*. Clinical Gastroenterology and Hepatology **4**(6): 754-759.

Buck, B. L., E. Altermann, T. Svingerud and T. R. Klaenhammer (2005). *Functional analysis of putative adhesion factors in Lactobacillus acidophilus NCFM*. Appl Environ Microbiol **71**(12): 8344-8351.

Cai, Y., J. Yang, H. Pang and M. Kitahara (2010). *Lactococcus fujiensis sp. nov., a lactic acid bacterium isolated from vegetable matter*. International Journal of Systematic and Evolutionary Microbiology **61**(7): 1590-1594.

Cao, X., R. Bansil, K. R. Bhaskar, B. S. Turner, J. T. LaMont, N. Niu and N. H. Afdhal (1999). *pH-dependent conformational change of gastric mucin leads to sol-gel transition.* Biophysical Journal **76**(3): 1250-1258.

Capozzi, V., P. Russo, M. T. Duenas, P. López and G. Spano (2012). *Lactic acid bacteria producing B-group vitamins: a great potential for functional cereals products*. Applied microbiology and biotechnology **96**(6): 1383-1394.

Castelain, M., E. Koutris, M. Andersson, K. Wiklund, O. Bjornham, S. Schedin and O. Axner (2009). *Characterization of the biomechanical properties of T4 pili expressed by Streptococcus pneumoniae--a comparison between helix-like and open coil-like pili*. Chemphyschem **10**(9-10): 1533-1540.

Celli, J. P., B. Gregor, B. Turner, N. Afdhal, R. Bansil and S. Erramilli (2005). *Viscoelastic properties and dynamics of porcine gastric mucin*. Biomacromolecules **6**: 1329-1333.

Celli, J. P., B. S. Turner, N. H. Afdhal, R. H. Ewoldt, G. H. McKinley, R. Bansil and S. Erramilli (2007). *Rheology of gastric mucin exhibits a pH-dependent sol-gel transition.* Biomacromolecules **8**(5): 1580-1586.

Celli, J. P., B. S. Turner, N. H. Afdhal, S. Keates, I. Ghiran, C. P. Kelly, R. H. Ewoldt, G. H. McKinley, P. So and S. Erramilli (2009). *Helicobacter pylori moves through mucus by reducing mucin viscoelasticity*. Proceedings of the National Academy of Sciences **106**(34): 14321-14326.

Chapot-Chartier, M.-P., E. Vinogradov, I. Sadovskaya, G. Andre, M.-Y. Mistou, P. Trieu-Cuot, S. Furlan, E. Bidnenko, P. Courtin, C. Pechoux and S. Kulakauskas (2010). *Cell surface of Lactococcus lactis is covered by a protective polysaccharide pellicle*. Journal of Biological Chemistry **285**(14): 10464-10471.

Chen, Y.-S., C.-H. Chang, S.-F. Pan, L.-t. Wang, Y.-c. Chang, H.-c. Wu and F. Yanagida (2012). *Lactococcus taiwanensis sp. nov., a novel lactic acid bacterium isolated from fresh cummingcordia*. International Journal of Systematic and Evolutionary Microbiology.

Cho, S.-L., S.-W. Nam, J.-H. Yoon, J.-S. Lee, A. Sukhoom and W. Kim (2008). *Lactococcus chungangensis sp. nov., a lactic acid bacterium isolated from activated sludge foam*. International journal of systematic and evolutionary microbiology **58**(8): 1844-1849.

Choi, H. J., C. I. Cheigh, S. B. Kim and Y. R. Pyun (2000). *Production of a nisin-like bacteriocin by Lactococcus lactis subsp. lactis A164 isolated from Kimchi*. Journal of Applied Microbiology **88**(4): 563-571.

Clark, A. and S. Ross-Murphy (1987). *Structural and mechanical properties of biopolymer gels*. Biopolymers, Springer Berlin Heidelberg. **83:** 57-192.

Cone, R. (2005). *Mucus*. Handbook of mucosal immunology. J. Mestecky, M. E. Lamm, W. Strober *et al.* London, Academic Press**:** 49-72.

Cone, R. A. (2009). *Barrier properties of mucus*. Advanced Drug Delivery Reviews **61**(2): 75-85.

Corfield, A. P. (2000). *Glycoprotein methods and protocols: the mucins*, Springer.

Corroler, D., I. Mangin, N. Desmasures and M. Gueguen (1998). *An ecological study of lactococci isolated from raw milk in the Camembert cheese registered designation of origin area*. Applied and Environmental Microbiology **64**(12): 4729-4735.

Crank, J. (1975). *The mathematics of diffusion*. Clarendon Oxford.

Crocker, J. C. (1997). *Measurement of the hydrodynamic corrections to the Brownian motion of two colloidal spheres*. Journal of Chemical Physics **106**(7): 2837-2840.

Crocker, J. C., M. T. Valentine, E. R. Weeks, T. Gisler, P. D. Kaplan, A. G. Yodh and D. A. Weitz (2000). *Two-point microrheology of inhomogeneous soft materials*. Physical Review Letters **85**(4): 888-891.

Crow, V. L., F. G. Martley, T. Coolbear and S. J. Roundhill (1995). *The influence of phage-assisted lysis of Lactococcus lactis subsp. lactis ML8 on cheddar cheese ripening*. International Dairy Journal **5**(5): 451-472.

Dague, E., D. T. L. Le, S. Zanna, P. Marcus, P. Loubière and M. Mercier-Bonin (2010). *Probing in vitro interactions between Lactococcus lactis and mucins using AFM*. Langmuir **26**(13): 11010-11017.

Dawson, M., E. Krauland, D. Wirtz and J. Hanes (2004). *Transport of polymeric nanoparticle gene carriers in gastric mucus*. Biotechnology Progress **20**(3): 851-857.

Dawson, M., D. Wirtz and J. Hanes (2003). *Enhanced viscoelasticity of human cystic fibrotic sputum correlates with increasing microheterogeneity in particle transport*. The journal of biological chemistry **278**(50): 50393-50401.

de Azevedo, M., J. Karczewski, F. Lefevre, V. Azevedo, A. Miyoshi, J. M. Wells, P. Langella and J.-M. Chatel (2010). *In vitro and in vivo characterization of DNA delivery using recombinant Lactococcus lactis expressing a mutated form of L. monocytogenes Internalin A*. BMC microbiology **12**(1): 299.

De La Fuente, L., E. Montanes, Y. Meng, Y. Li, T. J. Burr, H. C. Hoch and M. Wu (2007). *Assessing adhesion forces of type I and type IV pili of Xylella fastidiosa bacteria by use of a microfluidic flow chamber*. Appl Environ Microbiol **73**(8): 2690-2696.

Décavé, E., D. Garrivier, Y. Brechet, F. Bruckert and B. Fourcade (2002). *Peeling process in living cell movement under shear flow*. Physical Review Letters **89**(10): 108101.

Delgado-Reyes, V. A., E. G. Ramos-Ramirez, A. Cruz-Orea and J. A. Salazar-Montoya (2013). *Flow and Dynamic Viscoelastic Characterization of Non-Purified and Purified Mucin Dispersions*. International Journal of Polymer Analysis and Characterization **18**(3): 232-245.

Derjaguin, B. (1941). *Theory of the stability of strongly charged lyophobic sols and the adhesion of strongly charged particles in solutions of electrolytes*. Acta Physicochim. USSR **14**: 633-662.

Dieye, Y., V. Oxaran, F. Ledue-Clier, W. Alkhalaf, G. Buist, V. Juillard, C. W. Lee and J.-C. Piard (2010). *Functionality of sortase A in Lactococcus lactis*. Applied and Environmental Microbiology **76**(21): 7332-7337.

Dramsi, S., P. Trieu-Cuot and H. l. n. Bierne (2005). *Sorting sortases: a nomenclature proposal for the various sortases of Gram-positive bacteria*. Research in Microbiology **156**(3): 289-297.

Farkye, N. Y. (2004). *Cheese technology*. International Journal of Dairy Technology **57**(23): 91-98.

Farnworth, E. R. (2006). *Kefir-a complex probiotic*. Food Science and Technology Bulletin: Fu **2**(1): 1-17.

Felley, C. P., I. n. Corthesy-Theulaz, J.-L. B. Rivero, P. Sipponen, M. Kaufmann, P. Bauerfeind, P. H. Wiesel, D. Brassart, A. Pfeifer and A. L. Blum (2001). *Favourable effect of an acidified milk (LC-1) on Helicobacter pylori gastritis in man*. European Journal of Gastroenterology & Hepatology **13**(1): 25-29.

Fick, A. (1855). *V. On liquid diffusion*. The London, Edinburgh, and Dublin Philosophical Magazine and Journal of Science **10**(63): 30-39.

Finegold, S., V. Sutter and G. Mathisen (1983). *Human intestinal microflora in health and disease*. New York, Academic Press.

Forde, A. and G. F. Fitzgerald (1999). *Analysis of exopolysaccharide (EPS) production mediated by the bacteriophage adsorption blocking plasmid, pCI658, isolated from Lactococcus lactis ssp. cremoris HO2*. International Dairy Journal **9**(7): 465-472.

Gao, Y., Y. Lu, K.-L. Teng, M.-L. Chen, H.-J. Zheng, Y.-Q. Zhu and J. Zhong (2011). *Complete genome sequence of Lactococcus lactis subsp. lactis CV56, a probiotic strain isolated from the vaginas of healthy women*. Journal of Bacteriology **193**(11): 2886-2887.

Gardel, M. L., M. T. Valentine and D. A. Weitz (2005). *Microrheology. Microscale Diagnostic Techniques*, Springer**:** 1-49.

Georgiades, P., P. D. A. Pudney, D. J. Thornton and T. Waigh (2013). *Particle tracking microrheology of purified gastrointestinal mucins*. Biopolymers: n/a-n/a.

Giaouris, E., R. Briandet, M. Meyrand, P. Courtin and M.-P. Chapot-Chartier (2008). *Variations in the degree of D-alanylation of teichoic acids in Lactococcus lactis alter resistance to cationic antimicrobials but have no effect on bacterial surface hydrophobicity and charge*. Applied and Environmental Microbiology **74**(15): 4764-4767.

Giaouris, E., M. P. Chapot-Chartier and R. Briandet (2009). *Surface physicochemical analysis of natural Lactococcus lactis strains reveals the existence of hydrophobic and low charged strains with altered adhesive properties*. Int J Food Microbiol **131**(1): 2-9.

Gionchetti, P., F. Rizzello, A. Venturi, P. Brigidi, D. Matteuzzi , G. Bazzocchi, G. Poggioli, M. Miglioli and M. Campieri (2000). *Oral bacteriotherapy as maintenance treatment in patients with chronic pouchitis: a double-blind, placebo-controlled trial*. Gastroenterology **119**(2): 305-309.

Gittes, F., B. Schnurr, P. Olmsted, F. MacKintosh and C. Schmidt (1997). *Microscopic viscoelasticity: shear moduli of soft materials determined from thermal fluctuations*. Physical Review Letters **79**(17): 3286.

Godon, J. J., K. Jury, C. A. Shearman and M. J. Gasson (1994). *The Lactococcus lactis sex-factor aggregation gene cluA*. Molecular microbiology **12**(4): 655-663.

Górecki, R. K., A. Koryszewska-Baginska, M. Golebiewski, J. Zylinska, M. Grynberg and J. K. Bardowski (2011). *Adaptative potential of the Lactococcus lactis IL594 strain encoded in its 7 plasmids*. PloS One **6**(7): e22238.

Granato, D., G. E. Bergonzelli, R. D. Pridmore, L. Marvin, M. Rouvet and I. n. E. Corthésy-Theulaz (2004). *Cell surface-associated elongation factor Tu mediates the attachment of Lactobacillus johnsonii NCC533 (La1) to human intestinal cells and mucins*. Infection and Immunity **72**(4): 2160-2169.

Granato, D., F. Perotti, I. Masserey, M. Rouvet, M. Golliard, A. Servin and D. Brassart (1999). *Cell Surface-Associated Lipoteichoic Acid Acts as an Adhesion Factor for Attachment of Lactobacillus johnsoniiLa1 to Human Enterocyte-Like Caco-2 Cells*. Applied and Environmental Microbiology **65**(3): 1071-1077.

Guandalini, S. (2002). *Use of lactobacillus-GG in paediatric Crohn's disease*. Digestive and Liver Disease **34**: S63-S65.

Guimaraes, V. r. D., S. Innocentin, F. o. Lefevre, V. Azevedo, J.-M. Wal, P. Langella and J.-M. Chatel (2006). *Use of native lactococci as vehicles for delivery of DNA into mammalian epithelial cells*. Applied and Environmental Microbiology **72**(11): 7091-7097.

Gunning, A. P., A. R. Kirby, C. Fuell, C. Pin, L. E. Tailford and N. Juge (2013). *Mining the "glycocode"--exploring the spatial distribution of glycans in gastrointestinal mucin using force spectroscopy*. FASEB J **27**(6): 2342-2354.

Habimana, O., C. Le Goff, V. Juillard, M.-N. l. Bellon-Fontaine, G. Buist, S. Kulakauskas and R. Briandet (2007). *Positive role of cell wall anchored proteinase PrtP in adhesion of lactococci*. BMC Microbiology **7**(1): 36.

He, J. and J. X. Tang (2011). *Surface adsorption and hopping cause probe-size-dependent microrheology of actin networks*. Physical review. E, Statistical, nonlinear, and soft matter physics **83**(4 Pt 1): 041902.

Hele-Shaw, H. (1898). *Flow of water*. Nature **58**: 520.

Henriksson, R., L. Franzen, K. Sandstrom, A. Nordin, M. Arevarn and E. Grahn (1995). *Effects of active addition of bacterial cultures in fermented milk to patients with chronic bowel discomfort following irradiation*. Supportive Care in Cancer **3**(1): 81-83.

Hirayama, K. and J. Rafter (2000). *The role of probiotic bacteria in cancer prevention*. Microbes and Infection **2**(6): 681-686.

Holzapfel, W. H., P. Haberer, J. Snel and U. Schillinger (1998). *Overview of gut flora and probiotics*. International Journal of Food Microbiology **41**(2): 85-101.

Jeffrey, B., H. S. Udaykumar and K. S. Schulze (2003). *Flow fields generated by peristaltic reflex in isolated guinea pig ileum: impact of contraction depth and shoulders*. American Journal of Physiology. Gastrointestinal and Liver Physiology **285**(5): G907-G918.

Jimenez, M. (2013). *Étude du transfert de matière gaz/liquide en milieux complexes: quantification du transfert d'oxygène par technique optiques*, INSA.

Jimenez, M., N. Dietrich, A. Cockx and G. Hébrard (2013). *Experimental study of O2 diffusion coefficient measurement at a planar gas-liquid interface by planar laser-induced fluorescence with inhibition*. AIChE Journal **59**(1): 325-333.

Johansson, M. E., D. Ambort, T. Pelaseyed, A. Schutte, J. K. Gustafsson, A. Ermund, D. B. Subramani, J. M. Holmen-Larsson, K. A. Thomsson, J. H. Bergstrom and S. van der Post (2011). *Composition and functional role of the mucus layers in the intestine*. Cellular and Molecular Life Sciences **68**(22): 3635-3641.

Johansson, M. E., J. K. Gustafsson, J. Holmén-Larsson, K. S. Jabbar, L. Xia, H. Xu, F. K. Ghishan, F. A. Carvalho, A. T. Gewirtz and H. Sjovall (2013). *Bacteria penetrate the normally impenetrable inner colon mucus layer in both murine colitis models and patients with ulcerative colitis*. Gut.

Johansson, M. E., J. M. H. n. Larsson and G. C. Hansson (2011). *The two mucus layers of colon are organized by the MUC2 mucin, whereas the outer layer is a legislator of host-microbial interactions*. Proceedings of the National Academy of Sciences **108**(Supplement 1): 4659-4665.

Johansson, M. E., M. Phillipson, J. Petersson, A. Velcich, L. Holm and G. C. Hansson (2008). *The inner of the two Muc2 mucin-dependent mucus layers in colon is devoid of bacteria*. Proceedings of the National Academy of Sciences **105**(39): 15064-15069.

Juge, N. (2012). *Microbial adhesins to gastrointestinal mucus*. Trends Microbiol **20**(1): 30-39.

Kankainen, M., L. Paulin, S. Tynkkynen, I. von Ossowski, J. Reunanen, P. Partanen, R. Satokari, S. Vesterlund, A. P. A. Hendrickx, S. Lebeer, S. C. J. De Keersmaecker, J. Vanderleyden, T. Hämäläinen, S. Laukkanen, N. Salovuori, J. Ritari, E. Alatalo, R. Korpela, T. Mattila-Sandholm, A. Lassig, K. Hatakka, K. T. Kinnunen, H. Karjalainen, M. Saxelin, K. Laakso, A. Surakka, A. Palva, T. Salusjärvi, P. Auvinen and W. M. de Vos (2009). *Comparative genomic analysis of Lactobacillus rhamnosus GG reveals pili containing a human-mucus binding protein*. Proceedings of the National Academy of Sciences of the United States of America **106**(40): 17193-17198.

Karlsson, N. G., H. Nordman, H. Karlsson, I. Carlstedt and G. C. Hansson (1997). *Glycosylation differences between pig gastric mucin populations: a comparative study of the neutral oligosaccharides using mass spectrometry*. Biochem J **326 (Pt 3)**: 911-917.

Kato, H., Y. Shiwa, K. Oshima, M. Machii, T. Araya-Kojima, T. Zendo, M. Shimizu-Kadota, M. Hattori, K. Sonomoto and H. Yoshikawa (2012). *Complete genome sequence of Lactococcus lactis IO-1, a lactic acid bacterium that utilizes xylose and produces high levels of L-Lactic acid*. Journal of Bacteriology **194**(8): 2102-2103.

Khulusi, S., M. Mendall, S. Badve, P. Patel, C. Finlayson and T. Northfield (1995). *Effect of Helicobacter pylori eradication on gastric metaplasia of the duodenum*. Gut **36**(2): 193-197.

Kim, Y.-C. (1996). *Diffusivity of bacteria*. Korean Journal of Chemical Engineering **13**(3): 282-287.

Kim, Y. S. and S. B. Ho (2010). *Intestinal goblet cells and mucins in health and disease: recent insights and progress*. Current gastroenterology reports **12**(5): 319-330.

Kimoto, H., J. Kurisaki, N. Tsuji, S. Ohmomo and T. Okamoto (1999). *Lactococci as probiotic strains: adhesion to human enterocyte-like Caco-2 cells and tolerance to low pH and bile*. Letters in Applied Microbiology **29**(5): 313-316.

Kimoto, H., K. Mizumachi, T. Okamoto and J.-i. Kurisaki (2004). *New Lactococcus strain with immunomodulatory activity: enhancement of Th1-type immune response*. Microbiology and Immunology **48**(2): 75-82.

Kinoshita, H., H. Uchida, Y. Kawai, T. Kawasaki, N. Wakahara, H. Matsuo, M. Watanabe, H. Kitazawa, S. Ohnuma and K. Miura (2008). *Cell surface Lactobacillus plantarum LA 318 glyceraldehyde-3-phosphate dehydrogenase (GAPDH) adheres to human colonic mucin*. Journal of Applied Microbiology **104**(6): 1667-1674.

Kinoshita, H., H. Uchida, Y. Kawai, H. Kitazawa, K. Miura, K. Shiiba, A. Horii and T. Saito (2007). *Quantitative evaluation of adhesion of lactobacilli isolated from human intestinal tissues to human colonic mucin using surface plasmon resonance (BIACORE assay)*. J Appl Microbiol **102**(1): 116-123.

Kirch, J., A. Schneider, B. Abou, A. Hopf, U. F. Schaefer, M. Schneider, C. Schall, C. Wagner and C. M. Lehr (2012). *Optical tweezers reveal relationship between microstructure and nanoparticle penetration of pulmonary mucus*. Proc Natl Acad Sci U S A **109**(45): 18355-18360.

Kleerebezem, M., P. Hols, E. Bernard, T. Rolain, M. Zhou, R. J. Siezen and P. A. Bron (2010). *The extracellular biology of the lactobacilli*. FEMS Microbiol Rev **34**(2): 199-230.

Kleerebezem, M., R. van Kranenburg, R. Tuinier, I. C. Boels, P. Zoon, E. Looijesteijn, J. Hugenholtz and W. M. de Vos (1999). *Exopolysaccharides produced by Lactococcus lactis: from genetic engineering to improved rheological properties?* Lactic Acid Bacteria: Genetics, Metabolism and Applications, Springer**:** 357-365.

Kocevar-Nared, J., J. Kristl and J. Å mid-Korbar (1997). *Comparative rheological investigation of crude gastric mucin and natural gastric mucus*. Biomaterials **18**(9): 677-681.

Kraatz, M. (2011). *Isolation of Lactic Acid Related Bacteria from the Pig Mucosal Proximal Gastrointestinal Tract, Including Olsenella Umbonata Sp. Nov. and Veillonella Magna Sp. Nov*, Logos Verlag Berlin GmbH.

Lafitte, G., K. Thuresson and O. Söderman (2007). *Diffusion of nutrients molecules and model drug carriers through mucin layer investigated by magnetic resonance imaging with chemical shift resolution*. Journal of Pharmaceutical Sciences **96**(2): 258-263.

Lai, S. K., D. E. O'Hanlon, S. Harrold, S. T. Man, Y. Y. Wang, R. Cone and J. Hanes (2007). *Rapid transport of large polymeric nanoparticles in fresh undiluted human mucus*. Proc Natl Acad Sci U S A **104**(5): 1482-1487.

Lai, S. K., J. S. Suk, A. Pace, Y. Y. Wang, M. Yang, O. Mert, J. Chen, J. Kim and J. Hanes (2011). *Drug carrier nanoparticles that penetrate human chronic rhinosinusitis mucus*. Biomaterials **32**(26): 6285-6290.

Lai, S. K., Y. Y. Wang, R. Cone, D. Wirtz and J. Hanes (2009). *Altering mucus rheology to "solidify" human mucus at the nanoscale*. PLoS One **4**(1): e4294.

Lai, S. K., Y. Y. Wang, K. Hida, R. Cone and J. Hanes (2010). *Nanoparticles reveal that human cervicovaginal mucus is riddled with pores larger than viruses*. Proc Natl Acad Sci U S A **107**(2): 598-603.

Landau, L. and E. Lifshitz (1986). *Statistical Physics: Course of Theoretical Physics/Translated from the Russian by E. Peierls and RF Peierls*, Pergamon Press.

Lau, A. W., B. D. Hoffman, A. Davies, J. C. Crocker and T. C. Lubensky (2003). *Microrheology, stress fluctuations, and active behavior of living cells*. Physical review letters **91**(19): 198101.

Le, D.-T.-L. (2011). *Identification et caractérisation des déterminants physico-chimiques et biologiques mis en jeu dans l'adhésion de Lactococcus lactis à la mucine modèle PGM*, INSA.

Le, D. T. L., Y. Guérardel, P. Loubiere, M. Mercier-Bonin and E. Dague (2011). *Measuring Kinetic Dissociation/Association Constants Between Lactococcus lactis Bacteria and Mucins Using Living Cell Probes*. Biophysical Journal **101**(11): 2843-2853.

Le, D. T. L., S. Zanna, I. Frateur, P. Marcus, P. Loubière, E. Dague and M. Mercier-Bonin (2012). *Real-time investigation of the muco-adhesive properties of Lactococcus lactis using a quartz crystal microbalance with dissipation monitoring*. Biofouling **28**(5): 479-490.

Lebeer, S., I. Claes, H. L. Tytgat, T. L. Verhoeven, E. Marien, I. von Ossowski, J. Reunanen, A. Palva, W. M. de Vos and S. C. De Keersmaecker (2012). *Functional analysis of Lactobacillus rhamnosus GG pili in relation to adhesion and immunomodulatory*

interactions with intestinal epithelial cells. Applied and Environmental Microbiology **78**(1): 185-193.

LeBlanc, J. G., C. Aubry, N. G. Cortes-Perez, A. de Moreno de LeBlanc, N. Vergnolle, P. Langella, V. Azevedo, J. M. Chatel, A. Miyoshi and L. G. Bermudez-Humaran (2013). *Mucosal targeting of therapeutic molecules using genetically modified Lactic Acid Bacteria: an update*. FEMS Microbiology Letters.

Lee, S., M. Muller, K. Rezwan and N. D. Spencer (2005). *Porcine gastric mucin (PGM) at the water/poly (dimethylsiloxane)(PDMS) interface: influence of pH and ionic strength on its conformation, adsorption, and aqueous lubrication properties*. Langmuir **21**(18): 8344-8353.

Leifson, E. (1930). *A method of staining bacterial flagella and capsules together with a study of the origin of flagella*. Journal of bacteriology **20**(3): 203.

Leporanta, K. (2003). *The world of fermented milk: viili and langfil-exotic fermented products from Scandinavia*. Valio Foods & Functionals **2**: 3-5.

Levine, A. J. and T. Lubensky (2000). *One- and two-particle microrheology*. Physical Review Letters **85**(8): 1774.

Lieleg, O., R. M. Baumgartel and A. R. Bausch (2009). *Selective Filtering of Particles by the Extracellular Matrix: An Electrostatic Bandpass*. Biophysical Journal **97**(6): 1569-1577.

Lieleg, O., C. Lieleg, J. Bloom, C. B. Buck and K. Ribbeck (2012). *Mucin Biopolymers As Broad-Spectrum Antiviral Agents*. Biomacromolecules **13**(6): 1724-1732.

Lieleg, O., I. Vladescu and K. Ribbeck (2010). *Characterization of particle translocation through mucin hydrogels*. Biophysical Journal **98**(9): 1782-1789.

Linsalata, M., F. Russo, P. Berloco, M. L. Caruso, G. D. Matteo, M. G. Cifone, C. D. Simone, E. Ierardi and A. D. Leo (2004). *The influence of Lactobacillus brevis on ornithine decarboxylase activity and polyamine profiles in Helicobacter pylori: infected gastric mucosa*. Helicobacter **9**(2): 165-172.

Liu, J., M. L. Gardel, K. Kroy, E. Frey, B. D. Hoffman, J. C. Crocker, A. R. Bausch and D. A. Weitz (2006). *Microrheology probes length scale dependent rheology*. Physical Review Letters **96**(11): 118104.

Lo, P.-R., R.-C. Yu, C.-C. Chou and E. C. Huang (2004). *Determinations of the antimutagenic activities of several probiotic bifidobacteria under acidic and bile conditions against benzo[a]pyrene by a modified Ames test*. International Journal of Food Microbiology **93**(2): 249-257.

Looijesteijn, P., W. Van Casteren, R. Tuinier, C. Doeswijk-Voragen and J. Hugenholtz (2000). *Influence of different substrate limitations on the yield, composition and molecular*

mass of exopolysaccharides produced by Lactococcus lactis subsp. cremoris in continuous cultures. Journal of Applied Microbiology **89**(1): 116-122.

Looijesteijn, P. J., L. Trapet, E. de Vries, T. Abee and J. Hugenholtz (2001). *Physiological function of exopolysaccharides produced by Lactococcus lactis*. International Journal of Food Microbiology **64**(1): 71-80.

Lorthois, S., P. Schmitz and E. Angles-Cano (2001). *Experimental study of fibrin/fibrin-specific molecular interactions using a sphere/plane adhesion model*. Journal of colloid and interface science **241**(1): 52-62.

Lukic, J., I. Strahinic, B. Jovic, B. Filipic, L. a. Topisirovic, M. Kojic and J. Begovic (2012). *Different roles for lactococcal aggregation factor and mucin binding protein in adhesion to gastrointestinal mucosa*. Applied and Environmental Microbiology **78**(22): 7993-8000.

Ly, M., N. Vo, T. Le, J.-M. Belin and Y. Waché (2006). *Diversity of the surface properties of Lactococci and consequences on adhesion to food components*. Colloids and surfaces B: Biointerfaces **52**(2): 149-153.

Ly, M. H., M. Naitali-Bouchez, T. Meylheuc, M.-N. l. Bellon-Fontaine, T. M. Le, J.-M. Belin and Y. Wache (2006). *Importance of bacterial surface properties to control the stability of emulsions*. International Journal of Food Microbiology **112**(1): 26-34.

Mackenzie, D. A., F. Jeffers, M. L. Parker, A. Vibert-Vallet, R. J. Bongaerts, S. Roos, J. Walter and N. Juge (2010). *Strain-specific diversity of mucus-binding proteins in the adhesion and aggregation properties of Lactobacillus reuteri*. Microbiology **156**(Pt 11): 3368-3378.

Madigan, M. T. (2005). *Brock Biology of Microorganisms, 11th edn*, SciELO Espana.

Madsen, F., K. Eberth and J. Smart (1996). *A rheological evaluation of various mucus gels for use in in-vitro mucoadhesion testing*. Pharmacy and Pharmacology Communications **2**(12): 563-566.

Maier, B., L. Potter, M. So, C. D. Long, H. S. Seifert and M. P. Sheetz (2002). *Single pilus motor forces exceed 100 pN*. Proc Natl Acad Sci U S A **99**(25): 16012-16017.

Mandlik, A., A. Swierczynski, A. Das and H. Ton-That (2008). *Pili in Gram-positive bacteria: assembly, involvement in colonization and biofilm development*. Trends in Microbiology **16**(1): 33-40.

Maneval, W. (1941). *Staining bacteria and yeasts with acid dyes*. Biotechnic & Histochemistry **16**(1): 13-19.

Marraffini, L. A., A. C. DeDent and O. Schneewind (2006). *Sortases and the art of anchoring proteins to the envelopes of gram-positive bacteria*. Microbiology and Molecular Biology Reviews **70**(1): 192-221.

Marshall, V. M., E. N. Cowie and R. S. Moreton (1995). *Analysis and production of two exopolysaccharides from Lactococcus lactis subsp. cremoris LC330*. Journal of Dairy Research **62**(04): 621-628.

Martin, G., C. Marriott and I. Kellaway (1978). *Direct effect of bile salts and phospholipids on the physical properties of mucus*. Gut **19**(2): 103-107.

Mason, T. G. (2000). *Estimating the viscoelastic moduli of complex fluids using the generalized Stokes-Einstein equation*. Rheologica Acta **39**(4): 371-378.

Mason, T. G. and D. Weitz (1995). *Optical measurements of frequency-dependent linear viscoelastic moduli of complex fluids*. Physical Review Letters **74**(7): 1250.

Masuda, K. and T. Kawata (1983). *Distribution and chemical characterization of regular arrays in the cell walls of strains of the genus Lactobacillus*. FEMS Microbiology Letters **20**(2): 145-150.

Mayfield, C. and W. Inniss (1977). *A rapid, simple method for staining bacterial flagella*. Canadian Journal of Microbiology **23**(9): 1311-1313.

McGuckin, M. A., S. K. Lindén, P. Sutton and T. H. Florin (2011). *Mucin dynamics and enteric pathogens*. Nature Reviews Microbiology **9**(4): 265-278.

McLaughlin, J. (2002). *Gastrointestinal Physiology*, The Medicine Publishing Company Ltd.

Mercier-Bonin, M., M. Adoue, S. Zanna, P. Marcus, D. Combes and P. Schmitz (2009). *Evaluation of adhesion force between functionalized microbeads and protein-coated stainless steel using shear-flow-induced detachment*. J Colloid Interface Sci **338**(1): 73-81.

Mercier-Bonin, M., A. Dehouche, J. Morchain and P. Schmitz (2011). *Orientation and detachment dynamics of Bacillus spores from stainless steel under controlled shear flow: modelling of the adhesion force*. Int J Food Microbiol **146**(2): 182-191.

Mercier-Bonin, M., M.-P. Duviau, C. Ellero, N. Lebleu, P. Raynaud, B. Despax and P. Schmitz (2012). *Dynamics of detachment of Escherichia coli from plasma-mediated coatings under shear flow*. Biofouling **28**(9): 881-894.

Meyer, F. and A. Silberberg (1979). *The rheology and molecular organization of epithelial mucus*. Biorheology **17**(1-2): 163-168.

Meyrand, M., A. Guillot, M. Goin, S. Furlan, J. Armalyte, S. Kulakauskas, N. G. Cortez-Perez, G. Thomas, S. Chat and C. Pechoux (2013). *Surface proteome analysis of a*

natural isolate of Lactococcus lactis reveals the presence of pili able to bind human intestinal epithelial cells. Molecular & Cellular Proteomics: doi:10.1074/mcp.M1113.029066

Miorner, H., G. Johansson and G. Kronvall (1983). *Lipoteichoic acid is the major cell wall component responsible for surface hydrophobicity of group A streptococci*. Infection and Immunity **39**(1): 336-343.

Moore, M. E., T. Boren and J. V. Solnick (2011). *Life at the margins: modulation of attachement proteins in Helicobacter pylori*. Gut microbes **2**: 42-46.

Morelli, L. (2000). *In vitro selection of probiotic lactobacilli: a critical appraisal*. Current Issues in Intestinal Microbiology **1**(2): 59-67.

Motta, J.-P., L. G. Bermúdez-Humarán, C. l. Deraison, L. Martin, C. Rolland, P. Rousset, J. r. m. Boue, G. Dietrich, K. Chapman and P. Kharrat (2012). *Food-grade bacteria expressing elafin protect against inflammation and restore colon homeostasis*. Science Translational Medicine **4**(158): 158ra144-158ra144.

Mozes, N., A. Léonard and P. G. Rouxhet (1988). *On the relations between the elemental surface composition of yeasts and bacteria and their charge and hydrophobicity*. Biochimica et Biophysica Acta (BBA)-Biomembranes **945**(2): 324-334.

Nakajima, H., T. Hirota, T. Toba, T. Itoh and S. Adachi (1992). *Structure of the extracellular polysaccharide from slime-forming Lactococcus lactis subsp. cremoris SBT 0495*. Carbohydrate research **224**: 245-253.

Navarre, W. W. and O. Schneewind (1999). *Surface proteins of gram-positive bacteria and mechanisms of their targeting to the cell wall envelope*. Microbiology and Molecular Biology Reviews **63**(1): 174-229.

Nejadnik, M. R., H. C. van der Mei, H. J. Busscher and W. Norde (2008). *Determination of the shear force at the balance between bacterial attachment and detachment in weak-adherence systems, using a flow displacement chamber*. Appl Environ Microbiol **74**(3): 916-919.

Nelson, P. (2004). *Biological physics*, Freeman New York.

Nordman, H., J. R. Davies, A. Herrmann, N. G. Karlsson, G. C. Hansson and I. Carlstedt (1997). *Mucus glycoproteins from pig gastric mucosa: identification of different mucin populations from the surface epithelium*. Biochem J **326 (Pt 3)**: 903-910.

Nouaille, S., L. A. Ribeiro, A. Miyoshi, D. Pontes, Y. Le Loir, S. C. Oliveira, P. Langella and V. Azevedo (2003). *Heterologous protein production and delivery systems for Lactococcus lactis*. Genetics and Molecular Biology **2**(1): 102-111.

Olmsted, S. S., J. L. Padgett, A. I. Yudin, K. J. Whaley, T. R. Moench and R. A. Cone (2001). *Diffusion of macromolecules and virus-like particles in human cervical mucus*. Biophysical Journal **81**(4): 1930-1937.

Ottemann, K. M. and A. C. Lowenthal (2002). *Helicobacter pylori uses motility for initial colonization and to attain robust infection*. Infect Immun **70**: 1984-1990.

Ouwehand, A. C., E. M. Tuomola, S. Tolkko and S. Salminen (2001). *Assessment of adhesion properties of novel probiotic strains to human intestinal mucus*. Int J Food Microbiol **64**(1-2): 119-126.

Oxaran, V., F. Ledue-Clier, Y. Dieye, J. M. Herry, C. Pechoux, T. Meylheuc, R. Briandet, V. Juillard and J. C. Piard (2012). *Pilus biogenesis in Lactococcus lactis: molecular characterization and role in aggregation and biofilm formation*. PLoS One **7**(12): e50989.

Panorchan, P., D. Wirtz and Y. Tseng (2004). *Structure-function relationship of biological gels revealed by multiple-particle tracking and differential interference contrast microscopy: The case of human lamin networks*. Physical Review E **70**(4): 041906.

Passerini, D., C. Beltramo, M. Coddeville, Y. Quentin, P. Ritzenthaler, M.-L. Daveran-Mingot and P. Le Bourgeois (2010). *Genes but not genomes reveal bacterial domestication of Lactococcus lactis*. PloS One **5**(12): e15306.

Pelletier, V., N. Gal, P. Fournier and M. L. Kilfoil (2009). *Microrheology of microtubule solutions and actin-microtubule composite networks*. Phys Rev Lett **102**(18): 188303.

Perez-Vilar, J. and R. L. Hill (1999). *The structure and assembly of secreted mucins*. Journal of Biological Chemistry **274**(45): 31751-31754.

Pérez, T., J. L. Balcazar, A. Peix, A. Valverde, E. Velazquez, I. de Blas and I. Ruiz-Zarzuela (2011). *Lactococcus lactis subsp. tructae subsp. nov. isolated from the intestinal mucus of brown trout (Salmo trutta) and rainbow trout (Oncorhynchus mykiss)*. International Journal of Systematic and Evolutionary Microbiology **61**(8): 1894-1898.

Pierres, A., D. Touchard, A. M. Benoliel and P. Bongrand (2002). *Dissecting streptavidin-biotin interaction with a laminar flow chamber*. Biophys J **82**(6): 3214-3223.

Powell, D. (1987). *Intestinal water and electrolyte transport*. Physiology of the gastrointestinal tract **2**: 1267-1305.

Pretzer, G., J. Snel, D. Molenaar, A. Wiersma, P. A. Bron, J. Lambert, W. M. de Vos, R. van der Meer, M. A. Smits and M. Kleerebezem (2005). *Biodiversity-based identification and functional characterization of the mannose-specific adhesin of Lactobacillus plantarum*. Journal of bacteriology **187**(17): 6128-6136.

Proft, T. and E. Baker (2009). *Pili in Gram-negative and Gram-positive bacteria — structure, assembly and their role in disease*. Cellular and Molecular Life Sciences **66**(4): 613-635.

Pusch, O., D. Boden, S. Hannify, F. Lee, L. D. Tucker, M. R. Boyd, J. M. Wells and B. Ramratnam (2005). *Bioengineering lactic acid bacteria to secrete the HIV-1 virucide cyanovirin*. JAIDS Journal of Acquired Immune Deficiency Syndromes **40**(5): 512-520.

Qian, H., M. P. Sheetz and E. L. Elson (1991). *Single-particle tracking - analysis of diffusion and flow in 2-dimensional systems*. Biophysical Journal **60**(4): 910-921.

Ramos, H. C., M. Rumbo and J. C. Sirard (2004). *Bacterial flagellins: mediators of pathogenicity and host immune responses in mucosa*. Trends Microbiol **12**: 509-517.

Reid, J. R. and T. Coolbear (1999). *Specificity of Lactococcus lactis subsp. cremoris SK11 proteinase, lactocepin III, in low-water-activity, high-salt-concentration humectant systems and its stability compared with that of lactocepin I.* Applied and environmental microbiology **65**(7): 2947-2953.

Reunanen, J., I. von Ossowski, A. P. Hendrickx, A. Palva and W. M. de Vos (2012). *Characterization of the SpaCBA pilus fibers in the probiotic Lactobacillus rhamnosus GG*. Applied and Environmental Microbiology **78**(7): 2337-2344.

Robbe-Masselot, C., E. Maes, M. Rousset, J.-C. Michalski and C. Capon (2009). *Glycosylation of human fetal mucins: a similar repertoire of O-glycans along the intestinal tract*. Glycoconjugate Journal **26**(4): 397-413.

Robbe, C., C. Capon, E. Maes, M. Rousset, A. Zweibaum, J.-P. Zanetta and J.-C. Michalski (2003). *Evidence of regio-specific glycosylation in human intestinal mucins: presence of an acidic gradient along the intestinal tract*. Journal of Biological Chemistry **278**(47): 46337-46348.

Rogers, S. S., T. A. Waigh, X. B. Zhao and J. R. Lu (2007). *Precise particle tracking against a complicated background: polynomial fitting with Gaussian weight*. Physical Biology **4**(3): 220-227.

Rojas, M., F. Ascencio and P. L. Conway (2002). *Purification and characterization of a surface protein from Lactobacillus fermentum 104R that binds to porcine small intestinal mucus and gastric mucin*. Applied and Environmental Microbiology **68**(5): 2330-2336.

Roos, S. and H. Jonsson (2002). *A high-molecular-mass cell-surface protein from Lactobacillus reuteri 1063 adheres to mucus components*. Microbiology **148**(2): 433-442.

Ruas-Madiedo, P., J. Hugenholtz and P. Zoon (2002). *An overview of the functionality of exopolysaccharides produced by lactic acid bacteria*. International Dairy Journal **12**(2): 163-171.

Saulou, C., B. Despax, P. Raynaud, S. Zanna, A. Seyeux, P. Marcus, J.-N. Audinot and M. Mercier-Bonin (2012). *Plasma-mediated nanosilver-organosilicon composite films deposited on stainless steel: synthesis, surface characterization, and evaluation of anti-adhesive and anti-microbial properties on the model yeast saccharomyces cerevisiae*. Plasma Processes and Polymers **9**(3): 324-338.

Schleifer, K. and R. Kilpper-Balz (1987). *Molecular and chemotaxonomic approaches to the classification of streptococci, enterococci and lactococci: a review*. Systematic and Applied Microbiology **10**(1): 1-19.

Schuster, B. S., J. S. Suk, G. F. Woodworth and J. Hanes (2013). *Nanoparticle diffusion in respiratory mucus from humans without lung disease*. Biomaterials **34**(13): 3439-3446.

Sharon, N. and H. Lis (1990). *Legume lectins--a large family of homologous proteins*. The FASEB Journal **4**(14): 3198-3208.

Shen, H., Y. Hu and W. M. Saltzman (2006). *DNA diffusion in mucus: effect of size, topology of DNAs, and transfection reagents*. Biophys J **91**(2): 639-644.

Sheng, Y. H., S. Z. Hasnain, T. H. Florin and M. A. McGuckin (2012). *Mucins in inflammatory bowel diseases and colorectal cancer*. Journal of Gastroenterology and Hepatology **27**(1): 28-38.

Siezen, R. J., J. Bayjanov, B. Renckens, M. Wels, S. A. van Hijum, D. Molenaar and J. E. van Hylckama Vlieg (2010). *Complete genome sequence of Lactococcus lactis subsp. lactis KF147, a plant-associated lactic acid bacterium*. Journal of Bacteriology **192**(10): 2649-2650.

Siezen, R. J., J. R. Bayjanov, G. E. Felis, M. R. van der Sijde, M. Starrenburg, D. Molenaar, M. Wels, S. A. van Hijum and J. E. van Hylckama Vlieg (2011). *Genome-scale diversity and niche adaptation analysis of Lactococcus lactis by comparative genome hybridization using multi-strain arrays*. Microb Biotechnol **4**(3): 383-402.

Siezen, R. J., B. Renckens, I. van Swam, S. Peters, R. van Kranenburg, M. Kleerebezem and W. M. de Vos (2005). *Complete sequences of four plasmids of Lactococcus lactis subsp. cremoris SK11 reveal extensive adaptation to the dairy environment*. Applied and Environmental Microbiology **71**(12): 8371-8382.

Sijtsma, L., K. Hellingwerf and J. Wouters (1991). *Composition and phase binding capacity of cell walls isolated from Lactococcus lactis subsp. cremoris SK110 and SK112*. Nederlands melk en Zuiveltijdschrift **45**(2): 81-95.

Silva, A. J., K. Pham and J. A. Benitez (2003). *Haemagglutinin/protease expression and mucin gel penetration in EI Tor biotype Vibrio cholerae*. Microbiology **149**: 1883-1891.

Sleytr, U. B. and T. J. Beveridge (1999). *Bacterial S-layers*. Trends in Microbiology **7**(6): 253-260.

Sriamornsak, P. and N. Wattanakorn (2008). *Rheological synergy in aqueous mixtures of pectin and mucin*. Carbohydrate Polymers **74**(3): 474-481.

Steffe, J. F. (1992). *Rheological Methods in Food Process Engineering*, Freeman Press.

Steidler, L., S. Neirynck, N. Huyghebaert, V. Snoeck, A. Vermeire, B. Goddeeris, E. Cox, J. P. Remon and E. Remaut (2003). *Biological containment of genetically modified Lactococcus lactis for intestinal delivery of human interleukin 10*. Nature Biotechnology **21**(7): 785-789.

Suh, J., M. Dawson and J. Hanes (2005). *Real-time multiple-particle tracking: applications to drug and gene delivery*. Advanced drug delivery reviews **57**(1): 63-78.

Suk, J. S., S. K. Lai, Y. Y. Wang, L. M. Ensign, P. L. Zeitlin, M. P. Boyle and J. Hanes (2009). *The penetration of fresh undiluted sputum expectorated by cystic fibrosis patients by non-adhesive polymer nanoparticles*. Biomaterials **30**(13): 2591-2597.

Telford, J. L., M. l. A. Barocchi, I. Margarit, R. Rappuoli and G. Grandi (2006). *Pili in gram-positive pathogens*. Nature Reviews Microbiology **4**(7): 509-519.

Teubl, B. J., M. Absenger, E. Frohlich, G. Leitinger, A. Zimmer and E. Roblegg (2013). *The oral cavity as a biological barrier system: design of an advanced buccal in vitro permeability model*. Eur J Pharm Biopharm **84**(2): 386-393.

Theodossi, A., D. Spiegelhalter, J. Jass, J. Firth, M. Dixon, M. Leader, D. Levison, R. Lindley, I. Filipe and A. Price (1994). *Observer variation and discriminatory value of biopsy features in inflammatory bowel disease*. Gut **35**(7): 961-968.

Tian, P., M. Brandl and R. Mandrell (2005). *Porcine gastric mucin binds to recombinant norovirus particles and competitively inhibits their binding to histo-blood group antigens and Caco-2 cells*. Letters in Applied Microbiology **41**(4): 315-320.

Todorov, S., M. Botes, S. Danova and L. Dicks (2007). *Probiotic properties of Lactococcus lactis ssp. lactis HV219, isolated from human vaginal secretions*. Journal of Applied Microbiology **103**(3): 629-639.

Touhami, A., M. H. Jericho, J. M. Boyd and T. J. Beveridge (2006). *Nanoscale characterization and determination of adhesion forces of Pseudomonas aeruginosa pili by using atomic force microscopy*. J Bacteriol **188**(2): 370-377.

Tripathi, P., A. Beaussart, D. Alsteens, V. Dupres, I. Claes, I. von Ossowski, W. M. de Vos, A. Palva, S. Lebeer and J. Vanderleyden (2013). *Adhesion and nanomechanics of pili from the probiotic lactobacillus rhamnosus GG*. ACS Nano **7**(4): 3685-3697.

Tsubokawa, D., Y. Goso, A. Sawaguchi, M. Kurihara, T. Ichikawa, N. Sato, T. Suganuma, K. Hotta and K. Ishihara (2007). *A monoclonal antibody, PGM34, against 6-sulfated blood-group H type 2 antigen, on the carbohydrate moiety of mucin*. FEBS Journal **274**(7): 1833-1848.

Tuomola, E. M., A. C. Ouwehand and S. J. Salminen (2000). *Chemical, physical and enzymatic pre-treatments of probiotic lactobacilli alter their adhesion to human intestinal mucus glycoproteins*. Int J Food Microbiol **60**(1): 75-81.

Turner, B. S., K. R. Bhaskar, M. Hadzopoulou-Cladaras and J. T. LaMont (1999). *Cysteine-rich regions of pig gastric mucin contain von Willebrand factor and cystine knot domains at the carboxyl terminal*. Biochimica et Biophysica Acta (BBA)-Gene Structure and Expression **1447**(1): 77-92.

Turner, L., W. S. Ryu and H. C. Berg (2000). *Real-time imaging of fluorescent flagellar filaments*. Journal of Bacteriology **182**(10): 2793-2801.

Uchida, H., K. Fujitani, Y. Kawai, H. Kitazawa, A. Horii, K. Shiiba, K. Saito and T. Saito (2004). *A new assay using surface plasmon resonance (SPR) to determine binding of the Lactobacillus acidophilus group to human colonic mucin*. Bioscience, Biotechnology, and Biochemistry **68**(5): 1004-1010.

Uhlman, L., U. Schillinger, J. Rupnow and W. Holzapfel (1992). *Identification and characterization of two bacteriocin-producing strains of Lactococcus lactis isolated from vegetables*. International Journal of Food Microbiology **16**(2): 141-151.

Valentine, M. T., Z. E. Perlman, M. L. Gardel, J. H. Shin, P. Matsudaira, T. J. Mitchison and D. A. Weitz (2004). *Colloid surface chemistry critically affects multiple particle tracking measurements of biomaterials*. Biophys J **86**(6): 4004-4014.

Valyasevi, R., W. Sandine and B. Geller (1990). *The bacteriophage kh receptor of Lactococcus lactis subsp. cremoris KH is the rhamnose of the extracellular wall polysaccharide*. Applied and Environmental Microbiology **56**(6): 1882-1889.

van der Meer, J. R., J. Polman, M. M. Beerthuyzen, R. J. Siezen, O. P. Kuipers and W. De Vos (1993). *Characterization of the Lactococcus lactis nisin A operon genes nisP,*

encoding a subtilisin-like serine protease involved in precursor processing, and nisR, encoding a regulatory protein involved in nisin biosynthesis. Journal of bacteriology **175**(9): 2578-2588.

Van der Sluis, M., B. A. De Koning, A. C. De Bruijn, A. Velcich, J. P. Meijerink, J. B. Van Goudoever, H. A. Beller, J. Dekker, I. Van Seuningen and I. B. Renes (2006). *Muc2-deficient mice spontaneously develop colitis, indicating that MUC2 is critical for colonic protection*. Gastroenterology **131**(1): 117-129.

van Hylckama Vlieg, J. E., J. L. Rademaker, H. Bachmann, D. Molenaar, W. J. Kelly and R. J. Siezen (2006). *Natural diversity and adaptive responses of Lactococcus lactis*. Curr Opin Biotechnol **17**(2): 183-190.

Van Oss, C., R. Good and M. Chaudhury (1986). *The role of van der Waals forces and hydrogen bonds in "hydrophobic interactions" between biopolymers and low energy surfaces*. Journal of colloid and Interface Science **111**(2): 378-390.

Vanderpool, C., F. Yan and D. B. Polk (2008). *Mechanisms of probiotic action: implications for therapeutic applications in inflammatory bowel diseases*. Inflammatory Bowel Diseases **14**(11): 1585-1596.

Vasiljevic, T. and N. P. Shah (2008). *Probiotics - from Metchnikoff to bioactives*. International Dairy Journal **18**(7): 714-728.

Verwey, E. E. J. W., J. T. G. Overbeek and J. T. J. T. G. Overbeek (1999). *Theory of the stability of lyophobic colloids*, DoverPublications. com.

Von Kleist, S., E. Chany, P. Burtin, M. King and J. Fogh (1975). *Immunohistology of the antigenic pattern of a continuous cell line from a human colon tumor*. Journal of the National Cancer Institute **55**(3): 555-560.

von Ossowski, I., J. Reunanen, R. Satokari, S. Vesterlund, M. Kankainen, H. Huhtinen, S. Tynkkynen, S. Salminen, W. M. de Vos and A. Palva (2010). *Mucosal adhesion properties of the probiotic Lactobacillus rhamnosus GG SpaCBA and SpaFED pilin subunits*. Applied and environmental microbiology **76**(7): 2049-2057.

Wang, Y.-Y., S. K. Lai, C. So, C. Schneider, R. Cone and J. Hanes (2011). *Mucoadhesive nanoparticles may disrupt the protective human mucus barrier by altering its microstructure*. PloS One **6**(6): e21547.

Wang, Y., J. Wang and W. Dai (2011). *Use of GFP to trace the colonization of Lactococcus lactis WH-C1 in the gastrointestinal tract of mice*. J Microbiol Methods **86**(3): 390-392.

Wang, Y. Y., S. K. Lai, J. S. Suk, A. Pace, R. Cone and J. Hanes (2008). *Addressing the PEG mucoadhesivity paradox to engineer nanoparticles that "slip" through the human mucus barrier*. Angew Chem Int Ed Engl **47**(50): 9726-9729.

Wegmann, U., M. O'Connell-Motherway, A. Zomer, G. Buist, C. Shearman, C. Canchaya, M. Ventura, A. Goesmann, M. J. Gasson and O. P. Kuipers (2007). *Complete genome sequence of the prototype lactic acid bacterium Lactococcus lactis subsp. cremoris MG1363*. Journal of Bacteriology **189**(8): 3256-3270.

Wirtz, D. (2009). *Particle-tracking microrheology of living cells: principles and applications*. Annual Review of Biophysics **38**: 301-326.

Xu, C. P., N. P. Boks, J. de Vries, H. J. Kaper, W. Norde, H. J. Busscher and H. C. van der Mei (2008). *Staphylococcus aureus-fibronectin interactions with and without fibronectin-binding proteins and their role in adhesion and desorption*. Appl Environ Microbiol **74**(24): 7522-7528.

Yang, X. Y., K. Forier, L. Steukers, S. Van Vlierberghe, P. Dubruel, K. Braeckmans, S. Glorieux and H. J. Nauwynck (2012). *Immobilization of Pseudorabies Virus in Porcine Tracheal Respiratory Mucus Revealed by Single Particle Tracking*. Plos One **7**(12).

Yang, Z., M. Staaf, G. r. Widmalm and H. Tenhu (1999). *Separation, purification and characterisation of extracellular polysaccharides produced by slime-forming Lactococcus lactis ssp. cremoris strains*. International Dairy Journal **9**(9): 631-638.

Yanisch-Perron, C., J. Vieira and J. Messing (1985). *Improved M13 phage cloning vectors and host strains: nucleotide sequences of the M13mpl8 and pUC19 vectors*. Gene **33**(1): 103-119.

Zenteno, E., L. Vázquez, R. l. Chávez, F. l. Córdoba, J. M. Wieruszeski, J. Montreuil and H. Debray (1995). *Specificity of the isolectins from the plant cactus Machaerocereus eruca for oligosaccharides from porcine stomach mucin*. Glycoconjugate Journal **12**(5): 699-706.

Zhou, D., J. Li, N. Li and G. Yan (2004). *Study on viscosity property of gastrointestinal mucus*. Journal of Biomedical Engineering **21**(1): 72.

LIST OF TABLES AND FIGURES

LIST OF TABLES

LIST OF FIGURES

SUMMARY IN FRENCH

Caractérisation de la muco-adhésion de *Lactococcus lactis* par le développement d'approches biophysiques

Contexte et objectifs

L'épithélium digestif est recouvert d'une couche protectrice de mucus, qui est un hydrogel perméable et viscoélastique. Cette couche sert de niche écologique pour les bactéries commensales et/ou exogènes comme les probiotiques, elle joue également un rôle dans la défense contre les pathogènes. La couche de mucus est formée d'un réseau de fibres de mucines. Ces dernières sont des glycoprotéines de haut poids moléculaire avec un squelette protéique riche en sérine et thréonine, lié à une grande variété de O-glycanes qui représentent une source nutritionnelle pour les bactéries et/ou des ligands potentiels pour les adhésines bactériennes, contribuant ainsi probablement à la sélection et l'implantation d'un microbiote régio-spécifique. De nombreuses études sur la muco-adhésion des bactéries lactiques ont été réalisées avec des lactobacilles, dans le but de sélectionner de nouveaux probiotiques, dotés d'une meilleure faculté de persistance dans l'intestin. En revanche, peu de données sont actuellement disponibles sur les facteurs structurels et fonctionnels impliqués dans la muco-adhésion de *Lactococcus lactis*, le modèle des bactéries lactiques. Dans ce cadre, en collaboration avec l'Institut Micalis de Jouy-en-Josas, avec nous nous sommes focalisés sur la quantification multi-échelles des interactions entre la souche naturelle d'origine végétale *L. lactis* ssp. *lactis* TIL448 et une mucine modèle, la mucine gastrique de porc (PGM).

Démarche expérimentale

Nous nous sommes intéressés aux capacités muco-adhésives de *L. lactis* TIL448 par le couplage de (i) la microscopie à force atomique (AFM), à l'échelle de la cellule unique et en mode statique et (ii) la méthode hydrodynamique en chambre à écoulement cisaillé, à l'échelle de l'ensemble de la population bactérienne. Dans l'optique d'identifier la nature et le rôle fonctionnel des déterminants de surface mis en jeu, nous avons testé, outre la souche sauvage, la souche curée de plasmides TIL1230 et deux mutants TIL1289 et TIL1290, altérés dans la synthèse de pili et d'une protéine "mucus-binding", respectivement. En collaboration avec l'équipe "Transfert, Interface, Mélange" du laboratoire, nous avons également évalué l'aptitude à la migration de *L. lactis* au sein de gels de PGM, par la mise en œuvre de la

méthode "Diffusion Front Tracking". Ces essais se sont accompagnés d'une caractérisation de la microstructure, des propriétés mécaniques et rhéologiques des gels de PGM à différentes concentrations, par la technique de "Multi-Particle Tracking" à l'aide de nanosondes fonctionnalisées, ainsi que par la comparaison rhéométrie classique/microrhéométrie.

Résultats

Evaluation du rôle respectif des pili et de la protéine "mucus-binding" dans les propriétés muco-adhésives de *L. lactis*

Dans une première partie, les propriétés muco-adhésives de *L. lactis* TIL448 et des souches dérivées ont été quantifiées par AFM, à l'échelle de la cellule unique et en conditions statiques. Cette étude a été réalisée en collaboration avec le Laboratoire d'Analyse et d'Architecture des Systèmes et l'Institut des Technologies Avancées en sciences du Vivant de Toulouse. Les résultats sont présentés sur la **Figure 1**.

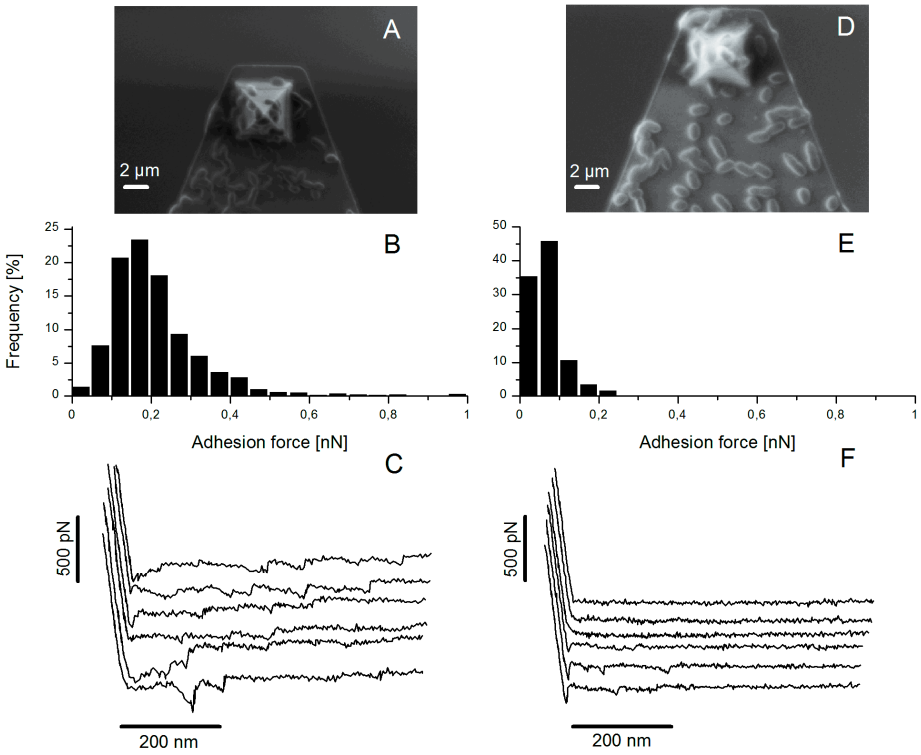

Figure 1. Résultats AFM pour la souche sauvage *L. lactis* TIL448 (à gauche) et la souche curée de plasmides TIL1230 (à droite). (A, D) Images par microscopie électronique à balayage des cellules bactériennes de *L. lactis* immobilisées sur la pointe AFM ; (B, E)

histogrammes des forces d'adhésion de la lacto-probe en contact avec la couche de PGM et (C, F) courbes force-distance caractéristiques.

L'adhésion forte de la souche TIL448 à PGM a été démontrée avec une force de 0,18 ± 0,04 nN, accompagnée d'un pourcentage faible d'événements non adhésifs (2%) et d'un pourcentage élevé d'événements adhésifs spécifiques (60%). La viabilité des bactéries sur la pointe AFM, estimée par un marquage au CFDA ("carboxyfluorescein diacetate"), a été établie (**Figure 2**).

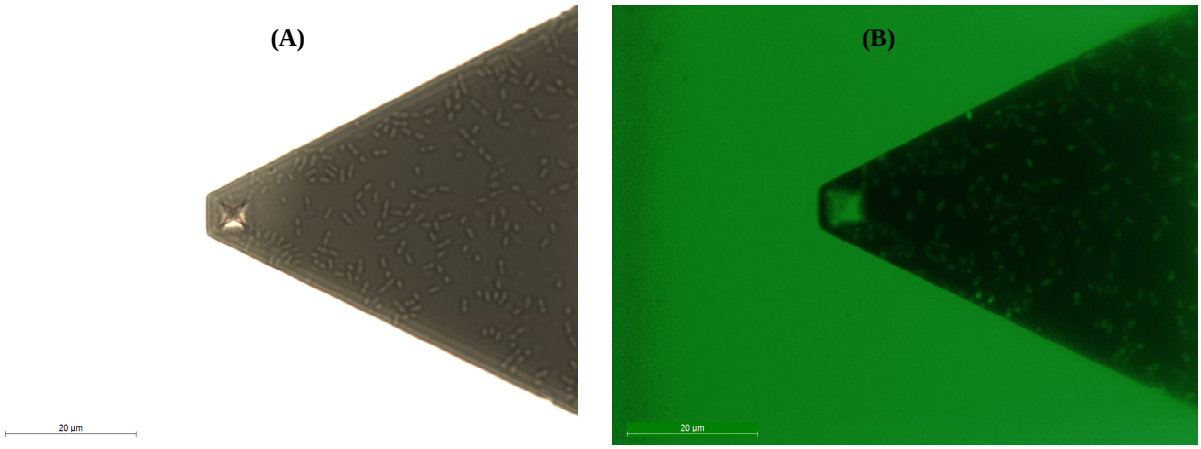

Figure 2. Viabilité de la lacto-pointe TIL448. (A) Image par microscopie en lumière blanche permettant de quantifier le nombre total de bactéries attachées sur la pointe AFM ; (B) Image par microscopie à épifluorescence pour estimer la viabilité des bactéries sur la pointe AFM, après marquage au CFDA. Les cellules viables sont marquées en vert. Barre d'échelle : 20 µm.

Des distances à la rupture ont été détectées à la fois à 100-200 nm et à plus de 600-800 nm, de manière cohérente avec la présence de pili (structures pouvant atteindre plusieurs µm de longueur). En revanche, l'adhésion de TIL1230 est nettement diminuée (**Figure 1**, **Tableau 1**), suggérant que les déterminants de la surface bactérienne impliqués dans la muco-adhésion de TIL448 sont portés par des plasmides. Cette hypothèse a été par la suite confirmée en testant les deux mutants TIL1289 et TIL1290 (**Tableau 1**). Par ailleurs, nous avons pu montrer par AFM la contribution équivalente des pili et de la protéine "mucus-binding ", du fait d'un pourcentage d'événements adhésifs spécifiques proche pour les deux mutants (**Tableau 1**).

Tableau 1. Forces d'adhésion et pourcentages d'événements non adhésifs, adhésifs non spécifiques et adhésifs spécifiques, obtenus par AFM pour les lacto-pointes TIL448, TIL1230, TIL1289 and TIL1290 en contact avec la couche de PGM.

		TIL448 (souche sauvage)	**TIL1230** (curée de plasmides)	**TIL1289** (mutant piline)	**TIL1290** (mutant protéine "mucus-binding")
Force (nN)		0,18 ± 0,04	0,09 ± 0,02	0,10 ± 0,03	0,12 ± 0,04
% événements	NA[a]	2%	37%	31%	20%
	A-NS[b]	38%	55%	43%	51%
	A-S[c]	60%	8%	26%	29%

[a] NA: événement non adhésif

[b] A-NS: événement adhésif non spécifique

[c] A-S: événement adhésif spécifique

Enfin, toujours par AFM, nous avons démontré, à partir d'essais de blocage avec PGM ou des fractions O-glycaniques purifiées (fractions totale, acide et neutre), que les oligosaccharides neutres jouent un rôle majeur dans les interactions TIL448/PGM (**Tableau 2**).

Tableau 2. Tests de blocage par AFM sur la souche TIL448 avec PGM ou des fractions O-glycaniques purifiées (fractions totale, acide et neutre). Avant blocage, le pourcentage d'événements non adhésifs est de 2%.

Solution	PGM	O-glycanes totaux	Fraction acide	Fraction neutre
% NA[a] après blocage	80 ± 4%	76 ± 5%	11 ± 5%	42 ± 10%

[a] NA: événement non adhésif

Dans une seconde partie, nous avons effectué des essais par méthode hydrodynamique, au niveau de la population bactérienne et en conditions d'écoulement laminaire, pour le même panel de souches de *L. lactis* : TIL448 (souche sauvage), TIL1230 (souche curée de plasmides), TIL1289 (mutant piline) et TIL129 (mutant protéine "mucus-binding"). Les résultats sont présentés sur la **Figure 3**. L'avantage de cette méthode est l'observation *in situ*

du processus de détachement des bactéries sous cisaillement contrôlé, plus "proche" des conditions physiologiques existant *in vivo*.

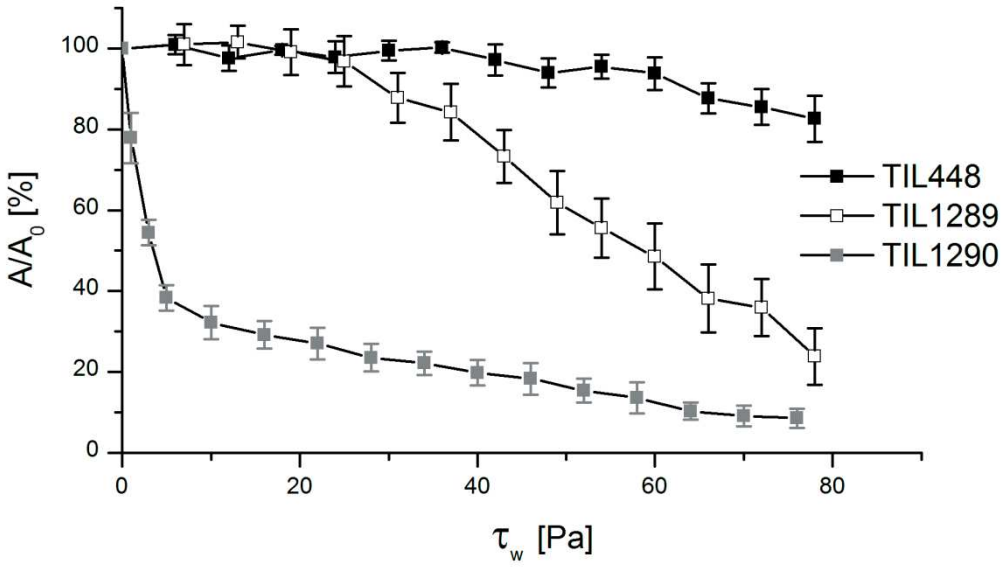

Figure 3. Profils de détachement sous cisaillement contrôlé de la souche sauvage TIL448 (carrés noirs), du mutant piline (carrés blancs) et du mutant protéine "mucus-binding" (carrés gris). A noter que, pour la souche curée de plasmides TIL1230, aucune adhésion à la couche de PGM n'a été observée.

La forte adhésion de TIL448 à PGM a été confirmée, avec près de 80% de bactéries restant adhérées pour la plus forte contrainte de cisaillement appliquée (80 Pa) **(Figure 3)**. La souche curée de plasmides TIL1230 n'adhère pas à PGM, même après 3 heures de contact. Le mutant protéine "mucus-binding" (TIL1290) adhère faiblement à PGM, alors que le mutant piline (TIL1289) présente un profil de détachement intermédiaire **(Figure 3)**. Ceci suggère qu'en conditions dynamiques, contrairement aux tendances observées par AFM, la protéine "mucus-binding" joue un rôle plus important que les pili dans le processus muco-adhésif de TIL448. Il faut toutefois noter que les deux méthodes diffèrent par la façon de "sonder" l'adhésion : par AFM, le contact puis le retrait de la lacto-pointe de la couche de PGM s'effectuent en mode forcé alors que, par méthode hydrodynamique, les conditions de détachement sont plus "douces".

L'ensemble de ce travail a fait l'objet d'une publication récemment acceptée dans le journal PLOS ONE.

Evaluation des capacités de migration de *L. lactis* au sein d'un hydrogel de PGM

Pour relier les propriétés muco-adhésives et diffusives de *L. lactis*, les capacités de migration de la souche TIL448 et de ses dérivés ont été évaluées dans des suspensions de PGM à concentration variable (0,5% et 5% (m/v)), en mettant en œuvre une nouvelle méthode "Diffusion Front Tracking" (DFT), précédemment développée au laboratoire pour mesurer le coefficient de diffusion de O_2 dans les liquides. Cette méthode consiste à suivre le front de diffusion de la suspension bactérienne au cours du temps au sein du réseau de PGM, dans une chambre de Hele-Shaw, couplée à une caméra CCD. Les bactéries *L. lactis* sont préalablement marquées avec la fuschine pour mieux visualiser le front de diffusion. Le dispositif expérimental est présenté sur la **Figure 4**. A noter que la viabilité et les propriétés de surface (hydrophobie, électronégativité) de l'ensemble des souches testées n'ont pas été modifiées de manière significative après marquage à la fuchsine (résultats non montrés).

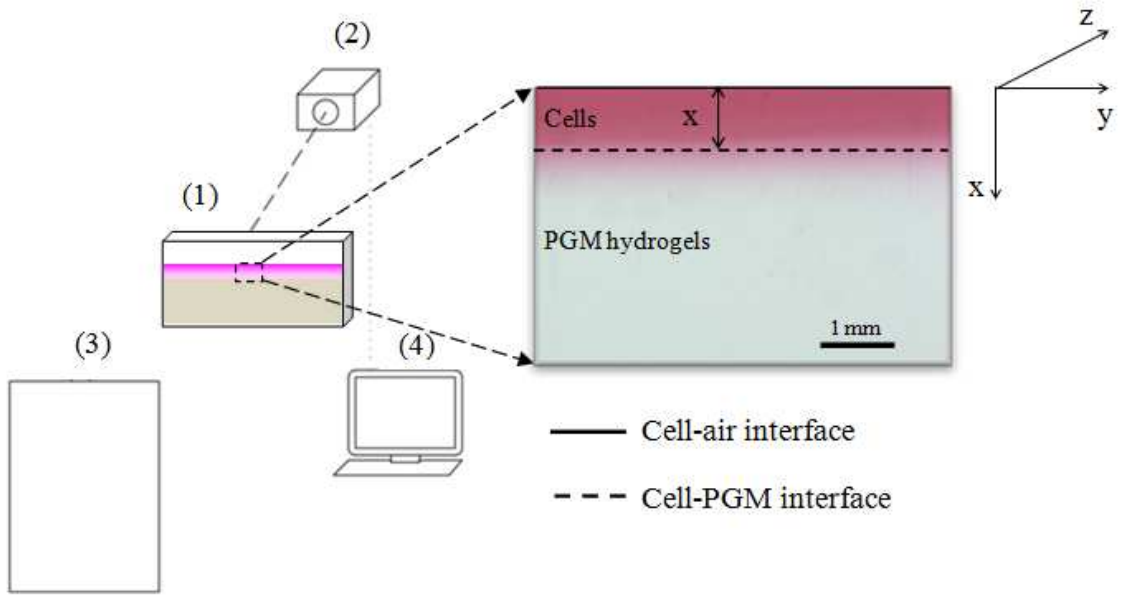

Figure 4. Dispositif expérimental pour les essais par DFT : (1) chambre de Hele-Shaw avec l'hydrogel de PGM et la suspension de *L. lactis* marquée à la fuschine et injectée en surface ; (2) caméra CCD ; (3) système d'éclairage ; (4) ordinateur d'acquisition.

La faisabilité de la méthode a tout d'abord été démontrée. Le coefficient de diffusion pour l'ensemble des souches testées a ensuite été déterminé (**Tableau 4**).

Tableau 4. Coefficient de diffusion (10^{-12} m^2/s) de *L. lactis* dans l'hydrogel de PGM pour les quatre souches étudiées et pour une concentration PGM de 0,5% et 5% (m/v).

	TIL1248* souche sauvage	**TIL1289** mutant piline	**TIL1290** mutant protéine "mucus-binding"	**TIL1250*** souche curée de plasmides
PGM 0,5% (m/v)	8,16 ± 0,41	12,90 ± 0,65	22,80 ± 1.14	89,80 ± 4,49
PGM 5% (m/v)	7,45 ± 0,37	9,00 ± 0,45	10,40 ± 0,52	68,80 ± 3,44

* à noter que, pour cette étude par DFT, les homologues de TIL448 et TIL1230 marqués à la GFP ("Green Fluorescent Protein") ont été utilisés (TIL1248 et TIL1250, respectivement).

Quelle que soit la concentration de PGM, le coefficient de diffusion le plus faible est obtenu pour la souche sauvage (TIL1248) alors que le plus élevé est atteint pour la souche curée de plasmides (TIL1250) (**Tableau 4**). Ces résultats sont une première indication que la migration de *L. lactis* dans l'hydrogel de PGM peut être influencée par son profil muco-adhésif, c'est-à-dire que la souche présentant des interactions fortes avec PGM a tendance à être plus "freinée" qu'un partenaire moins muco-adhésif. Cela a été confirmé par l'analyse des mutants de *L. lactis* : le mutant piline TIL1289 a un coefficient de diffusion plus faible que celui observé pour le mutant protéine "mucus-binding" TIL1290 (**Tableau 4**), ce qui est cohérent avec les conclusions émises précédemment sur la contribution plus importante de la protéine "mucus-binding" que les pili dans l'adhésion à PGM, comme observé en chambre à écoulement cisaillé (voir **Figure 3**). Toutefois, l'influence des propriétés de surface non spécifiques, comme l'hydrophobie, est également à prendre en considération. En effet, les souches les plus hydrophobes (TIL1248 et TIL1289) sont celles qui migrent le moins vite, probablement en raison d'interactions préférentielles avec les zones hydrophobes de PGM (régions riches en cystéine, par exemple). La taille et la morphologie des cellules bactériennes sont d'autres facteurs potentiellement impliqués avec, dans le cas des souches piliées, des phénomènes supplémentaires d'auto-agrégation.

Nous avons également démontré que les bactéries *L. lactis* ont tendance à être plus diffusives dans PGM 0,5% (m/v) que dans PGM 5% (m/v) (**Tableau 4**), probablement en lien avec des

propriétés structurales, mécaniques et rhéologiques du réseau de PGM différentes. Ce volet a été abordé dans une dernière partie de notre étude, présentée ci-dessous.

Caractérisation de la microstructure du réseau de mucines par des approches de microrhéométrie et de suivi de particules fluorescentes

Rhéométrie des mucines

Les propriétés viscoélastiques de solutions de PGM (à pH neutre, tampon PBS ou H_20 déionisée) ont été déterminées en utilisant un rhéomètre rotatif cône-plan (**Figure 5**) à vitesse de cisaillement contrôlée. La viscosité apparente a été caractérisée en fonction de la vitesse de cisaillement, allant de 10^{-3} à 300 s^{-1}, présentant un fort comportement rhéofluidifiant. En effet, la viscosité chute jusqu'à 2000 fois sur 5 décades dans le cas de PGM 0,5% (m/v). Par ailleurs, la courbe de viscosité est décrite par un plateau Newtonien à vitesse faible (10^{-3} s^{-1}), qui augmente avec la concentration (de 4,1 à 71,3 Pa.s) et qui s'étend vers les vitesses plus élevées à mesure que la concentration en PGM augmente, jusqu'à 10^{-2} s^{-1} dans le cas de PGM 20% (m/v). L'élasticité est prépondérante à faibles concentrations. Lorsque la concentration augmente de 2% à 20% (m/v), la viscosité domine sur l'élasticité, avec un angle de déphasage supérieur à 45°. Il a été proposé que PGM se comporte comme une solution dite semi-diluée auto-assemblée à faibles concentrations puis comme une solution diluée à concentrations élevées.

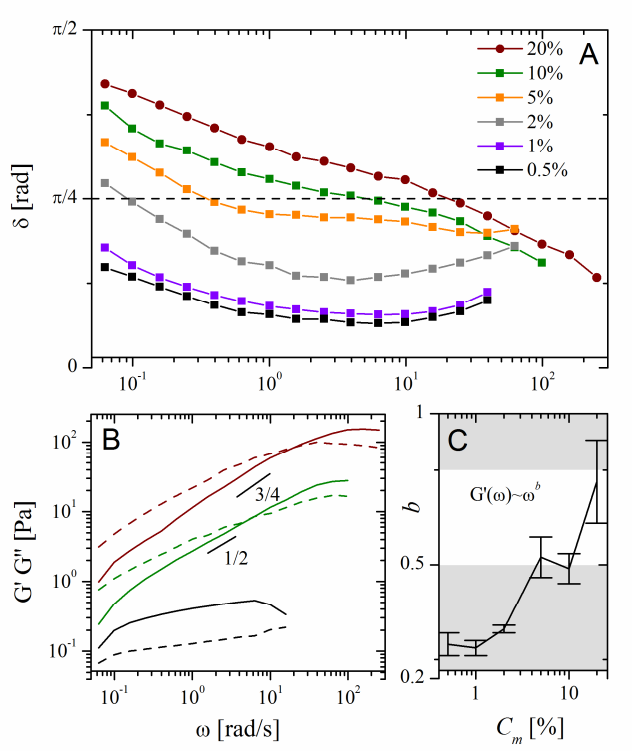

Figure 5. (A) Angle de déphasage en radians en fonction de la fréquence d'oscillation (rad/s), pour différentes concentrations de PGM (0,5-20% (m/v)) ; (B) Modules de perte (G", en pointillés) et de stockage (G', traits pleins) en fonction de la fréquence d'oscillation. Les pentes de 3/4 et 1/2 sur G' montrent le comportement en loi de puissance $G'(\omega) \sim \omega^b$, où l'exposant b est indiqué dans (C) en fonction de la concentration en PGM C_m.

Microstructure et propriétés microrhéologiques des mucines

La microstructure des solutions de PGM a été appréhendée par des techniques de suivi de particules fluorescences, appelées ici nanoparticules (NPs). Cette technique repose sur le suivi de la position des particules en fonction du temps. Les NPs, de diamètre 200 nm ou 500 nm, sont chargées négativement par des groupements carboxyl, chargées positivement par des groupements amines ou préalablement fonctionnalisées avec un agent neutre en charge, le polyéthylène glycol (PEG) qui annihile toute interaction d'origine électrostatique avec le milieu suspendant. L'efficacité de greffage a été vérifiée par la mesure du potentiel zeta des NPs. Une approche statistique a ensuite consisté à déterminer le déplacement quadratique moyen (MSD pour "Mean-Squared Displacement") de chaque traceur. Le MSD est relié à au temps par la relation $MSD = \Gamma \Delta t^{\alpha}$ avec une dépendance en loi puissance par l'exposant α qui est l'anomalie de diffusion. Le coefficient Γ n'est rien d'autre que $\Gamma = 4D$ dans le cas d'un

déplacement isotropique (*x~y*). *D* est le coefficient de diffusion (µm²/s) du traceur dans le milieu. Si α=1, alors la diffusion est considérée comme libre. Il a été montré que le coefficient de diffusion *D* diminue significativement avec la concentration en PGM. De plus, les particules les plus petites sont avantagées ainsi que les particules neutres (i.e. greffées avec PEG).

A partir des MSD, il est ensuite possible d'extraire des données mécaniques du réseau de mucines par l'intervention de la microrhéologie passive. Cette méthode consiste à déterminer le module complexe du milieu dont la déformation n'est induite que par l'action du mouvement brownien des traceurs et du réseau lui-même. Une première méthode, la microrhéologie *1 point* (1P), est gouvernée par l'autocorrélation du mouvement d'un traceur. La microrhéologie *2 points* (2P) se fonde, quant à elle, sur le postulat que la position de deux traceurs est corrélée soit parce que les fluctuations du réseau interfèrent sur leurs positions, soit parce que la position du premier influe sur celle du second. La seconde méthode décrite permet de s'affranchir des hypothèses d'homogénéité et d'incompressibilité du continuum et se montre plus adéquate dans le cas de PGM à une concentration supérieure à 2% (m/v). La **Figure 6** montre la superposition d'une méthode locale (2P) avec une méthode macroscopique (rhéométrie).

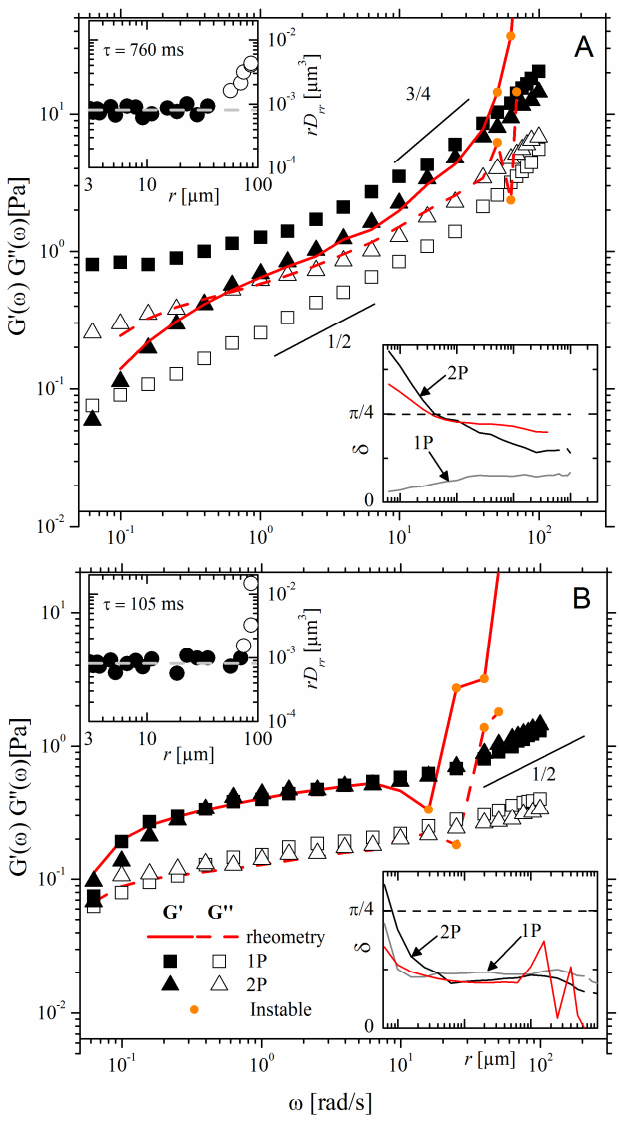

Figure 6. Modules visqueux (G'') et élastique (G') apparents en fonction de la fréquence d'oscillation pour (A) PGM 5% (m/v) et (B) PGM 0,5% (m/v) en utilisant les méthodes de rhéométrie cône-plan, microrhéometrie 1P et 2P. Les cercles pleins en orange représentent les données aberrantes (effet d'inertie de la géométrie à partir de 50 rad/s). Encart du haut : régression de rD_{rr} (coefficient de corrélation du mouvement des deux traceurs séparés d'une distance r) (μm^3) pour des temps de 0,76 s et 0,105 s, respectivement, utilisés pour obtenir les données relatives au module complexe G*(ω). Les valeurs prises en compte dans la régression sont identifiées par des symboles pleins et les valeurs aberrantes par des symboles ouverts c'est-à-dire hors de la plage $D_{rr} \sim 1/r$. Encart du bas : angle de déphasage δ en fonction de la fréquence (rad/s) en utilisant la même échelle que l'axe principal. Les valeurs obtenues en rhéométrie sont représentées par une ligne rouge continue (**Figure 5**) ; les lignes continues noire et grise sont obtenues à partir des méthodes 2P et 1P, respectivement.

Pour établir un lien entre la microstructure en termes de propriétés mécaniques, comme décrit précédemment et la perméabilité du réseau de PGM, un modèle d'obstruction, issu de la littérature, a été utilisé et permet d'accéder aux valeurs estimatives caractéristiques de la taille de pore du réseau. Les tailles ainsi obtenues varient de 470 nm à 240 nm pour des concentrations de PGM de 0,5% et 5% (m/v), respectivement. Ces valeurs sont parfaitement corrélées aux données de diffusivité et de microrhéologie. En effet, les particules de 500 nm de diamètre et greffées avec PEG sont piégées dans le réseau et restent quasi-statiques pour une concentration en PGM de 5% (m/v) tandis que les particules de 200 nm et greffées avec PEG sont, elles, capables d'évoluer librement. La forte hétérogénéité dans la taille de pore du réseau a toutefois été soulignée.

L'ensemble de ce travail fait l'objet d'une publication actuellement en préparation.

Conclusions

Notre étude, positionnée à l'interface Biologie/Physique et basée sur la combinaison d'approches biophysiques innovantes, a permis de disséquer le phénotype muco- adhésif de *L. lactis* TIL448, en relation avec la nature des déterminants de surface impliqués et les propriétés structurales, mécaniques et rhéologiques du réseau de PGM. Ces résultats permettront, à plus long terme, de proposer de nouvelles applications pour *L. lactis* dans le domaine de la santé (probiotique, vecteur pour délivrer des molécules d'intérêt thérapeutique).